Universidad Rey Juan Carlos

DOCTORAL THESIS

Construction of Efficient Intumescent Flame-Retardant Systems Based on Multi-Group Synergy: Properties and Mechanism in Polypropylene

Author:

Wei Tang

Supervisors:

De-Yi Wang
Silvia González Prolongo

Doctoral Program in Industrial Technologies: Chemical, Environmental, Energy, Electronics, Mechanics, and Materials

International Doctoral School

2025

ACKNOWLEDGEMENTS

As I come to the conclusion of my PhD journey, I would like to express my deepest gratitude to all those who have supported and accompanied me throughout this important stage of my academic and personal development.

First and foremost, I would like to sincerely thank my supervisors Prof. De-Yi Wang, Prof. Silvia González Prolongo and Prof. Lijun Qian. Your invaluable guidance, continuous support, and insightful academic advice have been instrumental in the completion of my research. Your rigorous scientific attitude and broad academic vision have been a constant source of inspiration and will continue to guide me in my future research career.

I would also like to express my heartfelt thanks to all members of the HPPN team of IMDEA Materials Institute. I am truly grateful for the professional research environment, technical support, and fruitful collaborations you have made. The exchanges and cooperation with you have greatly enriched my knowledge and skills, and I am honored to have made such good friends along the way.

My sincere appreciation also goes to the team at Beijing Technology and Business University. Thank you for your generous help, encouragement, and valuable academic discussions, which have made my research more productive and my PhD journey more rewarding.

I would like to give special thanks to my friends and family, whose companionship, understanding, and encouragement have always been a great comfort to me. It is your unwavering support that helped me persevere during challenging moments and made this long journey more enjoyable.

Finally, I am profoundly grateful for all the kindness and assistance I have received during my time in Spain. Whether in daily life or academic work, the help and encouragement from so many people have made me feel welcome and motivated in a foreign land.

To everyone who has helped me along this journey, I extend my heartfelt thanks. I wish you all continued success and happiness in your lives and careers.

Wei Tang

2025-10-01

RESUMEN

Esta disertación se centra en el diseño molecular y el desarrollo de sistemas avanzados de retardantes de llama intumescentes (IFR) con el fin de mejorar simultáneamente la resistencia a la llama, las propiedades mecánicas y el rendimiento multifuncional de los compuestos de polipropileno (PP). Mediante una combinación de estrategias de control de agregación molecular, copolimerización covalente y coordinación metal–ligando, se construyeron tres clases de sistemas IFR eficientes: macromoléculas basadas en nitrógeno/silicio (MNSi-n), un copolímero que contiene fósforo/nitrógeno/silicio (PNSi-co-MP) y una macromolécula híbrida basada en aluminio (Al-PAP). Se investigaron sistemáticamente las relaciones entre la estructura molecular, el comportamiento de dispersión, la formación de carbón y los mecanismos de acción retardante de llama, con el objetivo de establecer principios de diseño racionales para compuestos de PP de alto rendimiento.

En la primera parte, se sintetizó una serie de macromoléculas basadas en nitrógeno/silicio (MNSi-n, n = 1, 2, 3) mediante la inserción de esqueletos carbonosos de piperazina/fenil-silicio (NSi-n) con diferentes grados de agregación dentro de una red de ácido cianúrico de melamina (MCA) unida por enlaces de hidrógeno. Estas macromoléculas se combinaron con polifosfato de amonio (APP) para formar compuestos (MNSi-n/APP)/PP. Se examinó el efecto del grado de agregación del NSi-n sobre la eficiencia retardante y la formación de carbón mediante ensayos de hilo incandescente (GW), índice de oxígeno límite (LOI), UL 94 y calorimetría de cono. El PP puro mostró un índice de inflamabilidad del hilo incandescente (GWFI) de solo 725 °C, mientras que los compuestos de PP que contenían 28 % en peso de (MNSi-n/APP) alcanzaron la clasificación más alta, superior a 960 °C. El GWFI aumentó con el grado de agregación del NSi-n, confirmando que la estructura agrupada de piperazina/fenil-silicio era crucial para mejorar la resistencia a la llama. El valor de LOI del PP puro fue de 18.6 %, mientras que 22%(MNSi-3/APP)/PP alcanzó 25.7 %. Todos los compuestos (MNSi-n/APP)/PP con 28 % en peso superaron el 28 % de LOI y lograron una clasificación UL 94 V-0. En contraste, el sistema MCA/APP/PP (sin NSi-n) no superó la prueba UL 94, lo que puso de manifiesto el papel sinérgico del esqueleto NSi-n con APP. Los resultados del calorímetro de cono mostraron una notable resistencia al fuego: la tasa máxima de liberación de calor (PHRR) del PP puro fue de 1591 $kW \cdot m^{-2}$, mientras que para 25%(MNSi-n/APP)/PP se redujo a aproximadamente 400 $kW \cdot m^{-2}$. El índice de rendimiento al fuego (FPI) superó 0.055 $s \cdot m^2 \cdot kW^{-1}$ en todos los sistemas MNSi-n, frente a 0.018 $s \cdot m^2 \cdot kW^{-1}$ para el PP puro, mientras que el índice de crecimiento del fuego (FGI) disminuyó más del 40 %. MNSi-3 mostró la menor tasa de

liberación de calor (HRR) y liberación total de calor (THR), así como el FPI más alto, confirmando que un mayor grado de agregación del NSi-n promovió una eficiencia intumescente superior. El análisis termogravimétrico (TGA) mostró que (MNSi-n/APP)/PP se descomponía antes que (MCA/APP)/PP, favoreciendo la formación rápida de una capa protectora de carbón. A 500-600 °C, 25%(MNSi-n/APP)/PP retuvo más del 16 % de residuo, mientras que el PP puro no dejó prácticamente ninguno. Las observaciones por microscopía electrónica de barrido con espectroscopía de dispersión de energía (SEM-EDS) indicaron que MNSi-n/APP generó capas de carbón densas y continuas ricas en fósforo y silicio. La muestra 25%(MNSi-3/APP)/PP mostró los contenidos más altos de carbono (7.58 %) y silicio, lo que indica una mayor sinergia Si-P. La termografía infrarroja confirmó el fuerte efecto barrera: (MNSi-n/APP)/PP mantuvo su integridad estructural tras 60 s de exposición a la llama, mientras que (MCA/APP)/PP colapsó severamente. El análisis en fase gaseosa mediante espectroscopía infrarroja por transformada de Fourier (FTIR) demostró que MNSi-n/APP redujo la emisión de fragmentos hidrocarbonados (CH_3, CH_2, C=C) y liberó óxidos de fósforo (radicales $PO_x\cdot$), lo que disminuyó la eficiencia de combustión y mejoró la inhibición en fase gaseosa. En resumen, la incorporación de pequeñas cantidades de esqueletos de piperazina/fenil-silicio en la red de MCA generó macromoléculas de nitrógeno/silicio con agregación modulable. El compuesto optimizado (MNSi-3/APP)/PP mostró mejoras significativas en LOI, GWFI, FPI y rendimiento de residuo, junto con reducciones en HRR, THR y FGI. Este trabajo demuestra que controlar la agregación molecular dentro de estructuras carbonosas es una estrategia eficaz para diseñar sistemas IFR de alto rendimiento y baja carga para poliolefinas.

La segunda parte se centró en un nuevo copolímero dendrítico (PNSi-co-MP) que contiene fósforo (P), nitrógeno (N) y silicio (Si), sintetizado mediante copolimerización aleatoria de un monómero PNSi con fosfato de melamina (MP). Este copolímero actuó como un IFR eficiente para PP. La copolimerización interrumpió la regularidad monomérica, alterando la cristalinidad y el comportamiento térmico en comparación con el sistema MPNSi/polifosfato de melamina (MPP) auto-polimerizado. PNSi-co-MP presentó transición vítrea y ablandamiento térmico durante el procesado del PP, mejorando la dispersión y la adhesión interfacial con la matriz polimérica. El análisis morfológico reveló que las partículas de PNSi-co-MP pasaron de formas laminares (5-10 μm) a esferas o barras más pequeñas (200-300 nm), mejorando la transferencia de esfuerzo y la absorción de energía. En consecuencia, los compuestos PNSi-co-MP/PP mostraron fractura dúctil, mientras que MPNSi/MPP/PP se fracturó de forma frágil. El compuesto 16PNSi-co-4MP/PP presentó un aumento del 278 % en la elongación a la rotura y

una mejora del 33.3 % en la resistencia al impacto respecto a 16MPNSi/4MPP/PP, manteniendo una resistencia a la tracción similar. Las pruebas de retardancia de llama confirmaron un rendimiento superior: el compuesto con 20 % en peso de 12PNSi-co-8MP/PP alcanzó un GWFI superior a 960 °C, una temperatura de ignición del hilo incandescente (GWIT) de 875 °C, un LOI de 30.2 % y una clasificación UL 94 V-0. Los ensayos de calorimetría de cono mostraron reducciones del 93.6 % en PHRR y del 87.2 % en la tasa máxima de producción de humo (PSPR) respecto al PP puro. La combustión se inhibió eficazmente en 17 s tras la ignición, formándose una capa densa rica en Si/P/O/C/N que actuó como barrera térmica. La espectroscopía Raman indicó una mayor grafitización (menor relación ID/IG), mientras que la espectroscopía de fotoelectrones de rayos X (XPS) confirmó la presencia de enlaces Si-O-Si, P-O-C y P-N, demostrando una red sinérgica que reforzó la estabilidad del carbón. El rendimiento de residuo de 12PNSi-co-8MP/PP alcanzó el 61.4 %, mientras que THR y la liberación total de humo (TSR) disminuyeron un 57.6 % y 61.9 %, respectivamente, en comparación con MPNSi/MPP/PP. El índice de retardancia de llama (FRI) alcanzó 42.23, indicando una excelente seguridad contra incendios. Los análisis mecanísticos mediante TGA-FTIR y cromatografía de gases acoplada a espectrometría de masas (Py-GC/MS) demostraron que la copolimerización promovió una formación temprana de carbón y una degradación-carbonización sincronizada, generando menos especies volátiles y reacciones más rápidas en fase condensada. La integración de P, N y Si en una misma cadena molecular mejoró la carbonización en fase condensada y redujo la combustión en fase gaseosa al formar redes reticuladas estables. En conjunto, este estudio demostró que la copolimerización molecular equilibra eficazmente el refuerzo mecánico, la procesabilidad y la retardancia de llama en los compuestos de PP. El copolímero PNSi-co-MP representa una vía prometedora hacia IFRs de alto rendimiento con excelente combinación de tenacidad y seguridad frente al fuego.

En la parte final, se sintetizó una macromolécula híbrida (Al-PAP) que contiene fosfato de aluminio y fosfato de piperazina mediante policondensación, y se combinó con polifosfato de melamina (MPP) para construir un sistema IFR híbrido (Al-IFR) para PP. La inclusión de iones de aluminio (Al^{3+}) en la cadena fosfato facilitó el entrecruzamiento entre las fuentes ácidas, carbonosas y gaseosas, mejorando la compacidad y estabilidad térmica de la capa de carbón. Este enfoque resolvió el compromiso habitual entre retardancia de llama y conductividad térmica en sistemas IFR/PP. Con solo un 14 % en peso, Al-IFR elevó el LOI del PP a 28.3 %, equivalente al logrado con un 20 % de IFR convencional. Con 20 % en peso, el LOI aumentó a 32.2 %, GWIT alcanzó 850 °C, GWFI superó 960 °C y se obtuvo clasificación UL 94 V-0 a 3.2 mm y 1.6 mm. Los ensayos de calorímetro de cono mostraron reducciones del 84.7 % en

PHRR y del 72.2 % en PSPR respecto al PP puro. El FPI aumentó 4.7 veces y el FRI alcanzó el nivel "bueno" (1-10), demostrando alta seguridad frente al fuego y eficiencia en supresión de humo. Para mejorar aún más la conductividad térmica, se incorporaron Al_2O_3, nitruro de boro (BN) y nanotubos de carbono (MWCNTs) en los compuestos 20Al-IFR/PP. Al_2O_3 mostró la mejor sinergia, mejorando simultáneamente la conductividad térmica y la retardancia de llama. El compuesto 5Al_2O_3/20Al-IFR/PP mostró reducciones del 90.8 % en PHRR y 88.2 % en PSPR, junto con aumentos del 27.0 % en difusividad térmica y 48.9 % en conductividad térmica. En contraste, BN y MWCNT destruyeron la estructura intumescente, reduciendo el rendimiento retardante y aumentando la emisión de humo. Los estudios mecanísticos mediante FTIR, espectroscopía Raman y XPS indicaron que Al^{3+} y Al_2O_3 catalizaron interacciones fosfato-carbono, generando capas densas ricas en Si/P/O/C con alta grafitización (baja relación ID/IG). Los análisis TGA y Py-GC/MS confirmaron que las especies de aluminio redujeron la liberación de volátiles y promovieron estructuras fosfato-carbono térmicamente estables. El rendimiento de residuo aumentó de 11.2 % para 20Al-IFR/PP a 52.2 % para 5Al_2O_3/20Al-IFR/PP, confirmando una excelente estabilidad en fase condensada. Las pruebas mecánicas mostraron que el compuesto 5Al_2O_3/20Al-IFR/PP mantuvo una alta tenacidad, con una elongación a la rotura superior al 400 % y una resistencia al impacto sin muesca de 30 $kJ \cdot m^{-2}$. En resumen, la introducción de la macromolécula híbrida Al-PAP, junto con el relleno de Al_2O_3, permitió mejorar simultáneamente la retardancia de llama, la conductividad térmica y la supresión de humo, obteniéndose compuestos de PP multifuncionales con alta seguridad y buen rendimiento mecánico.

En conjunto, esta disertación establece una estrategia integral y sistemática de ingeniería molecular para diseñar sistemas IFR multifuncionales y altamente eficientes para polipropileno. A través de tres vías representativas - control de agregación molecular (sistema MNSi-n/APP), copolimerización covalente (sistema PNSi-co-MP) y coordinación metálica (sistema Al-IFR) - se demostró una clara relación estructura-función-rendimiento. Los resultados revelan que ajustar el grado de agregación de las estructuras carbonosas N/Si favorece la formación de capas compactas ricas en Si-P y una inhibición eficiente en fase gaseosa, mientras que la copolimerización de monómeros P-N-Si mejora la compatibilidad a nivel molecular y el equilibrio de propiedades mecánicas. Además, la introducción de iones y óxidos de aluminio refuerza la integridad del carbón y la conductividad térmica, logrando la combinación buscada entre seguridad frente al fuego y funcionalidad en compuestos de PP. Más allá de alcanzar una excelente retardancia y tenacidad, los sistemas IFR desarrollados contribuyen a comprender las interacciones sinérgicas entre los elementos P, N, Si y Al durante la combustión. Los

conocimientos adquiridos proporcionan una base teórica para el diseño racional de retardantes de llama de nueva generación que integren múltiples funcionalidades - como disipación térmica, supresión de humo y refuerzo estructural - en un solo marco molecular. Las estrategias propuestas no se limitan al PP, sino que pueden extenderse a otras poliolefinas y plásticos de ingeniería, abriendo el camino hacia materiales sostenibles de alto rendimiento para aplicaciones avanzadas en electrónica, automoción y construcción, donde la seguridad contra incendios y la durabilidad son requisitos simultáneos.

ABSTRACT

This dissertation focuses on the molecular design and development of advanced intumescent flame retardant (IFR) systems to simultaneously improve the flame retardancy, mechanical properties, and multifunctional performance of polypropylene (PP) composites. Through a combination of molecular aggregation control, covalent copolymerization, and metal–ligand coordination strategies, three classes of efficient IFR systems were constructed, namely nitrogen/silicon-based macromolecules (MNSi-n), a phosphorus/nitrogen/silicon-containing copolymer (PNSi-co-MP), and an aluminum-based hybrid macromolecule (Al-PAP). The relationships between molecular structure, dispersion behavior, char formation, and flame retardant mechanisms were systematically investigated to establish rational design principles for high-performance PP composites.

In the first part, a series of nitrogen/silicon-based macromolecules (MNSi-n, n = 1, 2, 3) were synthesized by inserting piperazine/phenyl-silicon charring skeletons (NSi-n) with varying aggregation degrees into a hydrogen-bonded melamine cyanuric acid (MCA) framework. These macromolecules were combined with ammonium polyphosphate (APP) to form (MNSi-n/APP)/PP composites. The effect of NSi-n aggregation on flame retardant efficiency and char formation was examined through glow-wire (GW), limiting oxygen index (LOI), UL 94, and cone calorimeter tests. Neat PP showed a glow-wire flammability index (GWFI) of only 725 °C, while PP composites containing 28 wt.% (MNSi-n/APP) achieved the highest classification of over 960 °C. The GWFI increased with the aggregation degree of the NSi-n structure, confirming that the clustered piperazine/phenyl-silicon framework was crucial for enhancing flame retardancy. The LOI value of neat PP was 18.6%, whereas 22%(MNSi-3/APP)/PP reached 25.7%. All 28 wt.% (MNSi-n/APP)/PP composites achieved LOI values above 28% and UL 94 V-0 rating. In contrast, MCA/APP/PP (without NSi-n) failed the UL 94 test, highlighting the synergistic role of the NSi-n skeleton with APP. Cone calorimeter results revealed remarkable fire resistance. The peak heat release rate (PHRR) of neat PP was 1591 $kW \cdot m^{-2}$, while 25%(MNSi-n/APP)/PP decreased to approximately 400 $kW \cdot m^{-2}$. The fire performance index (FPI) exceeded 0.055 $s \cdot m^2 \cdot kW^{-1}$ for all MNSi-n systems, compared to 0.018 $s \cdot m^2 \cdot kW^{-1}$ for neat PP, while the fire growth index (FGI) decreased by more than 40%. MNSi-3 exhibited the lowest heat release rate (HRR) and total heat release (THR), as well as the highest FPI, confirming that a higher aggregation degree of NSi-n promoted superior intumescent efficiency. Thermogravimetric analysis (TGA) showed that (MNSi-n/APP)/PP decomposed earlier than (MCA/APP)/PP, facilitating rapid formation of a protective char layer.

At 500-600 °C, 25%(MNSi-n/APP)/PP retained over 16% residue, while neat PP left nearly none. Scanning electron microscopy with energy-dispersive spectroscopy (SEM-EDS) indicated that MNSi-n/APP produced dense, continuous char layers rich in phosphorus and silicon. The 25%(MNSi-3/APP)/PP sample exhibited the highest carbon (7.58 wt.%) and silicon content, indicating enhanced Si-P synergism. Infrared thermal imaging further verified the strong barrier effect: (MNSi-n/APP)/PP maintained structural integrity after 60 s of flame exposure, while (MCA/APP)/PP collapsed severely. Gas-phase analysis using Fourier-transform infrared spectroscopy (FTIR) confirmed that MNSi-n/APP suppressed hydrocarbon fragment emissions (CH_3, CH_2, C=C) and released phosphorus oxides ($PO_x\cdot$ radicals), leading to reduced combustion efficiency and enhanced gas-phase inhibition. In summary, incorporating small amounts of piperazine/phenyl-silicon charring skeletons into the MCA framework generated nitrogen/silicon-based macromolecules with tunable aggregation. The optimized (MNSi-3/APP)/PP composite exhibited significantly improved LOI, GWFI, FPI, and residue yield, and reduced HRR, THR, and FGI values. This work demonstrates that controlling molecular aggregation within charring structures is an effective strategy to design high-performance, low-loading IFR systems for polyolefins.

The second part focused on a novel dendritic copolymer (PNSi-co-MP) containing phosphorus (P), nitrogen (N), and silicon (Si), synthesized via random copolymerization of a PNSi monomer with melamine phosphate (MP). This copolymer served as an efficient IFR for PP. Copolymerization disrupted monomer regularity, altering crystallinity and thermal behavior compared with the self-polymerized MPNSi/melamine polyphosphate (MPP) system. PNSi-co-MP displayed glass transition and thermal softening behavior during PP processing, improving dispersion and interfacial adhesion with the PP matrix. Morphological analysis revealed that PNSi-co-MP particles transformed from plate-like shapes (5-10 μm) into smaller spherical or rod-like particles (200-300 nm), enhancing stress transfer and energy absorption. Consequently, PNSi-co-MP/PP composites exhibited ductile fracture behavior, while MPNSi/MPP/PP fractured brittly. The 16PNSi-co-4MP/PP composite showed a 278% increase in elongation at break and a 33.3% improvement in impact strength compared with 16MPNSi/4MPP/PP, while maintaining similar tensile strength, demonstrating excellent balance between strength and toughness. Flame-retardant testing confirmed superior performance. The 20 wt.% 12PNSi-co-8MP/PP composite achieved a GWFI above 960 °C, a glow-wire ignition temperature (GWIT) of 875 °C, an LOI of 30.2%, and UL 94 V-0 rating. Cone calorimeter results showed reductions of 93.6% in PHRR and 87.2% in peak smoke production rate (PSPR) compared with neat PP. Combustion was effectively inhibited within

17 s after ignition, forming a dense Si/P/O/C/N-rich char layer that acted as an efficient thermal barrier. Raman spectroscopy indicated enhanced graphitization (lower I_D/I_G ratio), while X-ray photoelectron spectroscopy (XPS) confirmed the presence of Si-O-Si, P-O-C, and P-N bonds, demonstrating a synergistic network that reinforced char stability. The residue yield of 12PNSi-co-8MP/PP reached 61.4%, while THR and total smoke release (TSR) decreased by 57.6% and 61.9%, respectively, compared with MPNSi/MPP/PP. The flame retardant index (FRI) reached 42.23, indicating excellent overall fire safety. Mechanistic analyses using thermogravimetry coupled with FTIR (TG-FTIR) and pyrolysis-gas chromatography-mass spectrometry (Py-GC/MS) showed that copolymerization promoted early char formation and synchronized degradation-carbonization behavior, leading to fewer volatile species and faster condensed-phase reactions. The integration of P, N, and Si within one molecular backbone not only improved condensed-phase charring but also reduced gas-phase combustion by forming stable crosslinked structures. Overall, this study demonstrated that molecular copolymerization effectively balanced mechanical reinforcement, processability, and flame retardancy in PP composites. The PNSi-co-MP copolymer provides a promising pathway to high-performance IFRs with combined toughness and fire safety.

In the final part, a hybrid macromolecule (Al-PAP) containing aluminum phosphate and piperazine phosphate was synthesized via polycondensation and combined with melamine polyphosphate (MPP) to construct a hybrid IFR system (Al-IFR) for PP. The inclusion of aluminum ions (Al^{3+}) within the phosphate backbone facilitated crosslinking among acidic, carbon, and gas sources, thereby improving the compactness and thermal stability of the char layer. This approach addressed the common trade-off between flame retardancy and thermal conductivity in IFR/PP systems. At only 14 wt.% loading, Al-IFR raised the LOI of PP to 28.3%, equivalent to that achieved with 20 wt.% conventional IFR. With 20 wt.% Al-IFR, the LOI further increased to 32.2%, GWIT reached 850 °C, GWFI exceeded 960 °C, and UL 94 V-0 ratings were achieved at both 3.2 mm and 1.6 mm thicknesses. Cone calorimeter tests revealed an 84.7% reduction in PHRR and a 72.2% decrease in PSPR compared with neat PP. The FPI increased by 4.7 times, and the FRI reached the “good” level (1-10), demonstrating high fire safety and smoke suppression efficiency. To further improve heat conduction, alumina (Al_2O_3), boron nitride (BN), and multi-walled carbon nanotubes (MWCNTs) were incorporated into 20Al-IFR/PP composites. Al_2O_3 exhibited the best synergy, simultaneously enhancing thermal conductivity and flame retardancy. The 5Al_2O_3/20Al-IFR/PP composite showed a 90.8% reduction in PHRR, an 88.2% reduction in PSPR, and increases of 27.0% in thermal diffusivity and 48.9% in thermal conductivity. In contrast, BN and MWCNT disrupted the intumescent

char structure, resulting in inferior fire performance and higher smoke emission. Mechanistic studies using FTIR, Raman spectroscopy, and XPS indicated that Al^{3+} and Al_2O_3 catalyzed phosphate-carbon interactions, generating dense Si/P/O/C-based layers with high graphitization (low I_D/I_G ratio). TGA and Py-GC/MS confirmed that aluminum species suppressed volatile release and promoted thermally stable phosphate-carbon frameworks. The residue yield increased from 11.2% for 20Al-IFR/PP to 52.2% for $5Al_2O_3$/20Al-IFR/PP, confirming excellent condensed-phase stability. Mechanical testing showed that the $5Al_2O_3$/20Al-IFR/PP composite maintained high toughness, with elongation at break exceeding 400% and a non-notched impact strength of 30 $kJ \cdot m^{-2}$. In summary, the introduction of the Al-PAP hybrid macromolecule, together with Al_2O_3 fillers, enabled simultaneous enhancement of flame retardancy, thermal conductivity, and smoke suppression, producing multifunctional PP composites with high fire safety and robust mechanical performance.

Overall, this dissertation establishes a comprehensive and systematic molecular engineering strategy for designing high-efficiency, multifunctional intumescent flame retardant systems for polypropylene. Through three representative design pathways, including controlled molecular aggregation (MNSi-n/APP system), covalent copolymerization (PNSi-co-MP system), and metal coordination (Al-IFR system), a clear structure-function-performance relationship has been demonstrated. The results reveal that fine-tuning the aggregation degree of nitrogen/silicon charring structures can promote compact Si-P-rich char formation and efficient gas-phase inhibition, while copolymerization of phosphorus-nitrogen-silicon monomers achieve molecular-level compatibility and balanced mechanical performance. Furthermore, the introduction of aluminum ion and alumina enhances both char integrity and thermal conductivity, achieving the long-sought combination of fire safety and functional performance in PP composites. Beyond achieving superior flame retardancy and mechanical toughness, the developed IFR systems also contribute to understanding the synergistic interactions among P, N, Si, and Al elements during combustion. The insights gained from this work provide a theoretical foundation for the rational design of next-generation flame retardants that integrate multiple functionalities, such as heat dissipation, smoke suppression, and structural reinforcement, into a single molecular framework. The strategies proposed herein are not limited to PP but can be extended to other polyolefins and engineering plastics, paving the way for high-performance, environmentally sustainable materials for advanced applications in electronics, automotive components, and building materials where fire safety and durability are simultaneously required.

CONTENTS

ABBREVIATIONS

Al_2O_3	Alumina or Aluminum oxide
AlDHP	Aluminum dihydrogen phosphate
Antioxidant 1010	Pentaerythritol tetrakis[3-(3,5-di-tert-butyl-4-hydroxyphenyl) propionate]
Antioxidant 168	Tris(2,4-di-tert-butylphenyl) phosphite
APP	Ammonium polyphosphate
ATH	Aluminum hydroxide
av-COY	Average carbon monoxide yield
av-CO_2Y	Average carbon dioxide yield
av-EHC	Average effective heat of combustion
BN	Boron nitride
C_p	Specific heat capacity
DOPO	9,10-dihydro-9-oxa-10-phosphaphenanthrene-10-oxide
DSC	Differential scanning calorimetry
EDS	Energy dispersive spectrometer
EG	Expandable graphite
FGI	Fire growth index
FPI	Fire performance index
FR	Flame retardant
FRI	Flame retardant index
FTIR	Fourier-transform infrared spectroscopy
GC/MS	Gas chromatography/mass spectrometry
GW	Glow wire test
GWFI	Glow-wire flammability
GWIT	Glow-wire ignition temperature
HRR	Heat release rate
IFR	Intumescent flame retardant
LDH	Layered double hydroxide
LOI	Limiting oxygen index
MCA	Melamine cyanurate

MDH	Magnesium hydroxide
MEL	Melamine
MP	Melamine phosphate
MPOP	Melamine pyrophosphate
MPP	Melamine polyphosphate
MWCNT	Multi-walled carbon nanotubes
NMR	Nuclear magnetic resonance
PA	Polyamide
PAP	Piperazine phosphate
PEPA	Pentaerythritol phosphate
PER	Pentaerythritol
PHRR	Peak heat release rate
PMLR	Peak mass loss rate
PPAP	Piperazine pyrophosphate
PP	Polypropylene
PP-g-MA	Polypropylene grafted with maleic anhydride
PSPR	Peak smoke production rate
PTFE	Polytetrafluoroethylene
py-GC/MS	Pyrolyzer - gas chromatography/mass spectrometry
$T_{d,max}$	Temperature of the maximum decomposition rate
TGA	Thermogravimmetric analysis
THEIC	Tris(2-hydroxyethyl) isocyanate
THR	Total heat release
TPU	Thermoplastic polyurethane
TSR	Total smoke release
TTI	Time to ignition
TTP	Time to peak heat release rate
SEM	Scanning electron microscope
SPR	Smoke production rate
XPS	X-ray photoelectron spectroscopy
XRD	X-ray diffraction

α	Thermal diffusivity
κ	Thermal conductivity
ρ	Bulk density

CHAPTER 1

Introduction

1.1 Background: Polypropylene

Polypropylene (PP) is a polymer obtained through the polymerization of propylene monomers, as illustrated in Fig. 1.1. It is mainly synthesized via coordination polymerization using Ziegler–Natta catalysts, which remains the most widely applied method in industrial production. [1][2][3] This process employs transition metal compounds, such as titanium chlorides, in combination with organoaluminium co-catalysts to achieve high isotacticity, high molecular weight, and excellent mechanical properties. Polymerization is typically carried out under moderate temperature and pressure in bulk, solution, or gas-phase conditions. In addition to conventional Ziegler–Natta catalysts, metallocene catalysts have emerged as a more advanced alternative. These catalysts allow for precise control over polymer microstructure, molecular weight distribution, and comonomer incorporation. Although metallocene-based processes are not yet widely adopted in large-scale industrial applications, they are increasingly used to produce specialty polypropylene grades with enhanced transparency, elasticity, or heat resistance. [4][5] Free radical polymerization of propylene is also theoretically feasible under high-temperature and high-pressure conditions. However, due to poor control over polymer structure and broad molecular weight distribution, this method is rarely used in commercial production. [6][7]

Fig. 1.1 Synthesis route of polypropylene.

Owing to its excellent processing performance, low production cost, and well-balanced mechanical properties, polypropylene is one of the most widely used general-purpose thermoplastic polymers. [8][9] These characteristics make PP suitable for a wide range of applications, offering both economic and functional advantages. It also exhibits high tensile strength, good fatigue resistance, and outstanding chemical stability, which can be attributed to its saturated hydrocarbon chain structure. Because of these advantages, PP is extensively applied in automotive composites, household appliance housings, piping systems, toys, packaging films, and building materials. [10] Its versatility and cost-effectiveness have made it a preferred material in many industrial and consumer fields.

However, PP also has significant limitations, particularly in terms of fire risk. It is a highly flammable material, with a limiting oxygen index (LOI) of only around 18%, demonstrating its high flammability at air atmosphere. [11][12] Under thermal oxidative conditions, especially at temperatures above 300 degrees Celsius, the molecular chains of PP break down rapidly. This degradation produces low-molecular-weight substances such as short-chain olefins, aldehydes, and ketones, all of which are highly flammable. [13][14][15][16] Moreover, PP tends to form molten drips during combustion, increasing the risk of fire spread and secondary ignition. [17][18] In order to extend the range of applications for PP, especially in fields that require higher fire safety standards such as construction, transportation, and electronics, improving its flame retardant properties is essential.

1.2 Overview of flame retardant (FR) solutions for polypropylene

The state-of-the-art flame retardant strategies for polypropylene have evolved significantly beyond traditional halogenated systems, driven by growing environmental and regulatory pressures. [19][20][21] Current approaches emphasize halogen-free, environmentally friendly alternatives with high efficiency. Among these, intumescent flame retardant (IFR) systems have gained prominence due to their ability to form protective char layers during combustion, offering effective flame inhibition with limited toxic emissions. [22] Meanwhile, nanocomposite strategies employing materials such as layered silicates, carbon nanotubes, and graphene are being extensively explored for their barrier effects, thermal stability, and potential to enhance both flame retardancy and mechanical performance at low loadings. [23][24] Recent trends also include flame retardants functioning in the gas phase [25][26] and synergistic hybrid systems [27][28], combining multiple flame retardant components to optimize efficiency. Additionally, the development of bio-based and sustainable flame retardants aligns with the global shift toward greener materials. [29][30] Despite these advancements, challenges such as processability, cost, and compatibility remain, motivating continued research into multifunctional, high-performance flame retardant solutions for PP.

1.3 Intumescent flame retardant for PP

Among the various strategies developed to enhance the flame retardancy of polypropylene, the intumescent flame retardant system stands out as one of the most mature and effective approaches. IFR functions by forming a porous, expanded char layer upon exposure to heat, which provides flame retardancy through thermal insulation, oxygen barrier effects, and the suppression of volatile degradation products. Due to their halogen-free composition, low smoke and toxicity during combustion, and absence of molten drips, IFR have attracted

significant research interest in recent years and are widely regarded as a promising class of flame retardant systems. IFR can be broadly categorized into physical and chemical intumescent systems. The former typically relies on expandable graphite (EG) as the active component, while the latter is developed through the rational design of synergistic acid sources, gas sources, and carbon sources to achieve effective charring and expansion. [31][32]

1.3.1 Physical intumescent systems for PP

Upon thermal exposure, the intercalated compounds within expandable graphite rapidly vaporize, generating pressure between the graphite layers and triggering substantial expansion, as shown in Fig. 1.2. This process transforms EG from its original flake-like structure into a worm-like morphology. The expanded graphite, characterized by its extremely low density, forms a continuous insulating layer on the polymer surface, which is able to serve as a thermal barrier, effectively limiting heat transfer to the polymer matrix while simultaneously inhibiting the release of flammable volatiles, thereby enhancing flame retardancy. [33]

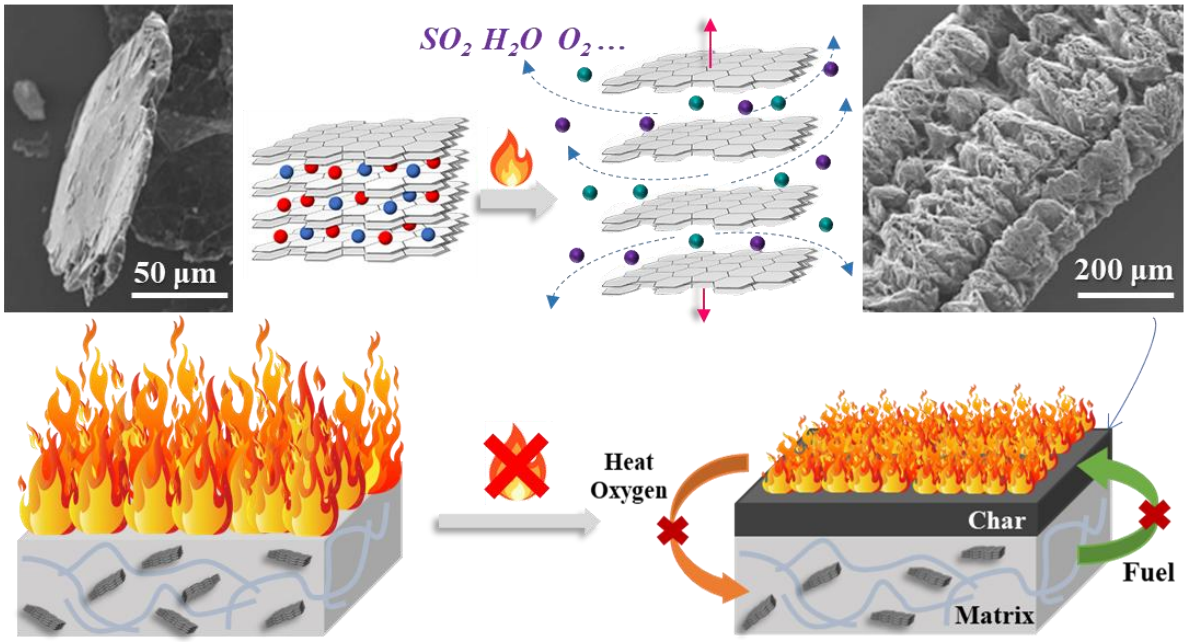

Fig. 1.2 The mechanism of expandable graphite.

When used alone, EG exhibits limited flame-retardant efficiency in polypropylene. At a loading of 25 wt.%, the limiting oxygen index (LOI) of the resulting PP composite is only around 23%, and the material fails to achieve any classification in the UL-94 vertical burning test. Nonetheless, it is noteworthy that despite its poor performance in LOI and vertical burning tests, 25 wt.% EG enables the PP composite to achieve a peak heat release rate (PHRR) below 200 $kW \cdot m^{-2}$ in cone calorimetry testing at 35 $kW \cdot m^{-2}$ heat flux. [34][35] This seemingly contradictory behavior may be attributed to the loose and structurally weak worm-like char

formed by EG, which is less likely to accumulate into a sufficiently thick protective layer during LOI and vertical burning tests but still provides good shielding in the horizontal mode of cone calorimetry.

Due to the limited efficiency of EG when used alone, current research efforts have primarily focused on multi-component synergistic formulations and modification. A representative approach involves the combination of EG with chemically intumescent flame retardants to construct a dual-intumescence system. Chemically intumescent agents can form a continuous and compact char barrier, compensating for the insufficient structural integrity of EG-derived char. At the same time, the low thermal conductivity and fluffy structure of the expanded EG contribute to improved insulation and flame-retardant performance, resulting in a synergistic effect between the two components. For example, a melamine polyphosphate (MPP) / dipentaerythritol system at a mass ratio of 3:1 exhibits optimal synergistic flame-retardant performance in polypropylene. When 30 wt.% of this IFR system is added, the resulting PP composite achieves a LOI of 28.7% and attains a UL-94 V-1 rating at a thickness of 1.6 mm. When 10 wt.% of EG is used to partially replace the IFR system, the LOI increases to 33.2%, and the composite passes the UL-94 V-0 rating at the same thickness. Additionally, the PHRR is reduced by approximately 50% compared to the EG-free formulation. These results suggest that the hybrid physical/chemical intumescence mechanism leads to a char structure with significantly enhanced barrier properties. [36] Similar synergistic flame-retardant effects have also been observed between EG and other intumescent systems, such as ammonium polyphosphate (APP) / char-forming agent system [37][38] and surface modified APP [39]. It is important to note, however, that the ratio between EG and chemically intumescent flame retardants is a critical factor. When the ratio is not optimized - for instance, a 1:9 mass ratio of EG to modified APP - flame-retardant performance can be significantly inferior compared to using modified APP alone. [40] To address the issue of poor char strength associated with EG, a hybrid ferrocene-based non-phosphorus polymer has been developed. [34] Under the catalytic action of this hybrid compound, EG can expand at relatively lower temperatures. Meanwhile, the decomposition products of the polymer act as catalysts to promote cross-linking within the polymer matrix and facilitate the formation of graphitic structures. During combustion, the resulting cross-linked networks generate a high-viscosity melt that fills the voids within the EG char and bridges adjacent expanded graphite layers, thereby eliminating the so-called “popcorn effect”. Moreover, for flame retardants with relatively low efficiency such as magnesium hydroxide (MH), achieving a UL-94 V-0 rating in PP typically requires a high loading exceeding 60 wt.%. Partial replacement of MH with EG

has been shown to reduce the total required flame retardant content while simultaneously increasing the LOI and suppressing heat release intensity. [41][42][43]

Modification of EG primarily involves surface functionalization and intercalation strategies. For example, silane coupling reactions can be employed to graft various silane monomers onto the hydroxyl groups present on the EG surface, resulting in surface-modified EG with improved compatibility and dispersion. Commonly used silane monomers include dimethyldiethoxysilane, dimethoxydiphenylsilane, phenyltrimethoxysilane, methyltrimethoxysilane, [35] as well as 9,10-dihydro-9-oxa-10-phosphaphenanthrene-10-oxide (DOPO) -grafted silanes [44]. These modifications have been shown to enhance both the interfacial interaction with the polymer matrix and the overall flame-retardant efficiency of EG. Furthermore, intercalation technology has recently emerged as a promising strategy for the modification of EG. Introducing nanoparticles (e.g., silica) or phosphorus-containing compounds (e.g., DOPO derivatives) between the graphite layers can significantly enhance the catalytic charring and expansion behavior of EG. [45][46][47]

In summary, expandable graphite exhibits excellent expansion ratio and rapid response upon fire exposure, providing effective barrier performance under varying fire scenarios. However, due to the inherently loose structure of its char, often referred to as the "popcorn effect," EG-based systems typically struggle to achieve high LOI values and favorable UL-94 vertical burning ratings with relatively low dosages. Therefore, future research should focus on strategies to improve the structural integrity and cohesion of the expanded residue.

1.3.2 Chemical intumescent systems for PP

Chemically intumescent flame retardant typically consists of three main structures: an acid source (dehydrating agent), a carbon source (char-forming agent, CFA), and a gas source (blowing agent). [48][49][50] Unless otherwise specified, all IFR systems mentioned hereafter refer to chemically intumescent systems.

The acid source plays a key role in catalyzing the esterification of the carbon source, thereby inducing dehydration. The traditional acid sources included diammonium phosphate and monoammonium phosphate, but due to their high water solubility, they have been largely phased out. More commonly used acid sources today include polyphosphate, pyrophosphate, and phytate. The carbon source provides the backbone for the formation of a foamed char layer by undergoing dehydration and carbonization during combustion. Traditional carbon sources are mostly polyhydric alcohols, such as pentaerythritol (PER) and starch. However, due to their hygroscopicity and thermal instability, these have been increasingly replaced by more stable

char-forming derivatives such as triazine compounds, amines, and phosphate esters. The gas source is responsible for releasing large volumes of non-flammable gases upon thermal decomposition, which facilitates the expansion of the system. Common gas-generating structures include melamine, APP (which releases ammonia), melamine cyanurate, and so on. [51][52][53] As a matter of fact, certain components within IFR systems can serve multiple functional roles. For instance, both APP and MPP can act simultaneously as acid sources and gas sources. Piperazine pyrophosphate functions as both an acid source and a carbon source. Moreover, some molecules are designed to incorporate all three functionalities - acid, carbon, and gas source, enabling them to serve as single-component IFR. As shown in Fig. 1.3. IFR functions primarily in the condensed phase by forming a porous and insulating char layer during combustion. The formation process can generally be divided into the following stages [54][55][56][57][58]:

(a) At relatively low temperatures, the acid source releases inorganic acids, which act as dehydrating agents to promote the esterification of polyols or amine-based carbon sources.

(b) During esterification, the system melts and may react with degradation products of polypropylene, resulting in the formation of a crosslinked network. Under the pressure of gases released by the gas source, the molten system expands to form foam.

(c) After these reactions, the system solidifies, and the resulting porous intumescent char layer acts as a barrier, inhibiting the release of combustible volatiles and blocking heat transfer from the external flame to the polymer matrix.

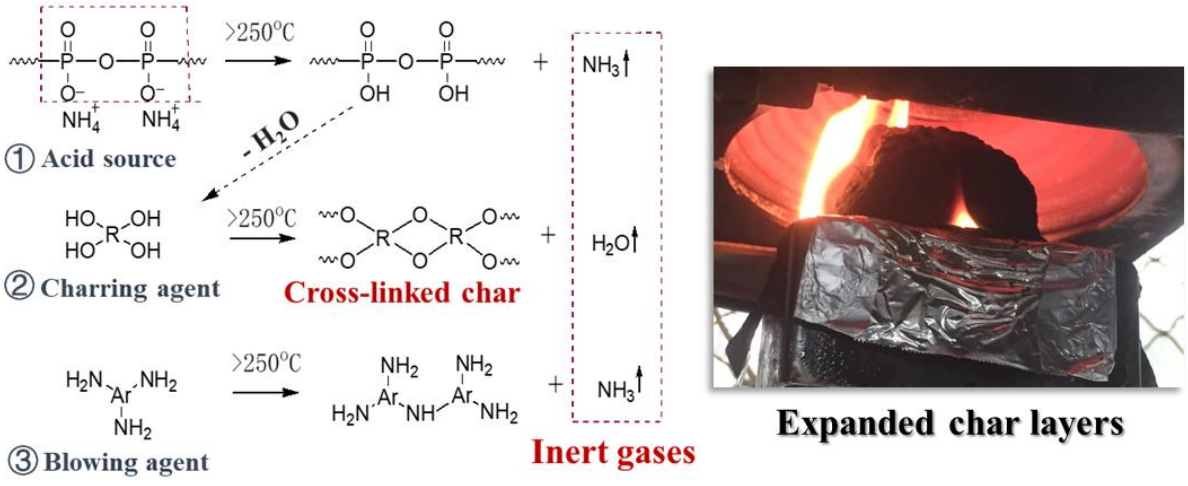

Fig. 1.3 The basic mechanism of intumescent flame retardant effect.

In IFR systems, the acid source is typically the major component and is theoretically regarded as the primary flame retardant, while the carbon and gas sources serve as auxiliary components that assist in the acid-induced formation of an intumescent char layer. However,

in practice, aside from the commonly used acid sources / structure mentioned above, few new and efficient acid-source molecules have been developed. This has made the design and synthesis of novel char-forming agents the most critical aspect of constructing effective IFR systems. In recent years, research efforts have primarily focused on the development of advanced carbon sources and on designing efficient IFR systems through the strategic arrangement of functional groups within the molecular structure. In addition, significant attention has been given to the development of synergistic flame-retardant systems to further enhance overall performance.

1.3.2.1 Char-forming agent for IFR/PP

The primary categories of char-forming agents include polyols and their derivatives, triazine-based compounds, organic amine derivatives, and phosphate esters. Among them, triazine and organic amine derivatives have emerged as the most extensively studied and widely applied due to their high efficiency and structural versatility.

a) Polyols and their derivatives CFA

The most representative polyol-based CFA is PER. The system composed of PER, APP, and melamine (MEL) was the first IFR formulation to be systematically studied and commercially applied. In 1984, Prof. G. Camino et al. conducted pioneering work on this system, thoroughly investigating the composition and structure of the char layer formed during the flame retardancy of polypropylene. Their work established a clear understanding of the intumescent flame-retardant mechanism, as described in previous sections. [55][56][57][58] Subsequent studies have developed more PER-based IFR systems for PP. [59][60][61] However, due to the high density of hydroxyl groups, PER exhibits strong hygroscopicity, while its flame-retardant efficiency still requires further improvement. Consequently, researchers have developed a variety of PER derivatives. A representative synthetic strategy involves the reaction of PER with trichlorophosphine to form caged pentaerythritol phosphate (PEPA), which can subsequently react with various functional groups to construct a series of CFA. [62] PEPA itself can be combined with APP or MPP for flame-retardant modification of PP. When the mass ratios of PEPA to APP and PEPA to MPP are 1:2 and 2:1, respectively, both the 30 wt.% PEPA/APP and 20 wt.% PEPA/MPP systems enable the LOI of PP to reach approximately 33% and also achieve V-0 rating in the UL-94 vertical burning test. [63][64] From **Table. 1.1**, it is obvious that the char-forming efficiency of PEPA becomes higher than that of PER in IFR. Owing to a hydroxyl group, PEPA still performed the potential to be designed into other CFAs, meanwhile the water resistance can be improved by eliminating the hydroxyl group. As a result,

extensive research has been conducted to develop a series of PEPA derivatives. Typical reactive ingredients include phosphoryl chloride, phenyl phosphoryl dichloride and so on. Based on these reactants, several representative PEPA derivatives have been synthesized, and their molecular structures and flame retardant efficiency in IFR are listed in Table 1.1. The acid source chemicals for forming corresponding IFR systems includ APP, MPP, and melamine pyrophosphate (MPOP). A comparison of LOI values and the suppression of PHRR indicates that IFR systems based on PEPA derivatives [65][66][67][68][69] exhibit flame-retardant efficiency in PP comparable to that of PEPA-based IFR systems. At a loading level of approximately 25-30 wt.%, these systems typically achieve LOI values around 30% and UL 94 V-0 rating, demonstrating that the flame-retardant performance primarily stems from the synergistic charring behavior between the basic PEPA structure and the acid, gas source components. However, from a theoretical perspective, these PEPA derivatives are expected to offer improved properties, particularly in terms of water resistance and compatibility.

Table 1.1 The structures, formulations and flame retardancy in PP for polyols-derivatives CFAs

CFA	Chemical Structures	IFR Formulation (Weight ratio)	IFR [a] (wt.%)	LOI	PHRR Red. [b]
PER [59]	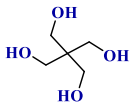	3APP/2PER	25	27.8%	52.5%
PEPA [63]	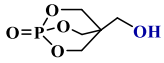	2APP:1PEPA	30	32.8%	/
PEPA [64]	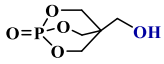	1MPP/2PEPA	20	33.0%	78.3%
BCPPO [65]	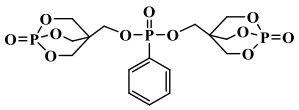	9APP/3MEL/3BCPPO	30	30.3%	83.2%
Trimer [66][67]	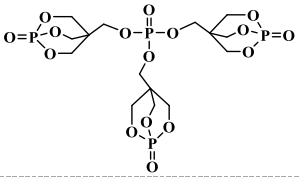	8.3APP/16.7Trimer	25	28.8%	/
Trimer [68]	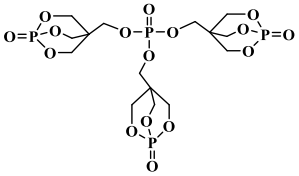	1MPOP/1Trimer	30	/	87.6%

SBCPO [69]	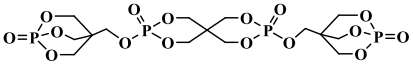	1APP/1SBCPO	25	30.5%	75.2%
BSPPO [70]	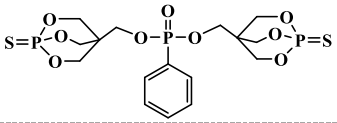	7APP/4MPP/4BSPPO	30	32.0%	82.5%
DOPNP [71]	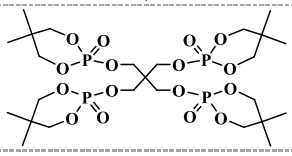	10APP/5MPP/1DOPNP	30	31.3%	~75.0%
SPSA [72]	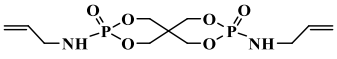	2APP/1SPSA	30	24.0%	58.6%
THEIC [73]	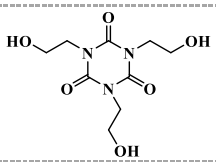	2APP/1THEIC	30	34.8%	78.6%
Homo-THEIC [74]	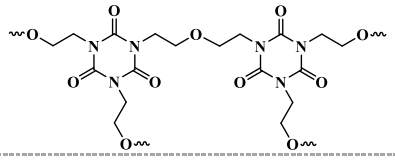	2APP/1Homo-THEIC	30	32.8%	71.8%
PN-HBP [75]	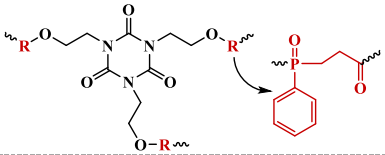	1APP/1PN-HBP	20	30.0%	86.9%
β-CD [76]	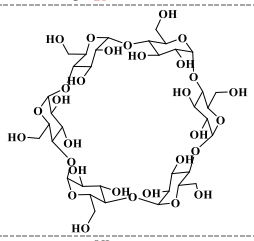	3APP/1β-CD	30	21.4%	/
HDI-CD [76]	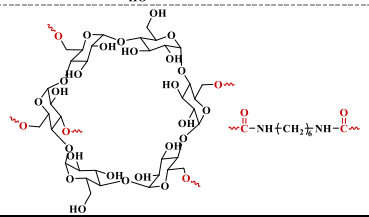	3APP/1HDI-CD	30	33.0%	/

[a] Apart from β-CD, all formulations listed in the table enable PP with UL **94 V-0 rating** (3.2 mm).
[b] PHHR reduction percentage of FR-PP compared to pure PP.

In addition, PER can react with thiophosphoryl chloride to form a sulfur-containing cage-like phosphate ester, structurally similar to PEPA. [70] This intermediate can further undergo a dehydrochlorination reaction with phenyl phosphoryl dichloride to yield a sulfur-containing PER derivative, BSPPO, whose structure closely resembles that of BCPPO. IFR system based on BSPPO exhibits a comparable ability to suppress the PHRR as that based on BCPPO, while providing a slightly higher LOI in flame-retardant polypropylene, which might be contributed

by the sulfur-containing structure. Another derivative, DOPNP, contains four phosphate ester groups and is synthesized from PER, neopentyl glycol, and phosphoryl chloride. [71] At an optimal formulation ratio, with a total IFR loading of 30 wt.%, the resulting PP composite achieves a LOI of 31.3% and passes the UL-94 vertical burning test with a V-0 rating. Notably, the loading amount of the DOPNP is significantly lower than that of other CFAs, demonstrating its high charring efficiency. Furthermore, the phosphate structure of DOPNP shows good compatibility with the PP matrix, ensuring effective flame retardancy while minimizing adverse effects on the mechanical properties. Further, a CFA molecule capable of chemically reacting with the PP matrix has also been synthesized from PER. [72] Although the IFR system based on SPSA exhibits only moderate flame-retardant efficiency, the use of electron beam treatment enables the double bonds in the CFA molecule to form covalent bonds with the PP chains. This chemical linkage helps to preserve the mechanical and thermal stability of the flame-retardant PP composites.

In addition to PER, other noteworthy polyol-based CFA molecules include tris(2-hydroxyethyl) isocyanate (THEIC) and its derivatives, as well as cyclodextrin derivatives. [73][74][75][76] THEIC is a triol containing a triazine-trione structure, where the triazine ring serves as a fundamental moiety that promotes char formation and is commonly employed in the construction of IFR systems. Additionally, its alkyl hydroxyl structure is similar to that of PER, suggesting inherently high charring efficiency. An IFR system composed of THEIC and APP at a loading of 30 wt.% can achieve a LOI of approximately 35% in PP, indicating a higher flame-retardant efficiency compared to the PER derivatives. However, a critical drawback of THEIC is its high water solubility. When 30 wt.% APP/THEIC is incorporated into PP, both the LOI and the flame-retardant rating of the composite significantly decrease with prolonged water immersion. After 96 hours of water treatment, the LOI of the 30IFR/PP composite decreases from 34.8% to 26.9%, and it fails to achieve any rating in the UL-94 vertical burning test. [73] Therefore, the same research team performed an intramolecular dehydration reaction on THEIC to obtain a crosslinked THEIC derivative. Due to the reduction of hydroxyl groups, the flame-retardant efficiency slightly decreased, particularly reflected in a lower LOI value. However, the water resistance of the derivative is expected to have improved significantly. [74] Additionally, the monomer 2-carboxyethyl (phenyl) phosphinic acid has been co-condensed with THEIC via dehydration to produce a phosphorus-containing THEIC derivative, PN-HBP. When combined with APP, this IFR system exhibits excellent charring and flame-retardant performance, achieving an LOI of 30% at a total loading of only 20 wt.%. This enhanced performance is likely attributed to the synergistic charring effect between THEIC and APP,

combined with the gas-phase flame-retardant action of the phosphine benzene structure. [75] Moreover, it is important to note that for polyol-based CFA derivatives, having more hydroxyl groups does not signify better performance, since cyclodextrin provides a good example. When β-CD is combined with APP, it exhibits almost no effective intumescent char-forming flame-retardant behavior. However, when some of the hydroxyl groups on cyclodextrin undergo an addition reaction with diisocyanatos to form crosslinked cyclodextrin molecules, the resulting chemical combined with APP exhibits excellent synergistic char-forming flame-retardant efficiency. This reaction introduces N-H groups, which function similarly to O-H groups and can also participate in dehydration reactions with the acid source to promote charring. [76]

In summary, polyols and their derivatives represent a class of highly efficient carbonization agents. However, most of these compounds are small molecules, and their long-term stability, particularly regarding water resistance and migration resistance, remains a concern. Among them, PEPA-based and THEIC-based derivatives, in which the hydroxyl groups have been partially or fully reacted, exhibit both high flame-retardant efficiency and improved stability, indicating promising application potential. Notably, some compounds such as PEPA and TRIMER have already been commercialized as flame retardants.

b) Triazine derivatives CFA

Among the various carbonization agents currently used for flame-retardant modification of PP, triazine-based CFAs exhibit the highest efficiency and have been the most extensively studied and applied. Several triazine-based products have already been commercialized. The triazine ring is a six-membered heterocycle containing three nitrogen atoms, with the molecular formula $C_3N_3H_3$ and exists in three isomeric forms. Due to its excellent chemical and thermal stability, the triazine structure is highly suitable for use in flame-retardant systems. Moreover, the tertiary nitrogen atoms in the ring enhance char formation, and the high nitrogen content can serve as a gas source during combustion, contributing to the intumescent mechanism. As a result, triazine derivatives are widely employed in the synthesis of CFA molecules. [77] Among the various triazine isomers, the 1,3,5-triazine structure is the most commonly used in CFA design. Representative compounds containing this structure include cyanuric chloride, melamine, and cyanuric acid. Of these, cyanuric chloride is the most frequently used precursor for synthesizing triazine-based derivatives, as it contains three reactive C-Cl groups that can undergo stepwise substitution reactions at different temperatures. These substitutions typically occur with nucleophilic O-H or N-H groups via a dehydrochlorination mechanism.

Based on their chemical structures, triazine-based CFAs can be classified into linear and non-linear molecules.

I Linear triazine derivatives CFAs

In the design and synthesis of linear triazine-based CFAs, the typical approach involves first substituting the first chlorine atom on cyanuric chloride at a low temperature (0-5 ℃) by using a small molecule, such as an amino alcohol. This yields a triazine compound with two remaining reactive C-Cl groups. The resulting difunctional compound is then reacted with diverse diamines to form linear macromolecular triazine-based CFAs. The synthesis route is displayed in Fig. 1.4. Numerous research groups have developed a series of linear CFAs by introducing various aliphatic amine backbones and side substituents into the molecular structure.

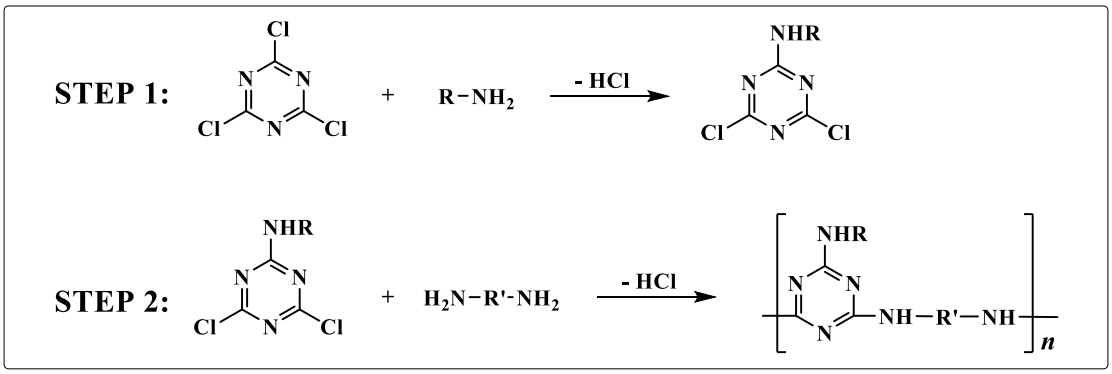

Fig. 1.4 The general preparation route for linear triazine-derivative CFAs.

Table 1.2 summarizes the linear triazine-based CFAs developed in recent years, along with their flame-retardant performance in intumescent flame-retardant PP systems. Based on the fundamental synthetic strategy described above, a variety of CFAs with different structures can be obtained by employing different reactive monomers. In the first step, the most commonly used end-capping agents are amine-based micro molecules, including the smallest ammonia [78], as well as organic aliphatic amines, [79][80][81][82][83][84] such as methylamine, methanolamine, ethylamine, ethanolamine, aniline, and so on. In addition, the PER-derived compound PEPA is also a suitable candidate due to its mono-hydroxyl structure. [89][90] Recent advances have also introduced aromatic compounds as end-capping agents, such as Schiff bases containing phenolic hydroxyl groups. [95] In the second step, concerning the design of the main chain backbone, aliphatic diamines are the most frequently used monomers, among which ethylenediamine [80][81][82][83][85][86][87] and piperazine [90][91][92][93][94][95] are the most widely employed. A review of the results and formulations in Table 1.2 reveals that this class of CFA molecules is most frequently combined

with ammonium polyphosphate. The resulting IFR systems demonstrate higher efficiency compared to those based on most polyols and their derivatives. In most cases, linear triazine-based IFR systems can enable PP to achieve a UL-94 V-0 rating at a loading level of only 20-25 wt.%. The primary flame-retardant mechanism of IFR systems based on triazine CFAs is similar to that of PER-based systems, in which the acid source (APP) decomposes upon heating and reacts with the carbon source to promote dehydration and charring. However, one key difference lies in the presence of the nitrogen-rich triazine ring within the CFA structures. Upon heating, triazine units can release non-flammable gases such as nitrogen and ammonia. Moreover, under acid catalysis, they facilitate the formation of carbonaceous layers with a higher degree of aromaticity, resulting in a stronger and thermally stable char barrier, thereby providing enhanced flame retardancy to the PP matrix.

Table 1.2 The structures, formulations and flame retardancy for linear triazine-derivative CFAs

CFA	Chemical Structures	IFR Formulation (Weight ratio)	IFR [a] (wt.%)	LOI	PHRR Red. [b]
CA [78]	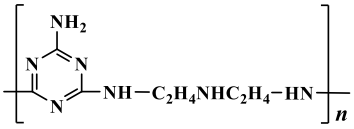	11APP:4CA	30	31.2%	/
TBM [79]	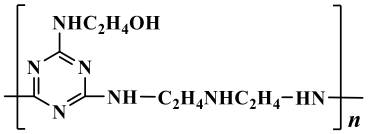	2MPP/1TBM	25	31.0%	77.1%
CFA [80]	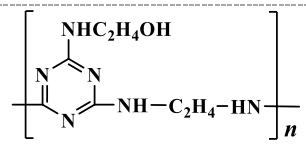	16APP/8CFA/1Zeolite 4A	25	37.0%	/
PETAT [81]	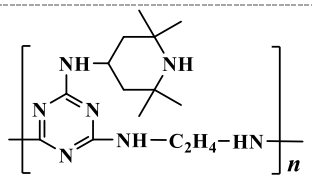	16.6APP/8.4PETAT	25	30.3%	72.9%
MTEC [82]	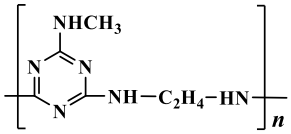	76APP/19MTEC/5SiO_2	22	29.6%	94.3%
CNCD-DA [83]	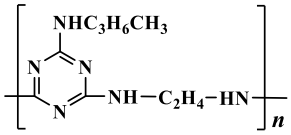	3APP:1CNCD-DA	25	/	86.7%
			30	36.5%	/
CNCO-HA [84]		4APP:1CNCO-HA	25	34.3%	81.5%

	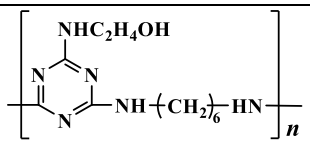		30	40.2%	/
CNCA-DA [85]	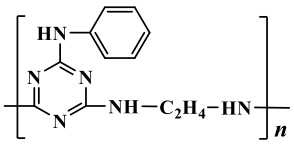	2APP:1CNCO-HA	20	27.1%	81.2%
			30	35.6%	/
PTCA [86]	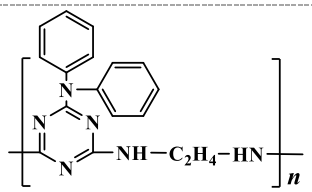	2APP/1PTCA	20	31.5%	90%
Si-MCA [87]	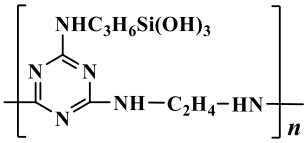	18.7APP/6.3Si-MCA	25	33.5%	79.9%
M*n*-CFA [88]	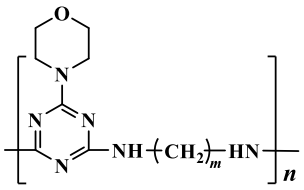	16APP/8Mn-CFA/1SiO_2	25%	31.9% (*m*=2) 35.5% (*m*=4) 34.3% (*m*=6)	/
PEPADC [89]	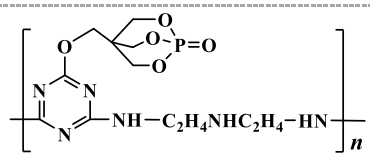	4APP/1PEPADC	30	35.5%	70.1%
PEPAPC [90]	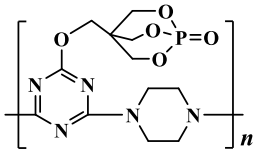	3APP/1PEPAPC	20	28%	81.3%
ETPC [91]	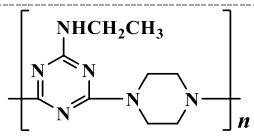	76APP/19ETPC/5SiO_2	24	34.1%	92.3%
TTPC [92]	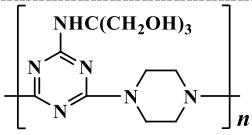	16APP/4TTPC/1ZB	21	29.6	85.1%
CFA-1 [93]	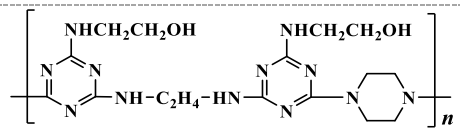	76APP/19CFA-1/5Zeolite 4A	22	38.2%	/

CFA-2 [93]	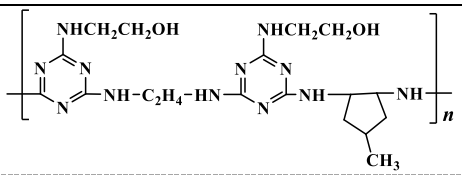	76APP/19CFA-2/5Zeolite 4A	22	35.2%	/
ETDPCs [94]	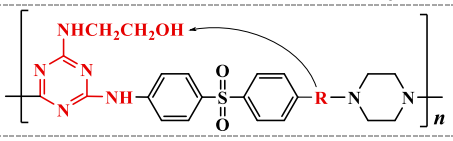	10APP/5MPP/5ETDPCs	20	30.4%	81.8%
S-CFA [95]	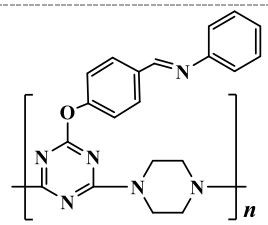	4APP/1S-CFA	24	28.9%	61.1%
HAPN [96]	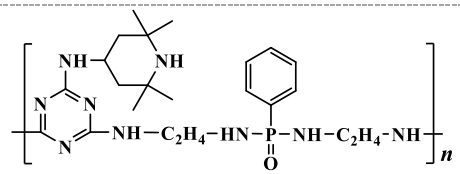	1APP:1HAPN	25	29.5%	72.1%

[a] All formulations listed in the table enable PP with **UL 94 V-0 rating** (3.2 mm).
[b] PHHR reduction percentage of FR-PP compared to pure PP.

In addition to the contribution of the triazine structure to char-forming ability, the end-capping structure on the side chain and the type of diamine moiety on the main chain have a more significant impact on the char-promotion behavior of CFA with other ingredients, since they are the primary groups involved in synergistic dehydration and char-forming reaction. At the same time, other properties of CFA, such as water resistance and thermal stability, are also closely related to these basic structures. For example, when the main chain consists of triazine and diethylenetriamine units, the TBM molecule with ethanolamine side groups exhibits higher flame-retardant performance than the CA molecule with amino side groups. To achieve a UL-94 V-0 rating and comparable LOI, the IFR system based on TBM requires a lower additive loading. [78][79] Furthermore, when the diethylenetriamine units in the TBM backbone are replaced with ethylenediamine, the resulting CFA, when combined with APP and zeolite as a synergist, enables the IFR system to reach an LOI of 37% at a total loading of 25 wt.%. [80] While the contribution of the synergist cannot be ignored, it generally enhances the LOI by less than 3%. Therefore, it can be inferred that the ethylenediamine structure contributes to higher flame-retardant efficiency. This also explains why ethylenediamine is commonly used in the construction of triazine-based CFAs. Based on this core structure, a series of linear triazine-ethylenediamine CFAs with various side groups have been developed. For instance, the PTCA molecule containing an N-phenylamine group enables its IFR system to achieve an LOI of 31.5% in PP at a loading of only 20 wt.%, while the PHRR value decreases by 90% compared to neat

PP, which is attributed to the aromatic structure to some extent, which is able to promotes the formation of graphitized carbon and improves the quality of the char layer to some extent. [86] However, different aromatic structures exhibit varying flame-retardant efficiencies. For instance, N-phenylaniline demonstrates greater effectiveness than aniline. A linear molecule containing a triazine/ethylenediamine backbone and an aniline side group, when also combined with APP in a 2:1 ratio to form an IFR system, achieves a LOI of 27.1% in PP at a loading of 20 wt.%, which is apparently lower than that achieved by the PTCA-based system. [85] In addition to ethylenediamine, other commonly used linear diamine structures for designing CFA include butanediamine, hexamethylenediamine, and diethylenetriamine. Studies have shown that when the morpholine structure is introduced as a side chain, the type of diamine used in the main chain can significantly influence the efficiency of linear triazine-based CFAs. CFA compounds derived from butanediamine and hexamethylenediamine exhibit superior performance in combination with APP, as demonstrated by higher limiting LOI values and significantly greater expansion ratios of the char layer. [88]

In addition to linear diamine molecules such as ethylenediamine, another commonly used building block for constructing the main chain backbone is the cyclic molecule piperazine. When alternately linked with triazine units, it forms a linear structure that also represents a typical class of CFAs. [90][91][92][95] his type of char-forming agent also exhibits excellent flame-retardant efficiency. When combined with APP to form an IFR system, the required loading to achieve a UL 94 V-0 rating in vertical burning tests typically falls within the range of 20-25 wt.%. For example, an IFR system based on the ETPC molecule with an ethylamino side chain achieved an LOI value of 34.1%, UL 94 V-0 rating, and a 92.3% reduction in PHRR at a loading of 24 wt.% under the catalytic effect of silica as a synergist. [91] However, the type of side chain also has a significant impact on the performance of linear triazine/piperazine-based CFA molecules. For instance, the S-CFA molecule featuring an aromatic Schiff base side chain exhibits excellent thermal stability, with a 1% weight-loss decomposition temperature of 328 °C and a maximum decomposition rate temperature approaching 500 °C. This level of thermal resistance ranks among the highest reported for CFA molecules to date and fully meets the processing requirements of engineering plastics and even some high-performance engineering plastics, indicating promising application potential. However, when blended with APP for use in PP, its flame-retardant efficiency is inferior to that of the aforementioned ETPC-based system. This reduced efficiency may be attributed to the excessively high decomposition temperature of S-CFA, which could delay the release of active species during combustion. [95] In addition, as previously discussed, polyols and their derivatives are considered promising

CFA candidates due to their inherent char-forming capability. Consequently, these structures are frequently introduced as side chains in triazine derivatives, such as PEPA and silanol-containing moieties. [87][89][90] The char-forming efficiency of these triazine- and amine-containing molecules is significantly higher than that of polyols alone, highlighting the synergistic advantage of integrating nitrogen-rich heterocycles with polyhydroxy structures.

In addition to employing single amine types, multiple amines can also be jointly utilized to construct the linear backbone of CFA molecules with triazine units. [93][94][96] This strategy is often adopted to balance synthesis cost and enhance charring efficiency. For example, a CFA molecule composed of a triazine/piperazine/ethylenediamine backbone, when combined with APP and Zeolite 4A as an IFR system, achieved an impressive LOI value of 38.2% at only 22 wt.% loading, placing it among the top-performing IFR systems reported to date. Based on the same design principle, replacing piperazine with 1,2-diamino-4-methylcyclopentane in the reaction led to a significant decrease in flame-retardant efficiency. [93] This further confirms the critical role of the piperazine structure in enhancing CFA performance. Additionally, the introduction of sulfur-containing 4,4'-diaminodiphenylsulfone into the triazine/piperazine framework resulted in the formation of ETDPCs. The presence of aromatic structures promoted the development of a highly graphitized char layer. The corresponding IFR system, formulated with APP and MPP, reached an LOI value of 30.4% and achieved UL-94 V-0 rating at only 20 wt.% loading, along with an 81.8% reduction in PHRR. [94] All the aforementioned CFA structures are phosphorus-free. However, efforts have also been made to incorporate phosphamide units into the CFA backbone, such as in the case of HAPN. Comparative studies revealed that HAPN exhibited flame-retardant performance on par with that of PETAT. Notably, the nitroxyl radicals generated by HAPN could efficiently inhibit or even extinguish flame propagation in the gas phase by quenching active combustion free radicals. [96]

In addition to char-forming flame-retardant efficiency, the water resistance of CFAs is also a critical factor in ensuring their long-term service stability. This is particularly important for most practical applications of flame-retardant polypropylene composites, which are typically required to pass the “85/85” standard test. Under this protocol, the materials must demonstrate excellent anti-migration performance when exposed to 85% relative humidity at 85 °C over an extended period. [97] Among the aforementioned CFA molecules, the ETPC-based material exhibited a water contact angle of 107°, indicating good hydrophobicity. Furthermore, polypropylene composites incorporating ETPC maintained nearly the same LOI value and retained their UL 94 vertical burning rating even after being treated in water at 70 °C for 168 hours. Interestingly, when the ethylamine side group in ETPC was replaced by ethanolamine,

the resulting CFA exhibited a water contact angle of 0°, indicating superhydrophilicity. [91] This comparison clearly demonstrates that hydroxyl groups exert a much stronger influence on hydrophilicity than imine groups. As a result, the TTPC molecule, which contains hydroxyl-rich side chains, also shows poor water resistance. [92] However, the TBM-based system with ethanolamine side chains unexpectedly exhibits good water resistance, which may be attributed to the presence of bulkier organic amine segments in the main chain. [79] If the side chains contain a high density of imine groups and the diamine segments in the main chain are relatively short, the resulting CFA molecule may still exhibit poor water resistance, even in the absence of hydroxyl groups. [81]

In summary, linear triazine-based charring agents represent the most extensively studied class of CFA structures, exhibiting excellent char-forming efficiency. Among them, ammonium polyphosphate is the most commonly employed synergistic acid source. The most representative and efficient backbone structures are triazine/piperazine and triazine/ethylenediamine frameworks. As for the side chains, optimal performance is typically achieved with ethylamine, ethanolamine, or methanolamine groups. For applications requiring water resistance, it is preferable to avoid side chains containing abundant hydroxyl groups. Nevertheless, even when hydroxyl groups are present, the overall water solubility of these linear macromolecules remains relatively low due to their triazine-based structures and polymeric nature. Compared to conventional small-molecule polyols, these triazine-derived CFAs still offer a significant advantage in water resistance.

II Non-Linear triazine derivatives CFA

As displayed in Table 1.3, in the case of non-linear triazine-based charring agents, the triazine units are primarily derived from cyanuric chloride, followed by melamine and triglycidyl isocyanurate, all of which are trifunctional monomers. [98][99][100][101][102][103][104][105] When these monomers react with monofunctional chemicals, they form small-molecule CFAs. [99] In contrast, reactions with multifunctional reactants lead to the formation of branched, high-molecular-weight CFA structures. [98][101][102][103][104][105][106][107] It is also feasible to obtain small-molecule CFAs from reactions between triazine monomers and multifunctional reactants by precisely controlling the feed ratio. [98][100] Unlike the preparation of linear triazine derivatives, the synthesis of non-linear triazine CFAs typically does not require an end-capping step. As a result, they are often synthesized via a one-pot method with simultaneous addition of reactants, offering a relatively simple and efficient preparation route.

Table 1.3 The structures, formulations and flame retardancy for non-linear triazine CFAs

CFA	Chemical Structures	IFR Formulation (Weight ratio)	IFR [a] (wt.%)	LOI	PHRR Red. [b]
PT [98]	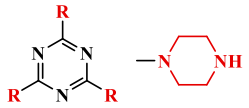	22APP/3PT	25	33.3%	/
		20APP/5PT	25	34.1%	73.4%
ST-DOPO [99]	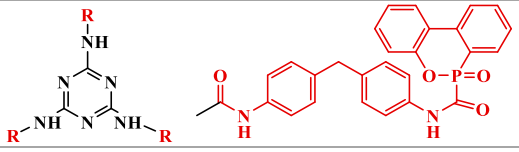	2ST-DOPO/1APP	30	35.0%	81.2%
PT-CA [100]	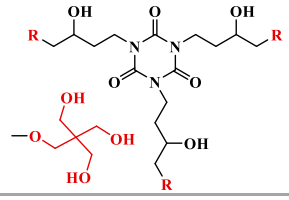	3APP/1MP/1PT-CA	30	31.5%	/
PT-Cluster [98]	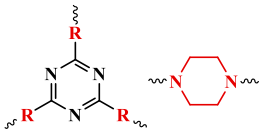	22APP/3PT-Cluster	25	32.7%	/
		20APP/5PT-Cluster	25	33.9%	80.5%
EA [101]	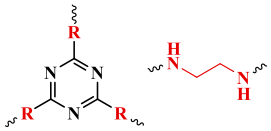	21.25APP/3.75EA	25	29.3%	71.3%
		17.5APP/7.5EA	25	32.3%	84.9%
BTETP [102]	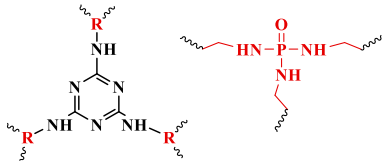	2APP/1BTETP	25	32.3%	83.0%
			20	31.6%	/
HPCFA [103]	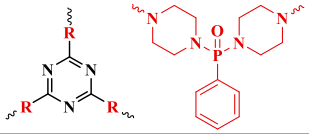	2APP/1HPCFA	20	31.0%	86.2%
PCAT [104]	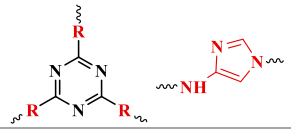	3PAPP/1PCAT	20	30.2%	84.7%
HCFA [105]	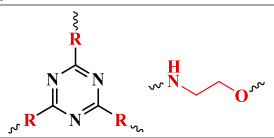	3APP/1HCFA	30	33.0%	76.6%
HBPPDA [106]	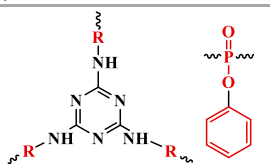	3APP/1HBPPDA	25	30.6%	76.1%
HBPU [107]	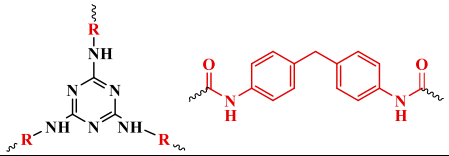	2APP/1HBPU	30	31.5%	81.1%

[a] All formulations listed in the table enable PP with **UL 94 V-0 rating** (3.2 mm).
[b] PHHR reduction percentage of FR-PP compared to pure PP.

In triazine-centered reactions based on cyanuric chloride, the primary co-reactants include piperazine and its derivatives, ethylenediamine and its derivatives, ethanolamine, and 3-amino-1,2,4-triazole. Among these options, CFA structures derived from piperazine and ethylenediamine exhibit the highest flame-retardant efficiency. For example, a system composed of only 3 wt.% of a small-molecule triazine-piperazine derivative (PT) and 22 wt.% of APP successfully imparted a UL 94 V-0 rating to polypropylene and achieved a LOI exceeding 33%. It has also been found that the ratio of triazine to piperazine, as well as the molecular aggregation state, can significantly influence CFA efficiency. When a macromolecular triazine-piperazine derivative, PT-Cluster, was used with APP, the resulting polypropylene composite exhibited a slightly lower LOI but provided a more pronounced suppression of PHRR. [98] Another example is the HPCFA compound, which is synthesized through the reaction between cyanuric chloride and phenyl di(piperazin-1-yl) phosphine oxide. The IFR system constructed with HPCFA achieved an LOI of 31.0% and a reduction in PHRR of 84.7% at a total loading of 20 wt.%. [103] This performance exceeds that of the APP/PT system. However, it is important to note that the CFA content in the APP/PT system is significantly lower than in the APP/HPCFA formulation. In industrial applications, IFR systems with lower CFA content are generally more desirable due to the relatively high production cost of CFA chemicals. Furthermore, another compound that can be used to construct non-linear triazine structures is melamine. While melamine alone typically serves as a gas source in conventional IFR systems, it can form effective CFA molecules when chemically bonded with organic amine segments. For instance, the amino groups on melamine can undergo addition reactions with isocyanate groups to yield polyurethane-based structures, such as ST-DOPO and HBPU. [99][107] Additionally, melamine can react with diphosphoryl chloride compounds via a hydrogen chloride elimination mechanism, resulting in crosslinked and branched CFA molecules such as HBPPDA. [106] The char-forming efficiency of these molecules strongly depends on the char-forming performance of the co-reactive monomers. IFR systems incorporating these CFAs generally require a total loading of 25 to 30 wt.% to achieve effective flame retardancy, which is lower in efficiency compared to the CFA structures derived from cyanuric chloride and organic amines. Moreover, the epoxy groups on triglycidyl isocyanurate can undergo ring-opening addition reactions with the hydroxyl groups of PER at elevated temperatures. This reaction yields polyol derivatives containing triazine structures, such as PT-CA. However, IFR systems incorporating such compounds typically require a high loading of around 30 wt.% to achieve effective flame retardancy, indicating relatively modest efficiency. [100]

In summary, among non-linear triazine-derived CFAs, those synthesized from cyanuric chloride and organic amines generally exhibit higher flame-retardant efficiency. However, a potential issue arises during the formation of branched or crosslinked structures. As the reaction progresses, increasing steric hindrance and the declining solubility of intermediates in the solvent may hinder complete substitution of the chlorine atoms. As a result, residual chlorine may remain in the final CFA product. This poses a risk for applications requiring halogen-free certification.

c) Other amine derivatives CFA

A summary of the triazine-derived compounds discussed above reveals that one of the most prominent structural features is the combination of triazine with organic amine groups. Organic amines play a critical role in initiating intumescent flame-retardant behavior through their interaction with acid sources. This highlights the potential of organic amines as key building blocks for synthesizing CFA molecules via reactions with other functional groups in addition to triazine-based chemicals. After reviewing literature, it is concluded that the representative amine is piperazine, as shown in Table 1.4. [108][109][110][111][112] A common strategy involves combining piperazine with phosphorus-containing structures to synthesize molecules such as piperazine pyrophosphate. However, the phosphorus content in such molecules is typically insufficient to induce an efficient intumescent flame-retardant effect on its own. As a result, these compounds still require blending with an additional acid source to construct a complete IFR system, and thus, they can also be classified as CFAs. Specifically, piperazine reacts with various phosphate groups to form a series of piperazine phosphate CFAs. [108][109][110][111] It also undergoes dehydrochlorination with hexachlorocyclotriphosphazene or phenylphosphinyl dichloride to produce macromolecular piperazine-based CFA structures. [112][113] Due to the presence of a certain proportion of acidic groups in these molecules, the overall amount of additional acid sources such as APP or MPP required in the formulation is generally reduced. Overall, the efficiency of these piperazine-derived compounds has been further improved, with most corresponding IFR systems achieving effective flame retardancy at around 20 wt.% loading. In addition to their chemical composition, another likely contributing factor, particularly for phosphorus-containing piperazine derivatives, is that these integrated acid and carbon source molecules promote intramolecular synergistic charring reactions. This type of charring response is likely faster and more effective than the intermolecular char-forming behavior observed in conventional systems.

Table 1.4 The structures, formulations and flame retardancy for amine CFAs

CFA	Chemical structures	IFR Formulation (Weight ratio)	IFR [a] (wt.%)	LOI	PHRR Red. [b]
PPAP [108]	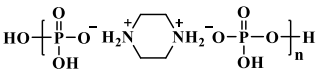	7.5APP/4PPAP/1MCA	20	33.6%	72.0%
PPAP [109]	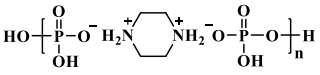	2PPAP/1MPP	20	29.5%	/
ATPIP [110]	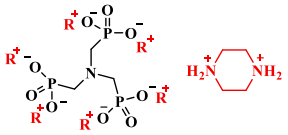	3APP/1ATPIP	25	30.0%	77.9%
HP-Mn [111]	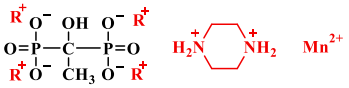	1APP/1HP-Mn	25	30.7%	74.2%
CPCFA [112]	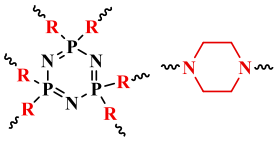	2APP/1CPCFA	30	37.5%	88.8%
BPOPA [113]	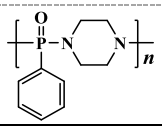	3APP/1BPOPA	30	36.0%	/

[a] All formulations listed in the table enable PP with **UL 94 V-0 rating** (3.2 mm).
[b] PHHR reduction percentage of FR-PP compared to pure PP.

d) Polymer plastic -type CFA

Based on the structural characteristics of highly efficient CFAs containing organic amine groups, it was inferred that some certain polymers containing amine functionalities also hold potential to serve as CFAs. Some studies have confirmed the effectiveness of thermoplastic polyurethane (TPU) [114][115][116] and polyamide (PA) [117][118][119][120][121][122][123][124][125] as carbon sources in IFR systems, as shown in Fig. 1.5. Firstly, TPU/APP combinations are capable of generating an effective intumescent flame-retardant effect. [114] The flame retardancy of PP/TPU/APP composites is influenced by the characteristics of TPU, particularly the type of polyol and the hard segment content. A higher hard segment content tends to enhance flame retardancy, which may be attributed to the increased amine group concentration associated with the hard segments, facilitating dehydration and crosslinking reactions in the presence of acid sources. However, the char-forming efficiency of TPU is relatively low, and its IFR system with APP may require a loading of up to 40 wt.% to achieve excellent flame retardant performance. Therefore, it can also be combined with conventional CFAs to optimize charring behavior while improving overall

material properties. For example, TPU-encapsulated PER can form a core–shell structured CFA, and the resulting IFR system shows improved flame retardancy, water resistance, migration resistance, and compatibility compared to traditional PER-based systems. [115]

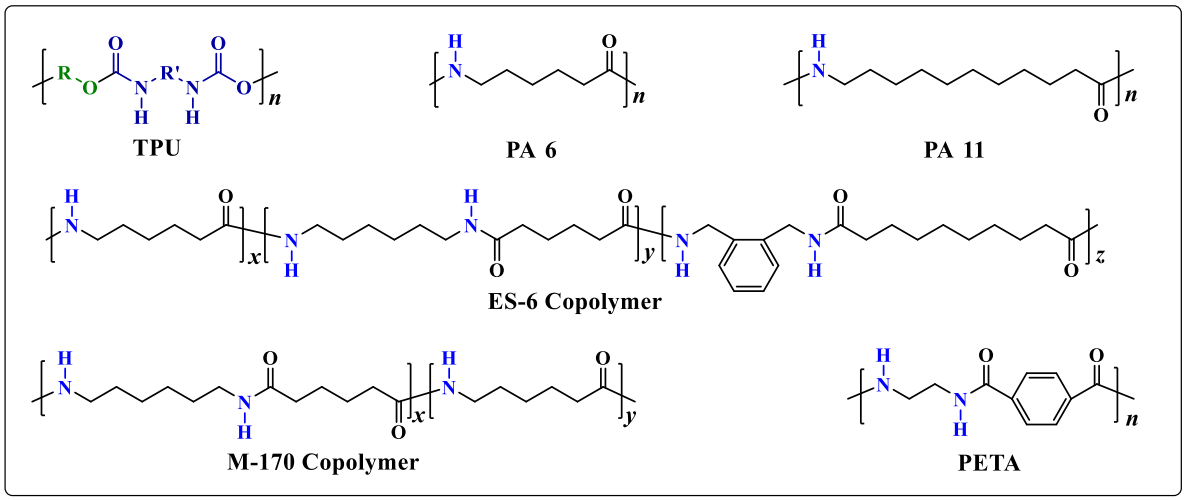

Fig. 1.5 Chemical structures of representative polymer plastic type CFAs.

Among polymeric polyamides, PA 6 and PA 11 are the most typical representatives. [117][118][119][120] When used individually as char-forming agents, their charring efficiency is relatively low. Compared to PA 6, PA 11 possesses a lower melting point and longer alkyl chains in its molecular structure, which contributes to improved compatibility with PP. And IFR systems incorporating PA 11 and PER as composite charring agents demonstrate superior char-forming performance compared to those based solely on PER. [118] When PA6 is used as a char-forming agent, the incorporation of a compatibilizer, such as carboxylated polypropylene, can effectively improve its compatibility with PP. A formulation consisting of PA6, APP, and MEL at a ratio of 10:10:5 exhibits optimal expansion ratio and char yield. However, this system suffers from severe melt dripping. The introduction of nanoclay, such as montmorillonite, can overcome this drawback. [121] In addition, PA6-based copolyamide char-forming agents can significantly improve the poor dispersion and compatibility of PA6 in PP matrices, such as the copolyamide molecules ES-6 and M-170. As low-melting-point polyamides, these materials also reduce processing temperatures and effectively suppress side reactions, particularly the degradation of APP. The composite char-forming agent system comprising these copolyamides and DPER demonstrates superior flame retardancy and mechanical properties compared to systems using only DPER or those containing PA6. However, a notable drawback remains the relatively high total IFR loading required in such systems. [122] To enhance the char-forming performance of such polyamide molecules, an effective strategy involves synthesizing high-molecular-weight linear polyamides through

polycondensation reactions between highly efficient diamine and dicarboxylic acid monomers. A typical example is the PETA molecule, synthesized from ethylenediamine and terephthalic acid. The IFR system based on PETA achieves a reduced effective loading level of approximately 25 wt.% in PP, with significantly improved flame-retardant efficiency compared to PA6 and PA11. [123][124][125]

Overall, polymer-based char-forming agents represented by TPU and PA exhibit various limitations in terms of efficiency and compatibility. However, inspired by these structures, future research could focus on designing novel CFA molecules through the incorporation of diverse monomer units, aiming to develop flame-retardant PP composites with superior comprehensive properties. Moreover, the inherent char-forming potential of TPU and PA in IFR systems may also inspire high-value recycling strategies and molecular redesign of these materials, aligning with the goals of green and sustainable development.

1.3.2.2 Monomolecular IFR systems

Intumescent flame retardants with a single-molecule design integrate the essential components including carbon source, acid source, and gas source into one molecular structure. This approach effectively avoids problems such as uneven distribution that are common in traditional multi-component systems. Compared to conventional flame retardants where char formation relies on intermolecular reactions, these single-molecule systems undergo faster reactions at elevated temperatures. As a result, they produce a dense and stable char layer. [126] Therefore, they have become a major focus of recent research. In general, these single-molecule flame retardants can be classified into two types. The first type involves molecular design and chemical bonding of fundamental structural units to form an IFR molecule. The typical structures are presented in Fig. 1.6. The second type is based on surface modification / particle bonding techniques which impart excellent synergistic charring ability to components that originally lack or have only weakly efficient charring features. A typical example is the surface modification of ammonium polyphosphate.

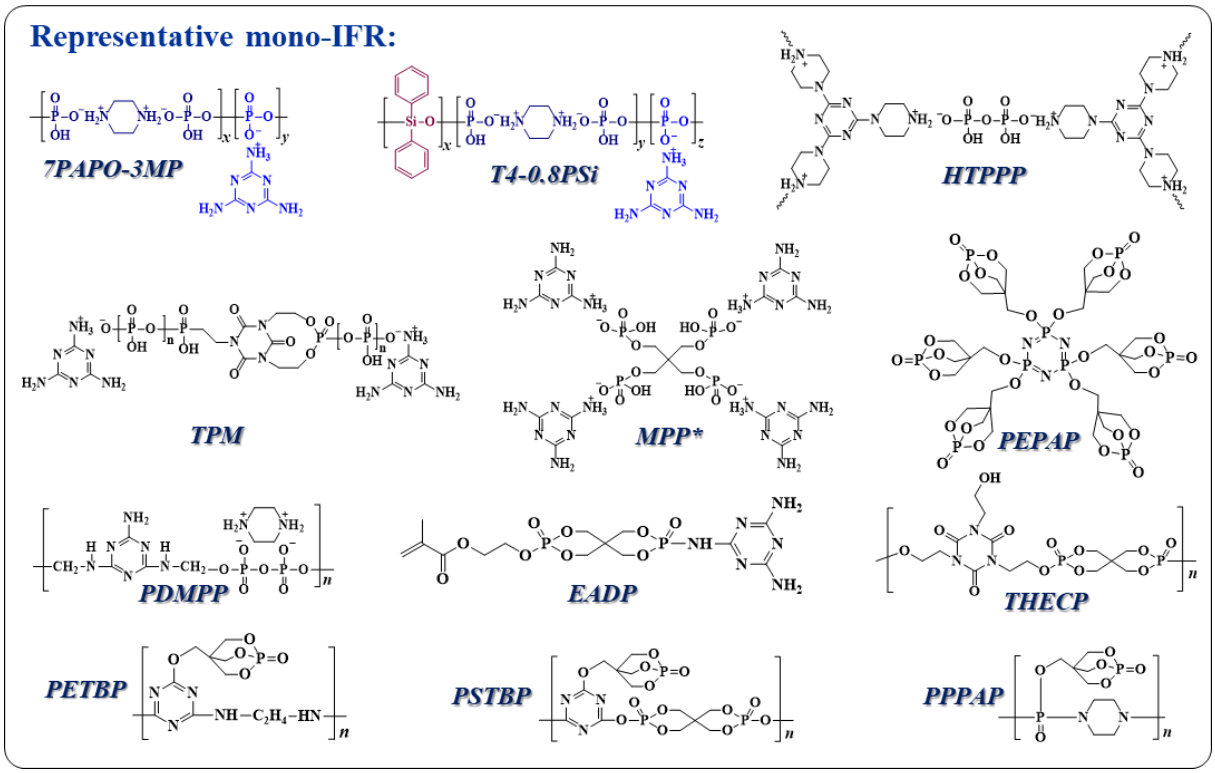

Fig. 1.6 Representative mono-IFR structures developed recently.

Firstly, Fig. 1.6 presents the structures of typical monomolecular IFR. It can be observed that their fundamental structural units are actually similar to those found in the previously discussed multi-component intumescent flame retardant systems, mainly including phosphoric acid groups [127][128][129][130][131][132], organic amines [127][128][129][132][135][137], polyols [131], melamine [127][128][130][131][132], triazine rings [129][134][135][136], pentaerythritol phosphate esters [135][136][137][138], and cyclo-triphosphinyl group [138]. Among them, certain copolymers of piperazine phosphate salts exhibit particularly outstanding flame-retardant performance, requiring addition levels of only around 20 wt.%, as shown in Table 1.5. It is worth noting that the copolymerization strategy disrupts the regularity of molecular arrangement, resulting in materials with toughening characteristics, in contrast to traditional systems which generally lack a softening point. [127][128] Certainly, when the types and proportions of basic chemical units are similar, single-molecule IFRs generally exhibit superior efficiency or faster action compared to blended systems. However, if the ratio of functional groups leads to an imbalance among acid, carbon, and gas sources, the resulting molecular efficiency will also be suboptimal. For example, the molecule PPPAP only achieves a UL 94 V-0 rating at a high loading of 40 wt.%, which is most likely due to an imbalance of functional components. [138] It is highly probable that its efficiency would be significantly improved when combined with APP. Similarly, THECP has also been shown to exhibit lower

efficiency as a single-molecule intumescent flame retardant compared to its performance in an IFR system when blended with APP. [134] Therefore, for single-molecule IFR, the type and proportion of basic groups in their molecular structure are crucial. In addition to the essential acid, carbon, and gas sources, the incorporation of certain metal ions and siloxane structures can also significantly enhance flame retardant efficiency. [126][127][128]

Table 1.5 The structures, formulations and flame retardancy for monomolecular IFR systems

Mono-IFR	IFR [a] (wt.%)	LOI	PHRR Red. [b]	Residue
7PAPO-3MP [127]	20	28.1%	81.2%	8.3%
T4-0.8PSi [128]	20	30.2%	85.1%	22.5%
HTPPP [129]	25	30.5%	93.7%	61.2%
TPM [130]	20	29.3%	76.6%	15.7%
MPP* [131]	20	30.9%	82.3%	21.0%
PDMPP [132]	23	26.7%	92.5%	12.6%
EADP [133]	25	31.5%	/	/
THECP [134]	20	29.3%	/	/
PETBP [135]	25	29.5%	71.0%	21.8%
PSTBP [136]	25	29.5%	/	/
PPPAP [137]	40	29.0%	79.8%	32.8%
PEPAP [138]	25	29.4%	52.9%	/

[a] All formulations listed in the table enable PP with **UL 94 V-0 rating** (3.2 mm).
[b] PHHR reduction percentage of FR-PP compared to pure PP.

In addition, particle micro-aggregation technology has emerged in recent years as an effective strategy for developing high-performance IFR systems. Specifically, at the macroscopic particle scale, different components are chemically bonded through reactive monomers such as tetramethyl tetravinyl cyclotetrasiloxane and TAIC. [139][140][141] On one hand, these micro-aggregated particles facilitate rapid interactions among components, while the bonding monomer structures contribute additional functionalities such as hydrophobicity. Moreover, they provide synergistic catalytic effects for char formation, further enhancing flame retardant efficiency.

Ammonium polyphosphate is a molecule that integrates acid and gas sources. However, due to the lack of a carbon source, it cannot generate an effective intumescent char-forming effect on its own. Therefore, surface coating and ion-exchange modification of APP to introduce carbon sources have proven to be effective approaches for constructing integrated

acid, gas, and carbon source systems. Initially, coating APP with polysiloxane and melamine-formaldehyde resin can moderately improve its char-forming ability and water resistance. Nevertheless, the flame-retardant efficiency remains insufficient, and additional char-forming agents are still required to achieve optimal performance. [142][143] Some studies have reported the use of silane coupling agents and hyperbranched polyesters for reactive crosslinking [144], as well as the crosslinking of 4,4'-diphenylmethane diisocyanate with melamine and dipentaerythritol [145], to construct crosslinked shell layers on the surface of APP, respectively. The resulting modified APPs can impart UL 94 V-0 flame retardancy to PP materials at a loading level of 20 wt.%. The modified APP with a crosslinked shell layer formed by hexamethylene diisocyanate and cyclodextrin enables PP to achieve a UL 94 V-0 rating at a loading level of 23 wt.%, which is superior to its corresponding physical blending system. [76][146]. Another modification approach involves introducing a carbon source by performing an ion exchange between organic amines and the ammonium ions in APP, thereby constructing a single-molecule IFR system. Commonly used organic amine monomers include piperazine [147], diethanolamine [148], ethylenediamine [149], and allylamine [150][151]. For example, the resulting piperazine polyphosphate achieves a UL 94 V-0 rating at a loading of 22 wt.% with a LOI of 31.2%, whereas 30 wt.% of unmodified APP only yields an LOI of 20.4% without attaining any UL 94 rating. [147] It is important to note that for modified APP obtained through either surface coating or ion exchange methods, improper selection of reactive units may lead to reduced thermal stability, which deserves to be aware in future research.

1.3.2.3 Synergists for IFR systems

Synergists in IFR systems play a crucial role in enhancing the flame retardancy. Their core mechanisms mainly involve catalyzing and promoting char formation, improving the structural integrity and intensity of the char layer, thus suppressing the release of toxic smoke and heat. [152] These synergists accelerate the dehydration of carbon sources within the intumescent system, facilitate the decomposition and cross-linking reactions of phosphates, and enable rapid char layer formation at lower temperatures, effectively preventing further release of heat and flammable gases. Currently, extensively studied synergists include metal oxides such as zinc oxide [153], magnesium oxide [154], lanthanum oxide [155], and cerium oxide [156][157]; metal salts and hydroxides like aluminum hydroxide [158], aluminum hypophosphite [159][160], aluminum phosphate [161], nickel cobaltate [162], nickel phosphate [163], and strontium carbonate [164]; as well as organic inorganic hybrid materials such as multi-walled carbon nanotubes coated with silica [165] and silica-modified Mexene [166]. These metal

components catalyze the dehydration of carbon sources through Lewis acid sites and promote the cross-linking and charring of phosphate intermediates, resulting in a dense heat-insulating char layer. Layered double hydroxides, due to their tunable metal composition, thermal stability, and slow-release properties, demonstrate excellent catalytic char formation and smoke suppression capabilities. [167][168] In recent years, silicon and boron based synergists including silicon dioxide [82][91], polysilsesquioxane [109][169], sepiolite [170], vermiculite [171], 4A zeolite [80][93][172], montmorillonite [173], silicone filled halloysite nanotubes [174], and zinc borate [92][175] have attracted attention. These materials not only improve the thermal stability of the char but also induce ceramic formation on the char surface, further enhancing fire resistance. The latest research trends focus on developing multifunctional synergists that integrate catalytic charring, smoke suppression, anti-dripping, and heat resistance functions within a single additive. Carbon nanomaterials such as nano carbon black [176], as well as metal organic frameworks [177][178], have been widely explored. These materials not only provide more efficient catalytic charring but also improve mechanical properties and thermal stability. Further, the dosage of synergists in IFR systems is critical; excessive amounts often compromise the original intumescent flame retardant performance. [179] In summary, catalytic IFR synergists are advancing toward higher efficiency, natural origin, and multifunctional integration, driving further development of intumescent flame retardant PP for high performance, low toxicity, and environmentally friendly applications.

1.4 Bio-based flame retardants

In recent years, the development of bio-based flame retardants for polypropylene still primarily focused on IFR systems or their individual components. The main biomass sources can be classified into three categories: phytic acid, biomass molecules containing amino groups, and biomass molecules containing hydroxyl groups, as exhibited in Fig. 1.7. Among them, phytic acid serves as a suitable alternative to conventional polyphosphate acid sources. Amino group-containing biomass molecules can provide the function of carbon or gas sources, while hydroxyl group-containing biomass molecules mainly act as carbon sources. [180]

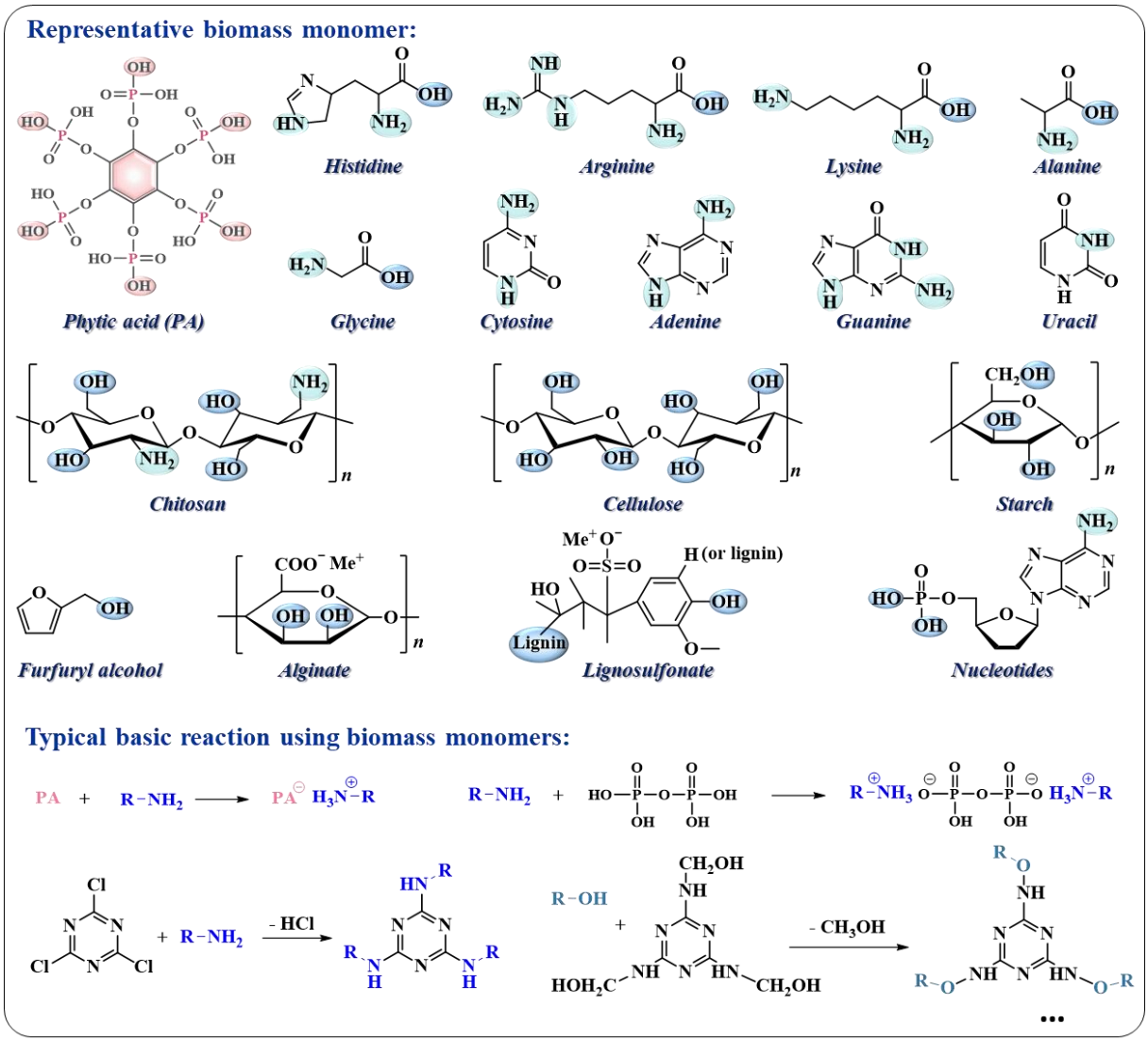

Fig. 1.7 Classic biomass monomers and reaction for flame retardants of PP.

Representatively, phytic acid can react with organic amines to produce phytate derivatives, with typical reactants including piperazine [181], melamine [182][183], biomass amino acids [184], and so on. Additionally, metal ions can be introduced to provide catalytic charring effects. [182] Specifically, a single-molecule IFR obtained from the reaction of phytic acid and piperazine at a molar ratio of 1:3 enables polypropylene to achieve a UL 94 V-0 rating at a loading of 20 wt.%. However, due to an unbalanced gas source content, the LOI is only 25.5%. [181] In another study, hyperbranched polyamide-amine-based molecules were synthesized from phytic acid and organic amines. With a mere 15 wt.% loading, the LOI of PP reached 30%, with a UL 94 V-0 rating, and the PHRR decreased by 83.8% compared to pure PP, while the mechanical properties were largely retained. [185] Moreover, phytic acid-melamine salts were used to modify layered double hydroxides for constructing single-molecule IFR system or to be combined with traditional IFR to enhance flame retardancy. [182][183] However, if

the amine structure is not properly selected in phytic acid-based IFR systems, the flame-retardant efficiency tends to be moderate. [184]

Regarding biomass-derived amine sources, they can be used to design char-forming agents. For instance, glycine and cytosine can react with cyanuric chloride to form small-molecule CFAs. [186][187] However, IFR systems constructed with these molecules generally exhibit relatively low efficiency and often require the addition of other carbon sources or synergists to achieve satisfactory flame retardancy. Cytosine can also react with pyrophosphate to produce a pyrophosphate salt that integrates both carbon and acid sources. An IFR system combining this compound with PER achieves UL 94 V-0 rating and a LOI of 30.0% at a total loading of 20 wt.%. [188] Alanine has been used as a side group in linear triazine/ethylenediamine-based CFA structures, where the resulting IFR system requires an additive loading of around 24 wt.% to achieve effective flame retardancy. [189] Besides, protein fiber also shows potential as CFA, exhibiting IFR characteristics when treated with phosphoric acid. [190] In addition to serving as a carbon source, some of these biomass-derived structures, like adenine, guanine, cytosine, and uracil, are capable of acting as gas sources to modulate IFR efficiency. [191] In addition, the amine group enables chitosan to be ion-exchanged with APP to obtain biomass-modified APP-based flame retardants, but with average efficiency. [192]

The main biomass sources containing hydroxyl groups include furfuryl alcohol [193], cellulose [194], starch [195], alginate [196], lignosulfonate [197][198][199], and nucleotides [200]. For instance, hydroxyethyl cellulose can undergo dehydration condensation with phosphoric acid and subsequently react with MEL to form a single-molecule IFR, which enables PP to achieve a UL 94 V-0 rating at a loading of 30 wt.%. [194] Starch was used in similar molecular designs but typically exhibits lower flame-retardant efficiency and thus needs to be combined with expandable graphite to achieve satisfactory performance. [195] Alginate and lignosulfonate are often used to modify layered double hydroxides, thereby improving their flame-retardant properties. [196][197][198][199] Specifically, sodium alginate-modified LDH enables PP to reach UL 94 V-0 classification at 30 wt.% loading. [196] Lignosulfonate-modified LDH, after being further coated with chitosan and metal phytate, achieves an LOI of 31.6% and UL 94 V-0 rating at 20 wt.% loading in PP. [197]Additionally, nucleotide structures can be chemically grafted into the melamine-formaldehyde resin network, and the resulting bio-based molecules can serve as effective synergists in APP/PER IFR systems. [200]

1.5. Other phosphorus-based flame retardants

Apart from intumescent flame retardants, some other phosphorus-based flame retardants are also candidates for flame-retarding PP. Red phosphorus is the simplest phosphorus flame retardant in terms of chemical structure. It can be used alone in PP materials, and at a loading of 10 wt.%, it enables glass fiber-reinforced PP to achieve a UL 94 V-0 rating and a LOI of 23.1%. [201] Red phosphorus is also commonly used in combination with expandable graphite to create a synergistic effect. [202] However, due to its tendency to oxidize and absorb moisture, most red phosphorus-based formulations use microencapsulated or coated red phosphorus, either on their own or blended with other flame retardants. For example, microencapsulated red phosphorus combined with magnesium hydroxide and zinc borate has been used for flame-retardant modification of PP. [203] Mechanistic studies indicate that adding microencapsulated red phosphorus enhanced thermal stability of PP. In addition, synergistic effects are observed when microencapsulated red phosphorus is combined with magnesium hydroxide or aluminum trihydrate. [204] During combustion, the metal hydroxides release water vapor, while red phosphorus decomposes between 400 and 500 ℃ to generate white phosphorus, leading to form a phosphoric acid coating on the surface of the material, providing a condensed-phase flame retardant effect.

Phosphate esters represent the largest category of phosphorus flame retardants by production volume. Traditional phosphates such as triphenyl phosphate can be used to flame retard PP. [205] For example, blending triphenyl phosphate with aluminum hypophosphite has been employed for flame-retardant modification of PP and wood flour composites. In this system, triphenyl phosphate primarily functions in the gas phase, while aluminum hypophosphite acts in the condensed phase, resulting in good flame retardancy. However, conventional phosphate esters generally have low molecular weight, which makes them susceptible to moisture absorption and migration. Furthermore, many phosphate esters are liquids, which leads to high smoke emissions and volatilization during processing, limiting their practical application. As a result, grafting phosphate ester group onto the side chain of polyolefin is an effective strategy to improve anti-migration properties and maintain long-term stability. [206] It is also important to note that phosphate esters often produce a plasticizing effect in polymers, which is considered when selecting flame retardants for PP.

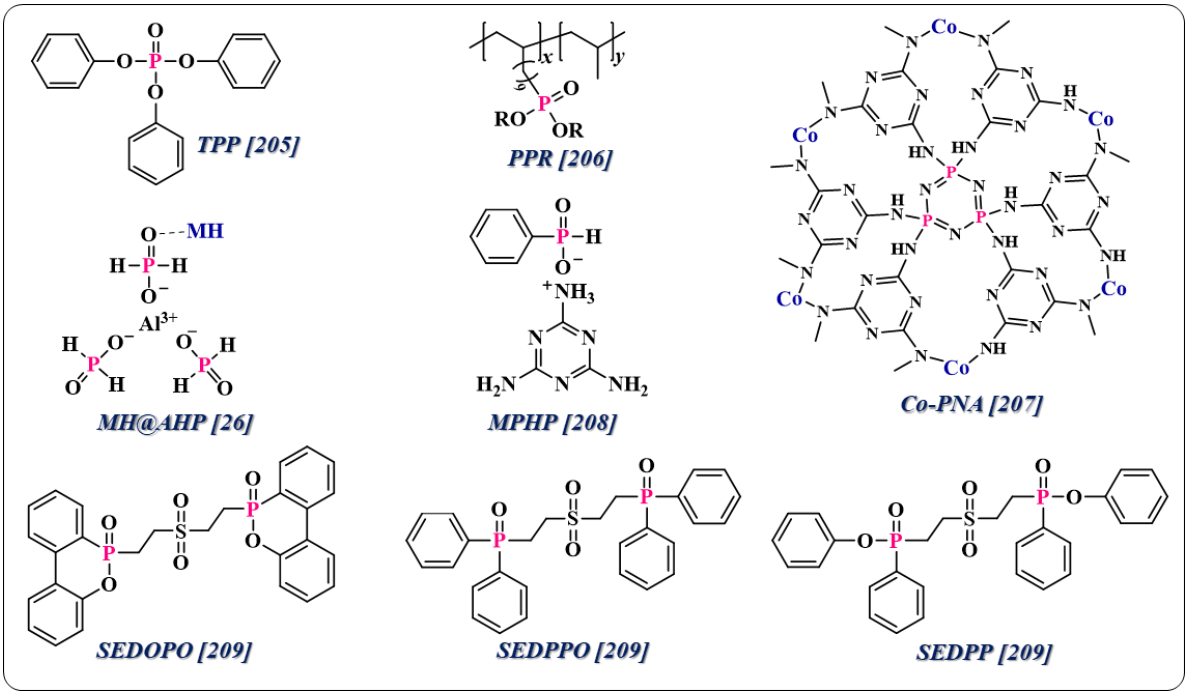

Fig. 1.8 The chemical structures of other phosphorus FRs.

As displayed in Fig. 1.8, polyphosphazenes, hypophosphite salts and phosphine derivatives due to their favorable gas-phase quenching effects, can also be used as flame retardants for PP. However, they are often combined with metal ions, hydroxides, silica, and other components to achieve enhanced flame-retardant efficiency. [26][207][208][209] For example, a hybrid structure formed by hexachlorocyclotriphosphazene, melamine, and cobalt ions enabled PP to achieve a UL 94 V-0 rating at a low loading of approximately 15.3 wt.%, with a LOI of 26.7%. [207]

In general, most of these flame retardants exhibit lower efficiency than IFR systems, especially in reducing peak heat release rate and achieving high LOI values. Nevertheless, IFRs have a significant drawback in that they can severely compromise the physical and mechanical properties of PP. Therefore, these phosphorus-containing flame retardant systems have been explored for applications where only moderate flame retardant performance is needed or where specific functional properties are required.

1.6 Inorganic flame retardants

Among inorganic flame retardants, magnesium hydroxide, aluminum hydroxide, and layered double hydroxides are the most widely used types. Structurally, these flame retardants are rich in hydroxyl groups, which release water vapor upon thermal decomposition and form protective layers of magnesium oxide or aluminum oxide. The released water vapor reduces the ambient temperature and dilutes flammable gases and oxygen, while the generated oxides

serve as physical barriers to inhibit combustion. [210] However, their main drawback is the requirement of high loading levels, generally exceeding 50 wt.% to achieve satisfactory flame retardancy. [211] This high loading often leads to a significant deterioration of mechanical properties; thus, they are commonly used in combination with other flame retardants or modified via surface treatments, microencapsulation, or nanotechnology to improve performance.

Magnesium hydroxide can be combined with clay minerals such as montmorillonite to enhance the efficiency. [212] When ATH and ammonium polyphosphate are used at 10 wt.% and 20 wt.% respectively, the PHRR and THR of the PP composites are reduced by 50% and 32% compared to neat PP. Additionally, ATH helps to reduce the smoke release commonly associated with APP. [213] Notably, the combination of ATH and MH demonstrates better flame-retardant performance than either alone. This synergistic effect is attributed to the higher heat absorption and lower decomposition temperature of ATH, approximately 140°C lower than that of MH, enabling a broader temperature range (235°C to 455°C) for endothermic reactions, thus more effectively inhibiting combustion. Therefore, several systems utilize combined MH, ATH, and zinc borate for the flame retardancy of PP. [214] LDHs typically show better flame-retardant efficiency than MH and ATH. Commercial LDHs usually involve carbonate-intercalated Mg-Al LDH (LDH-C). Studies have reported that phosphoric anion-intercalated LDH-P requires only 20 wt.% to achieve a UL 94 V-0 rating in PP, whereas LDH-C needs 30 wt.%. The LOI of LDH-P/PP composites is also higher than that of LDH-C/PP composites, attributed to the phosphorus groups in LDH-P enhancing char strength through crosslinking reactions during combustion. [215]

Surface modification nano structuring are key development directions for inorganic flame retardants. [216] For instance, La^{3+} surface modification of MH has been shown to increase the LOI of PP composites by 4.6% at only 0.2 wt.% La^{3+} loading. [217] Surface grafting of MH with poly(trimethylolpropane ester) yields hydrophobic MH particles that can raise the LOI of PP to 29.3% at 30 wt.% loading. [218] Additionally, surface treatments with titanate and zinc stearate can improve MH dispersion in the PP matrix, leading to better overall flame-retardant performance. [219] Besides, the strategy of preparing nano rod-like MH particles shows better dispersion and significantly enhances the thermal stability of PP composites, suggesting promising potential applications. [220] However, due to cost considerations, industrial applications of nano-metal hydroxides in PP remain limited, with most commercial products still relying on cost-effective options such as natural hydromagnesite. With increasingly stringent environmental regulations, the production capacity of mineral-ground

hydromagnesite is declining, while chemically synthesized hydroxides, especially those derived from waste brine from salt industries, are emerging as attractive alternatives. [26][221]

In conclusion, although magnesium-aluminum-based flame retardants generally exhibit moderate flame-retardant efficiency, they are widely studied in PP applications. Their excellent smoke suppression ability, potential to reduce material costs when used as fillers, and environmentally friendly characteristics ensure continued research and application prospects.

1.7 Summary

Based on the above review, it is evident that current efficient flame-retardant modification strategies for polypropylene mainly focus on halogen-free intumescent flame retardant systems, inorganic flame retardants, and nano-composite flame retardant systems. Among them, IFRs are particularly favored due to their environmental friendliness, low smoke emission, and low toxicity. However, they often suffer from poor dispersion and a detrimental impact on mechanical properties. The design and construction of efficient flame retardant groups in IFR is the key to achieving higher comprehensive performance. Nanomaterials, such as graphene, montmorillonite, and layered double hydroxides, exhibit promising potential in enhancing both flame-retardant efficiency and overall performance. Through synergistic effects, they enable excellent flame retardancy even at low loading levels. Looking ahead, the flame-retardant modification of polypropylene is expected to evolve towards high efficiency, environmental sustainability, low additive content, and improved mechanical performance. Key future research directions will include the development of green and sustainable flame retardants, the construction of multi-scale synergistic flame-retardant systems, and an in-depth understanding of flame-retardant mechanisms. Additionally, by leveraging interfacial regulation, surface modification, and intelligent functional design, it is anticipated that a balanced enhancement of flame retardancy, mechanical properties, processability, and multifunctionality can be achieved, thereby promoting the application of flame-retardant polypropylene in high-end fields.

1.8 Objectives

Based on the progress above, it was concluded that the development of highly efficient intumescent flame-retardant systems remains an effective strategy for producing polypropylene materials with enhanced fire safety performance. In particular, the selection of functional groups and the structural design of intumescent flame retardants are crucial factors in achieving high char-forming efficiency.

This dissertation aims to develop a series of novel intumescent flame retardant systems to systematically enhance the flame retardancy, mechanical performance, and multifunctional

properties of polypropylene composites. By employing molecular-level structural design and regulation, the research seeks to overcome common limitations of traditional flame retardants, such as high loading levels, deteriorated mechanical properties, and limited flame-retardant efficiency, thereby promoting the development of high-performance, application-oriented flame-retardant polypropylene materials. The specific objectives are as follows:

(1) To design and synthesize highly efficient nitrogen/silicon (N/Si)-based macromolecular charring agents with controlled molecular aggregation, achieving superior condensed-phase flame-retardant effects through synergistic interaction with phosphorus-based acid and gas sources, thus enhancing the overall fire safety of PP composites.

(2) To develop covalently bonded flame-retardant copolymers to address the dispersion and compatibility issues of physically blended IFR systems, achieving simultaneous improvements in flame retardancy and mechanical properties, including enhanced interfacial adhesion and processability of PP composites.

(3) To construct an aluminum-based intumescent flame retardant system through metal-ion coordination strategies, improving char stability and gas-phase inhibition at low additive loadings, and to further achieve integrated optimization of flame retardancy, smoke suppression, and thermal conductivity by introducing thermally conductive fillers.

Through a combination of “controlled aggregation,” “covalent grafting,” and “metal coordination” strategies, this dissertation systematically investigates the design of highly efficient, environmentally friendly, and multifunctional flame-retardant PP composites, providing innovative solutions for high-safety and multifunctional application scenarios.

CHAPTER 2

Materials and Characterization

2.1 Materials

All chemicals and materials utilized in this work included base polymers, processing aids, commercially flame retardants and functional fillers for the development of intumescent flame-retardant systems, as well as molecular precursors, solvents, and catalysts for the synthesis of novel flame-retardant compounds.

2.1.1 Base Polymers and Additives

The polypropylene (PP) employed throughout the formulations was a homopolymer grade (T30S) supplied by Zhong An United Coal Chemical Co., Ltd. A compatibilizer—polypropylene grafted with maleic anhydride (PP-g-MA, grafting ratio: 0.8%)—was sourced from Qingdao Sainuo Chemical Co., Ltd. Two types of antioxidants were incorporated: tris(2,4-di-tert-butylphenyl) phosphite (Antioxidant 168) and pentaerythritol tetrakis[3-(3,5-di-tert-butyl-4-hydroxyphenyl)propionate] (Antioxidant 1010), both obtained from Tokyo Chemical Industry Co., Ltd. Fig. 2.1 exhibits the specific structures for the base polymer and additives.

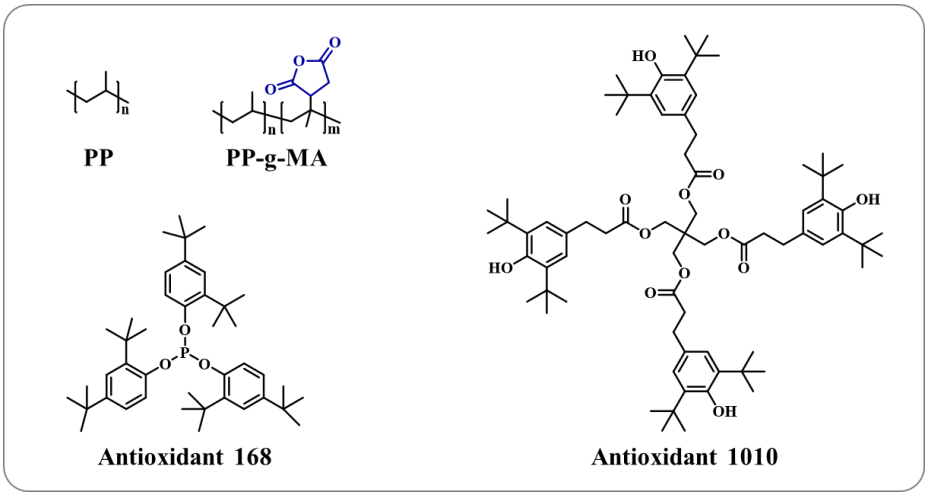

Fig. 2.1 The chemical structure of base polymers and additives in this thesis.

2.1.2 Flame retardants and functional additives

Ammonium polyphosphate (APP, FosFlam NH-1110CF) was provided by Guangzhou Addenda Chemical Co., Ltd., while melamine cyanurate (MCA) was obtained from Jinan Taixing Fine Chemical Co., Ltd. The anti-dripping agent, polytetrafluoroethylene (PTFE), was sourced from Daikin Fluorochemicals Co., Ltd. Melamine polyphosphate (MPP, particle size < 5 μm) was supplied by Shandong Weidong Chemical Co., Ltd. Nano-sized aluminum oxide

(Al_2O_3, PAT-G05A, 50 nm) was procured from Nanjing Paukert New Materials Co., Ltd., and boron nitride (BN, 50 nm) was purchased from Bisili New Materials Co., Ltd. Multi-walled carbon nanotubes (MWCNTs), with diameters of 10–20 nm and lengths ranging from 2–8 μm, were supplied by Shenzhen Guosen Pilot Technology Co., Ltd. Piperazine pyrophosphate (PPAP) was synthesized in-house following established procedures reported in the literature. [109] The chemical structures for main functional fillers are displayed in Fig. 2.2.

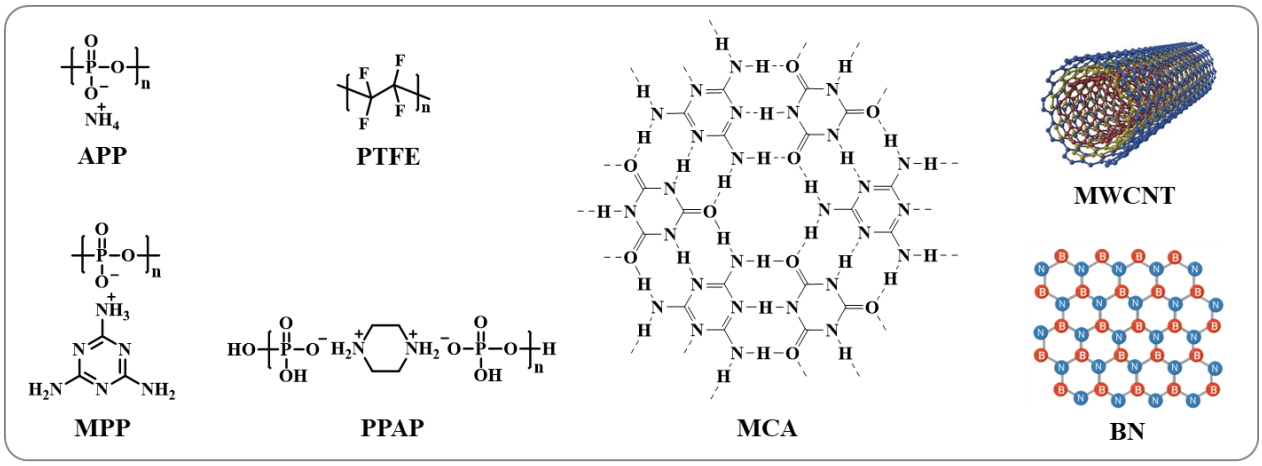

Fig. 2.2 The chemical structure of commercial functional additives in this thesis.

2.1.3 Chemicals for synthesis of novel flame retardants

The chemical precursors employed in this work included anhydrous piperazine (99%), sourced from Beijing Innochem Science & Technology Co., Ltd., and phenyl trichlorosilane (98%), purchased from Shanghai Aladdin Biochemical Technology Co., Ltd. High-purity melamine (> 99%, 20 μm) and cyanuric acid (> 99%) were obtained from Zhejiang Xusen Halogen-Free Smoke Suppression and Flame Retardant Co., Ltd. Aqueous phosphoric acid solution (85 wt.%) was acquired from Fuchen (Tianjin) Chemical Reagent Co., Ltd. Melamine phosphate (MP) was supplied by Shandong Brothers Technology Co., Ltd., while aluminum tris(dihydrogen phosphate) (AlDHP, 98%) was procured from Shanghai Macklin Biochemical Technology Co., Ltd. Piperazine phosphate (PAP) was synthesized in the laboratory following procedures adapted from previously published methods. [109] The structure of these chemicals are shown in Fig. 2.3.

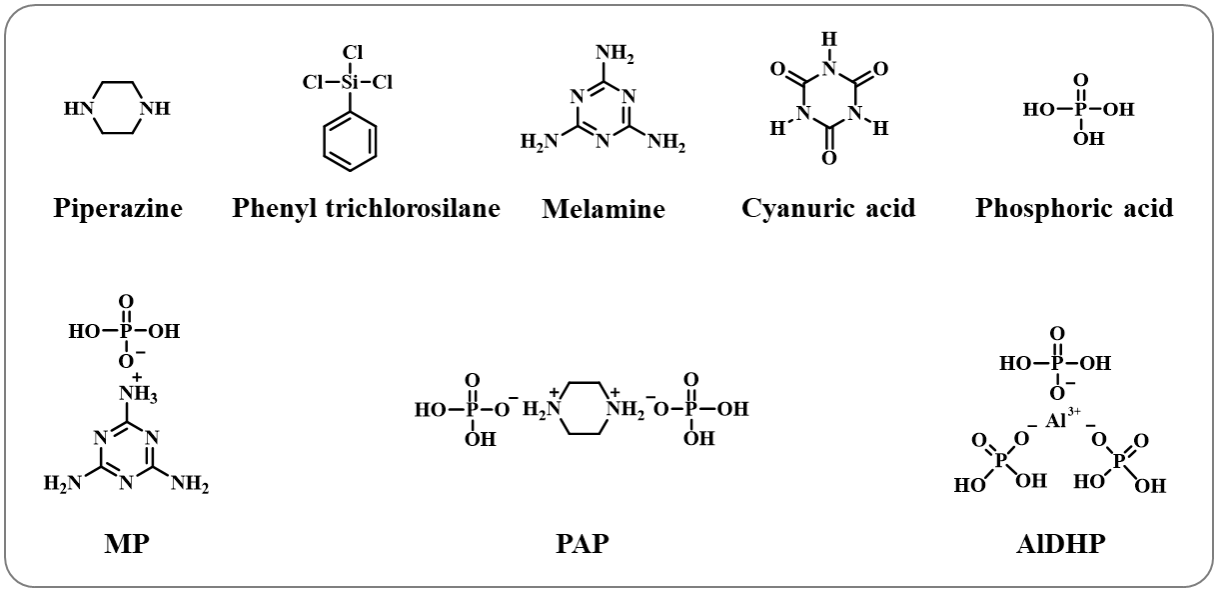

Fig. 2.3 The chemical structure of main precursors for synthesis in this thesis.

Dichloromethane (≥99.5%) and analytical-grade sodium hydroxide (NaOH) were obtained from Fuchen Chemical Reagent Co., Ltd. Prior to use, dichloromethane was thoroughly dried. Tetrabutylammonium (99%) was supplied by Beijing J&K Scientific Co., Ltd. Anhydrous ethanol (99%) was sourced from Fuchen (Tianjin) Chemical Reagent Co., Ltd. Unless stated otherwise, all water used throughout the experimental procedures was deionized and purified via a laboratory water purification system.

2.2 Characterization

2.2.1 Chemical Structure Characterization

The chemical structure of the synthesized materials was characterized using several advanced analytical techniques, including Fourier-transform infrared (FTIR) spectroscopy, solid-state nuclear magnetic resonance (solid-state NMR) spectroscopy, and X-ray diffraction (XRD).

Fourier-transform Infrared Spectroscopy: Structural information of the products and raw materials was obtained using an iN10MX-type FTIR spectrometer, which recorded spectra in the range of 4000-500 cm^{-1}. This technique helped identify the functional groups and analyze the chemical bonding and molecular interactions within the materials. The specific steps are as follows. First, the sample is mixed with anhydrous potassium bromide (KBr) powder at a specific ratio (typically 1:100) and then pressed into a transparent thin pellet using a press. Since KBr has good transparency in the infrared range, this pellet ensures that the sample's absorption characteristics in the infrared spectrum can be effectively measured. The resulting KBr pellet is then placed in the FTIR instrument for scanning, and the infrared absorption

spectrum of the sample is recorded. This method is widely used for chemical structure analysis of various solid samples, especially those that cannot be tested directly.

Solid-State Nuclear Magnetic Resonance (Solid-State NMR) Spectroscopy: The ^{29}Si, ^{13}C, ^{31}P, and ^{27}Al NMR spectra of synthesized molecules were acquired using a JNM-ECZ400R-type nuclear magnetic resonance spectrometer (JEOL Co., Ltd.) equipped with a 3.2 mm HX probe. These spectra provided detailed information about the chemical environments and the bonding characteristics.

X-ray Diffraction (XRD): The crystallinity and phase distribution of the samples were evaluated using an XRD-6000-type diffractometer. XRD patterns were collected with a scanning speed of 2.0°/min, covering the 2θ range of 5° to 60°. This technique provided information about crystalline and structural ordering, which is essential for understanding the physical properties of the materials.

2.2.2 Flame-Retardant Performance Evaluation

The flame retardant performance of the prepared samples was systematically assessed using several standard tests.

The glow wire ignition test simulates thermal stress caused by heated electrical components and assesses the material's resistance to ignition from a hot source. This test was conducted using a GPG-type apparatus (Wazau Co., Ltd.) in accordance with IEC 60695-2-12 and IEC 60695-2-13 standards to get glow-wire flammability index (GWFI) and glow-wire ignition temperature (GWIT). Test specimens measured 60.0 × 60.0 × 1.5 mm^3, with the glow wire penetrating the sample to a depth of 1.5 mm.

The limited oxygen index (LOI) measures the minimum concentration of oxygen required to sustain the combustion of a material in a controlled atmosphere, reflecting its flammability under oxygen-enriched conditions. LOI values were determined using a 300800-type instrument based on the ASTM D2863 standard, and the standard sample dimensions were 130.0 × 6.5 × 3.2 mm^3.

The UL-94 vertical burning test is widely used to classify the flame retardancy of plastic materials by observing dripping behavior, flame extinction time, and ignition of cotton beneath the specimen. This test was conducted using an FTT0802-type vertical combustion test chamber in accordance with ASTM D3801, with specimen dimensions of 130 × 13 × 3.2 mm^3. For each UL-94 vertical burning test, five specimens are required. The test involves a two-step ignition process. First, the bottom of the vertically clamped specimen is exposed to a flame for 10 seconds and then the flame is removed. The afterflame time (t_1) is recorded to determine

how long the specimen continues to burn. If the specimen self-extinguishes, a second 10-second ignition is applied, and the second afterflame time (t_2) is recorded. During the test, any dripping behavior is observed, particularly whether burning or non-burning droplets ignite the cotton positioned below the specimen, which is critical for determining the final UL-94 classification. The specific rating criteria are shown in table 2.1.

Table 2.1 The specific rating criteria of UL94 vertical burning test.

Criteria	V-0	V-1	V-2
Afterflame time after each flame application (s)	≤ 10	≤ 30	≤ 30
Total afterflame time (s) (10 flame applications)	≤ 50	≤ 250	≤ 250
Afterflame + afterglow time after 2nd ignition (s)	≤ 30	≤ 60	≤ 60
Dripping ignites cotton	No	No	Yes
Burn to clamp (complete specimen combustion)	No	No	No

The cone calorimeter test provides a comprehensive evaluation of fire safety by quantifying parameters such as heat release rate, total heat release, time to ignition, and smoke production. Cone calorimetry was carried out using an FTT cone calorimeter under a heat flux of 50 $kW \cdot m^{-2}$ according to the ISO 5660 standard. The specimens for this test were 100 × 100 × 3 mm^3 in size.

To assess the thermal insulation and barrier effect of the residual char formed during combustion, a T660-type thermal imager was used to record surface temperature profiles in real-time. This provides insight into the char layer's protective effectiveness and integrity. Samples used in this analysis had dimensions of 100.0 × 100.0 × 1.5 mm^3.

2.2.3 Mechanical Property Testing

The mechanical properties of the flame-retardant polypropylene composites were evaluated to investigate their structural integrity and applicability in practical scenarios.

The unnotched Charpy impact strength was tested to assess the material's resistance to sudden external force and crack initiation. Specimens with dimensions of 4.0 × 10.0 × 80.0 mm^3 were evaluated using an XJF-5 impact testing apparatus in accordance with the UNE EN ISO 179-1 standard. This test provides crucial information on the toughness and energy absorption capability of the composites under impact loading.

The tensile properties, including tensile strength, elongation at break, and Young's modulus, were measured to examine the composite's behavior under uniaxial stretching. The tests were conducted on a CMT6104-type electronic universal testing machine at a crosshead

speed of 10 mm/min, following the UNE EN ISO 527-1 standard. This characterization offers insight into the material's stiffness, ductility, and load-bearing capacity, which are essential for mechanical performance evaluation in engineering applications.

2.2.4 Thermal Conductivity Measurement

The thermal conductivity (κ, $W \cdot m^{-1} \cdot K^{-1}$) of the prepared polypropylene composite films was evaluated to investigate their heat transfer performance, which is a critical parameter for assessing the thermal insulation and fire resistance of flame-retardant materials. The thermal conductivity was calculated using the classical equation:

$$\kappa = \alpha \times C_p \times \rho$$

where α represents thermal diffusivity ($mm^2 \cdot s^{-1}$), C_p is the specific heat capacity ($J \cdot g^{-1} \cdot K^{-1}$), and ρ is the bulk density ($g \cdot cm^{-3}$) of the sample.

Thermal diffusivity measurements were performed at room temperature (25 °C) using a LFA 467 HyperFlash laser flash apparatus (Netzsch), which provides high-precision data and is particularly suitable for polymer-based thin films. The thickness and surface preparation of the specimens were carefully controlled to ensure test accuracy.

Specific heat capacity (C_p) was obtained through differential scanning calorimetry (DSC) using a PerkinElmer STA 6000 thermal analyzer. The measurements were conducted under a nitrogen atmosphere with a heating rate of 10 $°C \cdot min^{-1}$.

The density (ρ) of each sample was measured by the Archimedes method using an analytical balance, ensuring consistency across different formulations.

2.2.5 Thermal Behavior Analysis

The thermal stability and transition behavior of the materials were investigated by means of differential scanning calorimetry (DSC) and thermogravimetric analysis (TGA). These techniques are essential for understanding the thermal transitions, decomposition temperatures, and overall thermal robustness of flame-retardant systems.

DSC analysis was conducted using a PerkinElmer STA 6000 thermal analyzer in accordance with the UNE EN ISO 11357 standard. Approximately 10 ± 0.1 mg of each sample was weighed and sealed in an aluminum pan. The samples were heated from 20 °C to either 220 °C or 240 °C at a constant heating rate of 10 °C/min under a nitrogen flow of 20 mL/min to avoid oxidative degradation. The resulting DSC thermograms provided information on melting points, crystallization behavior, and possible thermal transitions related to the polymer matrix or flame-retardant additives.

The thermal decomposition behavior was evaluated by TGA using a PerkinElmer STA 8000 analyzer, following the UNE EN ISO 11358 standard. Samples were heated at a rate of 20 °C/min from room temperature to the degradation endpoint (typically above 800 °C), under a nitrogen atmosphere to simulate inert thermal degradation. The TGA curves allowed for determination of initial decomposition temperature, maximum decomposition rate temperatures, and residual char yields, which are important indicators of flame retardancy and thermal resistance.

Together, these thermal analyses provided a comprehensive evaluation of both the physical and chemical stability of the developed flame-retardant systems, offering critical insight into their suitability for fire-safe polymeric applications.

2.2.6 Morphological and Compositional Characterization

The morphology and elemental distribution of the gold-covered flame retardants, char layers, and fracture surfaces were thoroughly examined using scanning electron microscopy (SEM) coupled with energy dispersive X-ray spectroscopy (EDS). The analysis was conducted using a ProX facility at an operating voltage of 15 kV. SEM allows detailed visualization of the surface features, microstructure, and the formation of char layers after combustion. EDS provided additional insights into the elemental composition and distribution within the flame retardant systems, particularly identifying key elements such as phosphorus, nitrogen, and metals that are essential to the flame-retardant mechanism.

2.2.7 Condensed-Phase Flame-Retardant Mechanism Investigation

The chemical structures of the char residues obtained from the cone calorimeter tests were analyzed using X-ray photoelectron spectroscopy (XPS), utilizing a Thermo Fisher Scientific Escalab 250Xi equipped with Al Kα radiation (1486.68 eV). XPS provided detailed information on the elemental composition and chemical bonding states of the char, enabling an in-depth understanding of the surface characteristics and oxidation states of key elements present in the char layers.

Raman Spectroscopy was employed to investigate the molecular structure of the char residue. The Raman spectra were recorded using a HORIBA LabRAM Odyssey spectrometer with a 532 nm helium-neon laser as the excitation source. Raman analysis allowed for the detection of structural changes, such as the degree of graphitization or the presence of aromatic carbon structures, which are crucial in understanding the char's behavior under thermal stress.

Additionally, Fourier Transform Infrared Spectroscopy (FTIR) was used to further study the functional groups and bonding characteristics in the char residue. The FTIR spectra

provided valuable information about the presence of specific chemical groups, such as phosphates or hydroxyl groups, that play a role in the flame retardant mechanism and the char formation process during combustion.

These techniques, in combination, allowed for a comprehensive analysis of the char residue's chemical structure, which is essential in understanding the material's fire-retardant properties and the mechanisms of flame inhibition.

2.2.8 Gas-Phase Flame-Retardant Mechanism Investigation

The gas-phase products released during the thermal decomposition process were systematically analyzed to investigate the flame-retardant mechanisms. The pyrolysis fragments generated during thermogravimetric analysis (TGA) were captured and examined using a Frontier-type FTIR spectrometer. This setup provided valuable information on the chemical species and functional groups present in the gas phase, enabling a deeper understanding of the evolution of volatile compounds and their potential role in flame suppression.

To further investigate the gas-phase chemistry, thermal decomposition fragments from an EGA/PY-3030D-type pyrolysis apparatus were analyzed using a Clarus 680 gas chromatography system coupled with a Clarus SQ8T mass spectrometer (GC/MS). This combination of GC/MS allowed for the identification of specific volatile fragments released during the pyrolysis process. By detecting key gases such as hydrocarbons and phosphorus-based fragments, this technique helped elucidate the mechanisms by which these flame-retardant systems inhibit combustion in the gas phase.

Together, these techniques provided a comprehensive understanding of the gas-phase flame-retardant mechanisms, shedding light on how volatile fragments might interact with the combustion process to suppress flame propagation.

CHAPTER 3

Fabrication of Piperazine/Silane-Based Char-Forming Agent and Their Intumescent Flame Retardant Polypropylene

3.1 Introduction

Among the various components in IFR systems, the carbon source plays a pivotal role, and considerable efforts have been devoted to the design of novel charring molecules to improve intumescent efficiency. [101] Nitrogen-containing groups are commonly incorporated into the molecular structures of these char-forming agents. Representative examples include molecules based on piperazine/triazine [91][92], piperazine/triazine/ethylenediamine [93], piperazine/ethanolamine/triazine/diaminodiphenylsulfone [94], and triazine/p-phenylenediamine [222]. Compared to traditional polyol-based carbon sources, these nitrogen-rich molecules exhibit significantly enhanced charring ability and flame-retardant performance. Among them, piperazine-based moieties have demonstrated particularly strong charring effects in IFR/PP composites.

In parallel, the incorporation of silicon-containing units into charring agents or IFR systems has also proven effective for further improving flame retardancy. Notable examples include siloxanes [223][224], silsesquioxanes [225][226], and silicon dioxide [208], which have all contributed to more stable and protective char layers. Collectively, these findings suggest that combining nitrogen-containing piperazine structures with silicon-containing groups may synergistically enhance the charring performance in IFR/PP systems.

Intriguingly, our previous study [98] comparing two piperazine/triazine-based charring agents - PT (a small molecule) and PT-Cluster (a macromolecule with higher piperazine/triazine group density) - demonstrated that PT-Cluster outperformed PT in both charring efficiency and flame retardancy, despite having nearly identical chemical compositions. Similar observations have been reported for other systems, such as aggregated phosphaphenanthrene/siloxane [227][228] and phosphaphenanthrene/methylene [229] structures, which exhibited superior flame-retardant behavior compared to their monomeric counterparts. These studies underline the critical influence of molecular architecture, where even subtle variations - such as changes in the aggregation form of flame-retardant groups - can significantly enhance performance.

Building on these insights, this study designed a series of hydrogen-bonded macromolecular structures based on melamine cyanurate, incorporating nitrogen-rich

piperazine groups and phenyl-silicon units as core charring skeletons with tunable aggregation degrees. It is hypothesized that these charring cores, even in small quantities, could initiate a synergistic charring process with ammonium polyphosphate in PP. Furthermore, increasing the aggregation degree of the piperazine/phenyl-silicon structures is expected to further strengthen the intumescent charring and flame-retardant performance of the resulting IFR/PP composites.

3.2 Synthesis of macromolecules MNSi-n containing piperazine/silane skeletons

The specific preparation method of MNSi-n includes two steps. Firstly, the piperazine / silane skeletons NSi-n are synthesized by dehydrochlorination reaction between piperazine and phenyl trichlorosilane, as displayed in Fig. 3.1. Concretely, Anhydrous piperazine (38.80 g, 0.45 mol) was dissolved in 700 mL of dichloromethane at room temperature. Phenyl trichlorosilane (21.58 g, 0.10 mol) was then added dropwise to the piperazine solution while maintaining the temperature below 10 °C. The reaction mixture was subsequently stirred at 35 °C for 1 hour. After cooling the mixture to below 10 °C, tetrabutylammonium bromide (0.1 g) and an aqueous sodium hydroxide solution (5 wt.%, 100 g) were added slowly with continued stirring for 10 minutes. The resulting biphasic mixture was transferred to a separating funnel, and the lower aqueous layer was removed. The organic layer was then washed with 100 mL of water and separated again. This washing process was repeated three times to ensure complete removal of impurities. Finally, dichloromethane was removed by distillation under reduced pressure to obtain the product. For the synthesis of NSi-2 and NSi-3, the amounts of anhydrous piperazine used were 0.375 mol and 0.36 mol, respectively. All other reaction conditions and procedures remained the same as those used for NSi-1.

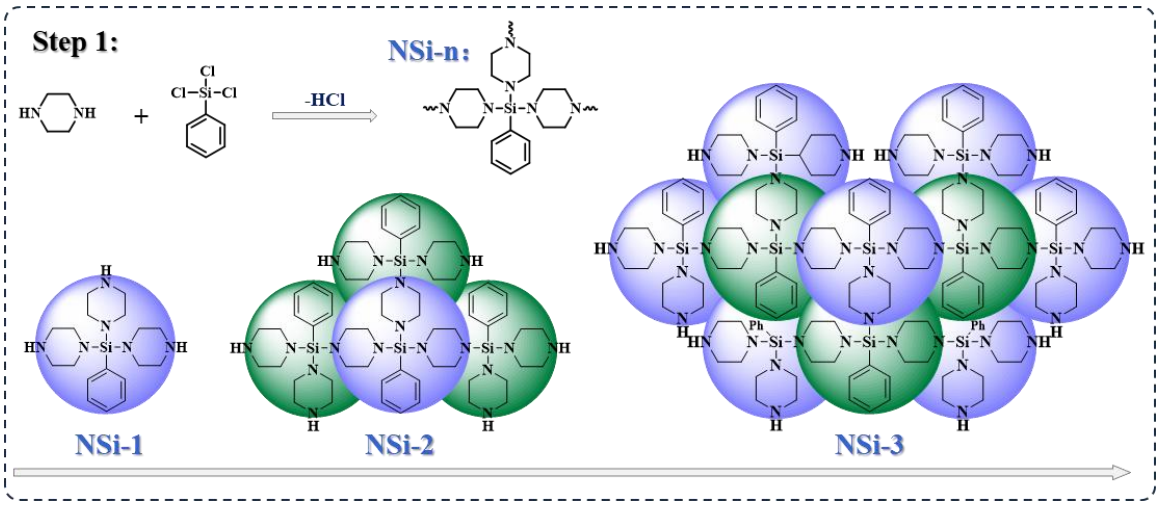

Fig. 3.1 The synthesis routes of intermediate NSi-n (n=1, 2, 3).

After that, the obtained NSi-n molecules are chemically bonded with melamine and cyanuric acid to obtain macromolecules MNSi-n through hydrogen bond self-assembly, as

exhibited in Fig. 3.2. Specifically, NSi-n (35.0 g) was dispersed in 500 mL of deionized water in a three-necked flask and stirred at 80 °C for 30 minutes. Subsequently, melamine (40.4 g) and cyanuric acid (112.7 g) were introduced into the mixture. The reaction was maintained at 90 °C for 1 hour under continuous stirring. After completion, the water was removed via vacuum distillation. The resulting solid was further dried at 150 °C to yield MNSi-n. The final product was ground to a particle size of less than 10 μm.

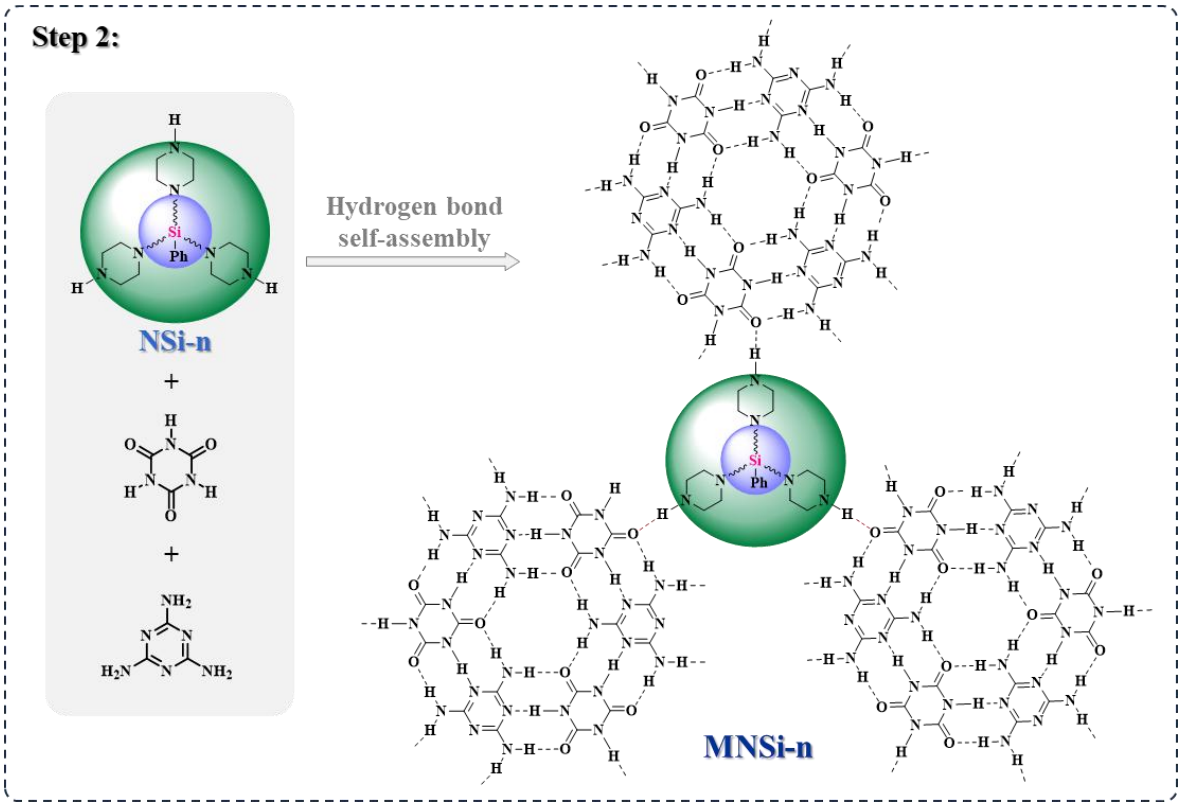

Fig. 3.2 The synthesis routes of macromolecules MNSi-n (n=1, 2, 3).

3.3 Construction of flame retardant PP composites

The PP-based composites were prepared through a melt blending process following the formulations provided in Table 3.1. The primary flame-retardant system utilized was an intumescent flame retardant composed of ammonium polyphosphate and MNSi-n at a fixed mass ratio of 3:1. For comparison, a reference sample was prepared using a system comprising APP and melamine cyanurate without char-forming skeletons, also at a mass ratio of 3:1. In the first step, all raw materials—including the PP matrix, IFR additives, and any additional modifiers—were weighed precisely according to the specified formulation. The components were then premixed in a high-speed mechanical mixer to ensure homogeneous dispersion before melting processing.

Table 3.1. The formulas (wt.%) of the IFR/PP composites.

	MNSi-n	MCA	APP	PP	Other additives*
PP	-	-	-	99	1
22%(MNSi-**1**/APP)/PP	5.5	-	16.5	77	1
22%(MNSi-**2**/APP)/PP	5.5	-	16.5	77	1
22%(MNSi-**3**/APP)/PP	5.5	-	16.5	77	1
22%(MCA/APP)/PP	-	5.5	16.5	77	1
25%(MNSi-**1**/APP)/PP	6.25	-	18.75	74	1
25%(MNSi-**2**/APP)/PP	6.25	-	18.75	74	1
25%(MNSi-**3**/APP)/PP	6.25	-	18.75	74	1
25%(MCA/APP)/PP	-	6.25	18.75	74	1
28%(MNSi-**1**/APP)/PP	7	-	21	71	1
28%(MNSi-**2**/APP)/PP	7	-	21	71	1
28%(MNSi-**3**/APP)/PP	7	-	21	71	1
28%(MCA/APP)/PP	-	7	21	71	1

***** Other additives included PTFE (0.4 wt.%), antioxidant 168 (0.3 wt.%), and antioxidant 1010 (0.3 wt.%).

The pre-blended mixture was fed into a co-rotating twin-screw extruder (Model: LHFS1-271822, Labtech Engineering Co., Ltd., Thailand) for compounding. The extrusion process was carried out at a barrel temperature of 190 °C, with the screw speed set to optimize both dispersion and thermal stability of the flame-retardant additives. The extrudate was cooled and pelletized for subsequent molding.

Standard test specimens were fabricated from the compounded pellets using two molding techniques:

Injection Molding: For mechanical and flammability testing samples, the pellets were processed in an injection molding machine (Model: TY-400, TAYU Machinery Co., Ltd., China). The barrel and mold temperatures were both maintained at 190 °C. Molding parameters such as injection pressure and cooling time were set according to the material flow behavior and mold design.

Compression Molding: For specific characterization (e.g., thermal analysis or limiting oxygen index tests), samples were also prepared using a compression molding press (Model: LP-S-50, Labtech Engineering Co., Ltd., Thailand). The molding was performed at 190 °C under a constant pressure of 50 MPa for a sufficient dwell time to ensure uniformity and eliminate internal voids.

After molding, all specimens were conditioned at room temperature (23 ± 2 °C, 50 ± 5% relative humidity) for at least 24 hours prior to testing, in accordance with relevant standards.

3.4 Structure characterization of intermediates and final products

The FTIR and NMR spectra of the synthesized intermediates NSi-n are presented in Fig. 3.3. In the FTIR spectra, a characteristic absorption band observed at 967 cm^{-1} corresponds to the Si–N stretching vibration, clearly indicating the formation of a covalent bond between anhydrous piperazine and phenyl trichlorosilane. In addition to this key peak, several other absorption bands were identified, corresponding to specific functional groups: N–H stretching at 3425 cm^{-1}, $–CH_2–$ stretching at 2944 and 2817 cm^{-1}, C–N stretching at 1108 cm^{-1}, aromatic C–H stretching at 3066 and 3044 cm^{-1}, aromatic ring vibrations at 1626 cm^{-1}, and Ph–Si bonds at 1144 cm^{-1}. The FTIR spectra of all three NSi-n compounds were found to be highly similar, reflecting their closely related chemical compositions. These spectral features were consistent with the expected molecular structures of the synthesized NSi-n intermediates. To further verify the molecular structure, nuclear magnetic resonance spectroscopy was employed. The ^{29}Si NMR spectra of the NSi-n series each displayed a single resonance peak, indicative of a symmetric silicon environment in the molecular structure. Minor variations in chemical shifts were observed among the samples, which can be attributed to differing degrees of aggregation or spatial distribution of piperazine and phenyl-silicon moieties. The ^{13}C NMR spectra (Fig. 3.3, a3–c3) provided additional structural confirmation. A signal appearing around 50 ppm (peak a) was assigned to the carbon atoms within the piperazine ring, while the signal at approximately 130 ppm (peak b) was attributed to the aromatic carbon atoms in the phenyl group. The theoretical molar ratios of carbon atoms from piperazine units to those from phenyl-silicon groups were calculated to be 2:1 for NSi-1, 1.5:1 for NSi-2, and 1.4:1 for NSi-3. The experimental integral area ratios (a:b) obtained from the ^{13}C NMR spectra were 1.93:1 (NSi-1), 1.53:1 (NSi-2), and 1.38:1 (NSi-3), which are in good agreement with the theoretical predictions. In summary, the combined FTIR and NMR results confirm that the NSi-n intermediates were successfully synthesized with well-defined structures.

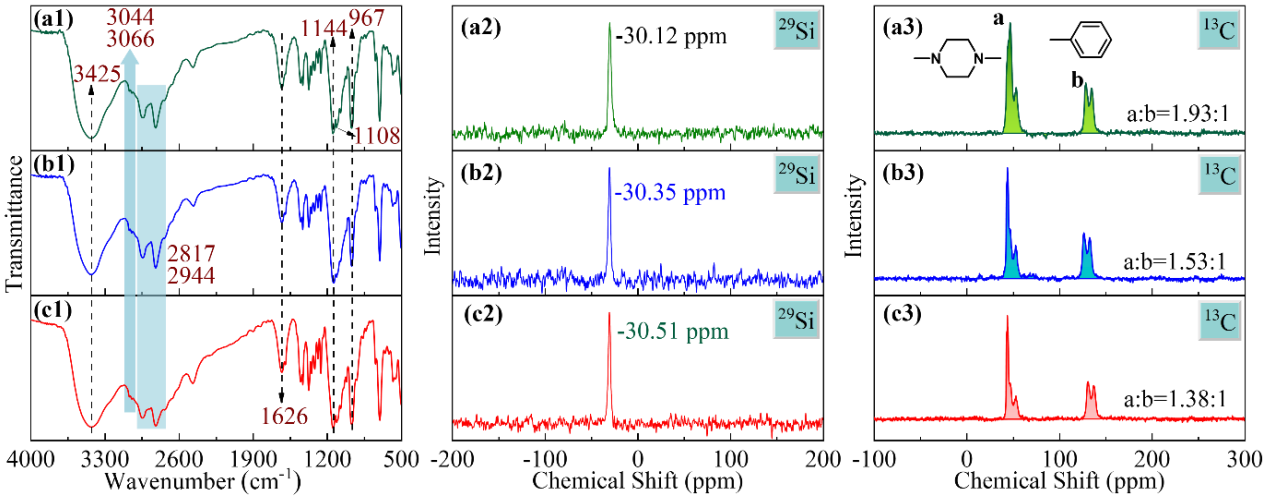

Fig. 3.3 The FTIR and NMR spectra of (a) NSi-1, (b) NSi-2, and (c) NSi-3.

The FTIR spectra of the synthesized macromolecular compounds MNSi-n are displayed in Fig. 3.4. A broad absorption band in the range of 2400–2700 cm^{-1} was observed, which is attributed to hydrogen bonding interactions. This feature confirms the formation of hydrogen bonds between the carbonyl groups (C=O) of cyanuric acid (from MCA) and the N–H groups of NSi-n intermediates, indicating the successful assembly of the MNSi-n macromolecular structure. Additionally, characteristic absorption peaks corresponding to the NSi-n components were also retained in the spectra, including N–H stretching at 3057 cm^{-1}, $–CH_2–$ vibrations at 2780, 2828, and 1396 cm^{-1}, aromatic skeletal vibrations at 1595 cm^{-1}, and Si–N stretching at 994 cm^{-1}. Notably, all these absorption bands exhibited slight shifts in comparison to the spectra of the NSi-n intermediates shown in Fig. 3.3(a1–c1), which further supports the presence of hydrogen bonding and the structural reorganization that occurred during MNSi-n formation.

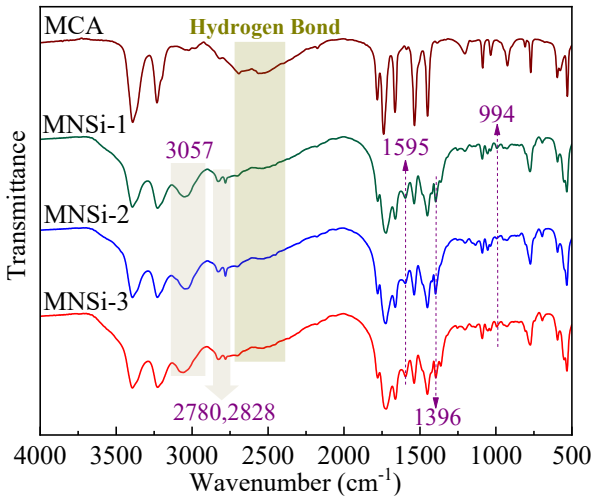

Fig. 3.4 The FTIR spectra of MNSi-n and MCA.

Thermogravimetric analysis, as illustrated in Fig. 3.5(a), demonstrated a significant improvement in thermal stability upon the formation of MNSi-n. Specifically, the decomposition onset temperature of MNSi-n was approximately 100 °C higher than that of the corresponding NSi-n intermediates. Furthermore, as shown in Fig. 3.5(b), the MNSi-3 compound exhibited superior thermal resistance compared to a simple physical mixture of MCA and NSi-3, highlighting the enhanced structural integration and thermal durability conferred by hydrogen bond-driven assembly. However, it is noteworthy that the thermal degradation behavior of MNSi-n changed at higher temperatures. Since cyanuric acid decomposes rapidly above 400 °C with negligible char residue, MNSi-n became less thermally stable than NSi-n in this high-temperature range, displaying a reduced residue yield beyond this threshold.

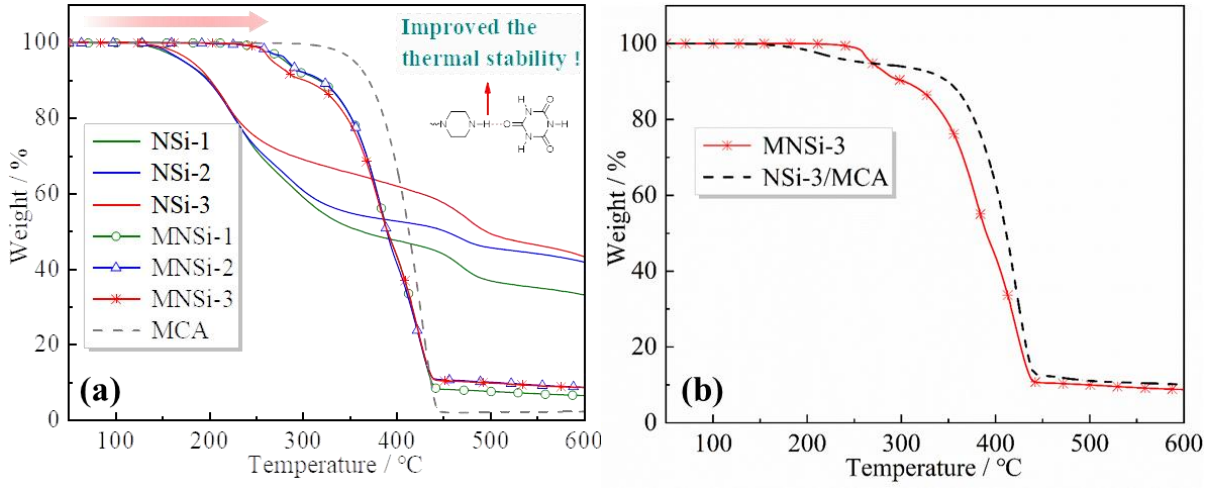

Fig. 3.5 The TGA curves of (a) NSi-n, MNSi-n, and (b) MNSi3, MCA

Morphological observations from SEM images (Fig. 3.6) revealed that MNSi-n formed larger, more compact particles compared to the MCA reference (Fig. 3.6, d). This morphological change is attributed to the supramolecular assembly among NSi-n, melamine, and cyanuric acid during synthesis. Moreover, elemental mapping using energy-dispersive X-ray spectroscopy confirmed the homogeneous distribution of carbon, oxygen, and nitrogen across the MNSi-n particle surface (excluding hydrogen, which is not detectable by EDS). This uniform distribution indicates that the NSi-n frameworks were effectively incorporated into the MCA-derived network, forming a well-organized macromolecular structure. In summary, the macromolecules MNSi-1, MNSi-2, and MNSi-3 were successfully constructed using NSi-1, NSi-2, and NSi-3, respectively, as functional intermediates. The resulting materials demonstrated enhanced thermal stability, and homogeneity, primarily driven by strong hydrogen bonding and effective molecular assembly.

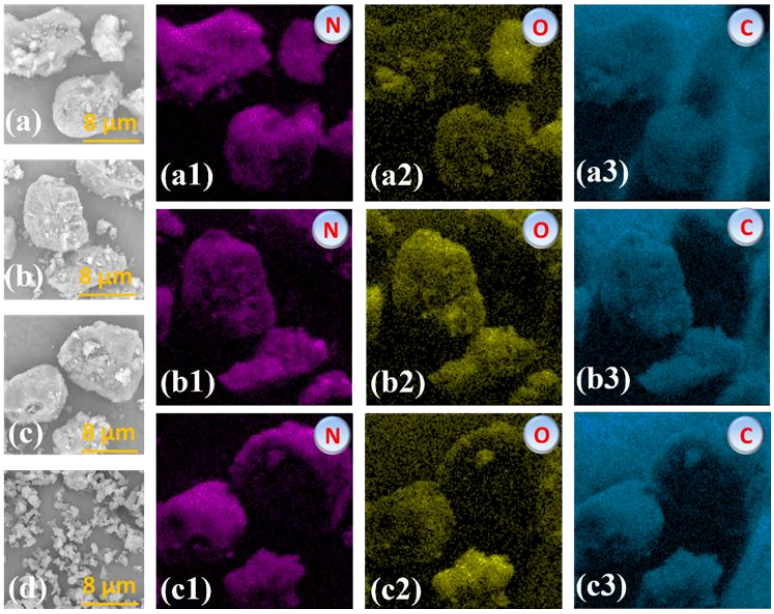

Fig. 3.6 The micromorphology and EDS maps: (a) MNSi-1, (b) MNSi-2, (c) MNSi-3, (d) MCA.

3.5 Flame retardancy of fabricated PP composites

To comprehensively evaluate the flame-retardant performance of the developed polypropylene composites, a series of standardized fire testing methods were employed. These included the glow-wire ignition test, limiting oxygen index test, UL-94 vertical burning test, and cone calorimeter test. Together, these methods provided a thorough and multi-faceted assessment of ignition resistance, flame propagation behavior, and heat release characteristics of the composites. The main results are detailed in Table 3.2.

Table 3.2. The results of GW, LOI, and UL 94 tests.

Samples	GW-test (3mm)		LOI	UL 94 (3.2mm)		
	GWFI	GWIT		t_1/(s)	t_2/(s)	Rating
PP	725°C	750°C	18.6%	Burn[a]	—	No
22%(MNSi-**1**/APP)/PP	825°C	775°C	24.8%	0	Burn[a]	No
22%(MNSi-**2**/APP)/PP	825°C	775°C	24.7%	0	Burn[a]	No
22%(MNSi-**3**/APP)/PP	850°C	775°C	**25.6%**	0	Burn[a]	No
22%(MCA/APP)/PP	750°C	750°C	22.7%	Burn*	—	No
25%(MNSi-**1**/APP)/PP	875°C	800°C	26.7%	0	4.5	V-0
25%(MNSi-**2**/APP)/PP	900°C	800°C	26.9%	0	3.9	V-0
25%(MNSi-**3**/APP)/PP	925°C	800°C	**27.3%**	0	3.8	V-0
25%(MCA/APP)/PP	800°C	775°C	23.4%	Burn*	—	No

28%(MNSi-**1**/APP)/PP	> 960℃	850℃	28.0%	0	2.9	V-0
28%(MNSi-**2**/APP)/PP	> 960℃	850℃	28.2%	0	2.8	V-0
28%(MNSi-**3**/APP)/PP	> 960℃	850℃	**28.6%**	0	2.9	V-0
28%(MCA/APP)/PP	825℃	775℃	24.2%	2.0	Burn*	No

* The flame burned to the clamp.

The glow-wire flammability test evaluates the ignition resistance of materials by bringing a heated metallic wire, typically ranging from 550 °C to 960 °C, into contact with the sample surface. The highest classification attainable is denoted as ">960 °C", indicating excellent thermal stability under direct thermal stimulus. As shown in Table 3.2 and Fig. 3.7, the GWFI of neat polypropylene was measured to be 725 °C, reflecting its inherent flammability. However, when 28 wt.% of an intumescent flame retardant system composed of APP and MNSi-n was incorporated into the PP matrix, the composite achieved the highest GWFI rating of ">960 °C". Furthermore, the GWIT of the 28%(MNSi-n/APP)/PP formulation was 100 °C higher than that of pure PP, indicating a significant enhancement in ignition resistance. In addition, Fig. 3.7 reveals that composites containing the (MNSi-n/APP) system consistently outperformed those based on the traditional (MCA/APP) system at equivalent loading levels. This clearly demonstrates that the piperazine - phenyl silicon core structure of the NSi-n intermediates played a pivotal role in enhancing the flame-retardant efficiency of the MNSi-n/APP system. Although the weight fractions of NSi-n cores were relatively low - 1.02 wt.% in 22%(MNSi-n/APP)/PP, 1.16 wt.% in 25%, and 1.30 wt.% in 28% formulations - their contribution to the charring process was substantial. The improved flame retardancy is attributed to the formation of a robust, silicon- and nitrogen-rich char layer derived from the macromolecular MNSi-n structure, in contrast to the limited charring capacity of MCA. Moreover, Fig. 3.7 illustrates a trend of increasing GWFI values with the degree of aggregation of piperazine/phenyl-silicon groups within the NSi-n skeleton. Specifically, MNSi-2 and MNSi-3, which possess a higher degree of structural aggregation compared to MNSi-1, exhibited superior flame-retardant performance. This indicates that enhanced interaction among charring groups significantly contributes to the thermal barrier effect and thereby to flame retardancy. In summary, the aggregation of piperazine and phenyl-silicon motifs within the NSi-n framework serves as a critical factor in enhancing the efficiency of the MNSi-n/APP IFR system in polypropylene composites.

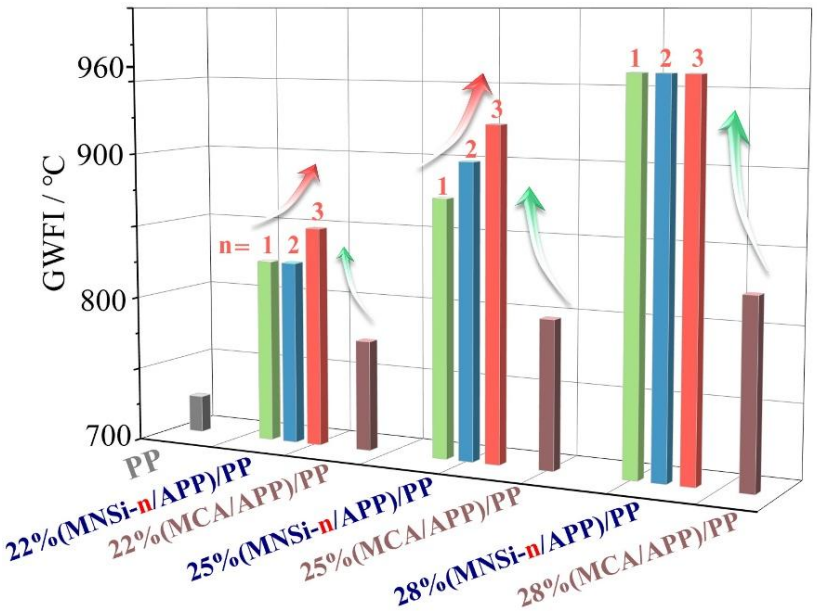

Fig. 3.7 The GWFI results of flame retardant PP composites and control samples.

The LOI test is commonly used to determine the minimum oxygen concentration required to sustain combustion. Neat polypropylene exhibited a low LOI value of only 18.6%, indicating its high flammability. However, with the incorporation of the MNSi-n/APP intumescent flame retardant system, the LOI values of the resulting composites were significantly enhanced. Specifically, the LOI of the 22 wt.% (MNSi-3/APP)/PP composite increased to 25.7%, representing a 7.1% improvement compared to pure PP. As the loading content was further increased to 28 wt.%, all three formulations—28%(MNSi-1/APP)/PP, 28%(MNSi-2/APP)/PP, and 28%(MNSi-3/APP)/PP—achieved LOI values exceeding 28%, demonstrating good flame retardancy. In addition to LOI enhancement, vertical burning tests based on the UL-94 standard revealed that both 25 wt.% and 28 wt.% MNSi-n/APP-modified PP composites attained the highest V-0 rating, indicating rapid self-extinguishing behavior and absence of flaming drips. In stark contrast, reference samples containing MCA/APP without the piperazine and phenyl-silicon functional groups—namely 22%(MCA/APP)/PP, 25%(MCA/APP)/PP, and 28%(MCA/APP)/PP—failed to achieve any UL-94 rating and showed significantly lower LOI values under identical flame retardant loading. These results underscore the critical role of the NSi-n core structure, particularly the piperazine and phenyl-silicon functionalities, in promoting an effective intumescent mechanism in combination with APP. The formation of a stable and insulating char layer is likely facilitated by these groups, which enhances the flame retardant efficiency of the composite. Moreover, among the three MNSi-n-based systems, the MNSi-3/APP/PP composite consistently exhibited the highest LOI values, which can be

attributed to the more extensive aggregation of piperazine and phenyl-silicon structures within the MNSi-3 framework.

Further, cone calorimeter tests were conducted under standardized conditions. As shown in Fig. 3.8(a), the neat PP exhibited a sharp and intense combustion process, with a peak heat release rate (PHRR) of 1591 $kW \cdot m^{-2}$. In contrast, the incorporation of 25 wt.% MNSi-n/APP intumescent flame retardant system significantly suppressed the heat release intensity, reducing the PHRR values of the composites to approximately 400 $kW \cdot m^{-2}$ - an impressive reduction of nearly 75%. Additionally, the times to PHRR (TTP) of neat PP, 25%(MCA/APP)/PP, and 25%(MNSi-n/APP)/PP were 125 s, 75 s, and about 55 s, respectively. The burning intensity of 25%(MNSi-n/APP)/PP was quickly suppressed to a greater extent compared with these control samples. These results indicate that although ignition and flame propagation occurred earlier in the flame-retardant samples, the combustion intensity was significantly mitigated, especially in the MNSi-n-based formulations, due to the rapid formation of protective char layers. To quantitatively assess the fire hazard potential, the fire performance index (FPI) and fire growth index (FGI) were calculated using the time to ignition (TTI), PHRR, and TTP values. FPI, defined as the ratio of TTI to PHRR, serves as a predictive indicator of material flammability and potential danger in a fire scenario - the higher the FPI, the safer the material. As shown in Fig. 3.8(b), the FPI values for the three 25%(MNSi-n/APP)/PP composites exceeded 0.055 $s \cdot m^2 \cdot kW^{-1}$, significantly surpassing that of pure PP (0.018 $s \cdot m^2 \cdot kW^{-1}$), indicating a substantial improvement in fire safety performance. Furthermore, the FGI values - indicative of the rate at which a fire develops - were also markedly reduced. As illustrated in Fig. 3.8(b), the FGI of the 25%(MNSi-n/APP)/PP samples remained below 7.5 $kW \cdot m^{-2} \cdot s^{-1}$, which is at least 41.7% lower than that of neat PP. This significant suppression of fire growth demonstrates the effectiveness of the MNSi-n/APP system in slowing down combustion propagation and reducing fire hazard.

In summary, the combined analysis of PHRR, TTP, FPI, and FGI clearly confirms that the 25%(MNSi-n/APP)/PP composites exhibit superior fire safety characteristics compared to both pure PP and MCA/APP-based formulations. The enhanced fire resistance can be attributed to the synergistic effects between APP and piperazine / phenyl-silicon skeletons within the MNSi-n macromolecular structure.

Table 3.3. Typical parameters of selected samples from cone calorimeter test.

Sample	TTI /s	PHRR /$kW \cdot m^{-2}$	THR /$MJ \cdot m^{-2}$	av-EHC /$MJ \cdot kg^{-2}$	TSR /$m^2 \cdot m^{-2}$	av-COY /$kg \cdot kg^{-1}$	av-CO_2Y /$kg \cdot kg^{-1}$	Residue

25%(MNSi-**1**/APP)/PP	23	411	119	41.2	2674	0.08	2.79	16.1%
25%(MNSi-**2**/APP)/PP	26	394	119	41.0	2601	0.08	2.85	17.6%
25%(MNSi-**3**/APP)/PP	24	**386**	116	**40.3**	2183	0.09	2.84	**20.3%**
25%(MCA/APP)/PP	24	525	132	44.7	1857	0.08	2.92	11.4%
PP	28	1591	151	52.7	2108	0.05	3.60	0.7%

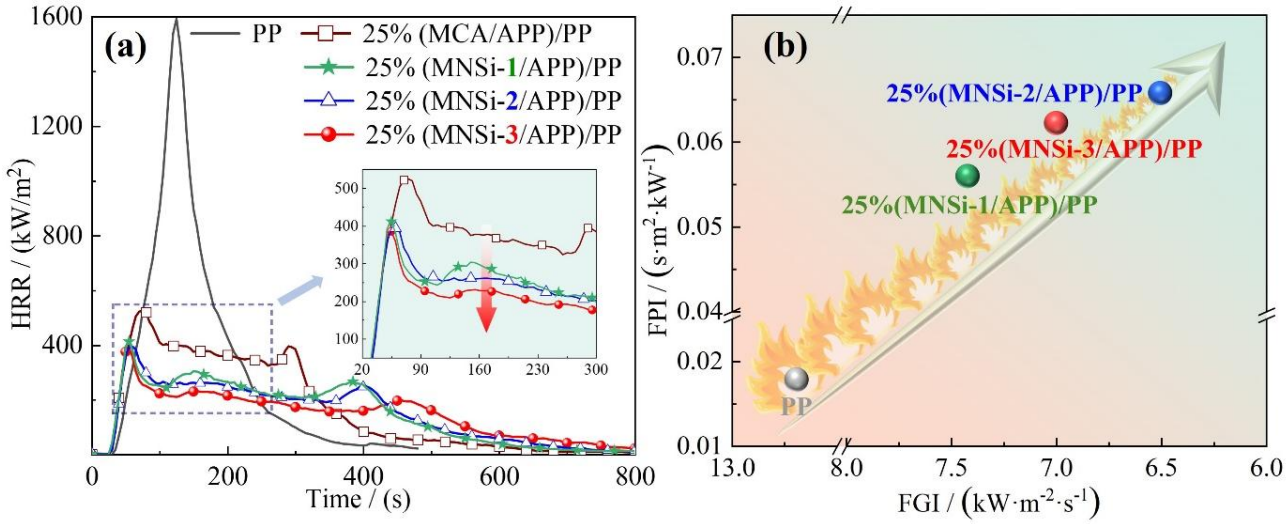

Fig. 3.8 The HRR curves, FPI, and FGI data of PP composites.

Despite the similar overall flame retardant system, the three 25 wt.% (MNSi-n/APP)/PP composites exhibited distinct differences in their combustion behaviors. As shown in Fig. 3.8(a), after reaching their PHRR, the 25%(MNSi-3/APP)/PP sample maintained the lowest heat release rate from approximately 100 s to 400 s, in comparison to the 25%(MNSi-1/APP)/PP and 25%(MNSi-2/APP)/PP. This extended suppression of HRR indicates a more sustained and effective barrier effect in the MNSi-3-containing system. Correspondingly, the fire safety indices, including FPI and FGI, shown in Fig. 3.8(b), revealed that both 25%(MNSi-3/APP)/PP and 25%(MNSi-2/APP)/PP possessed higher FPI values and lower FGI values than 25%(MNSi-1/APP)/PP. These data confirm that an increased aggregation degree of the piperazine/phenyl-silicon skeleton in NSi-n intermediates contributes to enhanced flame retardancy and improved overall fire safety of the resulting intumescent flame retardant systems in polypropylene matrix. A critical factor contributing to the improved flame resistance is the increased char residue generated during combustion. The char yields of all 25%(MNSi-n/APP)/PP composites exceeded 16 wt.%, in stark contrast to neat PP, which left negligible residue due to complete thermal decomposition into volatile fuel gases. Moreover, as the aggregation degree of the core NSi-n increased, the final char residue also increased,

demonstrating that MNSi-n promotes more efficient char formation. This char acts as a thermal barrier, insulating the underlying polymer and retarding heat and mass transfer.

The enhanced condensed-phase performance was also reflected in the reduced total heat release (THR) values, which decreased by more than 20% for the 25%(MNSi-n/APP)/PP composites compared to neat PP. FTIR analysis of the char residue (Fig. 3.9), combined with prior literature [98][230], suggests a plausible flame-retardant mechanism. At the early stage of combustion, the piperazine moieties in MNSi-n chemically interact with polyphosphate derived from APP to form intumescent char structures containing P-N and polyphosphate groups. As combustion progresses, these intermediate char layers undergo further structural evolution, incorporating segments of the PP matrix to generate P-C and P-O-C crosslinked structures. This process results in the formation of a dense, thermally stable, and expandable char layer that effectively isolates heat and oxygen, thereby enhancing flame retardancy.

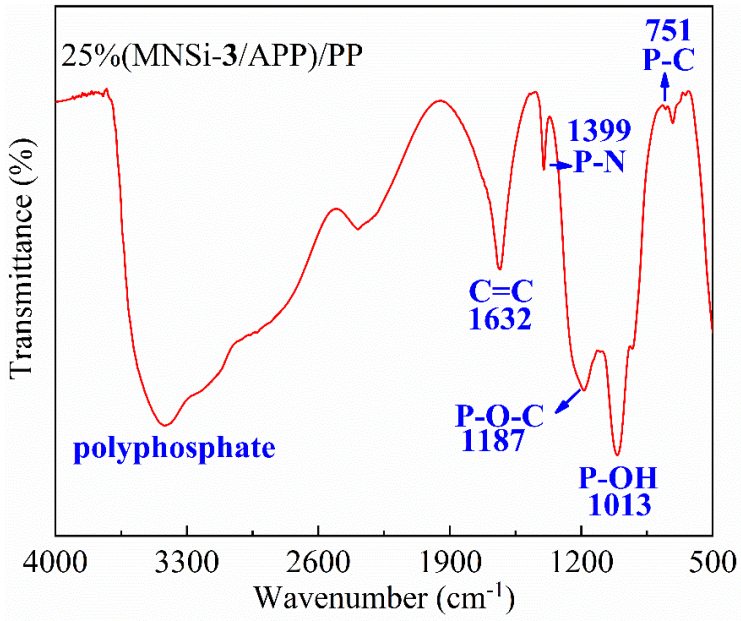

Fig. 3.9 The FTIR spectrum of residue from cone calorimeter test.

In the gas phase, the average effective heat of combustion (av-EHC) provides insight into the completeness of volatile combustion. All three 25%(MNSi-n/APP)/PP composites exhibited av-EHC values of approximately 41 $MJ \cdot kg^{-1}$, which were significantly lower than that of neat PP. This indicates an increased degree of incomplete combustion, further supported by the elevated average CO release (av-CO) values listed in Table 3.3. The mechanism behind this phenomenon is likely the release of phosphorus-containing free radicals (e.g., PO· and PO_2·) during thermal degradation of polyphosphate. These radicals scavenge high-energy species in the flame, interrupting the combustion chain reactions and imparting a gas-phase flame-retardant effect.

Smoke suppression is another critical aspect of fire safety. The total smoke release (TSR) of the composites varied with the aggregation degree of the MNSi-n structure. The 25%(MNSi-3/APP)/PP sample produced a TSR of 2183 $m^2 \cdot m^{-2}$, significantly lower than the values exceeding 2600 $m^2 \cdot m^{-2}$ for the 25%(MNSi-1/APP)/PP and 25%(MNSi-2/APP)/PP samples. The superior smoke suppression of MNSi-3 containing system is attributed to its stronger char-forming ability, which results from a higher degree of structural aggregation. This aggregation promotes the formation of a more compact and carbon-rich char layer, effectively trapping more decomposition products and reducing the emission of combustible volatiles.

In conclusion, the enhanced flame retardant and smoke suppression performance of the 25%(MNSi-3/APP)/PP composite can be attributed to the synergistic effects of its highly aggregated piperazine/phenyl-silicon framework and ammonium polyphosphate. This structural feature facilitates both gas-phase radical quenching and condensed-phase char formation, thereby delivering superior fire safety across multiple evaluation criteria.

3.6 Barrier effect evaluation of formed char residue

It is widely acknowledged that the formation of char layers with effective barrier properties is essential for the intumescent flame retardancy of polypropylene (PP) composites. To evaluate the thermal shielding capability of the char layers formed under high-temperature conditions, an intuitive infrared thermographic method was employed to monitor the back surface temperature during flame exposure. The infrared thermal images at various heating intervals are presented in Fig. 3.10, while the corresponding maximum surface temperatures recorded in the test area are summarized in Fig. 3.11. Upon direct flame application to the composite surface, charring reactions were initiated, promoting the development of thermally crosslinked protective layers. After 10 seconds of flame exposure, distinct temperature distributions were observed among the samples. Notably, the 25 wt.% (MNSi-n/APP)/PP composites exhibited smaller high-temperature regions compared to the 25 wt.% (MCA/APP)/PP sample, indicating superior thermal insulation performance. As flame exposure time increased, significant differences in thermal stability emerged. At 50 and 60 seconds, the 25%(MCA/APP)/PP sample displayed clear signs of thermal degradation and deformation. In contrast, the 25%(MNSi-n/APP)/PP composites maintained structural integrity and exhibited excellent shape stability, even after 60 seconds of direct flame exposure. The time-dependent changes in the maximum back-surface temperature, as shown in Fig. 3.11, further confirmed the enhanced thermal barrier effect of the MNSi-n/APP system. Among the MNSi-n-based formulations, the 25%(MNSi-3/APP)/PP composite demonstrated the smallest high-temperature area and the

lowest recorded maximum temperatures across all time points. This result highlights the pivotal role of the highly aggregated charring structures in MNSi-3, which contributed to the formation of denser and more effective char layers. Overall, these findings are consistent with the cone calorimeter results and support the conclusion that a higher aggregation degree of piperazine/phenyl-silicon groups within MNSi-n macromolecules enhances the thermal shielding performance of the resulting char layers, thereby improving the flame retardancy of the composite system.

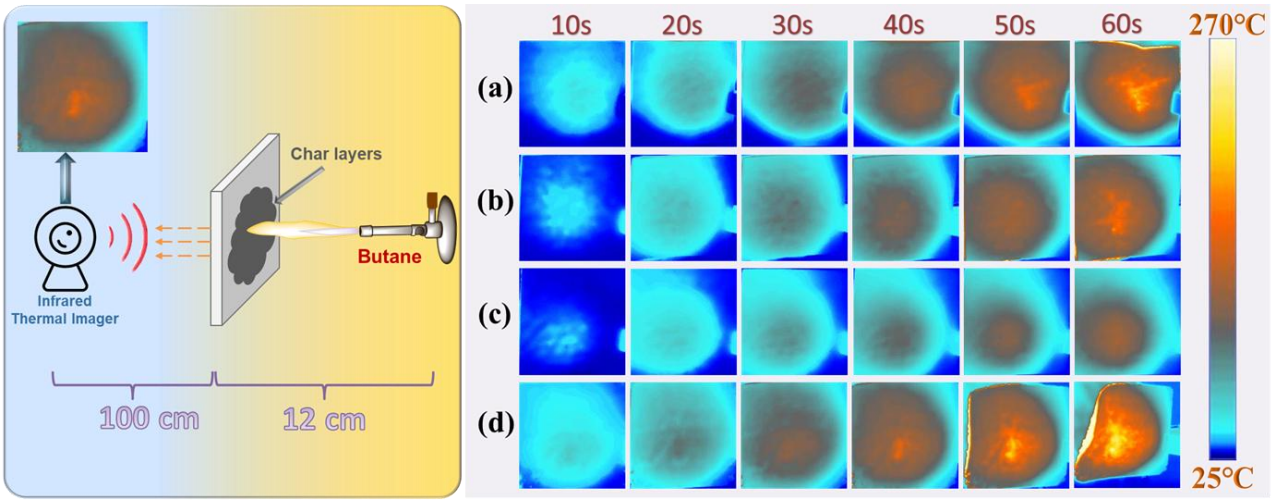

Fig. 3.10 The infrared thermal imaging pictures at different flame application times: (a) 25%(MNSi-1/APP)/PP; (b) 25%(MNSi-2/APP)/PP; (c) 25%(MNSi-3/APP)/PP; (d) 25%(MCA/APP)/PP.

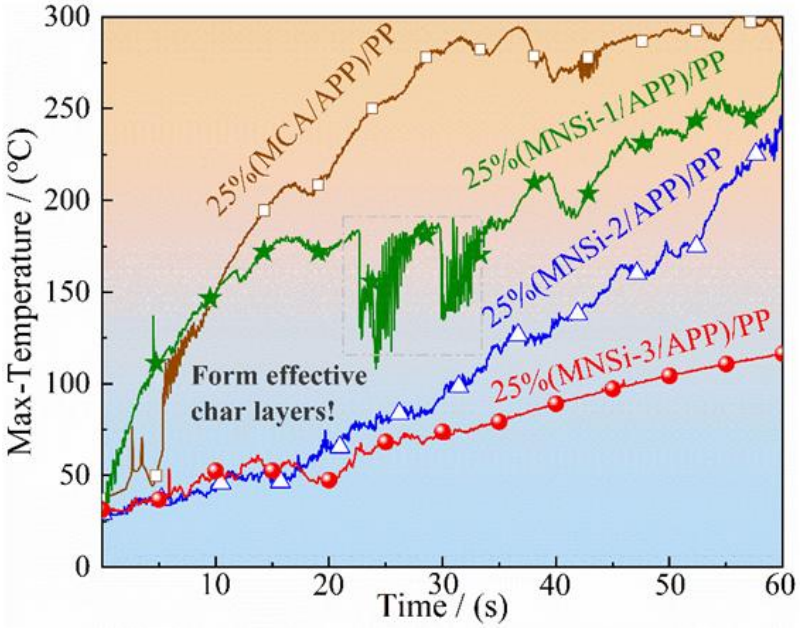

Fig. 3.11 The maximum temperature of the test area at different times.

3.7 Characterization of char residues

To further investigate the condensed-phase flame-retardant mechanism, the residual char layers obtained after cone calorimeter tests were analyzed using SEM and EDS. As shown in Fig. 3.12(e), neat PP left almost no residue after combustion, indicating its complete thermal decomposition into volatile flammable gases. In contrast, Fig. 3.12(d, d1) reveals that the char layer of the 25 wt.% (MCA/APP)/PP sample was severely disrupted and fragmented by gaseous volatiles during burning. This result clearly demonstrates that the MCA/APP system alone failed to produce a continuous and cohesive protective char structure within the PP matrix. In comparison, the surface morphologies of the 25 wt.% (MNSi-n/APP)/PP composites, shown in Fig. 3.12(a–c), displayed significantly more compact and uniform char layers than those of the MCA/APP system. These findings suggest that the incorporation of the piperazine/phenyl-silicon-based core skeleton (NSi-n) into the MCA structure resulted in a synergistic interaction with APP, effectively enhancing the char-forming ability of the system. The resulting MNSi-n/APP/PP composites produced denser and more robust char layers, thereby contributing to improved flame retardancy. Additionally, elemental mapping via EDS confirmed that silicon was uniformly distributed throughout the char layers of the MNSi-n/APP samples. The presence of silicon-based compounds, known for their thermal stability and incombustibility, played a crucial role in promoting the formation of compact, thermally resistant char layers. Moreover, among the MNSi-n/APP samples, the char surfaces of the 25%(MNSi-2/APP)/PP and 25%(MNSi-3/APP)/PP composites appeared more continuous and tightly packed compared to that of 25%(MNSi-1/APP)/PP. This observation further supports the conclusion that a higher degree of structural aggregation in the piperazine/phenyl-silicon core skeleton enhances the char quality, thus improving the flame-retardant performance. These structural features of the residual char layers are in strong agreement with the flame retardancy results observed in the GWFI, LOI, and cone calorimeter tests, further validating the effectiveness of the MNSi-n/APP system as an intumescent flame retardant in PP composites.

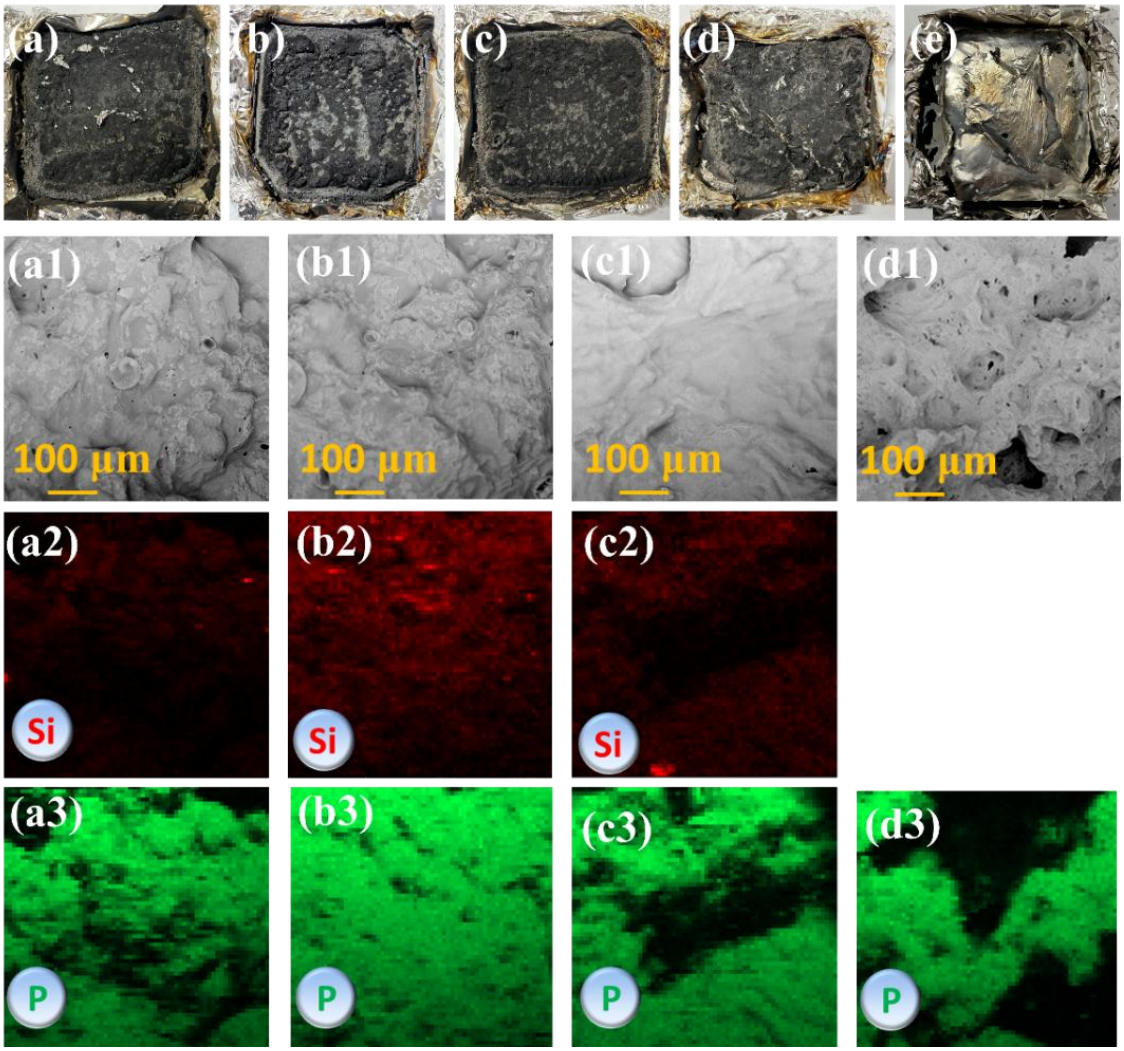

Fig. 3.12 The digital photos, micrograph photos, Si-element distribution, and P-element distribution on the surficial char layer: (a) 25%(MNSi-1/APP)/PP; (b) 25%(MNSi-2/APP)/PP; (c) 25%(MNSi-3/APP)/PP; (d) 25%(MCA/APP)/PP; (e) PP.

To further elucidate the chemical composition of the residual char and clarify the interaction mechanism among the flame-retardant components, elemental analysis was performed using EDS, and the results are summarized in Table 3.4. Notably, the 25 wt.% (MCA/APP)/PP composite, which lacked the core NSi-n structure, exhibited only 3.22 wt.% carbon in the residue - significantly lower than the carbon content found in the three 25 wt.% (MNSi-n/APP)/PP composites. This result clearly indicates that the incorporation of the NSi-n structure plays a critical role in retaining carbon-containing fragments in the condensed phase, thereby enhancing char formation. Among the MNSi-n-based systems, the 25%(MNSi-3/APP)/PP composite displayed the highest residual carbon content at 7.58 wt.%, compared to 5.87 wt.% for 25%(MNSi-1/APP)/PP and 6.60 wt.% for 25%(MNSi-2/APP)/PP. These results suggest that the higher degree of structural aggregation in the piperazine/phenyl-silicon

backbone of MNSi-3 promotes more efficient charring during combustion, further enhancing the flame-retardant performance. Additionally, the residue from 25%(MNSi-3/APP)/PP showed elevated levels of both silicon and phosphorus, which implies that the excellent flame retardancy of this composite is mainly attributed to the strong synergistic interaction between MNSi-3 and APP. As confirmed by the EDS mapping in Fig. 3.12, the Si and P elements were homogeneously distributed across the surface of the residual char, which likely contributed to the formation of more compact and thermally stable char layers. This uniform dispersion of flame-retardant elements reinforces the barrier properties of the char, leading to enhanced condensed-phase flame retardant effects.

Table 3.4 The elements contents of surface char layers.

Samples	Si (wt.%)	P (wt.%)	N (wt.%)	O (wt.%)	C (wt.%)
25%(MNSi-1/APP)/PP	0.15	14.60	11.12	68.26	5.87
25%(MNSi-2/APP)/PP	0.22	15.17	11.28	66.73	6.60
25%(MNSi-3/APP)/PP	0.25	16.18	10.29	65.70	7.58
25%(MCA/APP)/PP	0.00	19.46	9.19	68.12	3.22

3.8 Introduction

Thermal stability and decomposition characteristics of the materials are critical for elucidating the underlying flame-retardant mechanisms. As illustrated in Fig. 3.13, the initial decomposition temperatures of the 25 wt.% (MNSi-n/APP)/PP composites were all lower than that of the 25 wt.% (MCA/APP)/PP sample. This observation suggests that the MNSi-n/APP system can accelerate the thermal degradation of the PP matrix. Compared with the MCA molecule, the piperazine/phenyl-silicon core structure present in MNSi-n macromolecules is more reactive, which likely facilitates earlier decomposition through interactions with other flame-retardant components. Such early decomposition behavior is advantageous for intumescent flame retardancy, as it enables the rapid formation of protective char layers in the initial stages of combustion. Moreover, all (MNSi-n/APP)/PP composites exhibited higher residual yields than (MCA/APP)/PP in the temperature range of 500-600 °C, indicating that the NSi-n core structure significantly promotes char formation in the condensed phase. However, it was also observed that the residual char from 25 wt.% (MNSi-n/APP)/PP began to decompose at temperatures above 600 °C. This suggests that although the NSi-n core contributes to enhanced char formation, the thermal stability of the char may be limited, potentially due to the relatively low loading of the NSi-n structure or insufficient structural integrity within the charred residue.

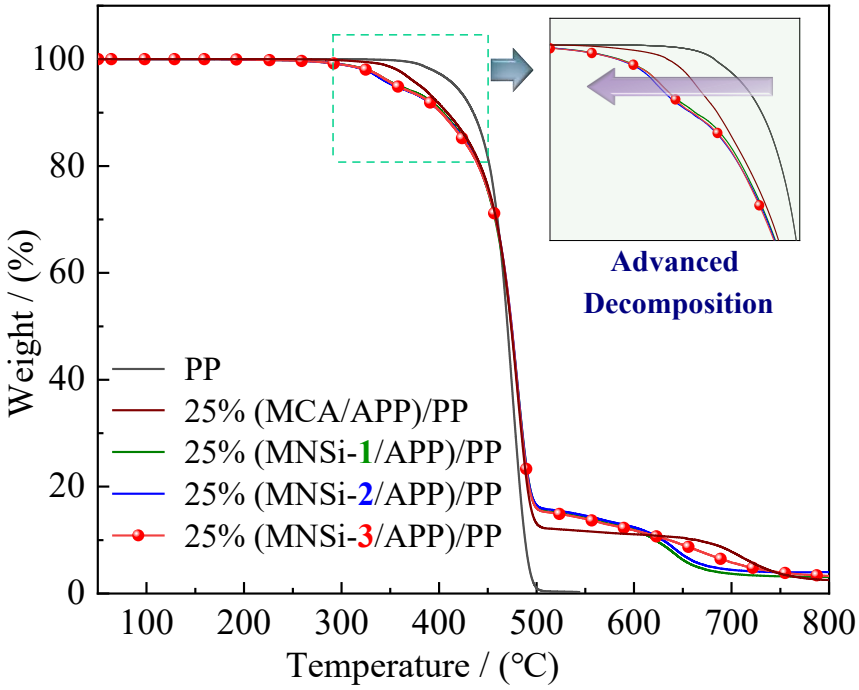

Fig. 3.13 The TGA curves of PP composites.

The volatile pyrolysis products released at the maximum decomposition temperature were analyzed using FTIR spectroscopy, and the corresponding spectra are presented in Fig. 3.14(a). For neat PP, the predominant volatile products were hydrocarbon fragments, including -CH_3 (2966, 1380 cm^{-1}), -CH_2- (2923, 1459 cm^{-1}), C-C (1153 cm^{-1}), =CH (3079, 968, 890 cm^{-1}), and C=C (1647 cm^{-1}), consistent with previous reports [135][231]. In contrast, the spectra of 25 wt.% (MNSi-n/APP)/PP composites showed significantly attenuated absorption peaks at 2966, 1380, 2923, 1459, and 890 cm^{-1}, indicating a notable reduction in hydrocarbon fragment release due to the incorporation of the MNSi-n/APP system. This suggests that the flame-retardant system can effectively interact with or trap hydrocarbon volatiles during thermal degradation. Further comparison in Fig. 3.14(b) reveals that 25%(MNSi-2/APP)/PP and 25%(MNSi-3/APP)/PP exhibited even lower absorption intensities for -CH_3 vibrations compared to 25%(MNSi-1/APP)/PP. This observation confirms that a higher aggregation in the piperazine/phenyl-silicon core structure enhances the system's ability to suppress the evolution of flammable gaseous products. Additionally, phosphorus-containing species were also detected. Specifically, the absorption bands at 1049 and 1102 cm^{-1} correspond to P-O-P and PO_x species, respectively [101][232]. Among the tested samples, 25%(MNSi-3/APP)/PP showed the weakest absorption at these wavelengths, suggesting that the higher aggregation degree of MNSi-3 promoted the retention of phosphorus-containing components within the condensed phase. This effect is consistent with the EDS results, further confirming the enhanced char-forming and flame-retardant efficiency of the MNSi-n/APP system.

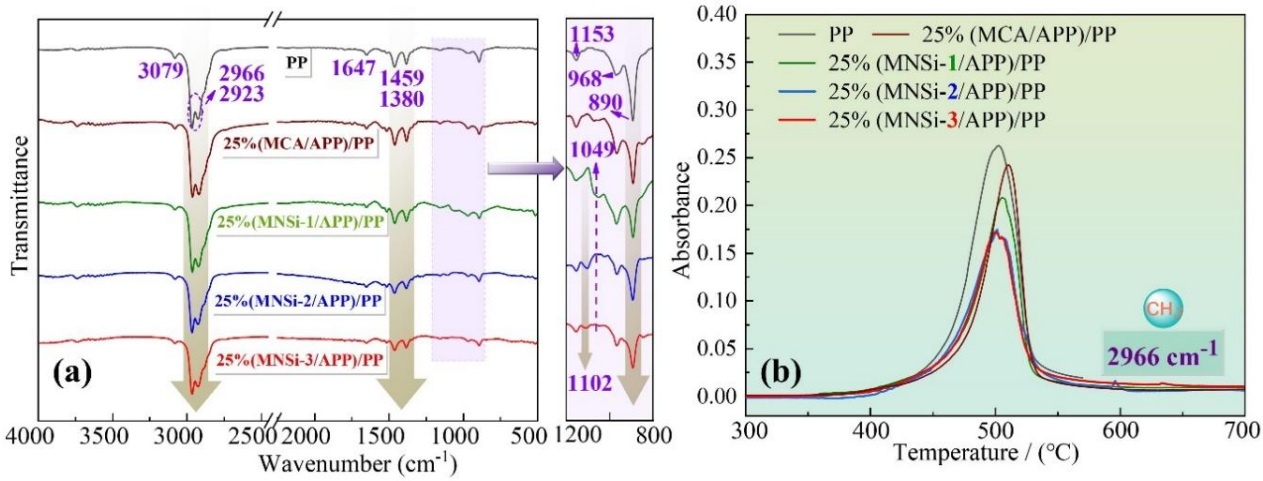

Fig. 3.14 (a) The FTIR curves of pyrolysis products at $T_{d,max}$, and (b) the released intensity of CH_3 group during heating.

3.9 Mechanical properties of PP composites

The mechanical performance of the PP composites is shown in Fig. 3.15. Neat PP exhibited an impact strength of approximately 124 kJ/m² and an elongation at break exceeding 600%. However, the incorporation of flame retardant additives led to a significant reduction in both parameters. A clear negative dose - effect relationship was observed: as the loading content of flame retardants increased, both impact strength and elongation at break decreased notably. This deterioration is primarily attributed to the disruption of matrix continuity caused by the introduction of flame retardant particles. As shown in Fig. 3.6, MCA possessed a regular sheet-like morphology with relatively small particle size, whereas MNSi-n tended to aggregate into larger particles due to hydrogen bonding-induced self-assembly. Consequently, the (MCA/APP)/PP composites exhibited higher impact strength and elongation at break than their (MNSi-n/APP)/PP counterparts.

In contrast, the tensile strength of the composites remained largely unaffected by the addition of flame retardants, indicating a negligible influence on this property. Overall, despite some reduction in toughness and flexibility, the mechanical properties of the (MNSi-n/APP)/PP composites remain within acceptable limits for general application.

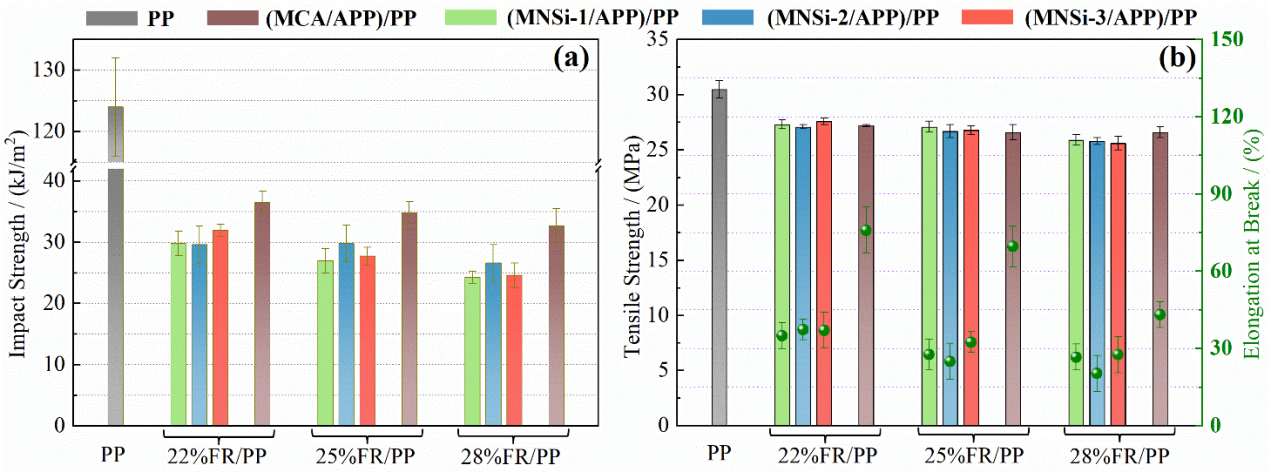

Fig. 3.15 Results of mechanical properties: (a) impact test; (b) tensile test.

3.10 Conclusion

As shown in the graphical summary of Fig. 3.16, a series of N/Si-based charring macromolecules (MNSi-n) were successfully constructed by introducing charring skeletons (NSi-n) with varying degrees of aggregation into hydrogen-bonded MCA frameworks. The core skeleton NSi-n played a crucial role in enhancing the intumescent flame retardant efficiency of (MNSi-n/APP)/PP composites. Compared to the MCA/APP system, the MNSi-n/APP system imparted significantly improved flame retardant properties to the PP matrix, including higher limiting oxygen index, glow-wire flammability index, glow-wire ignition temperature, and a UL-94 V-0 rating. Additionally, the (MNSi-n/APP)/PP composites exhibited lower PHRR and total THR, demonstrating improved fire safety. These improvements were mainly attributed to the synergistic charring effect between the NSi-n core and both APP and the PP matrix, which led to the formation of compact and thermally stable char layers enriched with silicon and phosphorus elements. Notably, PP composites containing MNSi-3 or MNSi-2 - with aggregated piperazine/phenyl-silicon structures - displayed superior flame retardant performance, as evidenced by higher LOI, GWFI, FPI, and residue yield, along with lower THR and FGI values, compared to the (MNSi-1/APP)/PP sample. This demonstrated that a higher degree of aggregation in the piperazine/phenyl-silicon core structure facilitates a more efficient interaction between MNSi-n and APP, thereby enhancing the overall charring effect. In summary, the incorporation of a small amount of NSi-n core structures markedly improved the flame retardant performance of MNSi-n macromolecules, offering a promising strategy for the design of high-efficiency, low-cost intumescent flame retardant PP materials.

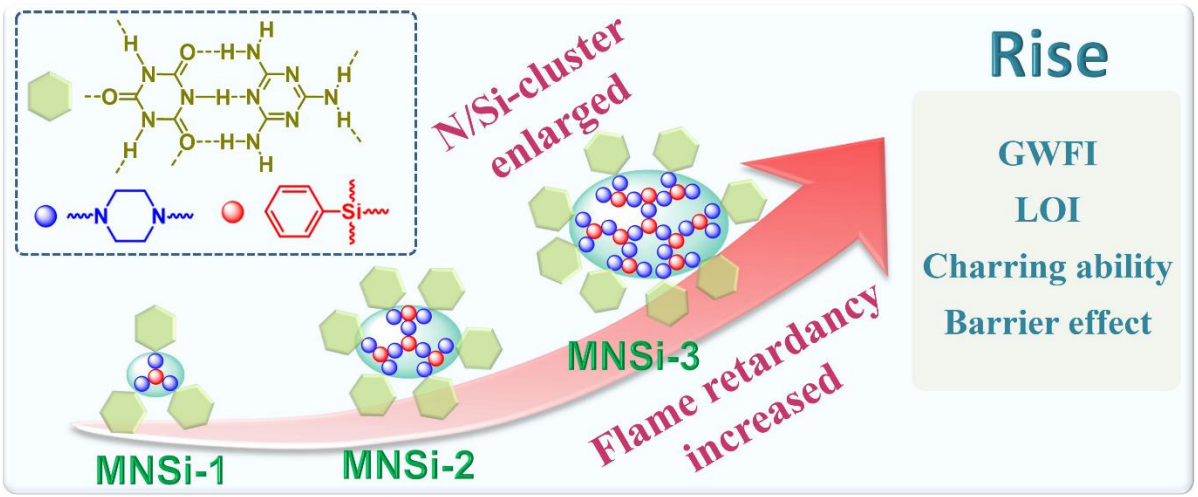

Fig. 3.16 The graphical summary of this chapter.

CHAPTER 4

Construction of Piperazine/Silane-Based Dendritic Molecule and Its Toughening / Intumescent Flame Retardant Polypropylene

4.1 Introduction

In the previous chapter, a synergistic flame-retardant system combining a piperazine/phenylsilicon framework with a polyphosphoric acid structure was developed, which significantly enhanced the flame retardancy of polypropylene. Experimental results demonstrated that this system effectively improved the fire safety of PP by initiating a synergistic charring mechanism. However, the system exhibits a clear limitation: the UL-94 vertical burning V-0 rating can only be achieved when the total loading of the flame retardant exceeds 25 wt.%. This drawback is primarily attributed to the relatively low content of the piperazine/phenyl silicon component, which inherently lacks sufficient thermal stability and thus requires stabilization through a hydrogen-bonding network formed by melamine and cyanuric acid. Nevertheless, the melamine-cyanurate complex functions predominantly as a gas-phase blowing agent and does not significantly contribute to char layer formation, thereby limiting the system's overall charring efficiency.

In addition, the mechanical property analysis presented in Chapter 3 revealed a marked decline in toughness at high flame-retardant loadings. This deterioration is mainly due to the poor compatibility between the flame retardant and the PP matrix, resulting in weak interfacial adhesion. To address this, it is crucial to design novel flame-retardant molecules with thermoplastic deformation behavior, enabling better interaction with the PP matrix during melt blending and thereby improving both dispersion and overall composite performance.

Recent studies have highlighted that the molecular arrangement and aggregation behavior of flame-retardant groups have a significant impact on the performance of intumescent flame-retardant systems. For example, the aggregation of piperazine/triazine-based charring groups has been shown to effectively enhance the synergistic interaction with ammonium polyphosphate, leading to improved flame retardancy. [98] Furthermore, the chemical linkage modes between flame-retardant groups play an important role in tuning their thermal behavior. Previous research has demonstrated that block copolymerization of piperazine phosphate, melamine phosphate, and oxosilane monomers yields flame-retardant block copolymers with superior performance compared to physically blended systems of the same composition. Notably, such block copolymerization disrupts the chain regularity of polyphosphates, resulting

in a thermal softening effect that promotes better interfacial compatibility and mechanical properties in the final composites. [128]

These advances underline the critical importance of molecular composition and structural design in the development of efficient IFR systems. By precisely tuning the chemical linkage architecture, it is possible to simultaneously optimize flame-retardant efficiency, thermal behavior, and mechanical performance. Based on these insights, this chapter focuses on the design of a novel phosphorus-, nitrogen-, and silicon-containing flame-retardant monomer derived from the NSi-1 structure. This monomer was copolymerized with melamine phosphate at various feed ratios to synthesize a series of branched flame-retardant polymers. The objective is to achieve a synergistic improvement in both flame retardancy and mechanical properties of polypropylene, offering a new strategy for the development of high-performance IFR polypropylene composites.

4.2 Synthesis of PNSi-co-MP copolymers

The synthesis described in this section consists of two steps. In the first step, NSi-1 reacts with phosphoric acid to yield an intermediate - phenyltris(piperazinyl)silane phosphate (PNSi). In the second step, the monomer PNSi undergoes a dehydration reaction with melamine phosphate to form a randomly copolymerized macromolecule, PNSi-co-MP. The synthetic route is illustrated in Figure 4.1.

Initially, an 85 wt.% orthophosphoric acid solution (39.2 g, 0.34 mol) was dispersed in 500 mL of anhydrous ethanol under stirring to ensure uniform mixing. The mixture was then heated to 40 °C. Subsequently, a solution of NSi-1 (40 g, 0.11 mol) in 500 mL of dichloromethane was added dropwise into the ethanol-based system. During this process, dichloromethane introduced into the system was continuously removed via atmospheric distillation. Upon completion of the addition, the reaction mixture was maintained at 70 °C for 2 hours. The resulting intermediate, PNSi, was finally isolated by filtration.

As illustrated in Fig. 4.1, PNSi-co-MP copolymers were synthesized through a dehydration reaction between PNSi and MP. Four variants were prepared with different mass ratios of PNSi to MP (10:10, 12:8, 14:6, and 16:4). The synthesis procedure was as follows: PNSi and MP were weighed according to the ratios listed in Table 4.1 and thoroughly mixed. The resulting mixture was transferred to a vacuum oven, where it was heated to 280 °C for 1 hour under a vacuum of approximately 0.1 MPa. After cooling to room temperature inside the oven, PNSi-co-MP copolymers with various monomer ratios were successfully obtained, with a yield exceeding 99.0%.

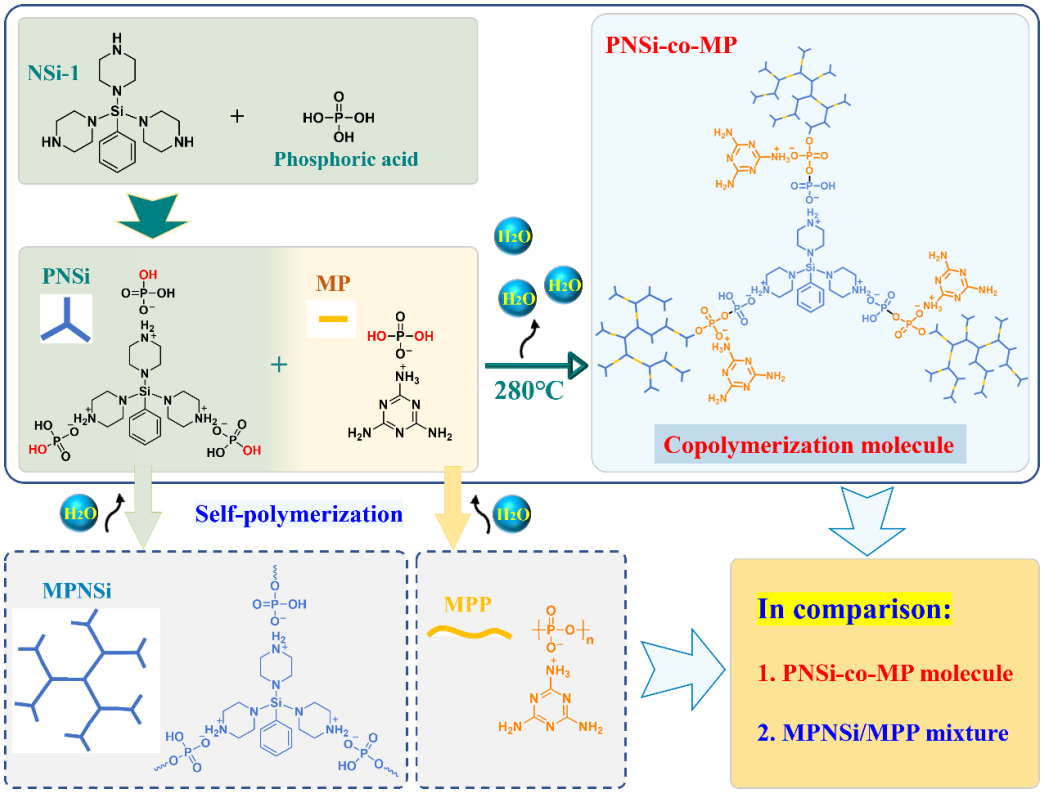

Fig. 4.1 The preparation of PNSi-co-MP molecule and the self-polymerized macromolecule (MPNSi) / MPP mixture.

Table 4.1 Feeding amounts of PNSi and MP monomers.

	10PNSi-co-10MP	12PNSi-co-8MP	14PNSi-co-6MP	16PNSi-co-4MP
PNSi:MP	10:10	12:8	14:6	16:4
PNSi/(g)	100	120	140	160
MP/(g)	100	80	60	40

In addition, a self-polymerized molecule from monomer PNSi was also prepared for building the mixture system MPNSi/MPP, as displayed in Fig. 4.2. A total of 200 g of the PNSi monomer was placed in a vacuum oven and subjected to a dehydration reaction at 280 °C for 1 hour under a vacuum pressure of approximately 0.1 MPa. After cooling, the resulting product, MPNSi, was obtained by grinding. By the way, the purchased MPP was also manufactured by the dehydration process of MP monomer.

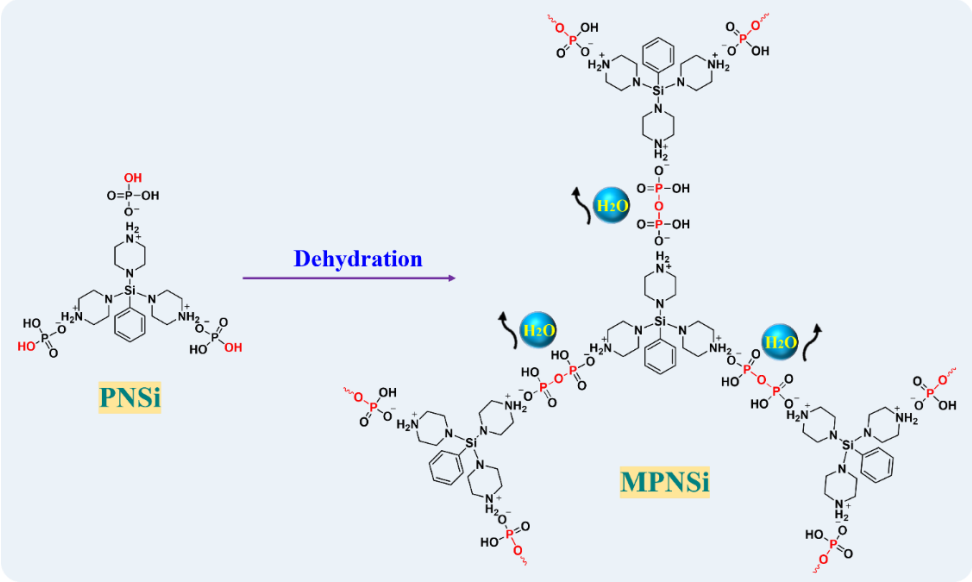

Fig. 4.2 The preparation process of MPNSi.

4.3 Fabrication of PP composites

The flame-retardant polypropylene composites were prepared according to the formulations listed in Table 4.2. The processing and molding techniques employed included extrusion, injection molding, and compression molding. The detailed procedures were consistent with those described in Section 3.3.

Table 4.2 Formulation (wt.%) of flame retardant PP composites.

	*m*PNSi-co-*n*MP	MPNSi	MPP	PP	Others*
PP	0	0	0	99	1
10PNSi-co-10MP/PP	20	0	0	79	1
10MPNSi/10MPP/PP	-	10	10	79	1
12PNSi-co-8MP/PP	20	-	-	79	1
12MPNSi/8MPP/PP	-	12	8	79	1
14PNSi-co-6MP/PP	20	-	-	79	1
14MPNSi/6MPP/PP	-	14	6	79	1
16PNSi-co-4MP/PP	20	-	-	79	1
16MPNSi/4MPP/PP	-	16	4	79	1

* Other additives included PTFE (0.4 wt.%), antioxidant 168 (0.3 wt.%), and antioxidant 1010 (0.3 wt.%).

4.4 Structural characterization of PNSi and MPNSi

The primary raw material, NSi-1, consists of Si, C, H, and N elements, as illustrated in Fig. 4.3(b). It should be noted that hydrogen (H) could not be detected by the employed EDS

equipment. Following the acid–base reaction between NSi-1 and orthophosphoric acid (H_3PO_4), the resulting product, PNSi, is expected to contain P, O, Si, C, H, and N—an elemental composition that was verified by the EDS results shown in Fig. 4.3(a).

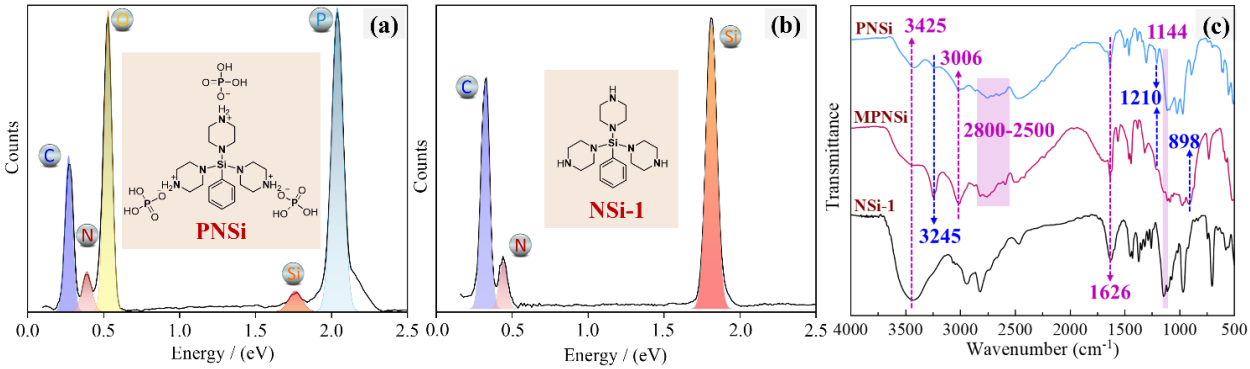

Fig. 4.3 The characterization results of PNSi monomer and MPNSi control sample: EDS results for (a) PNSi and (b) NSi-1; (c) FTIR curves of PNSi, MPNSi and NSi-1.

Further structural confirmation was provided by FTIR spectroscopy. As shown in Fig. 4.3(c), PNSi exhibited characteristic absorption bands at 3006 and 2800-2500 cm^{-1}, attributed to the presence of $-NH_2^+$ groups, indicating the formation of ionic assemblies. Additional FTIR signals corroborated the presence of other functional groups within the PNSi structure [127][233][234], including N-H (3425 cm^{-1}), phenyl (Ph) skeletal vibrations (1626 cm^{-1}), Si-Ph (1144 cm^{-1}), P=O (1210 cm^{-1}), and P-OH (3245 cm^{-1}). These spectral features provided further evidence supporting the chemical composition of PNSi. The proposed reaction pathway for MPNSi synthesis is illustrated in Fig. 4.2. Due to its similar backbone, MPNSi exhibited an FTIR profile closely resembling that of PNSi. The key difference, however, was the appearance of a new absorption peak at 898 cm^{-1}, corresponding to the P-O-P bond. This peak indicated that a dehydration condensation reaction occurred among the -OH groups of PNSi. Moreover, as shown in Fig. 4.4(b), the ^{31}P NMR spectra of MPNSi and PNSi revealed distinct phosphorus chemical shifts, further confirming that self-polymerization led to changes in the chemical environment of the phosphorus-containing structures. Collectively, these analytical results demonstrate the successful synthesis of both the PNSi monomer and the MPNSi polymer.

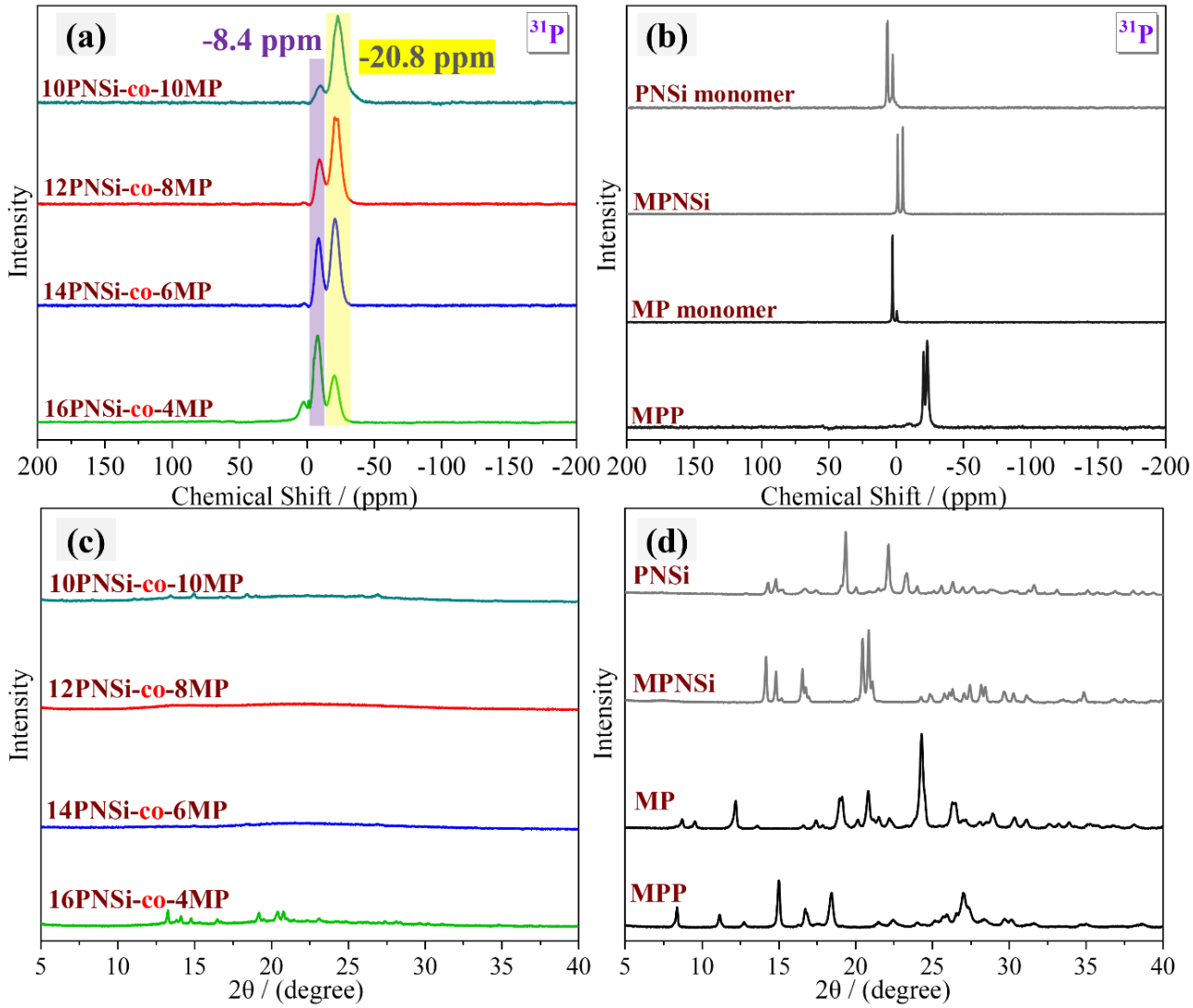

Fig. 4.4 Solid-state ^{31}P NMR spectra (a,b) and XRD patterns (c,d) of PNSi-co-MP and monomers and their self-polymerization products, respectively.

The PNSi-co-MP copolymers were synthesized via a random dehydration reaction between the P–OH groups of the PNSi and MP monomers. As shown in Fig. 4.5, all four FTIR spectra of the resulting PNSi-co-MP samples exhibited a characteristic absorption peak at 896 cm^{-1}, attributed to the formation of P–O–P linkages. This observation confirmed the occurrence of the polymerization reaction.

Further structural characterization was conducted using solid-state ^{31}P NMR and XRD analyses, as presented in Fig. 4.4. In the ^{31}P NMR spectra (Fig. 4.4a), chemical shifts at −8.4 and −20.8 ppm were assigned to phosphorus atoms in the PNSi and MP units, respectively. The spectra of PNSi, MP, and their self-polymerized products displayed sharp peaks (Fig. 4.4b), whereas the four PNSi-co-MP copolymers showed broader signals. This broadening was attributed to the random nature of copolymerization, which led to phosphorus atoms occupying

diverse chemical environments within the macromolecular structure. In contrast, the self-polymerization processes (i.e., PNSi to MPNSi and MP to MPP) only caused minor alterations in the P atom chemical shifts. Additionally, the relative intensities of the two peaks correlated well with the feed ratios of the respective monomers. XRD analysis further revealed that both monomers and their self-polymerized counterparts exhibited high crystallinity (Fig. 4.4d), whereas the PNSi-co-MP copolymers demonstrated nearly amorphous characteristics (Fig. 4.4c). This significant loss of crystallinity was attributed to the disruption of molecular regularity caused by the random copolymerization, further supporting the conclusion that the reaction was a copolymerization rather than independent self-polymerization of the two components. Finally, morphological analysis by SEM (Fig. 4.6) revealed that the PNSi-co-MP copolymers exhibited a distinct plate-like morphology with a thickness of approximately 2 μm. In contrast, MPNSi and MPP appeared as irregularly shaped particles. These findings collectively confirm the successful synthesis of the four PNSi-co-MP copolymers.

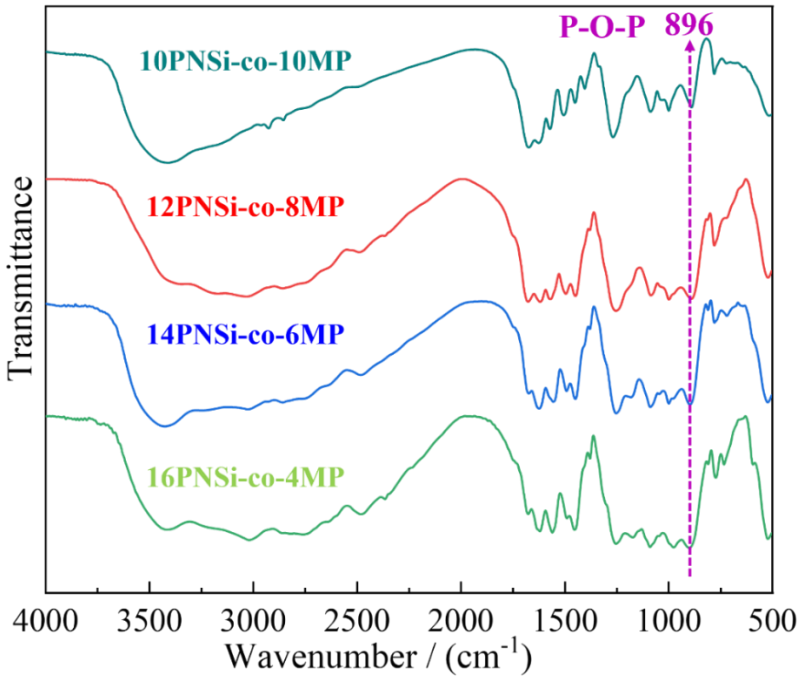

Fig. 4.5 The FTIR spectra of copolymer PNSi-co-MP.

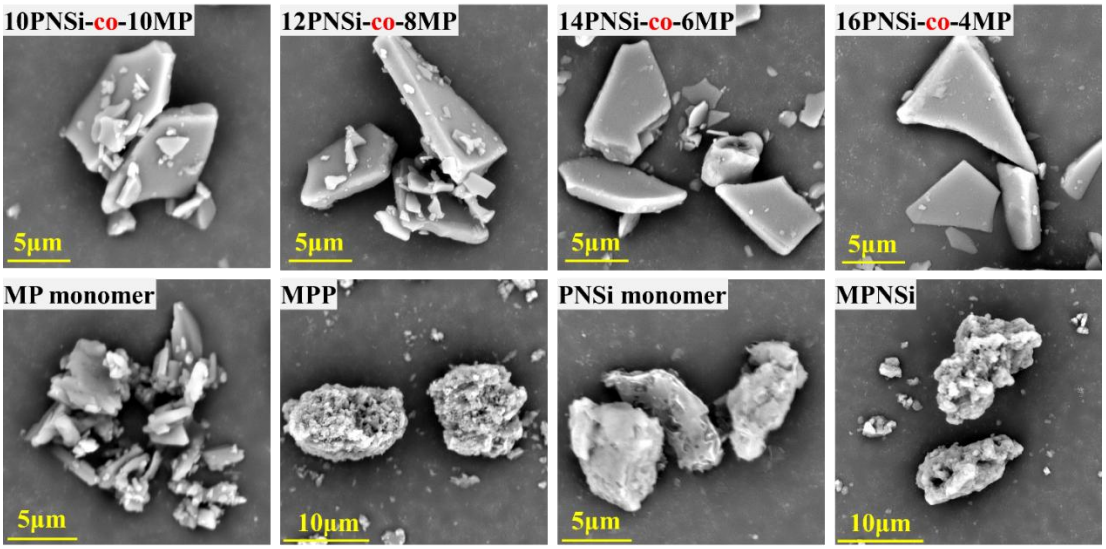

Fig. 4.6 SEM morphologies of four PNSi-co-MP, PNSi, MPNSi, MP and MPP.

4.5 The mechanical properties of PP composites

The representative mechanical properties of the composites are presented in Fig. 4.7. As shown in Figs. 4.7 (a) and 3(e), all four polypropylene composites containing 20 wt.% of PNSi-co-MP copolymer exhibited significantly higher elongation at break values compared to those incorporating the mixed MPNSi/MPP system. Notably, the 16PNSi-co-4MP/PP composite achieved an elongation at break of 120.8%, approximately 278% higher than that of the 16MPNSi/4MPP/PP counterpart. The stress–strain behavior of the flame-retardant composites is illustrated in Fig. 4.7 (d). For the MPNSi/MPP/PP samples, a sharp decline in tensile stress occurred after yielding, leading to abrupt fracture at an elongation of roughly 30%. In contrast, the PNSi-co-MP/PP composites demonstrated a "slow ductile fracture" mode. After the cold drawing stage, the tensile stress gradually diminished to approximately 0 MPa, indicating a progressive tearing process under tensile loading. This behavior suggests that the PP matrix retained considerable ductility despite the high filler loading (20 wt.%) of the copolymerized flame retardant. Typically, maintaining such toughness in PP at this filler level would require the addition of a compatibilizer. Moreover, the tensile strengths of the PNSi-co-MP/PP and MPNSi/MPP/PP samples were found to be nearly equivalent, as shown in Fig. 4.7(e). However, regarding impact performance, the PNSi-co-MP/PP composites outperformed those with the mixed IFR system. For instance, the 16PNSi-co-4MP/PP sample exhibited an unnotched impact strength 33.3% higher than that of its 16MPNSi/4MPP/PP counterpart. These findings clearly demonstrate that the copolymerized flame-retardant macromolecules and the self-polymerized IFR blends imparted fundamentally different mechanical behaviors to the PP composites, despite having nearly identical chemical compositions.

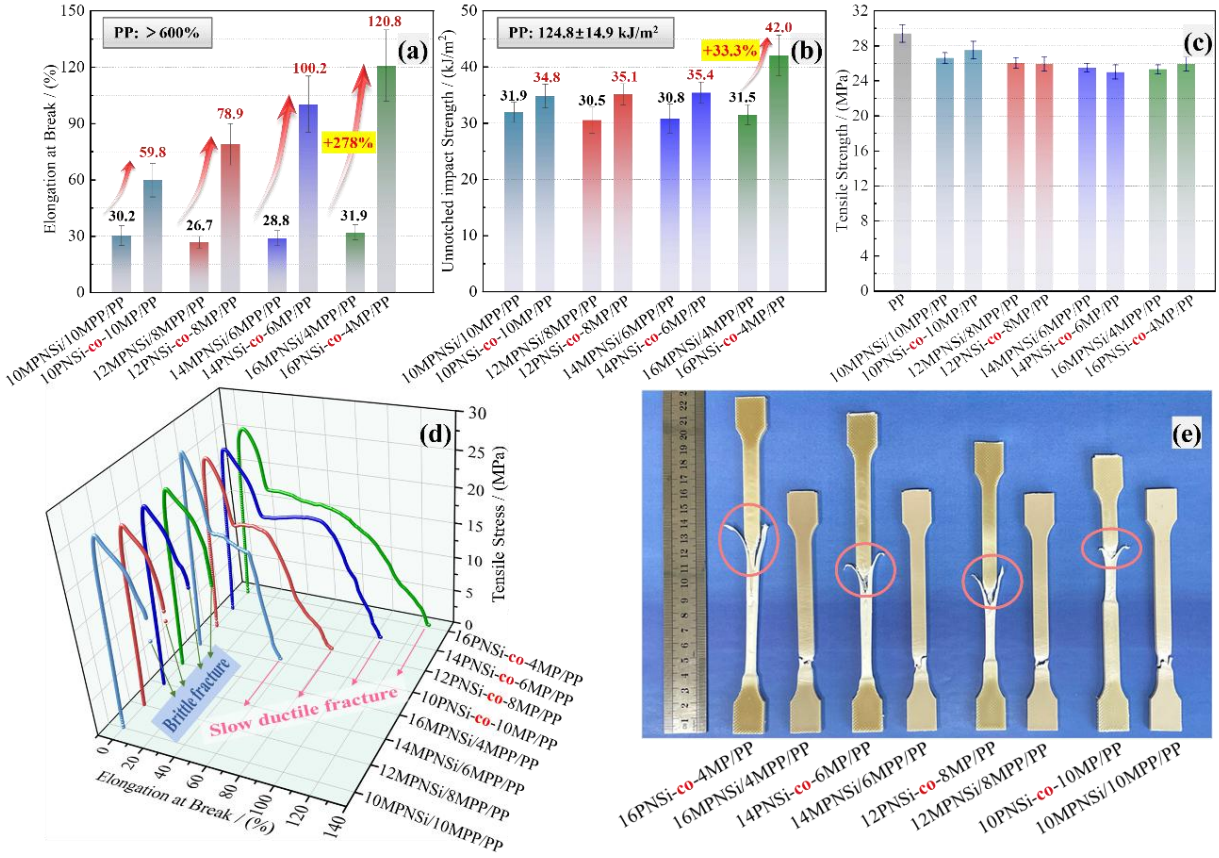

Fig. 4.7 The mechanical performance of PP composites.

4.6 Mechanical failure mechanism

To elucidate the mechanism underlying the superior mechanical properties of PP composites containing copolymerized molecules compared to those with MPNSi/MPP, scanning electron microscopy was employed to examine the fracture surfaces, as shown in Fig. 4.8. The SEM images in Figs. 4.8(e1–e3) clearly demonstrate poor interfacial compatibility between the 16MPNSi/4MPP mixture and the PP matrix. Evident filler–matrix separation and a lack of interfacial adhesion were observed, along with severe agglomeration of MPNSi and MPP particles within the polymer phase. These morphological features are consistent with the diminished mechanical performance observed in the MPNSi/MPP/PP composites. In contrast, the PNSi-co-MP-filled composites exhibited markedly improved morphological characteristics. As shown in Figs. 4.8(a1–d1) and (a2–d2), the copolymerized flame retardants did not exhibit noticeable aggregation. Furthermore, Figs. 4.8(a3–d3) reveal that the PNSi-co-MP particles were well integrated into the PP matrix, indicating favorable interfacial interactions. Interestingly, the morphology and size of the PNSi-co-MP particles embedded in the PP matrix differed from their original plate-like morphology (~5–10 μm). This transformation is explained by the DSC analysis (Fig. 4.9), which revealed that PNSi-co-MP possesses a glass

transition temperature, implying its ability to undergo thermal softening during melt processing. As a result, composites with 12PNSi-co-8MP and 14PNSi-co-6MP showed spherical copolymer particles uniformly dispersed throughout the matrix. Additionally, some rod-like PNSi-co-MP structures were observed in the 16PNSi-co-4MP/PP sample (Figs. 4.8 a1 and a2). These rod-shaped particles were fractured under external stress, potentially contributing to enhanced energy absorption compared to spherical particles. Most of the dispersed copolymer particles were within the 1–3 μm size range, with a minor fraction as small as 200–300 nm. The uniform dispersion along with strong interfacial adhesion between the PNSi-co-MP and the PP matrix, collectively contributed to the improved mechanical behavior of the copolymer-modified composites.

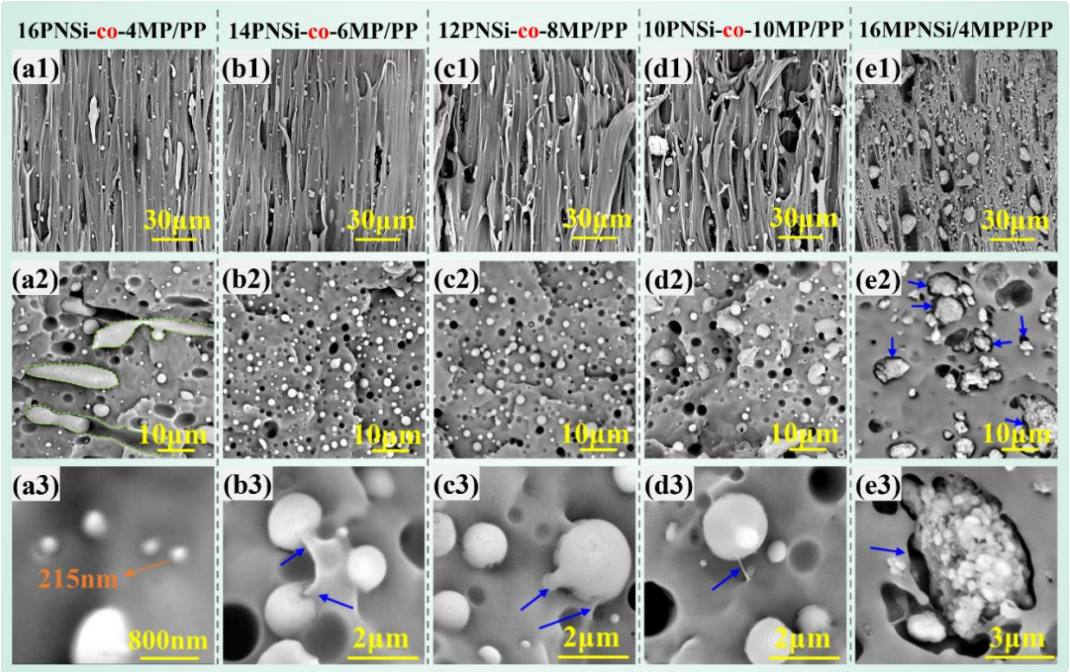

Fig. 4.8 SEM photographs of (a1–e1) tensile and (a2–e3) impact fracture surfaces.

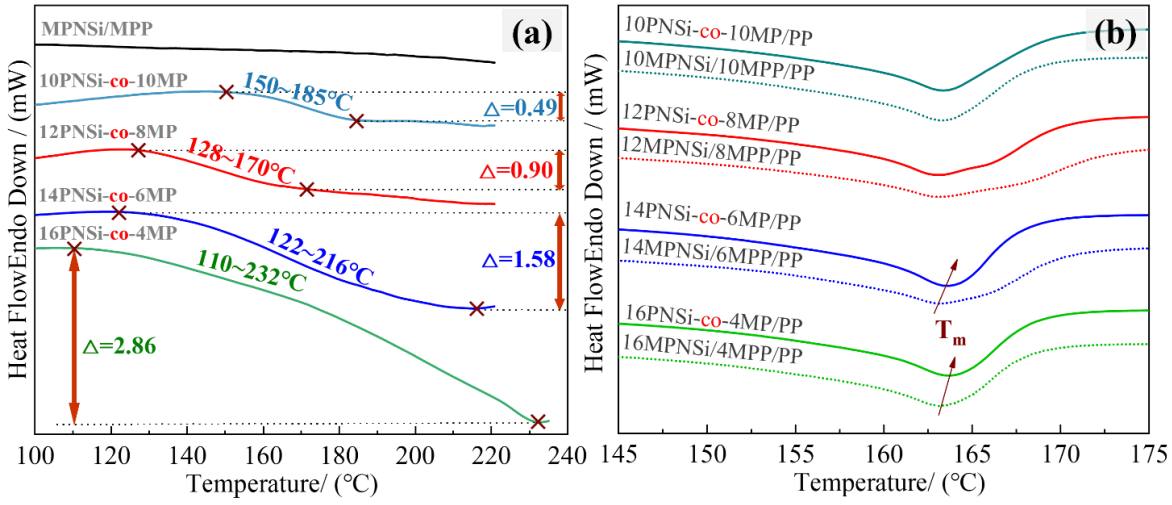

Fig. 4.9 DSC curves of (a) PNSi-co-MP and (b) PP composites.

To further elucidate the morphological transformation of the copolymerized PNSi-co-MP molecules during melt blending with the PP matrix, differential scanning calorimetry was performed, and the results are presented in Fig. 4.9. As shown in Fig. 4.9(a), the PNSi-co-MP copolymers exhibited distinct glass transition behavior, whereas the MPNSi/MPP mixture showed no noticeable endothermic transitions below 220 °C. This difference is attributed to the crystallinity of the respective compounds. The random copolymerization disrupted the regular packing of monomer units, thereby reducing crystallinity and allowing the material to undergo glass transition at lower temperatures. In contrast, the highly crystalline MPNSi and MPP structures remained thermally stable below the PP processing temperature. Moreover, the onset temperature of the glass transition decreased with increasing PNSi content in the PNSi-co-MP copolymer, accompanied by an enhanced heat absorption signal. This indicates that the molecular mobility and softening behavior of the copolymer increased as the PNSi fraction rose. As a result, the copolymerized molecules underwent shape transformation during melt processing, driven by both glass transition effects and mechanical shear from extrusion. Additionally, Fig. 4.9(b) reveals that the melting temperatures (T_m) of 16PNSi-co-4MP and 14PNSi-co-6MP were slightly elevated compared to those of their control counterparts. This phenomenon suggests the presence of intermolecular interactions—specifically, between the piperazine or phenyl groups in the PNSi backbone and the PP molecular chains. Such interactions are likely to facilitate interfacial bonding, as also reflected in the morphological features observed in Figs. 4.9 b3, c3, and d3. These intermolecular associations not only promoted morphological integration but also played a critical role in enhancing the mechanical performance of the resulting composites.

4.7 Flame retardancy

The flame-retardant performance parameters, including glow-wire ignition temperature, glow-wire flammability index, limiting oxygen index, and UL-94 vertical burning classification, are summarized in Fig. 4.10. The incorporation of PNSi-co-MP copolymers substantially enhanced the flame resistance of pure polypropylene. Notably, the composite containing 20 wt.% 12PNSi-co-8MP achieved a GWFI exceeding 960 °C, a GWIT of 875 °C, an LOI of 30.2%, and a UL-94 V-0 rating. Crucially, although the PNSi-co-MP copolymers and MPNSi/MPP mixtures performed equivalent chemical compositions and additive loadings, the copolymerized systems exhibited significantly superior flame-retardant efficiencies. For instance, 10PNSi-co-10MP/PP attained a UL-94 V-0 classification, whereas the corresponding 10MPNSi/10MPP/PP composite failed to pass any UL-94 level test. Similarly, the LOI value

of 12PNSi-co-8MP/PP surpassed that of 12MPNSi/8MPP/PP by 2.3%. In terms of thermal ignition properties, the 12PNSi-co-8MP/PP sample demonstrated GWIT and GWFI values that were 50 °C and 135 °C higher, respectively, than those of MPNSi/MPP-based PP. These comparative results clearly indicate that covalently integrating the flame-retardant functional groups within a single macromolecular structure significantly boosts flame-retardant efficiency, relative to physically blended multi-component systems.

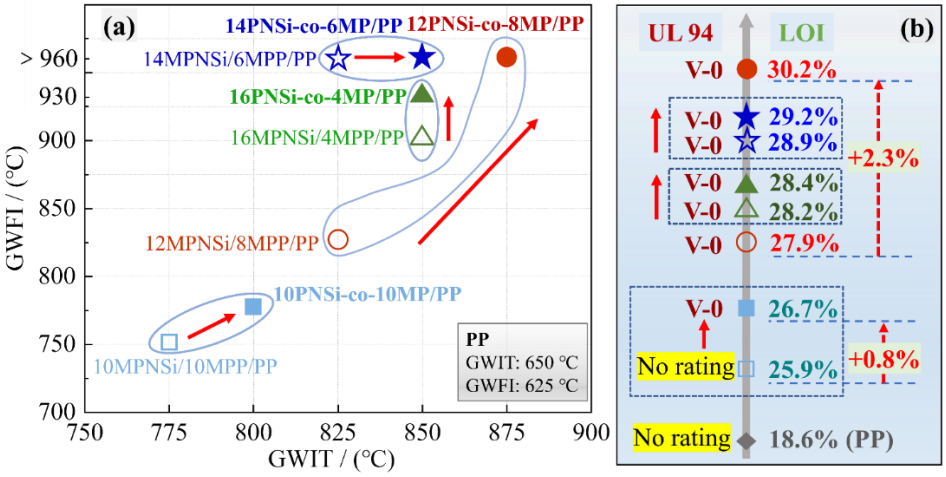

Fig. 4.10 Typical flame retardancy of designed PP composites.

The results of the glow-wire test for the 12PNSi-co-8MP/PP and 12MPNSi/8MPP/PP composites are illustrated in Fig. 4.11. Upon contact with an 875 °C glow wire for 5 and 10 seconds, the surface of 12PNSi-co-8MP/PP exhibited a notably smaller flame than that observed on 12MPNSi/8MPP/PP. Moreover, in the case of 12PNSi-co-8MP/PP, the flame self-extinguished at 15 and 25 seconds, whereas in the MPNSi/MPP-based sample, complete flame extinction occurred only at 25 seconds. These results suggest that 12PNSi-co-8MP/PP experienced significantly less thermal degradation under identical test conditions. This enhanced performance is attributed to the rapid formation and superior integrity of the char layer generated by the PNSi-co-MP system. As revealed by the FTIR spectra in Fig. 6, the char residue from the 12PNSi-co-8MP/PP composite was richer in carbonaceous structures, such as P–O–C linkages, C=C and C–C bonds, and aliphatic –CH_n groups, than the reference sample. This observation supports the hypothesis that the covalent integration of PNSi and MP units within a single macromolecular framework facilitates rapid intramolecular charring reactions. Additionally, it promotes crosslinking between the flame-retardant moieties and the PP matrix, effectively immobilizing more carbonaceous species within the condensed-phase residue.

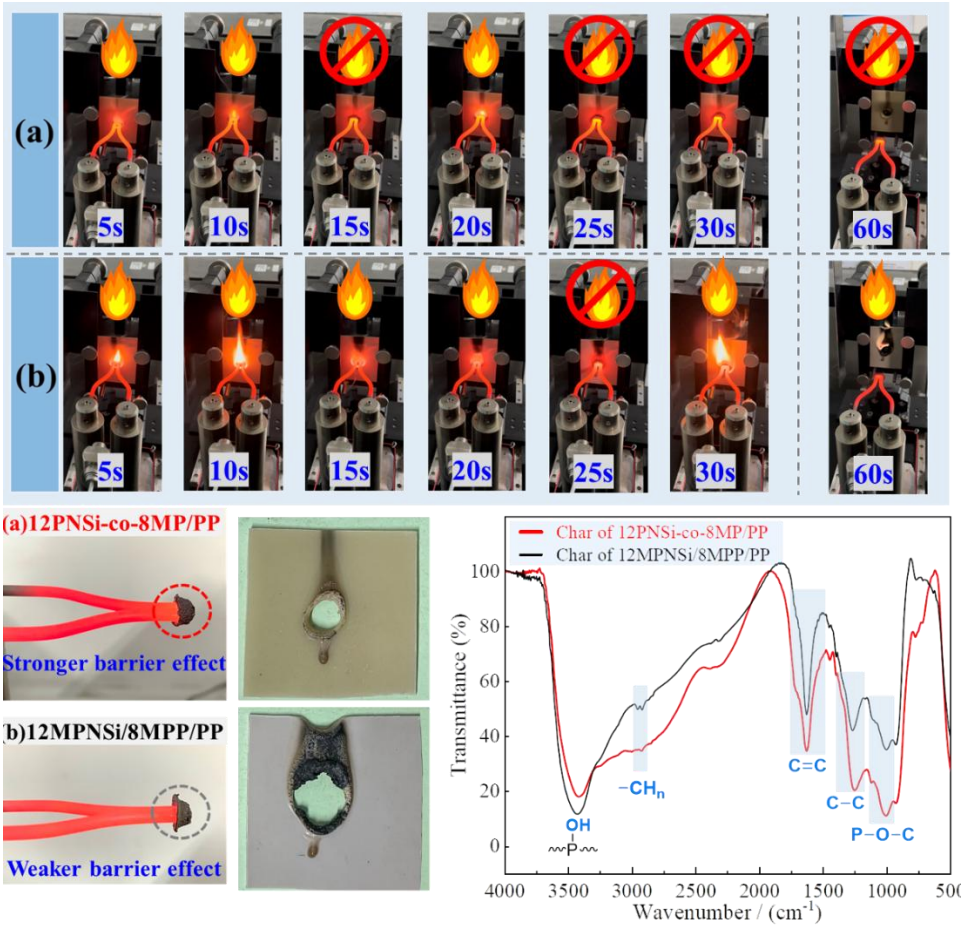

Fig. 4.11 The glow-wire test (875℃) phenomenon and char layer analysis.

Under forced irradiation in the cone calorimeter test, the polypropylene composites incorporating PNSi-co-MP copolymers exhibited outstanding fire-safety performance. As shown in Figs. 4.12(a, b) and summarized in Table 4.3, all four PNSi-co-MP/PP composites demonstrated significantly reduced peak heat release rates and peak smoke production rates compared to neat PP. Among them, the dendritic macromolecule 12PNSi-co-8MP, synthesized via copolymerization of PNSi and MP at a mass ratio of 12:8, showed the most pronounced flame-retardant efficiency. Specifically, its composite exhibited a remarkably low PHRR of 102 $kW \cdot m^{-2}$ and a PSPR of 0.021 $m^2 \cdot s^{-1}$, representing reductions of 93.6% and 87.2%, respectively, relative to unmodified PP. These findings highlight the efficacy of incorporating both PNSi and MP motifs within a single macromolecular structure to form an efficient intumescent flame-retardant (IFR) system. Furthermore, the PNSi-to-MP ratio was found to critically influence the fire performance of the resulting copolymers. When the proportion of PNSi was excessively high, the flame-retardant performance diminished. For instance, both 14PNSi-co-6MP/PP and 16PNSi-co-4MP/PP exhibited secondary peaks at 500–600 s in their HRR and SPR curves, as seen in Figs. 4.12(a) and 7(b), suggesting that volatile decomposition

products breached the char layer, triggering a resurgence in combustion. This phenomenon was further supported by SEM images in Figs. 10(c) and (d), which revealed morphological flaws in the char layers of these samples. It is inferred that an overabundance of the PNSi component characterized by its rigid siloxane and phenyl groups may compromise the mechanical integrity and elasticity of the protective char, leading to premature structural failure during combustion.

Furthermore, as illustrated in Figs. 4.12(a, b), 12PNSi-co-8MP/PP composite exhibited PHRR and PSPR values that were 49.0% and 62.5% lower, respectively, than those of the 12MPNSi/8MPP/PP sample. This significant difference in flame-retardant performance highlights the superior efficiency of the copolymerized 12PNSi-co-8MP structure over the physically blended MPNSi/MPP mixture, despite both systems having nearly identical chemical compositions and loadings. A more visually intuitive comparison is presented in Fig. 4.12(c), where the 12PNSi-co-8MP/PP sample suppressed flame propagation more rapidly in the early stages of combustion. This enhanced initial flame inhibition is likely attributed to the prompt onset of the charring reaction following ignition, resulting in the rapid formation of a protective carbonaceous layer that acts as an effective thermal and mass barrier. Collectively, these results underscore that, beyond the elemental composition, the molecular architecture, specifically the covalent linkage of functional groups within the macromolecule, plays a decisive role in dictating flame-retardant effect.

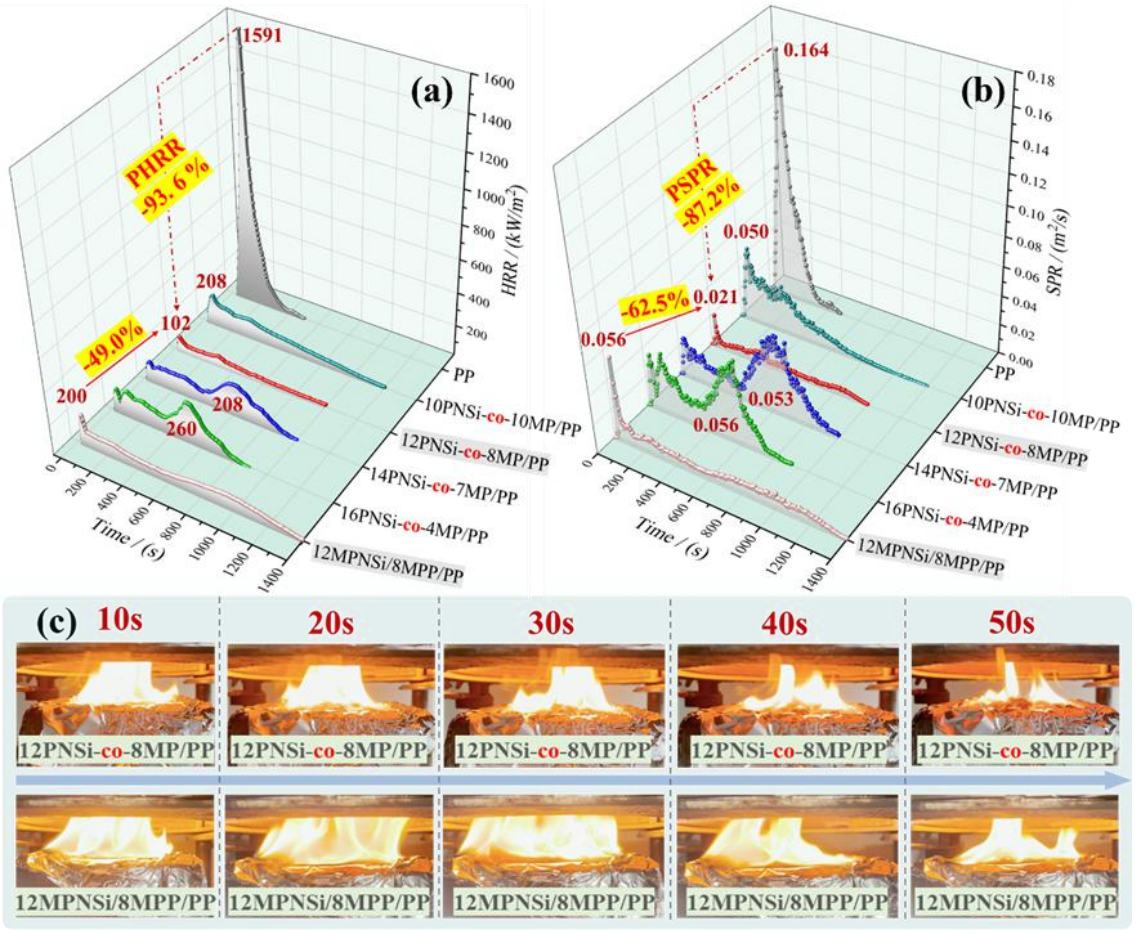

Fig. 4.12 (a) HRR and (b) SPR curves and (c) combustion conditions in initial stage.

Table 4.3 Typical parameters of samples from cone calorimeter tests.

Sample	TTI /s	PHRR /kW·m^{-2}	PSPR /m^2·s^{-1}	THR /MJ·m^{-2}	av-EHC /MJ·kg^{-2}	TSR /m^2·m^{-2}	FPI /s·m^2·kW^{-1}	Residue /%	FRI
PP	28	1591	0.164	151.6	52.7	2109	0.018	0.7	-
10PNSi-co-10MP/PP	26	208	0.050	108.4	40.1	1473	0.125	25.1	9.93
12PNSi-co-8MP/PP	23	**102**	**0.021**	**46.0**	**36.2**	**408**	**0.225**	**61.4**	**42.23**
14PNSi-co-6MP/PP	20	208	0.053	113.3	41.6	2195	0.096	13.3	7.31
16PNSi-co-4MP/PP	18	260	0.056	110.9	41.4	2116	0.069	15.4	5.38
12MPNSi/8MPP/PP	23	200	0.056	108.4	42.2	1070	0.115	20.8	9.14

As shown in Fig. 4.13(d), the time to ignition of the PP composites containing PNSi-co-MP compounds was shorter than that of neat PP. Moreover, a higher PNSi content in the copolymer correlated with a further reduction in TTI, suggesting that the PNSi backbone played a critical role in interacting with the PP matrix and initiating thermal decomposition. The fire performance index (FPI), defined as TTI divided by the PHRR, is indicative of the delay in flash ignition under large-scale fire conditions - a higher FPI value corresponds to lower fire

risk. Although the copolymerized flame-retardant systems exhibited lower TTI values than neat PP, their significantly reduced PHRR resulted in notably higher FPI values. Specifically, both the 12PNSi-co-8MP/PP and 12MPNSi/8MPP/PP composites showed a TTI of 23 s and a time to PHRR of 40 s, indicating that only 17 s were required for flame retardants to effectively suppress fire growth. However, due to its much lower PHRR, 12PNSi-co-8MP/PP exhibited an FPI value that was 95.7% higher than that of the 12MPNSi/8MPP/PP sample, as shown in Fig. 4.14. Additionally, the fire growth index, calculated as PHRR divided by TTP, provides insight into the speed of fire development - a lower FGI signifies lower fire hazard. The FGI of 12PNSi-co-8MP/PP was 49.0% lower than that of its MPNSi/MPP-based sample, indicating a slower and safer combustion process. Furthermore, the flame retardancy index (FRI) [11][235], which offers a comprehensive assessment of fire resistance, further confirmed the outstanding performance of the copolymerized system. The FRI value of 12PNSi-co-8MP/PP exceeded 40, while all other samples registered values below 10. These findings demonstrate the superior flame-retardant efficiency of the 12PNSi-co-8MP copolymer. The combination of high FPI, low FGI, and outstanding FRI clearly illustrates that copolymerization is an effective strategy to enhance the fire safety performance of PP composites when compared to simple physical mixtures of flame-retardant components.

The average effective heat of combustion values, calculated as the ratio of the heat release rate to the mass loss rate, are listed in Table 4.3. This parameter reflects the extent of combustion of volatile substances in the gas phase. Neat polypropylene underwent complete combustion and exhibited an av-EHC of 52.7 $MJ \cdot kg^{-1}$. Upon incorporation of the flame-retardant systems, all composite samples showed significantly reduced av-EHC values, indicating a lower degree of volatile-phase combustion. Notably, the 12PNSi-co-8MP/PP sample exhibited the lowest av-EHC value of 36.2 $MJ \cdot kg^{-1}$, demonstrating the superior gas-phase flame-retardant performance of the copolymerized PNSi-co-MP molecule, which effectively suppressed full combustion in the gas phase. The av-EHC values were also closely related to the char-forming ability of the composites. As shown in the mass loss curves in Fig. 4.13(c), the 12PNSi-co-8MP/PP sample retained a high residual yield of 61.4% after combustion, highlighting its excellent charring capability. In contrast, the control sample 12MPNSi/8MPP/PP exhibited a much lower residue yield of only 20.8%. The substantial char yield of 12PNSi-co-8MP/PP indicated that a significant portion of the flame-retardant components remained in the condensed phase, thereby reducing the amount of combustible volatiles available for gas-phase reactions. As a result, the total heat release and total smoke release (TSR) of the 12PNSi-co-8MP/PP composite were measured to be 46 $MJ \cdot m^{-2}$ and 408

$m^2 \cdot m^{-2}$, respectively. These values represent reductions of 57.6% and 61.9%, respectively, compared to the composite containing the mixed 12MPNSi/8MPP system, as shown in Figs. 4.13(a) and (b). These results clearly demonstrate that copolymerizing PNSi and MP monomers into a single macromolecule significantly enhances the flame-retardant performance of PP composites. This improvement is attributed to the fact that the charring and flame-retardant reactions initiated within a single molecular framework are more efficient and faster than those occurring between separate flame-retardant components.

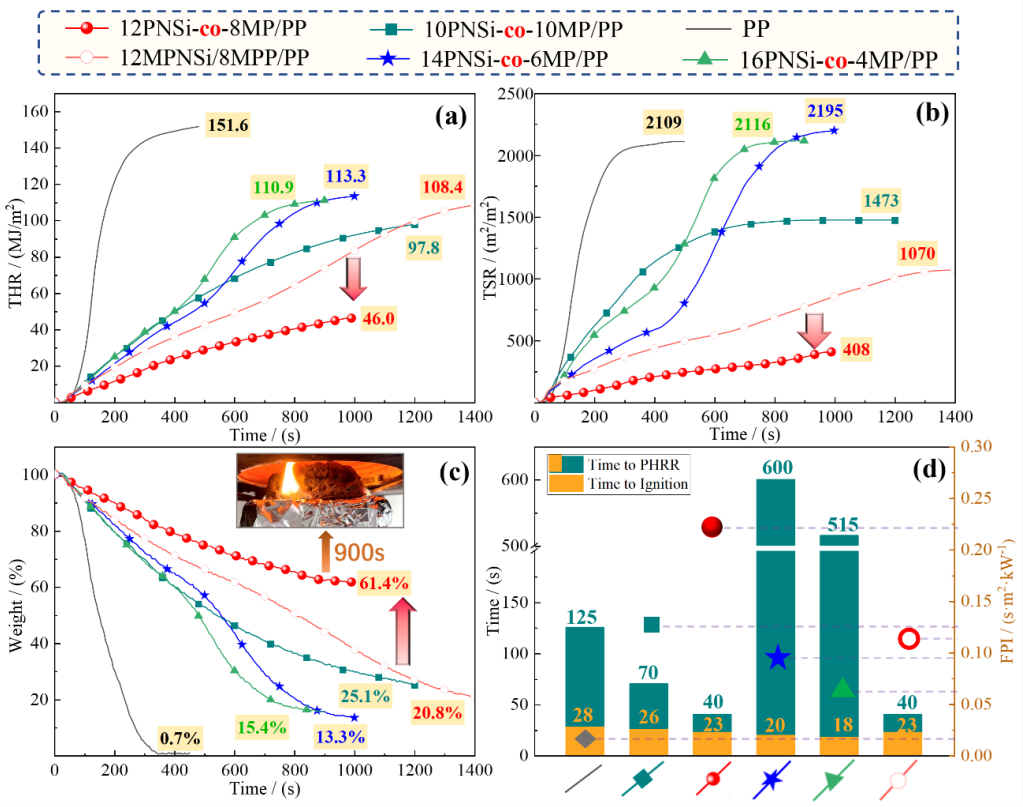

Fig. 4.13 (a) THR, (b) TSR and (c) mass loss curves and (d) some typical parameters of fire safety performance.

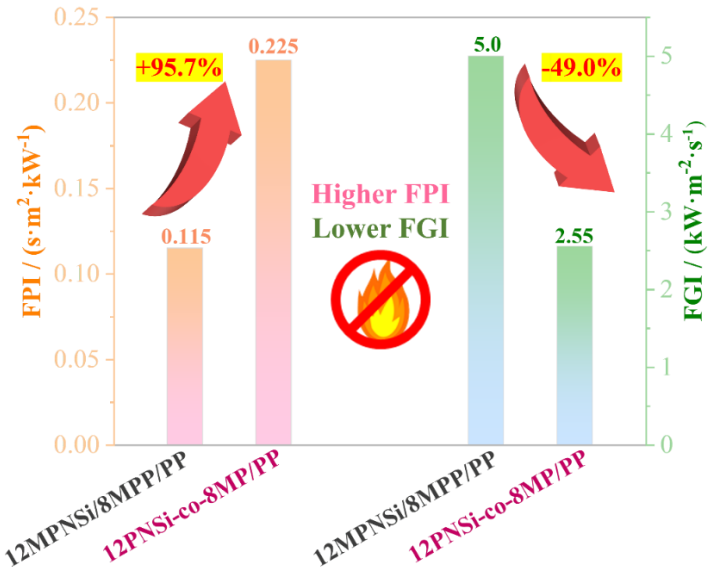

Fig. 4.14 The fire safety performance of copolymer 12PNSi-co-8MP/PP and mixed 12MPNSi/8MPP/PP samples.

4.8 Barrier effect of char layers

The barrier effect of the char layer plays a pivotal role in the performance of intumescent flame retardants. To evaluate this effect, particularly the thermal insulation capability of the char layer, an infrared thermal imager was employed to monitor the back-surface temperature of PP plate samples during combustion. The surface temperature distributions of the samples are presented in Fig. 4.15. Under identical flame exposure conditions, it is evident from Fig. 4.15 that the 12PNSi-co-8MP/PP sample exhibited a significantly smaller high-temperature region compared to the 12MPNSi/8MPP/PP sample. This observation indicates that the copolymerized 12PNSi-co-8MP molecule facilitated the formation of effective char layers with the PP matrix more rapidly than the physically blended 12MPNSi/8MPP mixture. The earlier formation of these char layers resulted in enhanced suppression of heat and mass transfer, thereby contributing to better flame-retardant performance. Since it is considerably more challenging to inhibit combustion after flame propagation has intensified, the rapid development of protective char layers at the early stages of ignition is critical. The molecular-level integration of PNSi and MP in the copolymer structure evidently accelerated the charring reaction, thereby significantly improving the barrier effect and overall fire resistance of the composite.

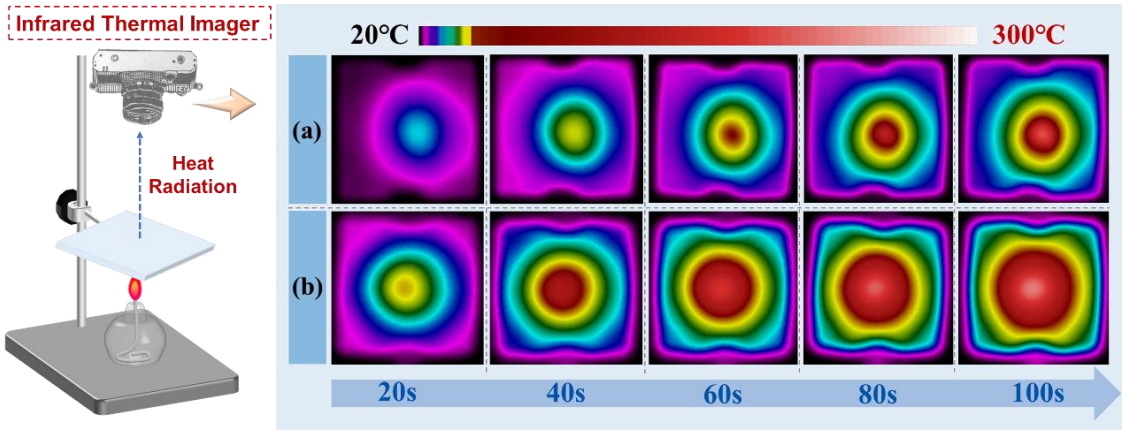

Fig. 4.15 Infrared thermal images of (a) 12PNSi-co-8MP/PP and (b) 12MPNSi/8MPP/PP.

4.9 Characterization of char residue

The surface morphology and EDS elemental maps of the char layers after cone calorimeter testing are shown in Fig. 4.16. A substantial amount of residue was retained in the condensed phase for the PNSi-co-MP/PP composites, demonstrating the excellent charring ability of the copolymerized PNSi-co-MP structures in conjunction with the PP matrix. Among all samples, 12PNSi-co-8MP/PP exhibited the best flame retardancy, primarily due to the formation of relatively compact and dense char layers, as illustrated in Fig. 4.16(b1). In contrast, the sample containing the physically blended 12MPNSi/8MPP system exhibited a loose and porous char structure with numerous voids, as shown in Fig. 4.16(e1). A closer examination of the char layers in the magnified images (Figs. 4.16(b2) and (e2)) revealed the presence of embedded particles, which were primarily composed of silicon (Si), phosphorus (P), and oxygen (O), based on the EDS elemental distribution. These findings suggest that chemical reactions occurred between the silicon-containing groups and phosphoric acid groups, leading to the formation of Si–P–O-based particles that may contribute to reinforcing the char layer. Notably, in Fig. 4.16(b2), these particles were uniformly distributed throughout the char, whereas in Fig. 4.16(e2), particle agglomeration was evident, potentially weakening the structural integrity of the char layer. To further elucidate the interactions between the flame retardant and the PP matrix, elemental compositions obtained from SEM-EDS analysis are listed in Table 4.4. A striking difference was observed in the carbon (C) content: the char from 12PNSi-co-8MP/PP contained approximately 30.5 wt.% C, which was 10.0 wt.% higher than that of the 12MPNSi/8MPP/PP sample. This result indicates that the copolymerized 12PNSi-co-8MP exhibited a significantly enhanced charring capability when combined with the PP matrix, compared to the mixed system. Moreover, the nitrogen (N) content in the 12PNSi-co-8MP/PP char was also slightly higher than that in the 12MPNSi/8MPP/PP char, which may be attributed

to the presence of piperazine units - an N-containing structure that likely plays a vital role in promoting the charring process. In conclusion, these results confirm that the copolymer structure of 12PNSi-co-8MP markedly enhances its interaction with the PP matrix, leading to more effective carbon- and nitrogen-rich char formation and thereby improving the overall flame-retardant performance of the composite.

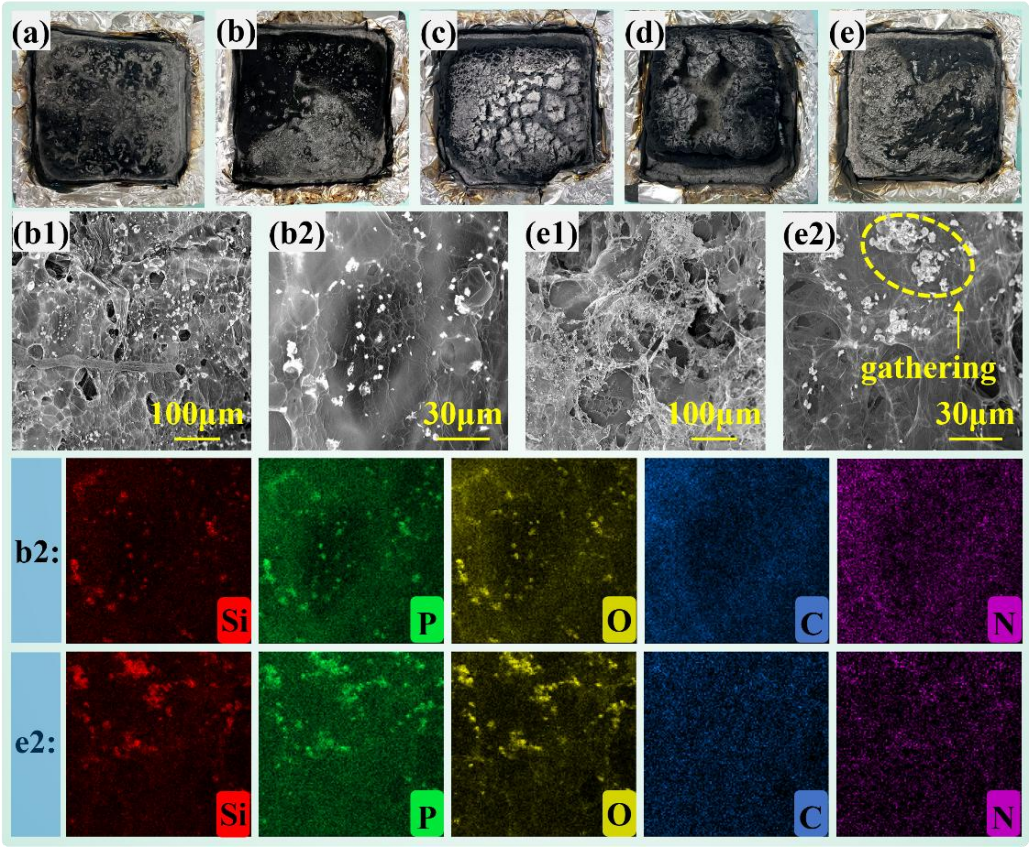

Fig. 4.16 Morphology and EDS maps of surficial char layers: (a) 10PNSi-co-10MP/PP; (b) 12PNSi-co-8MP/PP; (c) 14PNSi-co-6MP/PP; (d) 16PNSi-co-4MP/PP; (e) 12MPNSi/8MPP/PP.

Table 4.4 The element contents (wt.%) of chars from cone calorimeter tests by SEM-EDS.

Sample	C	N	P	O	Si
12PNSi-co-8MP/PP	**30.5±2.8**	13.9±0.7	6.5±0.4	47.6±5.1	1.5±0.2
12MPNSi/8MPP/PP	24.5±3.5	9.9±1.0	13.1±0.4	50.1±4.5	2.4±0.3

Furthermore, Raman spectroscopy was employed to evaluate the degree of graphitization in the char residues. As shown in Fig. 4.17, both char samples exhibited characteristic D and G bands, corresponding to disordered carbon and graphitic (crystalline) carbon structures, respectively. [236] Notably, the intensity ratio of the D to G bands (I_D/I_G) for the 12PNSi-co-8MP/PP sample was lower than that of the 12MPNSi/8MPP/PP sample, indicating a higher

degree of graphitization in the char formed by the copolymerized flame retardant. This suggests that the char layer of 12PNSi-co-8MP/PP possessed a more ordered carbon structure and thus was mechanically stronger and more resistant to breakage compared to that of the 12MPNSi/8MPP/PP formulation. In addition, visual observations revealed that the 12PNSi-co-8MP/PP and 10PNSi-co-10MP/PP samples formed continuous, intact char layers after combustion. In contrast, the char layers of 14PNSi-co-6MP/PP and 16PNSi-co-4MP/PP were visibly disrupted and fractured due to the pressure of volatile gases during combustion. This phenomenon is likely attributed to the excessively high content of silicon-containing structures in the latter two copolymers, which may have compromised the mechanical toughness and integrity of the resulting char layers.

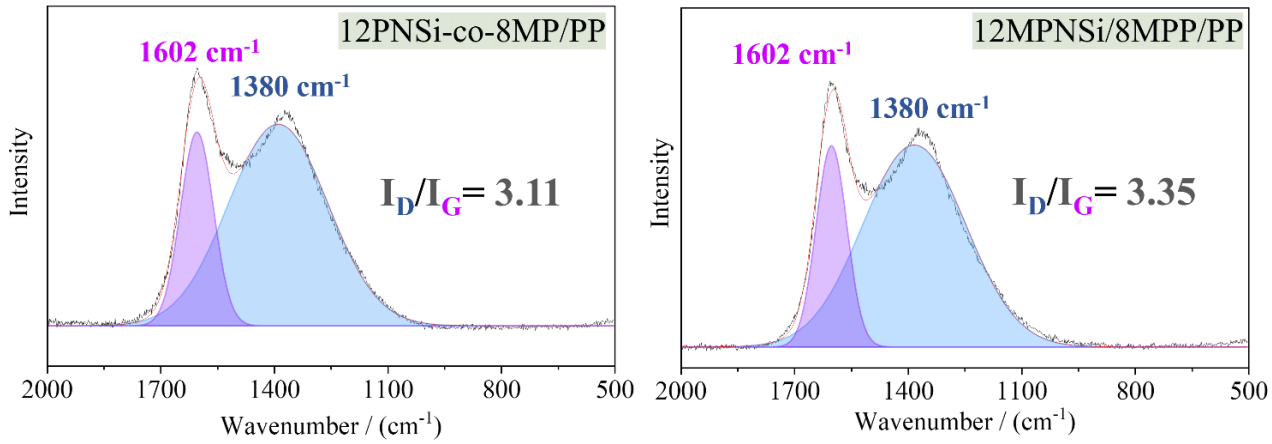

Fig. 4.17 The Raman spectra of char from cone calorimeter test.

To clarify the charring mechanism of PNSi-co-MP in PP, XPS of the 12PNSi-co-8MP/PP char was further conducted to provide more information regarding its chemical structure, as shown in Fig. 4.18. The results are listed as follows [185][237][238]: ***C 1s***: C=C (283.7 eV), C-C/C-H (284.6 eV), C-N/C=N (285.2 eV), C-O (286 eV); ***P 2p***: P-O-P/P-O-C (133.5 eV), P=O (134.4 eV), P-O-Si/P-N (135.4 eV); ***Si 2p***: Si-O-Si (102.7 eV), Si-O-C (103.4 eV), Si-O-P (103.9 eV); ***N 1s***: C-N/P-N (399.0 eV), C=N (401.1 eV). It was clear that the P-, N- and Si-based groups of the flame-retardant system were all involved in the synergistic reaction and formed the char layers. The matrix, especially the C-based composition, was locked by the P/N/Si-based structures and formed some crosslinking structures, including P-O-C, P-O-Si, C-O-Si and so on. In addition, the N-based structures, such as C=N, C-N and P-N, were generated by the degradation of 12PNSi-co-8MP and enhanced the stability of the char layers. [98] The silicon-based structures, like Si-O-Si, also played a role in strengthening the quality of the char. [109] All these structural features ensured the excellent barrier effect of the expandable char layers and endowed PP with outstanding intumescent flame retardancy.

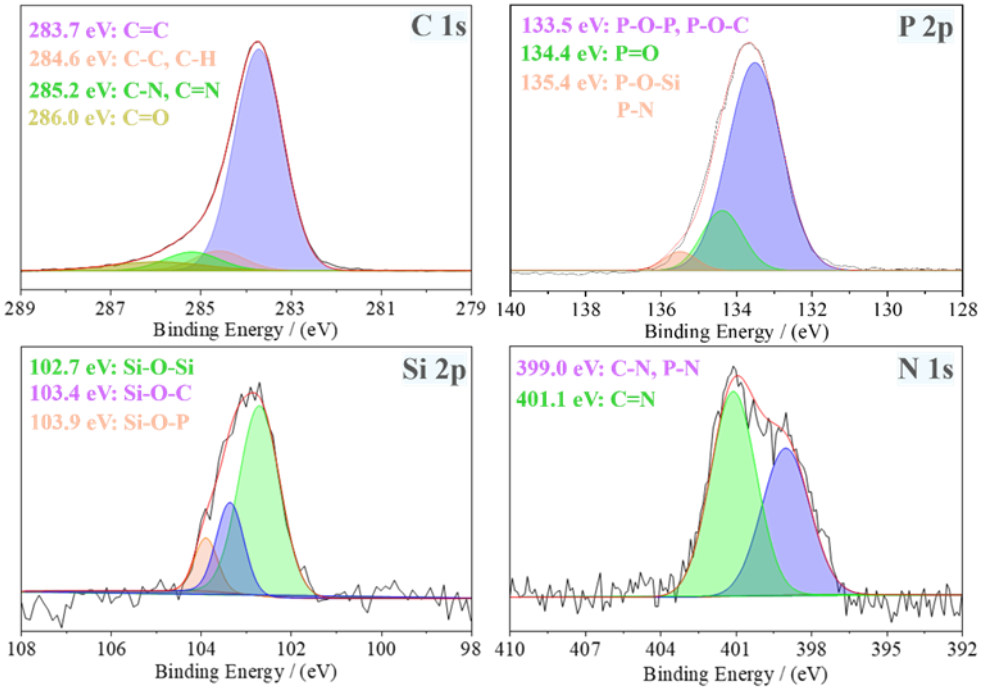

Fig. 4.18 X-ray photoelectron spectra of 12PNSi-co-8MP/PP char.

4.10 Thermal decomposition behavior

As illustrated in Fig. 4.19(a), the synthesized copolymerized compounds exhibited residue yields exceeding 30%, confirming the excellent charring ability of PNSi-co-MP due to the effective integration of the PNSi and MP structures. This high char yield serves as the foundation for the intumescent flame-retardant performance of PNSi-co-MP in the PP matrix. Among the evaluated samples, 12PNSi-co-8MP, which demonstrated the highest flame retardant efficiency, exhibited a distinct thermal decomposition behavior compared to the mixed 12MPNSi/8MPP system, despite their similar chemical compositions. As shown in Fig. 4.19(b), 12PNSi-co-8MP achieved a residue yield of 33.2% at 800 °C, approximately 6% higher than that of the 12MPNSi/8MPP mixture. This difference highlights the benefit of covalently linking PNSi and MP moieties within a single macromolecule, which facilitates more efficient char formation. In contrast, the lack of chemical bonding in the physically mixed system limited the extent of synergistic char-forming reactions. Moreover, 12PNSi-co-8MP displayed superior thermal stability below 500 °C compared to the 12MPNSi/8MPP mixture. However, when incorporated into PP, the 12PNSi-co-8MP/PP composite exhibited slightly lower thermal stability than 12MPNSi/8MPP/PP, indicating that 12PNSi-co-8MP more effectively promoted the early thermal decomposition of the PP matrix. This observation supports the conclusion that the charring reaction between PNSi-co-MP and PP occurred more readily than in the system containing unlinked MPNSi and MPP components.

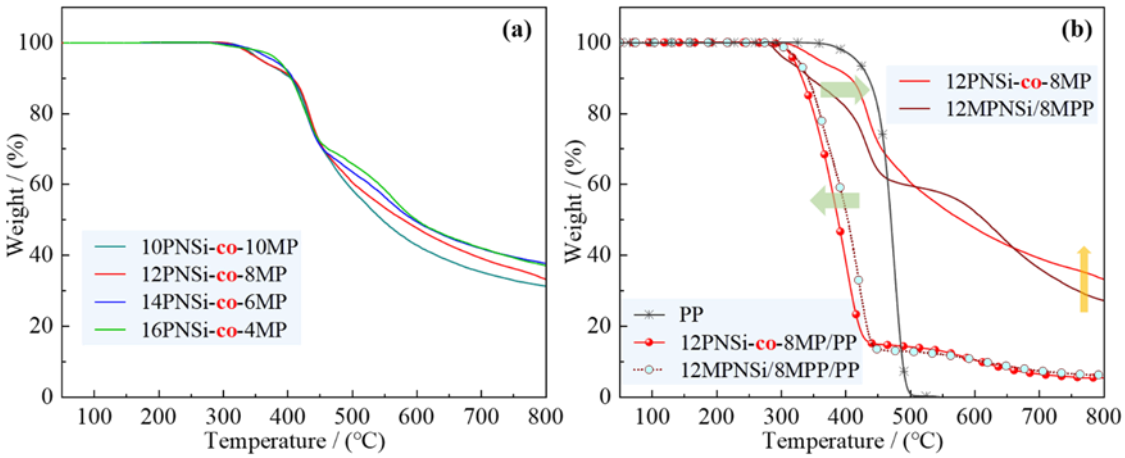

Fig. 4.19 TGA curves of flame retardants and typical PP composites.

To make clear the interaction mechanism between the flame retardants and the PP matrix, the volatile products released during thermal degradation were monitored in real-time using thermogravimetric analysis coupled with Fourier-transform infrared spectroscopy. The major gaseous fragments detected were hydrocarbons, primarily including -CH_n groups and C=C bonds. As shown in Figs. 4.20(a) and (b), the 12PNSi-co-8MP/PP composite released hydrocarbon fragments in a single-peak mode during thermal decomposition, whereas the 12MPNSi/8MPP/PP system exhibited a distinct double-peak release profile. This difference can be attributed to the limited interaction between the physically mixed MPNSi and MPP components with the PP matrix in the early stages of decomposition. In the 12MPNSi/8MPP/PP system, PP initially degraded on its own, resulting in the first release peak. As the temperature increased, a delayed charring reaction between MPNSi/MPP and PP partially inhibited further hydrocarbon evolution, forming the first peak. However, this inhibition was insufficient, and further decomposition at higher temperatures generated the second peak. In contrast, 12PNSi-co-8MP effectively initiated earlier degradation of the PP matrix and rapidly formed crosslinked structures, thereby facilitating a quicker charring reaction. This rapid char formation process led to a more uniform and concentrated release of hydrocarbons, manifesting as a single-peak profile. Moreover, as illustrated in Fig. 4.20(d), the intensity of hydrocarbon release for 12PNSi-co-8MP/PP was higher than that of 12MPNSi/8MPP/PP at 350 °C, but significantly lower at the temperature corresponding to the maximum decomposition rate. This observation suggests that 12PNSi-co-8MP promoted early-stage decomposition and effectively suppressed hydrocarbon release at higher temperatures, thereby reducing fuel availability for combustion. Additionally, Fig. 4.20(c) reveals that the -CH_3 release intensity of 12PNSi-co-8MP/PP was 18.6% lower than that of 12MPNSi/8MPP/PP, indicating reduced generation of combustible volatiles. This finding further supports the superior flame-retardant performance

of 12PNSi-co-8MP, demonstrating its enhanced ability to interact with the PP matrix and suppress the release of flammable degradation products.

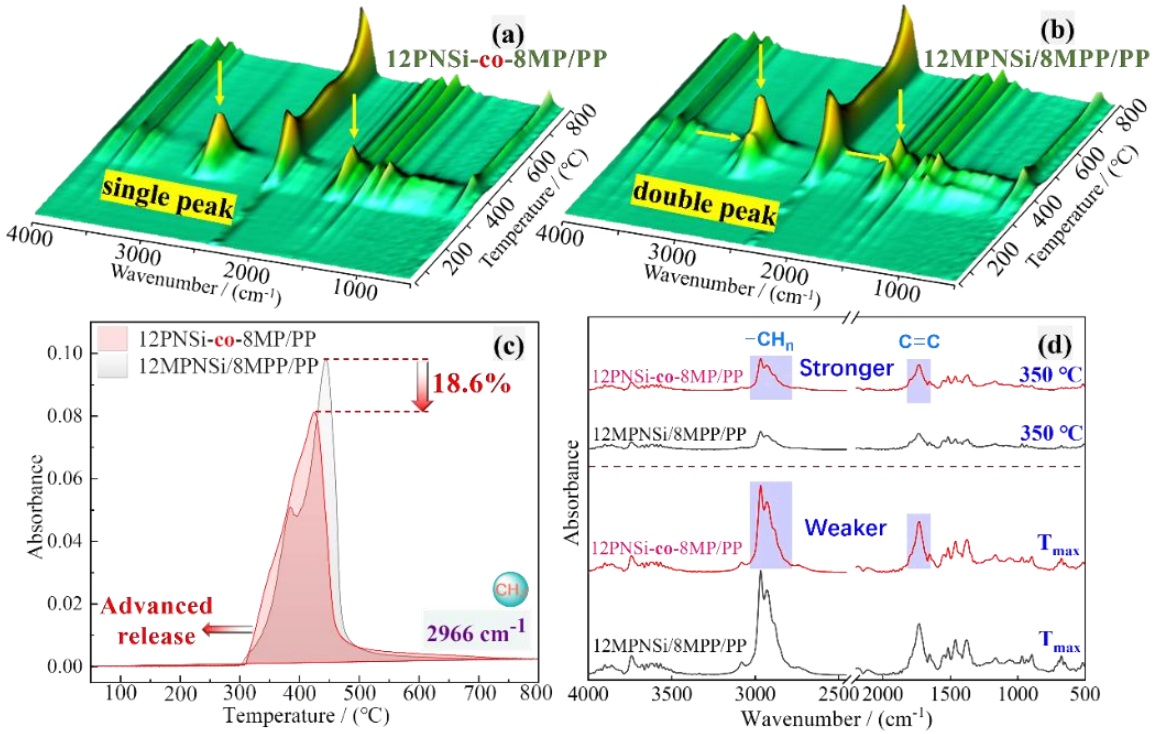

Fig. 4.20 Real-time FTIR spectra of 12PNSi-co-8MP/PP and 12MPNSi/8MPP/PP.

4.11 The py-GC/MS analysis of flame retardants

To investigate the differences in pyrolysis behavior between the synthesized copolymer flame retardant and the physically mixed intumescent flame retardant system, pyrolysis-gas chromatography/mass spectrometry was performed, and the results are presented in Fig. 4.21. Notably, 12PNSi-co-8MP released significantly fewer pyrolysis fragments compared to 12MPNSi/8MPP, as indicated by peaks A and B in the GC spectra. This suggests that 12PNSi-co-8MP underwent a rapid charring reaction, thereby limiting the release of volatile degradation products. Given that the pyrolysis process rapidly heats the sample to 500 °C, the occurrence of early-stage char formation effectively suppressed the evolution of gaseous fragments. In contrast, the absence of timely charring in 12MPNSi/8MPP resulted in the release of a larger quantity of pyrolysis products. Moreover, the chemical nature of the released volatiles differed between the two systems. The 12MPNSi/8MPP mixture predominantly emitted phosphorus-containing species such as PO and P-O-P, which are typically derived from the decomposition of acid sources. In contrast, 12PNSi-co-8MP mainly produced P-O-CH_n-O-P based fragments, indicating that a synergistic interaction between the acid and carbon sources occurred promptly during pyrolysis. This rapid interaction is attributed to the covalent integration of the PNSi and MP structures within a single copolymer chain. In summary, the

molecular integration of PNSi and MP in 12PNSi-co-8MP facilitated early-stage char formation and significantly enhanced condensed-phase flame-retardant behavior, distinguishing it from the physically blended system.

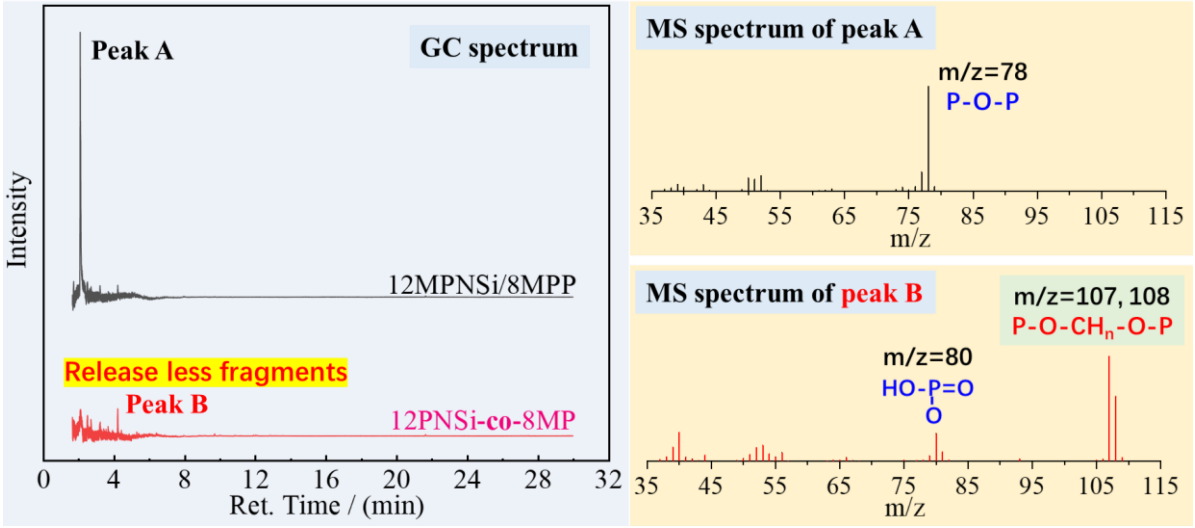

Fig. 4.21 GC and MS spectra of 12PNSi-co-8MP and 12MPNSi/8MPP.

4.12 Conclusion

In this work, dendritic copolymers PNSi-co-MP with varying ratios of PNSi to MP monomers were synthesized and compared with physically blended IFR systems composed of self-polymerized MPNSi and MPP. The PNSi-co-MP copolymers were found to disperse uniformly within the polypropylene matrix and establish strong interfacial interactions, whereas the MPNSi/MPP mixture tended to agglomerate, exhibiting poor compatibility with PP. As a result, the PNSi-co-MP/PP composites demonstrated significantly improved mechanical performance. Specifically, PNSi-co-MP/PP exhibited ductile fracture behavior, while MPNSi/MPP/PP underwent brittle failure. The elongation at break and unnotched impact strength of the PNSi-co-MP/PP composites were markedly higher than those of the MPNSi/MPP/PP counterparts. This enhancement was attributed to the excellent thermal softening behavior and low crystallinity of PNSi-co-MP, which enabled morphological adaptation during melt blending. Consequently, some PNSi-co-MP particles were thermally deformed to sizes around 200 nm, promoting better dispersion and mechanical reinforcement. In addition to mechanical improvements, PNSi-co-MP also imparted superior flame retardancy to the PP composites. Remarkably, with 20 wt.% loading, 12PNSi-co-8MP/PP achieved a glow-wire flammability index above 960 °C, a glow-wire ignition temperature of 875 °C, a limiting oxygen index (LOI) of 30.2%, and UL-94 V-0 classification. In contrast, 12MPNSi/8MPP/PP with the same loading exhibited inferior flame-retardant properties, including a GWFI and GWIT of 825 °C, an LOI

of 27.9%, and the same UL-94 V-0 rating, but with less effective flame inhibition. Furthermore, the 12PNSi-co-8MP/PP composite achieved a flame-retardant index (FRI) value of 42.23, indicating its excellent overall flame retardancy. This superior performance can be ascribed to the rapid charring mechanism facilitated by the covalent integration of PNSi and MP within a single molecular structure. The copolymer configuration enabled fast and synergistic interactions with the PP matrix, resulting in an efficient condensed-phase barrier effect. In summary, the molecular linkage of flame-retardant monomers rather than their physical mixture proved to be a critical strategy for enhancing both the mechanical and flame-retardant properties of PP composites.

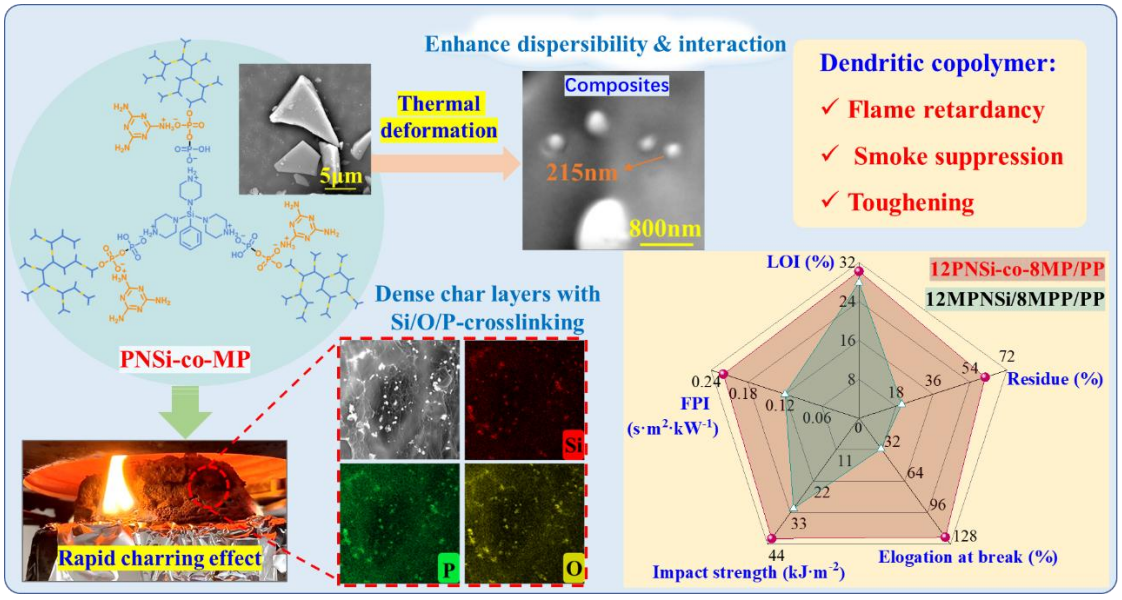

Fig. 4.22 The graphical summary of this chapter.

CHAPTER 5

Macromolecular Piperazine / Aluminum Phosphate Hybrid and Its Potential in Intumescent Flame Retardant / Thermal Conductive Polypropylene

5.1 Introduction

Multifunctional polymer composites with outstanding flame retardancy are increasingly becoming a critical focus in materials research, particularly in response to the growing demands of the high-end manufacturing sector. [239][240][241] Among these functions, high thermal conductivity is especially important for specific applications, such as housing materials in electronic devices. Without effective thermal dissipation, the accumulation of waste heat not only elevates the risk of fire but also shortens the service life of electronic devices operating at elevated temperatures for extended periods. [242][243][244] Polypropylene, being a widely used material for electrical and electronic housings, stands as a prime candidate for functional enhancement. Therefore, the development of multifunctional PP composites that simultaneously possess flame retardant and thermally conductive properties is of great significance for modern electronics applications.

However, achieving a balance between flame retardancy and thermal conductivity in PP remains challenging. [245] Intumescent flame retardant, recognized as some of the most effective flame retardants for PP, functions by forming compact, insulating char layers during combustion. The introduction of high-load functional additives holds high possibility to disrupt the formation and integrity of formed protective char layers. [246][247][248] Hence, the critical challenge lies in identifying strategies that allow both properties to coexist without compromising each other. To address this, two key directions are proposed. (a). Designing highly efficient IFR systems: If the flame retardant system exhibits sufficient efficacy, it allows room for integrating additional functional fillers without significantly impairing flame retardancy. Even in cases where the introduction of fillers slightly compromises the flame retardant performance, the overall performance may still meet the application requirements. (2) Optimizing thermally conductive fillers: The ideal fillers do not affect or slightly affect the charring behavior of the intumescent flame retardant system. If such fillers are employed, the synergistic realization of flame retardancy and thermal conductivity becomes feasible.

In the previous chapter, it was demonstrated that integrating different flame-retardant groups into a single molecule significantly improves the charring efficiency and barrier performance, thereby delivering superior fire safety for PP composites. This molecular-level

design approach, which combines multiple synergistic flame-retardant units in one macromolecule, offers a promising pathway for creating high-performance, multifunctional IFR systems. Based on this concept, a novel organic–inorganic hybrid macromolecule was synthesized by chemically bonding an aluminum-containing group with piperazine phosphate. Subsequently, this newly designed intumescent flame retardant system was combined with several commonly used thermally conductive fillers to investigate the compatibility between the flame retardant system and different thermal conduction systems. The aim was to develop a formulation capable of simultaneously enhancing both the flame retardancy and thermal conductivity for polypropylene materials.

5.2 Synthesis of hybrid macromolecule Al-PAP

The synthesis route of Al-PAP is illustrated in Fig. 5.1. Random copolymerization between the piperazine phosphate monomer and aluminum dihydrogen phosphate was initiated at a temperature exceeding 240 °C. Under these conditions, a hybrid charring macromolecule, Al-PAP, was formed via a dehydration reaction between the two monomers. The detailed procedure is as follows: 90 g of PAP and 10 g of AlDHP were thoroughly mixed using a high-speed grinder. The resulting blend was then transferred into a vacuum oven set to 260 °C under a vacuum of 0.1 MPa. To minimize oxygen interference, the oven atmosphere was purged twice with nitrogen. After maintaining the reaction for 1 hour, the copolymerization product, Al-PAP, was collected. Finally, the obtained Al-PAP was ground to a particle size of approximately 5-10 μm for use as an additive in polypropylene composites.

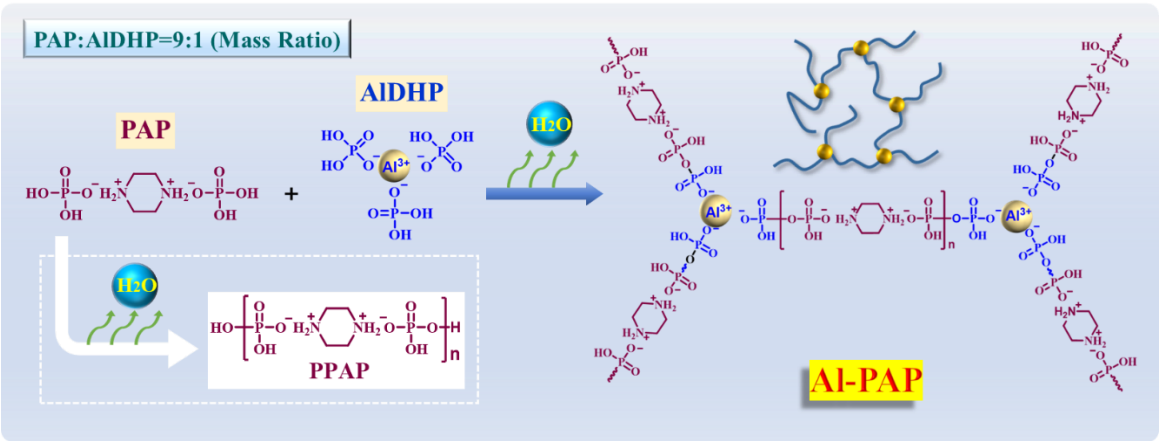

Fig. 5.1 The preparation route of hybrid-charring macromolecule Al-PAP.

5.3 Fabrication of flame retardant PP composites

All designed PP samples including flame retardant composites and flame retardant / thermal conductivity composites were fabricated according to the formula in Table 5.1. The Al-IFR system was obtained by mixing Al-PAP and MPP with a mass ratio of 7:3, and the IFR system

was formed by compounding the PPAP and MPP with a mass ratio of 7:3. The processing and molding techniques employed included extrusion, injection molding, and compression molding. The detailed procedures were consistent with those described in Section 3.3.

Table 5.1 The formula (wt. %) of PP composites.

	Al-PAP	PPAP	MPP	Al_2O_3	BN	MWCNT	PP	PP-g-MA	Others*
Neat PP	-	-	-	-	-	-	99	0	1
14Al-IFR/PP	9.8	-	4.2	-	-	-	80	5	1
16Al-IFR/PP	11.2	-	4.8	-	-	-	78	5	1
18Al-IFR/PP	12.6	-	5.4	-	-	-	76	5	1
20Al-IFR/PP	14	-	6	-	-	-	74	5	1
20IFR/PP	-	14	6	-	-	-	74	5	1
1Al_2O_3/20Al-IFR/PP	14	-	6	1	-	-	73	5	1
3Al_2O_3/20Al-IFR/PP	14	-	6	3	-	-	71	5	1
5Al_2O_3/20Al-IFR/PP	14	-	6	5	-	-	69	5	1
7Al_2O_3/20Al-IFR/PP	14	-	6	7	-	-	67	5	1
9Al_2O_3/20Al-IFR/PP	14	-	6	9	-	-	65	5	1
30Al_2O_3/PP	-	-	-	30	-	-	64	5	1
5BN/20Al-IFR/PP	14	-	6	-	5	-	69	5	1
5MWCNT/20Al-IFR/PP	14	-	6	-	-	5	69	5	1

***** Other additives included PTFE (0.4 wt.%), antioxidant 168 (0.3 wt.%), and antioxidant 1010 (0.3 wt.%).

5.4 Characterization of hybrid macromolecule Al-PAP

The hybrid macromolecule Al-PAP was synthesized via a dehydration copolymerization reaction between the P–OH groups of PAP and AlDHP. The FTIR spectra of Al-PAP and its constituent monomers are shown in Fig. 5.2(a). After copolymerization, a new absorption peak at 912 cm^{-1} which was attributed to P–O–P linkages appeared in the spectrum of Al-PAP, confirming the occurrence of a dehydration reaction among P–OH groups. [109][249] In addition, characteristic absorption peaks corresponding to other functional groups in Al-PAP were also observed: O-H (3245 cm^{-1}), N-H (3420 cm^{-1}), NH_2^+ (3004 cm^{-1}), hydrogen bonds (2755, 2431, and 1634 cm^{-1}), CH_2 (2818 cm^{-1}), P-O (951 cm^{-1}), and P=O (1086 cm^{-1}). [127][250][251] Furthermore, Fig. 5.2(b) illustrates a distinct change in the phosphorus chemical environment from the raw monomers to the Al-PAP copolymer. The ^{31}P NMR chemical shift in the range of -17.4 to 2.5 ppm supports the successful formation of Al-PAP via

random copolymerization between PAP and AlDHP. Additionally, the ^{27}Al solid-state NMR spectra in Fig. 5.2(c) confirm the chemical incorporation of AlDHP into the macromolecular structure. XRD analysis, as shown in Fig. 5.3, further supports these findings: after copolymerization, Al-PAP exhibited an amorphous structure due to the random arrangement of the monomers, in contrast to the high crystallinity observed in PPAP derived from self-polymerized PAP. Collectively, these results confirm the successful synthesis of the Al-PAP hybrid macromolecule.

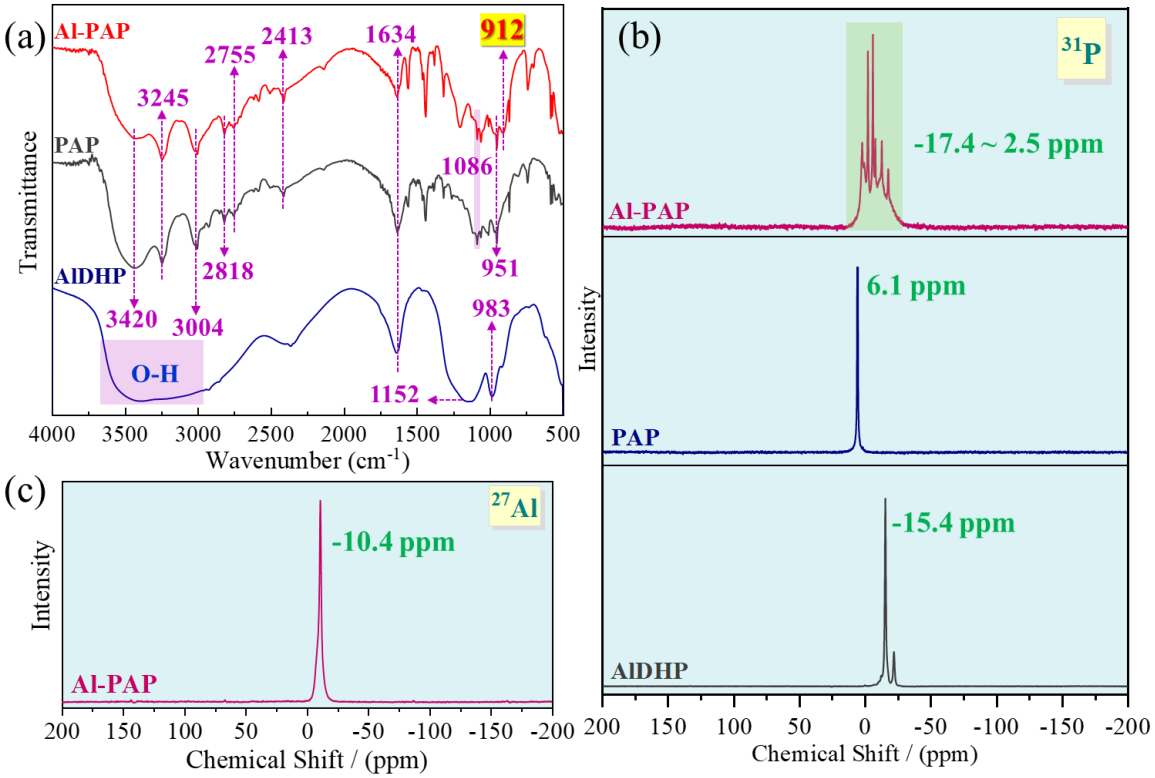

Fig. 5.2 The FTIR (a), ^{31}P (b) and ^{27}Al (c) solid-NMR spectra of Al-PAP and raw materials.

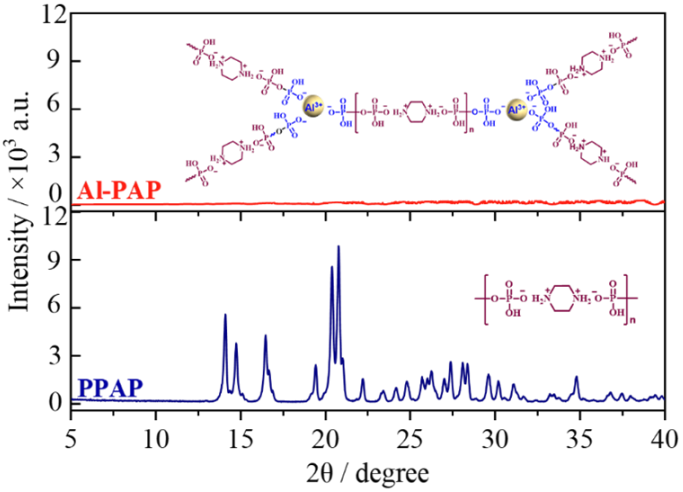

Fig. 5.3 The XRD spectra of copolymerized Al-PAP and self-polymerized PPAP.

5.5 Thermal stability of hybrid macromolecules

The thermal decomposition and char-forming behaviors of Al-PAP, PPAP, and the raw reactants are presented in Fig. 5.4. It can be observed that Al-PAP exhibited an initial decomposition temperature exceeding 300 °C, indicating its thermal stability is sufficient to meet the processing requirements of polypropylene. Furthermore, Al-PAP achieved a residue yield of 27.1% at 800 °C, which is notably higher than the 22.5% yield observed for PPAP. This result suggests that the incorporation of Al^{3+}-based structures effectively enhanced the char-forming capability when combined with the piperazine phosphate groups. Additionally, as shown in the DTG curves in Fig. 5.4(b), Al-PAP displayed a higher temperature corresponding to the maximum decomposition rate compared to PPAP. This shift further indicates the higher thermal stability and robustness of the char formed by the hybrid Al-PAP macromolecule.

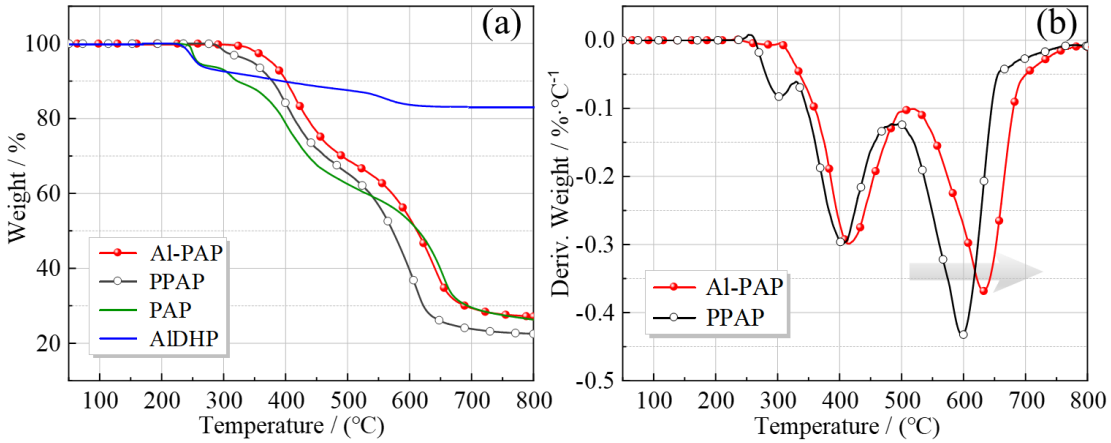

Fig. 5.4 The TG (a) and DTG (b) curves of Al-PAP, PPAP and raw materials.

5.6 Flame retardancy

The flame retardant properties, including limiting oxygen index, UL 94 vertical burning ratings, glow-wire ignition temperature, and glow-wire flammability index are summarized in Table 5.2.

Table 5.2 The GW, LOI, and UL 94 results of PP composites.

	GW (1.5mm)		LOI	UL 94			
	GWIT	GWFI		3.2 mm		1.6 mm	
				t_1/t_2 (s)	Rating	t_1/t_2 (s)	Rating
Neat PP	650°C	625°C	18.6%	Burn*/-	No	Burn*/-	No
14Al-IFR/PP	775°C	>960°C	28.3%	1.7/19.7	V-1	Burn*/-	No
16Al-IFR/PP	775°C	>960°C	29.1%	0.9/7.9	V-0	3.8/Burn*	No
18Al-IFR/PP	825°C	>960°C	30.6%	0/1.0	V-0	0.7/5.1	V-0

20Al-IFR/PP	850℃	>960℃	32.2%	0/0	V-0	0/1.7	V-0
20IFR/PP	825℃	>960℃	28.5%	0/0.8	V-0	0/11.9	V-1
1Al_2O_3/20Al-IFR/PP	875℃	>960℃	33.8%	0/0	V-0	0/0	V-0
3Al_2O_3/20Al-IFR/PP	825℃	>960℃	30.7%	0/5.8	V-0	0.5/18.9	V-1
5Al_2O_3/20Al-IFR/PP	825℃	>960℃	31.6%	0/0.5	V-0	0/5.8	V-0
7Al_2O_3/20Al-IFR/PP	825℃	>960℃	28.3%	0/0.7	V-0	1.9/4.4	V-0
9Al_2O_3/20Al-IFR/PP	775℃	800℃	23.8%	Burn*/-	No	Burn*/-	No
30Al_2O_3/PP	650℃	625℃	19.6%	Burn*/-	No	Burn*/-	No
5BN/20Al-IFR/PP	775℃	750℃	21.7%	Burn*/-	No	Burn*/-	No
5MWCNT/20Al-IFR/PP	750℃	725℃	23.3%	Burn*/-	No	Burn*/-	No

* The flame burned to the clamp.

Owing to its high flammability, neat polypropylene exhibited poor fire resistance, with an LOI of only 18.6%, a GWIT of 650 °C, a GWFI of 625 °C, and failed to achieve a UL 94 rating. Upon incorporation of 14 wt.% of the Al-based intumescent flame retardant, the 14Al-IFR/PP composite achieved a notable improvement, with a LOI of 28.3%, a GWFI exceeding 960 °C, and passed the UL 94 V-1 rating at a thickness of 3.2 mm. As the Al-IFR loading increased, the flame retardancy of the PP composites was further enhanced. The 16Al-IFR/PP formulation passed the UL 94 V-0 test at 3.2 mm thickness and attained an LOI of 29.1%. Remarkably, the 18Al-IFR/PP sample satisfied the UL 94 V-0 criteria for both 3.2 mm and 1.6 mm thicknesses, demonstrating its suitability for thin-walled PP applications. This sample also reached an LOI value exceeding 30%. With a further increase to 20 wt.%, the Al-IFR/PP composite achieved an LOI of 32.2%, a GWIT of 850 °C, a GWFI over 960 °C, and maintained UL 94 V-0 ratings at both tested thicknesses. Moreover, Al-IFR demonstrated much higher efficiency than the system based on PPAP. Specifically, a 20 wt.% loading of the PPAP-based IFR only achieved an LOI of 28.5%, comparable to the 14Al-IFR/PP formulation. Under identical loading levels, the 20Al-IFR/PP outperformed the 20IFR/PP in terms of LOI, GWIT, and UL 94 rating, indicating the superior flame retardant efficiency of Al-IFR.

This distinction was visually supported by combustion tests in 30% oxygen concentration (Figs. 5.5 b, c), where 20Al-IFR/PP self-extinguished after 19 s, while 20IFR/PP burned down to the 5 cm mark. These results underscore the critical role of Al^{3+} in the hybrid Al-PAP macromolecule in enhancing the intumescent flame retardant effect. FTIR analysis of the char residues (Fig. 5.6) revealed that the residue from 20Al-IFR/PP contained more hydrocarbon structures (–CH_n, C=C) and P–O–C skeletons formed through the interaction between

polyphosphates and the PP matrix, compared to the IFR/PP residue. This finding confirms that Al^{3+} facilitates crosslinking reactions among the IFR components and the matrix during combustion. [101][252] Collectively, these results demonstrate that the Al-IFR system, incorporating the hybrid macromolecule Al-PAP, is a highly effective flame retardant strategy for developing multifunctional PP composites with superior fire safety performance.

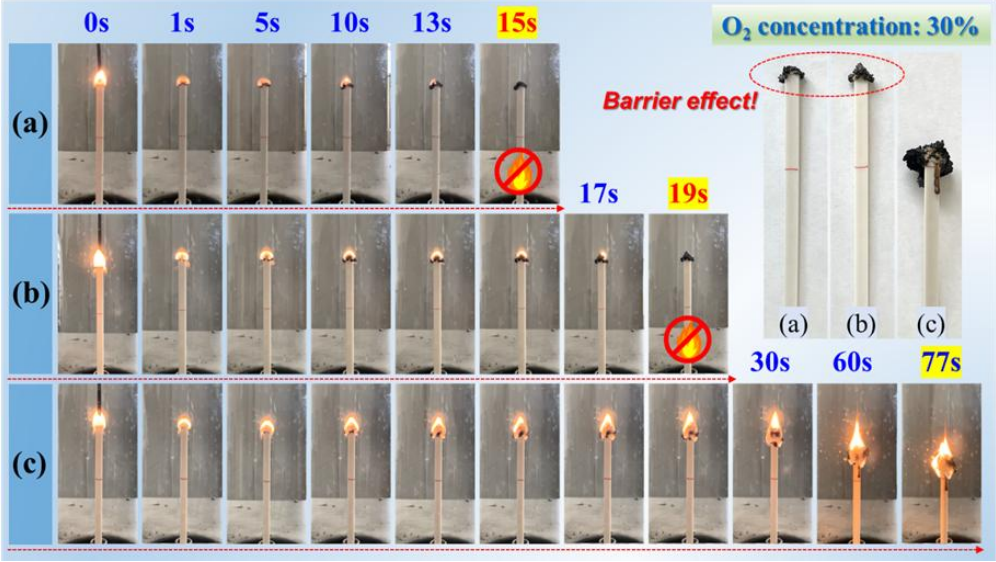

Fig. 5.5 The combustion process of $1Al_2O_3$/20Al-IFR/PP (a), 20Al-IFR/PP (b), and 20(PPAP/MPP)/PP (c) in LOI test under a 30% of oxygen concentration.

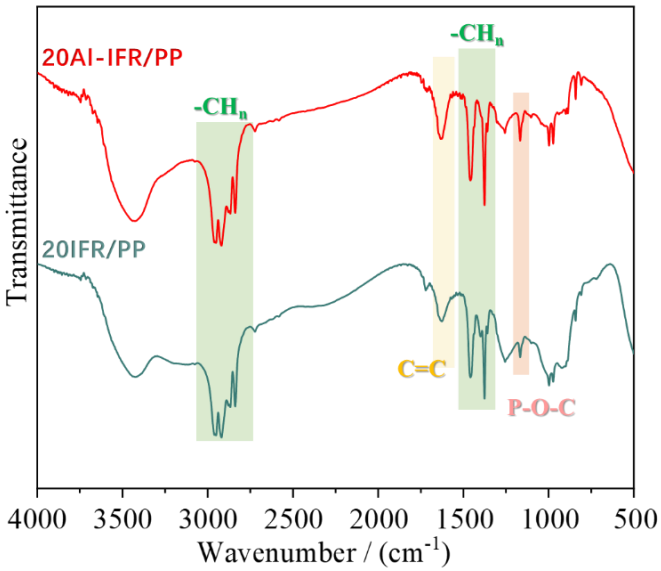

Fig. 5.6 The FTIR spectra of char residues after LOI tests.

Generally, the barrier effect of the char layer plays a crucial role in determining the intumescent flame retardancy of polypropylene composites. However, the integrity and compactness of the char can be adversely affected by the introduction of other functional fillers, particularly those aimed at enhancing thermal conductivity. To address this challenge, three

typical thermally conductive additives aluminum oxide, including boron nitride, and multi-walled carbon nanotubes, were individually incorporated into the Al-IFR system to identify a formulation that balances both flame retardancy and thermal conductivity. The flame retardant performance of these hybrid systems is also summarized in Table 5.2. Aluminum oxide, when used alone, exhibits negligible flame retardant properties in PP. Interestingly, its inclusion at a low loading (1 wt.%) in the 20Al-IFR/PP matrix led to a notable enhancement in fire resistance. Specifically, the LOI of the 1Al_2O_3/20Al-IFR/PP composite reached 33.8%, a remarkably high value for intumescent flame-retardant PP composites at comparable total loadings. As shown in Fig. 5.5(a), this sample was capable of self-extinguishing within 15 seconds under a 30% oxygen atmosphere. However, further increases in Al_2O_3 content resulted in a progressive deterioration of flame retardant performance. For instance, the LOI of the 9Al_2O_3/20Al-IFR/PP composite dropped to 23.8%, and the material failed to achieve any UL 94 rating, despite the high overall filler content of 29 wt.%. These results indicate that excessive Al_2O_3 disrupts the formation and expansion of effective char layers, thereby undermining the intumescent mechanism. Nevertheless, moderate loadings of Al_2O_3 (5 wt.% and 7 wt.%) maintained acceptable flame retardant performance. Both the 5Al_2O_3/20Al-IFR/PP and 7Al_2O_3/20Al-IFR/PP samples achieved UL 94 V-0 ratings at both 3.2 mm and 1.6 mm thicknesses. Additionally, the LOI of 5Al_2O_3/20Al-IFR/PP remained above 30%, suggesting its suitability for high-end applications requiring stringent fire safety. In contrast, the introduction of 5 wt.% BN or MWCNTs significantly compromised the flame retardancy of the Al-IFR/PP system. Both 5BN/20Al-IFR/PP and 5MWCNT/20Al-IFR/PP failed to meet UL 94 criteria and exhibited a marked reduction in LOI values compared to the 20Al-IFR/PP baseline. These findings demonstrate that BN and MWCNTs severely hinder the charring process, possibly due to their interference with the formation of an intumescent and cohesive char structure. In conclusion, alumina was identified as the most compatible thermally conductive filler for use with Al-IFR in PP composites, offering a viable route to develop materials that simultaneously exhibit enhanced thermal conductivity and excellent flame retardant properties.

To evaluate the comprehensive fire-safety performance, the cone calorimeter test was carried out with 50 $kW \cdot m^{-2}$ to provided key parameters, including time to ignition, time to peak of heat release rate, peak of heat release rate, total heat release, peak value of smoke production rate, total smoke release, residue yield, peak value of mass loss rate and average effective heat of combustion, which are all listed in Tables 5.3 and 5.4. Besides, the heat and smoke release behaviors of typical composites are displayed in Fig. 5.7.

Table 5.3. Key parameters of typical samples in cone calorimeter test.

Sample	TTI /s	TTP /s	PHRR /kW·m^{-2}	THR /MJ·m^{-2}	PSPR /m^2·s	TSR /m^2·m^{-2}	R_{end}	PMLR /g·s^{-1}
PP	28	105	1462	159.7	0.169	2604	0.0%	0.232
16Al-IFR/PP	20	520	290	123.5	0.076	2958	6.0%	0.078
20Al-IFR/PP	20	935	223	117.6	0.047	1723	13.4%	0.054
20IFR/PP	23	895	203	123.1	0.052	2196	11.2%	0.085
1Al_2O_3/20Al-IFR/PP	22	1080	90	105.1	0.018	1383	17.5%	0.044
5Al_2O_3/20Al-IFR/PP	21	320	135	117.8	0.020	1511	17.5%	0.057
5BN/20Al-IFR/PP	24	60	429	122.3	0.100	3080	14.7%	0.115
5MWCNT/20Al-IFR/PP	17	55	447	111.7	0.133	3702	10.7%	0.127

Table 5.4. Key parameters and fire safety index of typical samples in cone calorimeter test.

Sample	av-EHC /MJ·kg^{-2}	Av-COY kg/kg	FGI /kW·m^{-2}·s^{-1}	FPI /s·m^2·kW^{-1}	FRI
PP	52.7	0.06	13.92	0.019	1.0
16Al-IFR/PP	41.5	0.06	0.56	0.069	4.7
20Al-IFR/PP	40.7	0.10	0.24	0.090	6.4
20IFR/PP	42.0	0.10	0.23	0.113	7.7
1Al_2O_3/20Al-IFR/PP	40.2	0.06	0.08	0.244	19.4
5Al_2O_3/20Al-IFR/PP	41.9	0.07	0.42	0.156	11.0
5BN/20Al-IFR/PP	41.7	0.08	7.15	0.056	3.8
5MWCNT/20Al-IFR/PP	37.1	0.15	8.13	0.038	2.8

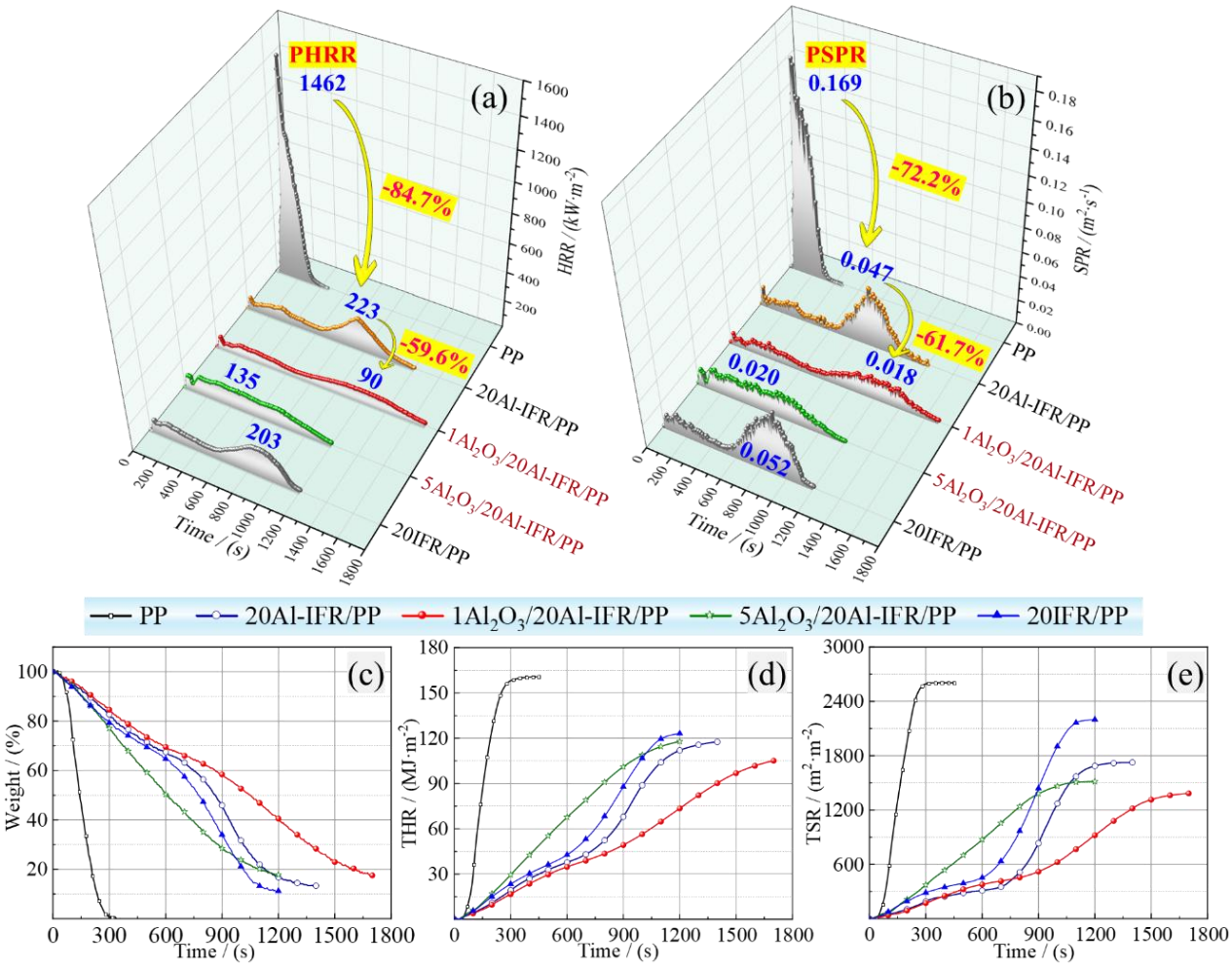

Fig. 5.7 The (a) HRR and (b) SPR, (c) weight loss, (d) THR, and (e) TSR curves of typical samples.

First, the TTI and TTP of neat PP were 28 s and 105 s, respectively, implying that the combustion intensity of PP increased rapidly to a high level after ignition, which can be also observed in Fig. 5.8(a). The combustion process was completed within approximately 400 s, leaving virtually no residue, as seen in Fig. 5.7(a). Consequently, PP demonstrated a high PHRR of 1462 kW·m^{-2} and a THR of 159.7 MJ·m^{-2}. Additionally, smoke production was substantial, indicating a significant fire hazard. Upon incorporation of 20 wt.% Al-IFR, the flame retardancy of the composite (20Al-IFR/PP) improved significantly. The PHRR was reduced to 223 kW·m^{-2}, which was an 84.7% reduction compared to neat PP, while the PSPR dropped by 72.2% to 0.047 m²·s. Furthermore, both THR and TSR decreased markedly, as shown in Table 5.3. This enhancement can be attributed to the formation of a compact, intumescent char layer early in the combustion process, which effectively inhibited heat and mass transfer (Fig. 5.8 b). Importantly, the 20Al-IFR/PP composite retained 13.4% of its mass post-combustion, in stark contrast to the complete burnout observed in neat PP. To evaluate

flame retardancy more quantitatively, the flame growth index, flame performance index, and flame retardancy index were calculated (Fig. 5.9 and Table 5.4). The FGI of 20Al-IFR/PP was 98.3% lower than that of neat PP, indicating a much slower flame propagation rate. The FPI was 4.7 times higher, reflecting a substantial improvement in overall flame suppression. The FRI value of the composite fell within the range of 1–10, corresponding to a "Good" classification of flame retardancy. [235]When compared with the traditional IFR system (without Al-based structure), the Al-IFR exhibited superior charring ability. Specifically, 20Al-IFR/PP showed a 2.2% higher residual mass than 20IFR/PP, despite their similar overall compositions. This enhancement suggests that the Al^{3+}-based structure in Al-PAP facilitated stronger condensed-phase interactions, promoting carbonaceous char formation and thereby reducing gas-phase volatilization. As a result, 20Al-IFR/PP achieved lower peak mass loss rate, THR, and TSR values compared to 20IFR/PP. These findings confirm that the hybrid charring macromolecule Al-PAP, when used synergistically with melamine polyphosphate, delivers an effective and comprehensive intumescent flame-retardant effect in PP composites.

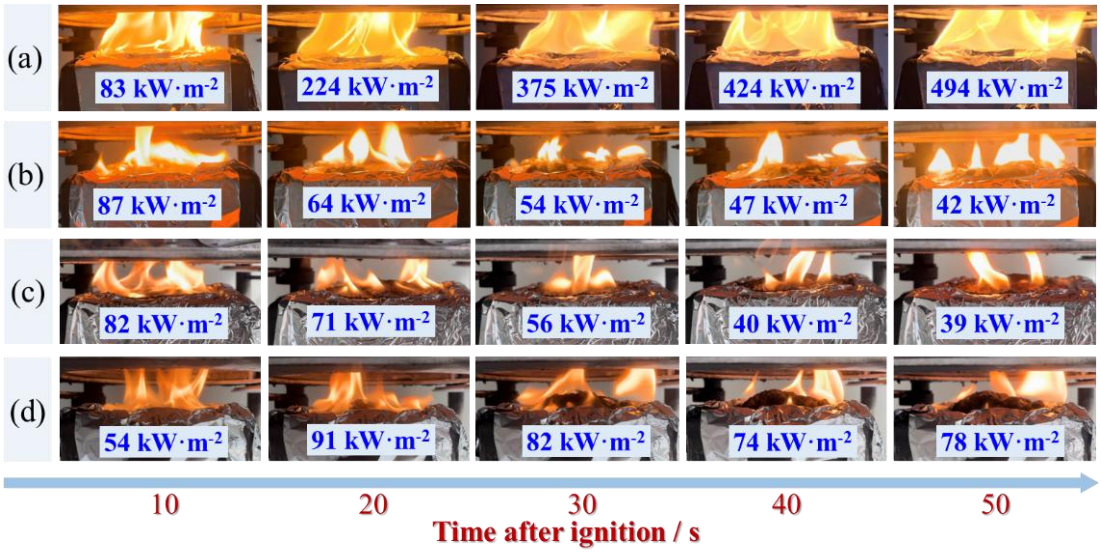

Fig. 5.8 The flame images and HRR values at the initial burning stage of (a) PP, (b) 20Al-IFR/PP, (c) 1Al_2O_3/20Al-IFR/PP, and (d) 20IFR/PP.

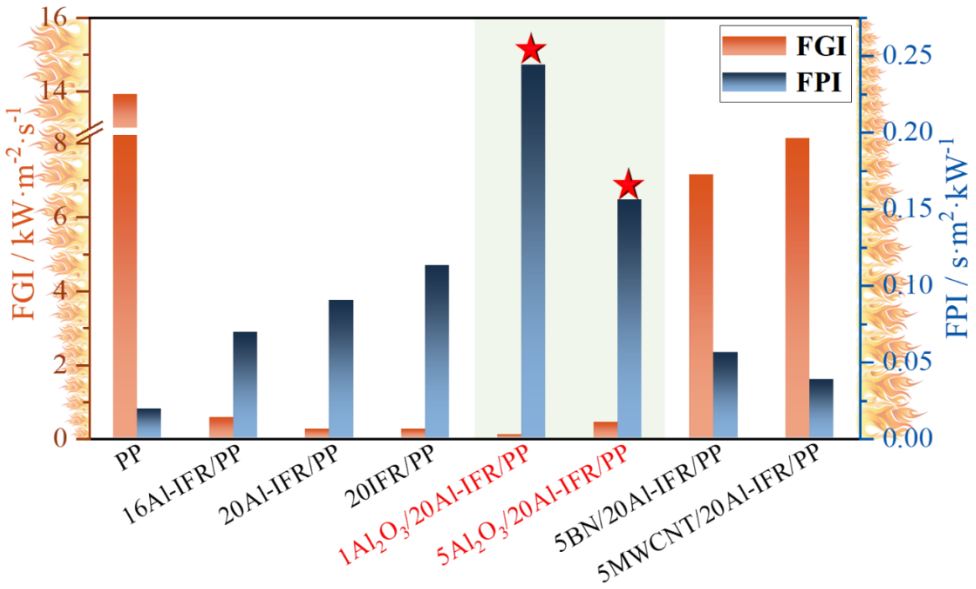

Fig. 5.9 The FGI and FPI parameters of PP composites.

As anticipated, the incorporation of Al_2O_3 into the Al-IFR system brought notable improvements in the fire safety performance of polypropylene composites. Notably, the residue yields of both 1Al_2O_3/20Al-IFR/PP and 5Al_2O_3/20Al-IFR/PP increased to 17.5%, compared to 11.2% for 20Al-IFR/PP, indicating a synergistic charring effect between Al_2O_3 and the Al-IFR system. This enhancement in char formation significantly contributed to the suppression of heat and smoke release during combustion. Specifically, the THR and TSR of 1Al_2O_3/20Al-IFR/PP were reduced by 34.2% and 46.9%, respectively, compared to neat PP. The PHRR for 1Al_2O_3/20Al-IFR/PP and 5Al_2O_3/20Al-IFR/PP were measured at just 90 $kW \cdot m^{-2}$ and 135 $kW \cdot m^{-2}$, corresponding to reductions of 93.8% and 90.8% relative to neat PP, and 59.6% and 39.5% compared to 20Al-IFR/PP. Importantly, the heat release rate curves of both Al_2O_3-containing composites showed no distinct sharp peaks, signifying that the resulting char layers were compact, thermally stable, and resistant to rupture by volatile decomposition products. In terms of smoke suppression, the PSPR of the Al_2O_3/Al-IFR/PP composites were significantly lower than those of both neat PP and 20Al-IFR/PP. This indicates that Al_2O_3 not only reinforces the condensed-phase structure but also contributes to reducing gas-phase emissions. Furthermore, the high flame performance index and low flame growth index values, as presented in Fig. 5.9, further confirm the outstanding flame retardancy of the Al_2O_3/Al-IFR system at optimized ratios. Notably, both 1Al_2O_3/20Al-IFR/PP and 5Al_2O_3/20Al-IFR/PP achieved flame retardancy index values exceeding 10, qualifying them for the "Excellent" category of flame retardant materials.

Furthermore, the HRR, weight loss, THR, and TSR curves for the composites incorporating 5 wt.% of Al_2O_3, BN, and MWCNTs in combination with 20 wt.% Al-IFR are

presented in Fig. 5.10. Among them, the fire safety performance of 5BN/20Al-IFR/PP and 5MWCNT/20Al-IFR/PP was unexpectedly poor, consistent with the trends observed in the LOI and UL 94 tests. As illustrated in Fig. 5.11, these two samples failed to form continuous and effective char layers during combustion, leading to a rapid increase in heat release rate at the early stage. The corresponding TTP values were only 60 s for 5BN/20Al-IFR/PP and 55 s for 5MWCNT/20Al-IFR/PP, significantly lower than that of 5Al_2O_3/20Al-IFR/PP. In addition, the TSR values of 5BN/20Al-IFR/PP and 5MWCNT/20Al-IFR/PP exceeded 3000 $m^2 \cdot m^{-2}$, much higher than that of neat PP, indicating a significant smoke hazard. These samples also exhibited lower av-EHC, reduced char residue, and higher CO yields. Such trends suggest a shift in the flame-retardant mechanism toward gas-phase activity, predominantly driven by the excessive release of phosphorus-containing volatiles, which exert quenching effects but lead to incomplete combustion. As a result, more smoke particles were generated, and the overall flame-retardant performance was compromised. Although some reduction in PHRR was observed for both BN- and MWCNT-containing samples, the absence of stable, expandable char structures with high integrity significantly limited their effectiveness. These results indicate that both BN and MWCNTs interfere with the intumescent char-forming mechanism, likely by disrupting the synergistic interactions between Al-PAP and MPP. In contrast, Al_2O_3 demonstrated excellent compatibility with the Al-IFR system, supporting the formation of robust char layers and yielding superior fire safety performance. Therefore, Al_2O_3 emerges as a more suitable additive for developing thermally conductive PP composites with enhanced intumescent flame retardant behavior.

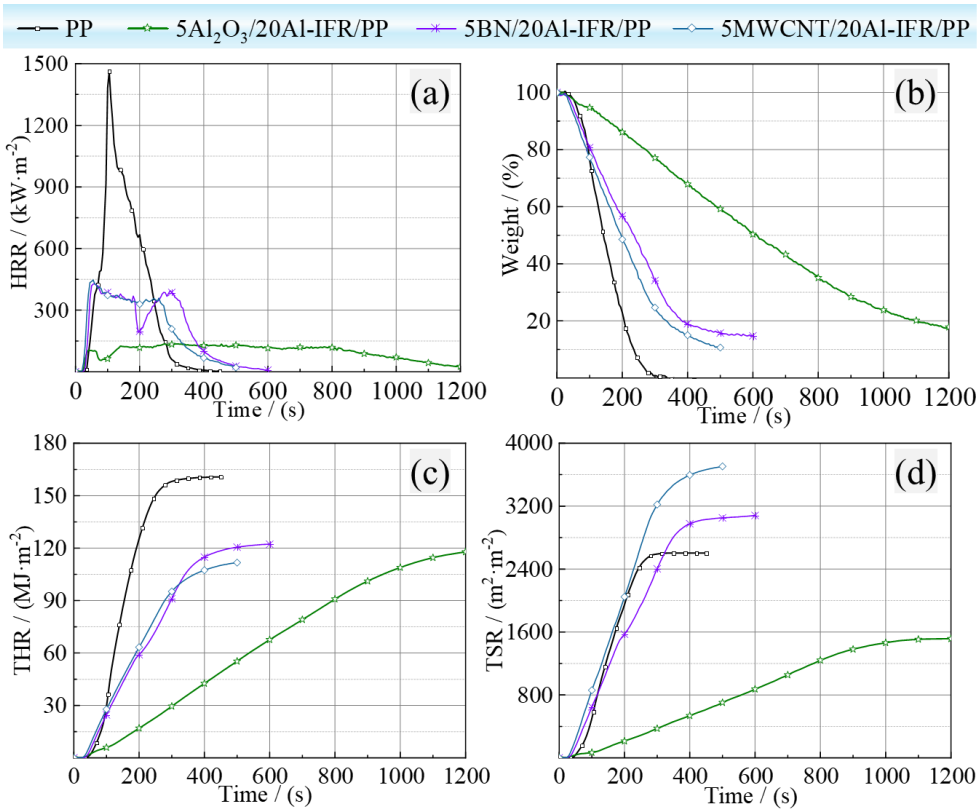

Fig. 5.10 (a) HRR, (b) weight loss, (c) THR, and (d) TSR curves of neat PP and PP containing different thermal conductive fillers.

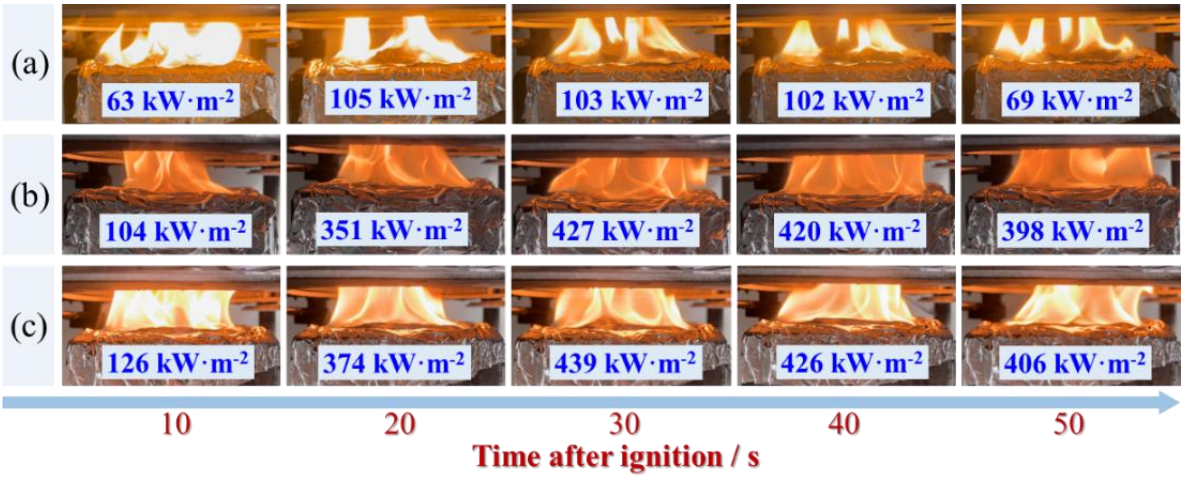

Fig. 5.11 The flame images and HRR values at the initial burning stage of (a) $5Al_2O_3$/20Al-IFR/PP, (b) 5BN/20Al-IFR/PP, and (c) 5MWCNT/20Al-IFR/PP.

5.7 Characterization of char residue

The appearance and micromorphology of the char residues obtained from the cone calorimeter tests are presented in Fig. 5.12. It is evident that while neat PP left no residual structure post-combustion, the composites incorporating Al-IFR and Al_2O_3/Al-IFR formed visibly expanded and cohesive char layers. These intumescent char layers act as physical barriers, limiting the

transfer of heat and gaseous degradation products, thereby contributing to the suppression of flame propagation and reduction of fire intensity. As shown in Fig. 5.12(b1, b2), the 20Al-IFR/PP composite formed a char layer approximately 3 cm in height, with a relatively dense outer surface. However, the presence of a visible perforation in the central region of the char residue, as illustrated in Fig. 5.12(b), suggests partial collapse or rupture of the barrier during the later combustion stages. This structural failure correlates with the peak heat release rate observed in the HRR curve, indicating that the thermal stability of the char layer formed solely by Al-IFR may be insufficient under prolonged heat exposure. In contrast, the addition of Al_2O_3 significantly improved the structural integrity of the char layers. Composites such as 1Al_2O_3/20Al-IFR/PP and 5Al_2O_3/20Al-IFR/PP produced continuous and compact char residues without obvious ruptures, as shown in Fig. 5.12(c, d). These enhanced char layers remained intact under thermal stress and resisted erosion by volatile decomposition products, which corresponds to their notably lower PHRR values. Furthermore, high-resolution SEM images (e.g., Fig. 5.12(c3)) revealed that Al-containing particles were well-dispersed and embedded within the char matrix, suggesting a possible catalytic role of Al_2O_3 in promoting char formation and stabilizing the carbonaceous structure during combustion. On the other hand, the char residues from 5BN/20Al-IFR/PP and 5MWCNT/20Al-IFR/PP composites displayed negligible expansion and lacked the formation of protective layers, as seen in Fig. 5.12(e, e1, f, f1). The absence of intumescent barrier structures in these samples likely accounts for their inferior flame retardant performance, as previously indicated by their high PHRR and TSR values. These observations confirm that Al_2O_3 is a superior synergistic additive in the Al-IFR system, capable of reinforcing the char layer and enhancing flame retardancy in PP composites.

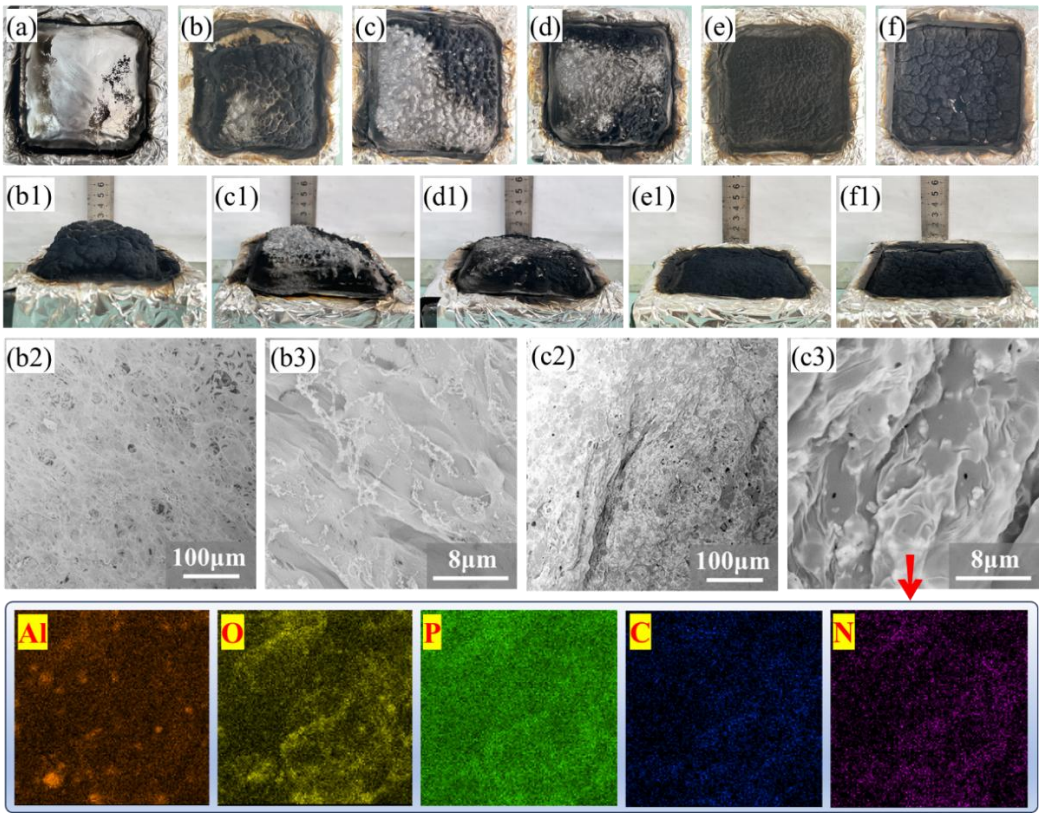

Fig. 5.12 The charred layers morphology of (a) PP, (b, b1, b2, b3) 20Al-IFR/PP, (c, c1, c2, c3) 1Al_2O_3/20Al-IFR/PP, (d, d1) 5Al_2O_3/20Al-IFR/PP, (e, e1) 5BN/20Al-IFR/PP, (f, f1) 5MWCNT/20Al-IFR/PP and the Al-EDS map of 1Al_2O_3/20Al-IFR/PP.

To further elucidate the enhancement mechanism imparted by Al_2O_3 in the Al-IFR system, X-ray photoelectron spectroscopy was employed to analyze the elemental composition of the char residues, with the data summarized in Table 5.5. Notably, the residue from the 1Al_2O_3/20Al-IFR/PP composite exhibited a significantly higher carbon content (51.80 wt.%) compared to that of 20Al-IFR/PP (21.60 wt.%), despite both samples containing equivalent levels of phosphorus-based components. This observation suggests that the presence of Al_2O_3 enhanced the retention of carbonaceous species during combustion. Additionally, the char of 1Al_2O_3/20Al-IFR/PP displayed a more intense signal corresponding to the P–O–C structure, as confirmed by FTIR analysis following the LOI test. This indicates a more extensive interaction between phosphoric acid derivatives and the PP matrix, likely leading to the formation of a more robust and interconnected char network. These findings imply that Al_2O_3 plays a catalytic role in promoting crosslinking reactions between the phosphorus-containing components of Al-IFR and the PP matrix during thermal degradation. The improvement in char structure quality was further supported by Raman spectroscopy results (Fig. 5.13). Both char residues exhibited characteristic D- and G-band peaks, associated with disordered and graphitic carbon structures, respectively. The intensity ratio (I_D/I_G) of 1Al_2O_3/20Al-IFR/PP was notably lower

than that of 20Al-IFR/PP, indicating a higher degree of graphitization in the former. This suggests that the char formed in the presence of Al_2O_3 possesses greater structural order and thermal stability, making it more resistant to degradation under combustion conditions. Overall, the incorporation of Al_2O_3 not only facilitates the formation of a denser, more thermally stable carbonaceous barrier but also enhances the crosslinking and charring efficiency of the Al-IFR system. These synergistic effects are key contributors to the superior flame retardant performance observed in the $1Al_2O_3$/20Al-IFR/PP composite.

Table 5.5 The element contents (wt. %) of chars after cone calorimeter test.

Sample	C	N	O	P	Al
20Al-IFR/PP	21.60	4.90	46.29	25.99	1.22
$1Al_2O_3$/20Al-IFR/PP	51.80	3.59	26.66	15.98	1.97

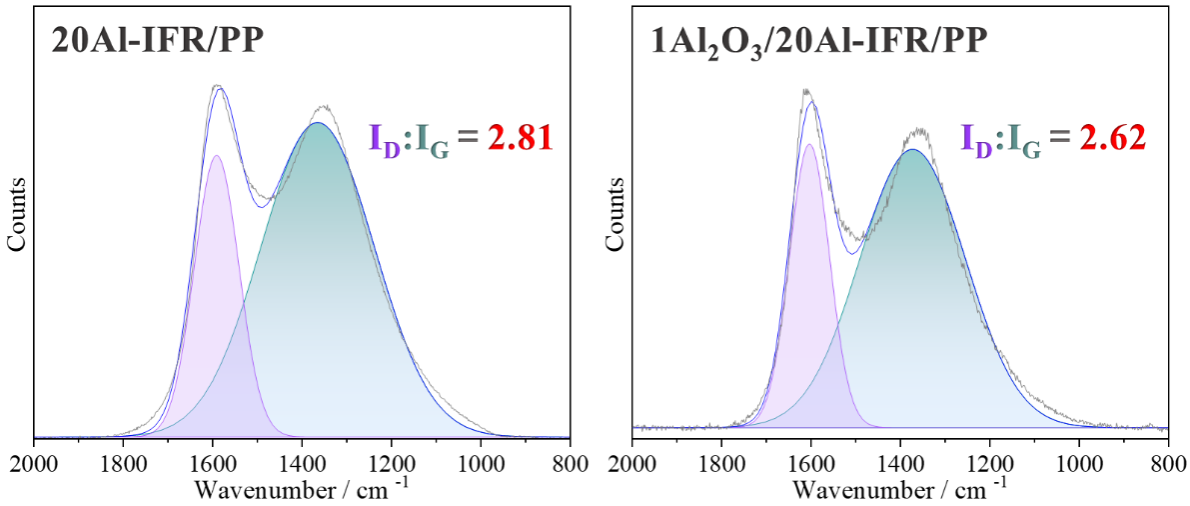

Fig. 5.13 The Raman spectra of chars after cone colorimeter test.

To assess the structural stability of intumescent char layers, composites consisting of 20 wt.% Al-IFR combined with 5 wt.% of different inorganic fillers, including Al_2O_3, BN, and MWCNT, were subjected to thermal treatment at 800 °C in a muffle furnace. The resulting char morphologies are illustrated in Fig. 5.14, while corresponding residue yields in TGA test are presented in Fig. 5.15. Notably, the three fillers demonstrated markedly different effects on the charring behavior and structural integrity of the Al-IFR system. The introduction of BN and MWCNT significantly disrupted the expansion and continuity of the char layers. In particular, MWCNT appeared to interfere with the crosslinking reactions among IFR components, resulting in negligible char expansion and poor residue formation. Similarly, BN incorporation led to weakened char structures, as evidenced by the hollow and brittle residue morphology, indicating its detrimental effect on char layer mechanical integrity. In contrast, Al_2O_3 exhibited

a favorable synergistic interaction with Al-IFR, promoting the formation of more compact and continuous char layers. This structural enhancement is critical for establishing an effective barrier against heat and mass transfer during combustion. However, an excessive Al_2O_3 loading (e.g., 9 wt.%) in the 20Al-IFR/PP system resulted in deteriorated flame retardancy, with the composite failing the UL-94 vertical burning test and showing a reduced limiting oxygen index. This decline highlights the threshold beyond which excessive inorganic filler loading can compromise the charring reaction, impair quality, and ultimately negate the flame retardant benefits of the IFR system. Overall, while high filler content can disrupt the charring process, Al_2O_3 stands out as the most compatible additive among the tested fillers. Its integration with Al-IFR shows greater tolerance and better preserves the flame retardant performance, making it a promising candidate for constructing thermally conductive, and flame-retardant PP composites.

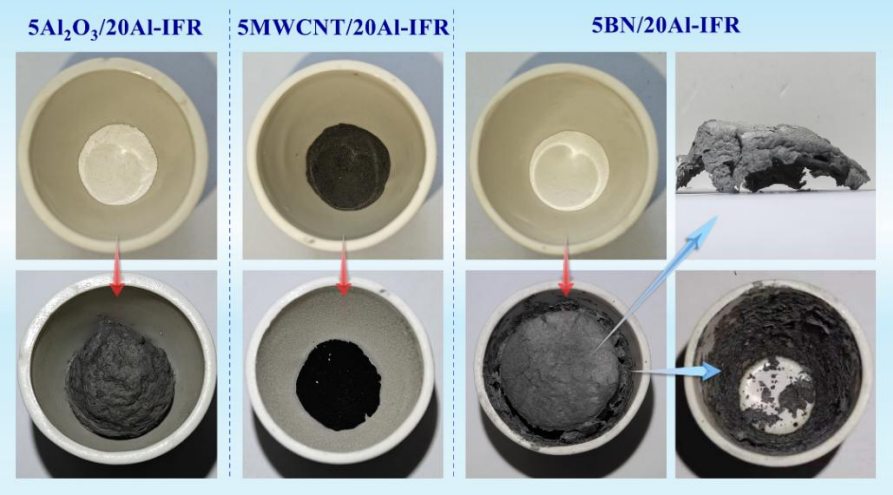

Fig. 5.14 The residue morphology of Al-IFR/thermal conductive fillers after heating to 800 ℃.

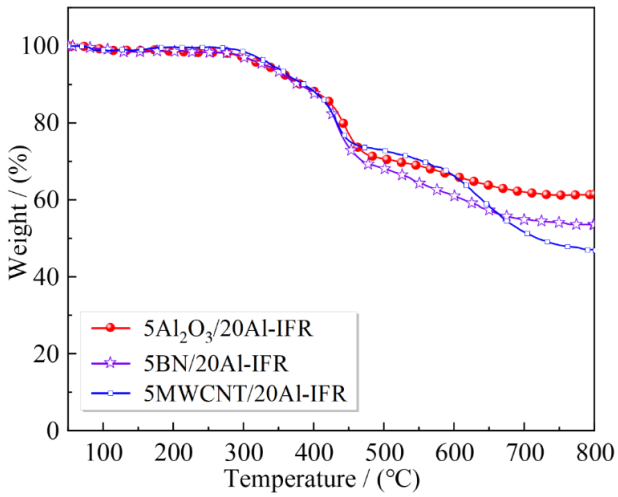

Fig. 5.15 The TGA curves of Al-IFR/thermal conductive fillers.

5.8 Thermal decomposition behavior

The thermogravimetric analysis curves of the flame retardants and representative PP composites are presented in Fig. 5.16 to evaluate their thermal stability and charring capacity. As shown in Fig. 5.16(a), the Al-IFR system exhibited a significantly higher residue yield of 17.2% compared to 10.9% for the conventional IFR. This enhancement is attributed to the presence of aluminum ions in Al-PAP, which likely facilitate synergistic charring reactions among phosphoric acid, piperazine, and melamine moieties. Moreover, in comparison to the PPAP/MPP system, the Al-PAP/MPP system displayed a slower decomposition rate beyond 500 °C, indicating that its thermal degradation products were more stable. The improved thermal stability and higher char residue of Al-IFR underpin its superior performance in flame retardancy, as confirmed by its favorable outcomes in LOI, UL-94, glow wire, and cone calorimeter tests. Notably, the inclusion of Al_2O_3 further enhanced the thermal stability of the system. The residue yields of 1Al_2O_3/20Al-IFR and 5Al_2O_3/20Al-IFR reached 32.9% and 52.2%, respectively, demonstrating a substantial increase relative to that of Al-IFR alone. In contrast, the theoretical residue yields - calculated assuming no interaction between Al-IFR and Al_2O_3 - were only 21.4% and 33.76%, respectively. This deviation indicates a strong synergistic effect between Al-IFR and Al_2O_3 in promoting char formation. Further evidence of this synergy is shown in Fig. 5.16(b), where the thermal decomposition of 1Al_2O_3/20Al-IFR was significantly suppressed above 500 °C, despite the low Al_2O_3 mass fraction (approximately 1/21 of the total). These results suggest that Al_2O_3 not only enhances the char-forming efficiency but also stabilizes the decomposition pathway of the flame retardant system.

Additionally, as shown in Fig. 5.16(c), the incorporation of intumescent flame retardants increased the initial decomposition temperature of the PP composites in air, indicating improved thermal resistance. The charring ability of these composites corresponded closely with the intrinsic char-forming potential of their respective flame retardant systems. Overall, the integration of Al_2O_3 into the Al-IFR system represents an effective strategy for enhancing both the thermal stability and char-forming efficiency of intumescent flame retardant PP composites. Nevertheless, it is important to note that a higher char yield alone does not necessarily equate to improved flame retardancy. The barrier efficiency of the char layer which was determined by both its quantity and structural integrity plays a critical role. Therefore, achieving an optimal balance between the amount and the quality of char is essential for maximizing the performance of intumescent flame retardant systems.

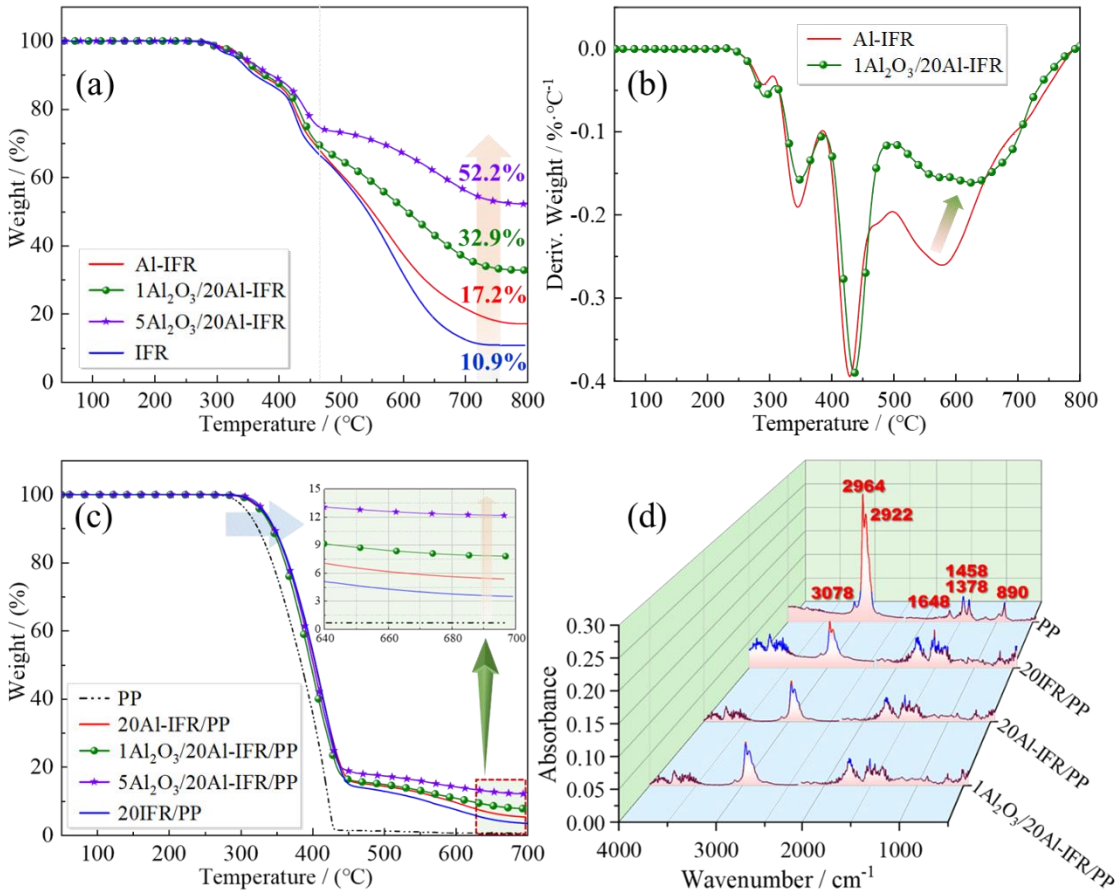

Fig. 5.16 (a) TG curves and (b) DTG curves of typical flame retardant, and the (c) TG curves and (d) released fragments' FTIR curves of typical PP composites.

Furthermore, real-time Fourier-transform infrared spectroscopy was employed to monitor the chemical structure of volatile decomposition products in the gas phase. As shown in Fig. 5.16(d), the FTIR spectra at the maximum decomposition temperature revealed that the main pyrolysis products of neat PP were hydrocarbons, as evidenced by characteristic absorption peaks corresponding to $–CH_3$ (2964, 1458, and 1378 cm^{-1}), $–CH_2$ (2922 cm^{-1}), $=CH_2$ (3078 and 890 cm^{-1}), and C=C (1648 cm^{-1}) functional groups. These fragments are known to be highly flammable, which explains the intense combustion behavior of unmodified PP. Upon incorporation of intumescent flame retardant systems into the PP matrix, the release intensity of these flammable hydrocarbon species was markedly reduced, indicating effective interaction between the flame retardants and the polymer matrix to form char. Notably, the 20Al-IFR/PP and $1Al_2O_3$/20Al-IFR/PP composites exhibited significantly weaker hydrocarbon absorption bands compared to 20IFR/PP, suggesting enhanced char formation and reduced generation of combustible volatiles. These findings, when considered alongside the TGA results, demonstrate that aluminum-based components, including Al^{3+} ions and Al_2O_3, play a crucial role in promoting charring and improving the condensed-phase flame retardant performance.

Additionally, the 1Al_2O_3/20Al-IFR sample released detectable phosphorus-containing species, such as P–O groups, during decomposition, indicative of a gas-phase flame inhibition mechanism. This was further corroborated by the FTIR spectra in Fig. 5.17. Overall, these results confirm the dual-phase flame retardant mechanism of the Al_2O_3/Al-IFR system in PP, which combines condensed-phase charring with gas-phase radical quenching, thereby significantly enhancing the flame retardant performance.

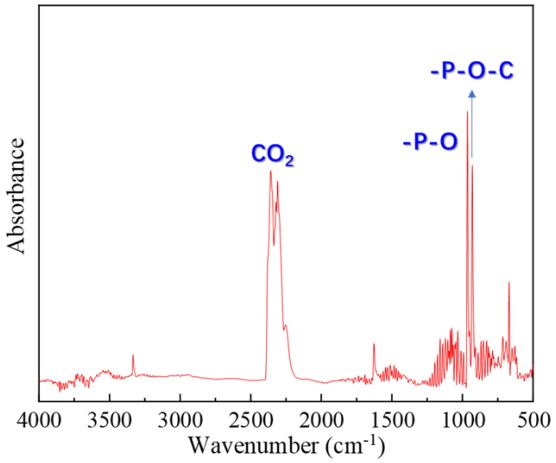

Fig. 5.17 The FTIR spectrum of fragments for 1Al_2O_3/20Al-IFR samples at the maximum decomposition rate.

5.9 Pyrolysis behavior of flame retardants

The differing flame retardant efficiencies observed among the systems suggest that their thermal degradation behaviors vary significantly. To further elucidate these differences, in addition to thermogravimetric analysis, pyrolysis-gas chromatography/mass spectrometry was employed to investigate the decomposition characteristics of IFR, Al-IFR, and 1Al_2O_3/20Al-IFR at a pyrolysis temperature of 500 °C. The resulting spectra are presented in Fig. 5.18. As shown in Fig. 5.18(a), both Al-IFR and 1Al_2O_3/20Al-IFR exhibited markedly lower fragment intensities compared to conventional IFR, indicating a more complete char-forming process and reduced release of volatile degradation products. Notably, the intensity of peak C was the lowest for 1Al_2O_3/20Al-IFR, further confirming the enhanced charring behavior in the presence of Al_2O_3. Additionally, IFR displayed two distinct peaks, including a prominent shoulder peak that disappeared in the spectra of Al-IFR and 1Al_2O_3/20Al-IFR. This phenomenon suggests that the aluminum-modified flame retardant systems underwent altered decomposition pathways, resulting in fewer and less volatile products than the PPAP/MPP-based IFR. The major pyrolysis products were identified from the mass spectra shown in Fig. 5.18(b). In Py-GC/MS testing, rapid heating favors the formation of hybrid degradation fragments only when

strong interactions exist between the flame retardant components. Otherwise, the components decompose independently. For the conventional IFR, the major volatile products were phosphorus-containing fragments derived from polyphosphoric acid (MPP) and pyrophosphoric acid (PPAP), along with nitrogen-containing species from melamine, indicating limited interaction between PPAP and MPP during decomposition. By contrast, the Al-IFR system generated larger and more complex molecular fragments, such as –CH–O–P(=O)–OH and –P(=O)–O–NH_2. These structures point to a more integrated degradation mechanism, where aluminum ions facilitate stronger interactions between phosphoric acid, nitrogen species, and carbon-rich components. Furthermore, the inclusion of Al_2O_3 in the 1Al_2O_3/20Al-IFR system enhanced the formation of phosphorus/carbon/oxygen hybrid structures, suggesting that Al_2O_3 acts synergistically with Al^{3+} to promote crosslinking and char formation. In summary, the presence of both aluminum ions and alumina fundamentally alters the pyrolysis behavior of intumescent flame retardant systems. Compared to conventional IFR, these aluminum-based systems encourage deeper integration among acid, carbon, and gas sources during decomposition, thereby enhancing char yield and thermal stability.

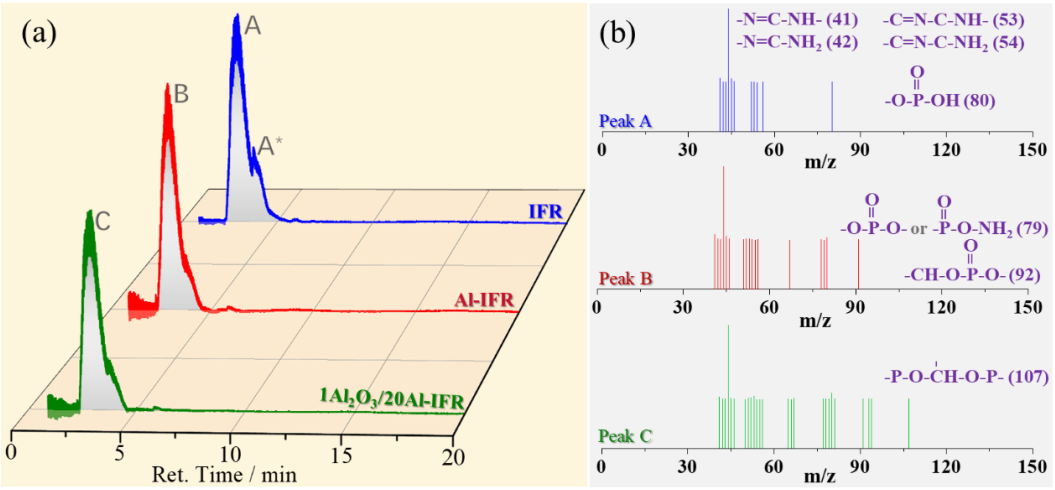

Fig. 5.18 The (a) GC and (b) MS spectrum of intumescent flame retardant systems.

5.10 Thermal conductivity performance

The effects of Al_2O_3 and the Al-IFR system on the thermal conductivity performance of PP composites were evaluated by measuring thermal diffusivity (α) and thermal conductivity (κ), as reported in Fig. 5.19(a, b) and Table 5.6. Both α and κ values were significantly increased in the samples containing Al-IFR and Al_2O_3/Al-IFR, in comparison to neat PP, indicating improved heat transfer performance. Notably, the incorporation of Al_2O_3 had a more pronounced effect on enhancing thermal conductivity than Al-IFR alone. Specifically, the composite containing 5 wt.% Al_2O_3 and 20 wt.% Al-IFR exhibited α and κ values of 2.07×10^{-7}

$m^2 \cdot s^{-1}$ and 0.414 $W \cdot m^{-1} \cdot K^{-1}$, respectively—corresponding to increases of 27.0% and 48.9% relative to neat PP.

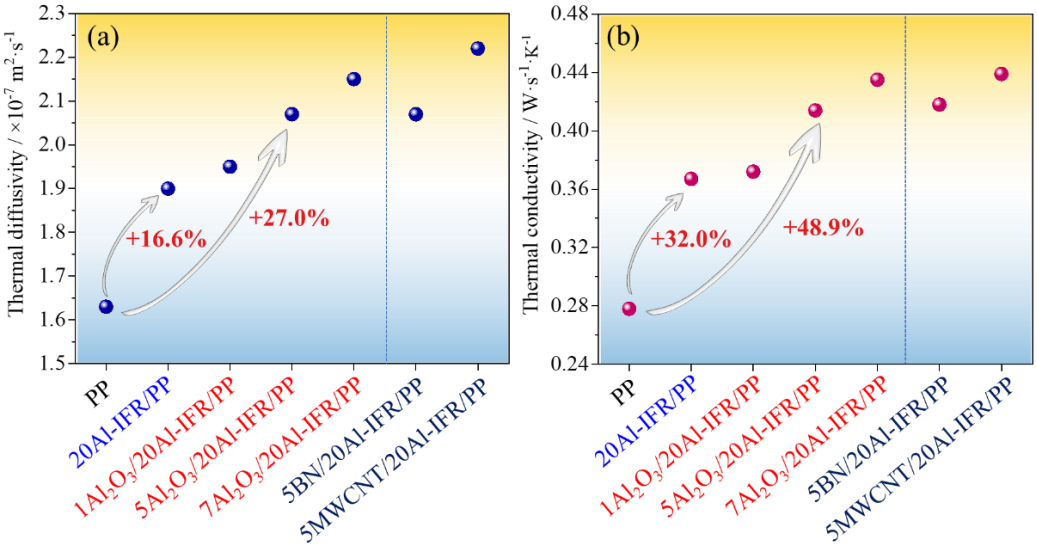

Fig. 5.19 The thermal diffusivity and thermal conductivity results of typical samples.

Table 5.6 The thermal-conductive performance of typical samples.

	Thermal diffusivity /$m^2 \cdot s^{-1}$	Thermal conductivity /$W \cdot s^{-1}K^{-1}$
PP	1.63×10^{-7}	0.278
20Al-IFR/PP	1.90×10^{-7}	0.367
$1Al_2O_3$/20Al-IFR/PP	1.95×10^{-7}	0.372
$5Al_2O_3$/20Al-IFR/PP	2.07×10^{-7}	0.414
$7Al_2O_3$/20Al-IFR/PP	2.15×10^{-7}	0.435
5BN/20Al-IFR/PP	2.07×10^{-7}	0.418
5MWCNT/20Al-IFR/PP	2.22×10^{-7}	0.439

In addition to Al_2O_3, boron nitride and multi-walled carbon nanotubes also contributed to enhanced thermal conductivity due to their inherently high thermal conduction and good dispersion within the matrix. To visualize thermal conductivity more intuitively, 3 mm-thick sheet-shaped samples were placed on a 100 °C heating platform, and their back-side temperatures were recorded in real time. As illustrated in Fig. 5.20, the $5Al_2O_3$/20Al-IFR/PP sample exhibited consistently higher maximum and average temperatures on the backside compared to neat PP, indicating faster heat transfer. Furthermore, the comparison between Figs. 5.20 (c) and (d) confirmed that the internal heat conduction rate was markedly improved in the Al_2O_3-modified system. Enhancing the Al_2O_3 content further improved thermal conductivity. The composite with 7 wt.% Al_2O_3 and 20 wt.% Al-IFR achieved α and κ values of 2.15×10^{-7}

$m^2 \cdot s^{-1}$ and 0.435 $W \cdot m^{-1} \cdot K^{-1}$, respectively. Although BN and MWCNT also exhibited effective thermal conduction, practical application demands a balance between flame retardancy and thermal conductivity. Among the three fillers, Al_2O_3 demonstrated superior overall performance, as it not only enhanced heat transfer but also maintained satisfactory flame retardancy. Within the evaluated formulation range, the optimal Al_2O_3 content for maintaining flame retardant performance was found to be 7 wt.% in conjunction with 20 wt.% Al-IFR. For applications requiring even higher thermal conductivity, both Al_2O_3 and Al-IFR loadings may be increased proportionally, provided that the balance between flame retardancy and thermal conduction is preserved.

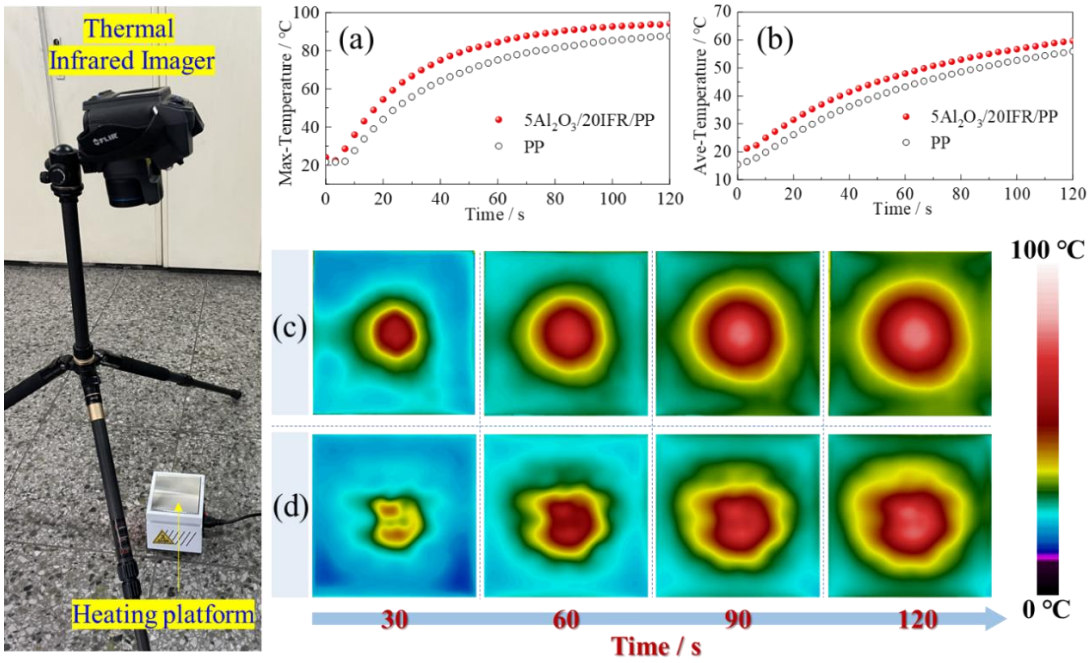

Fig. 5.20 (a) The max-temperature/time curve, (b) av-temperature/time curve, and the thermal infrared images of (c) $5Al_2O_3$/20Al-IFR/PP and (d) PP.

5.11 Mechanical properties

Polypropylene is widely recognized for its excellent toughness, characterized by high elongation at break and impact resistance. Therefore, the evaluation of mechanical performance is essential for extending the applicability of flame-retardant PP materials. The typical mechanical properties of selected composites are presented in Fig. 5.21 and Table 5.7. Neat PP exhibited an elongation at break exceeding 750% and a non-notched impact strength of 124.8 ± 14.9 $kJ \cdot m^{-2}$. Upon the incorporation of Al-IFR, both the elongation at break and tensile strength experienced modest reductions, while the impact resistance declined more substantially. For instance, the 20Al-IFR/PP composite maintained a tensile strength of

26.6 ± 0.4 MPa and an elongation at break of 518.9 ± 42.6%, indicating that ductility remained relatively high despite the flame retardant loading. However, the non-notched and notched impact strengths decreased sharply to 35.8 ± 4.7 $kJ \cdot m^{-2}$ and 3.13 ± 0.18 $kJ \cdot m^{-2}$, respectively. Fracture surface analysis revealed the formation of interfacial voids attributed to the detachment of Al-IFR particles during tensile deformation (Figs. 5.21 c, d). While the small particle size of Al-IFR limited the occurrence of cavitation, the weak interfacial adhesion between Al-IFR and the PP matrix hindered energy dissipation during impact, leading to stress concentration and reduced impact resistance (Figs. 5.21 e, f). Unexpectedly, aluminum oxide exhibited a minimal negative effect on the mechanical properties of PP, even at high loadings. For example, the 30Al_2O_3/PP composite with 30 wt.% Al_2O_3 showed an elongation at break of 723.2 ± 38.7% and a non-notched impact strength of 106.7 ± 13.3 $kJ \cdot m^{-2}$ - values comparable to those of neat PP. This favorable performance is likely due to the relatively small particle size of Al_2O_3 (hundreds of nanometers to ~2 μm), which avoids large-scale void formation under mechanical stress, as well as good compatibility with the PP-g-MA compatibilizer. When Al-IFR was combined with Al_2O_3, the resulting flame-retardant and thermally conductive composites still retained good toughness. The 5Al_2O_3/20Al-IFR/PP sample achieved an elongation at break exceeding 400% and a non-notched impact strength over 30 $kJ \cdot m^{-2}$, despite the total additive loading reaching 25 wt.%. Although the mechanical performance was slightly compromised, the reductions were acceptable in light of the substantial improvements in flame retardancy and smoke suppression. In summary, both Al-IFR and Al-IFR/Al_2O_3-modified PP composites maintained favorable mechanical properties, confirming their potential for practical applications that require a balance of flame retardancy, thermal conductivity, and mechanical toughness.

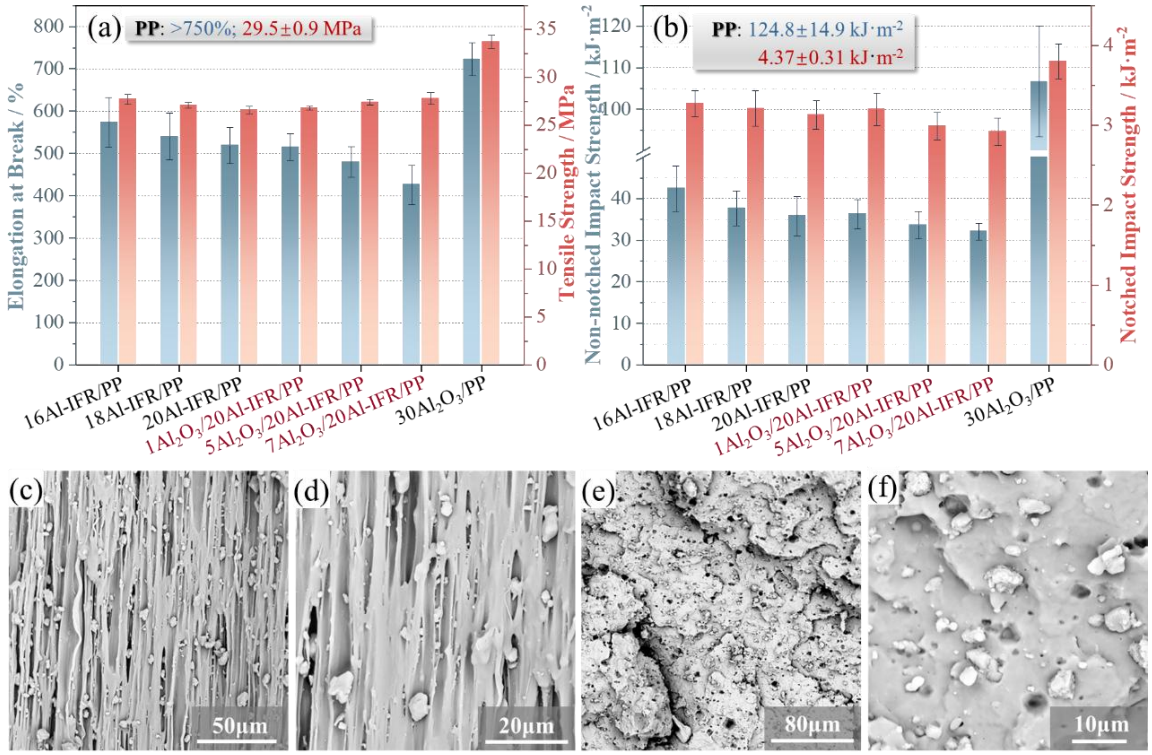

Fig. 5.21 The (a) tensile and (b) impact properties of PP composites, and the (c, d) tensile and (e, f) impact fracture micromorphology of 20Al-IFR/PP.

Table 5.7 The tensile and impact properties of PP composites.

	Elongation at break /%	Tensile Strength /MPa	Non-notched impact strength /kJ·m^{-2}	Notched impact strength /kJ·m^{-2}
PP	> 750	29.5±0.9	124.8±14.9	4.37±0.31
16Al-IFR/PP	573.2±58.8	27.7±0.5	42.4±5.5	3.27±0.16
18Al-IFR/PP	540.0±55.3	27.1±0.3	37.7±4.2	3.21±0.22
20Al-IFR/PP	518.9±42.6	26.6±0.4	35.8±4.7	3.13±0.18
1Al_2O_3/20Al-IFR/PP	515.0±31.5	26.8±0.2	36.3±3.5	3.20±0.20
5Al_2O_3/20Al-IFR/PP	479.9±36.8	27.4±0.3	33.6±3.3	2.99±0.17
7Al_2O_3/20Al-IFR/PP	425.6±45.9	27.8±0.6	32.1±2.0	2.92±0.17
5BN/20Al-IFR/PP	225.6±65.0	28.0±0.9	30.1±2.6	2.92±0.30
5MWCNT/20Al-IFR/PP	327.7±53.6	27.7±0.7	32.1±3.6	2.95±0.24
30Al_2O_3/PP	723.2±38.7	33.7±0.7	106.7±13.3	3.80±0.22

5.12 Summary

In this work, a novel hybrid charring macromolecule, Al-PAP, was successfully synthesized via the dehydration reaction between aluminum ion-based phosphate and piperazine-based phosphate at a weight ratio of 1:9. As shown in Fig. 5.22, this aluminum-coordinated structure

demonstrated excellent intumescent flame retardancy when combined with melamine polyphosphate to form the Al-IFR system for polypropylene composites. With only 14 wt.% of Al-IFR, the limiting oxygen index of the PP composite reached over 28%, comparable to that of a traditional system containing 20 wt.% PPAP/MPP. This result highlights the effectiveness of metal-ion–phosphate hybridization in enhancing charring and flame-retardant performance. Further improvements were observed with increasing Al-IFR content. UL 94 V-0 ratings were achieved at 16 wt.% and 18 wt.% loadings for 3.2 mm and 1.6 mm thick specimens, respectively. At 20 wt.% loading, the 20Al-IFR/PP composite exhibited a PHRR of only 223 $kW \cdot m^{-2}$ and a PSPR of 0.047 $m^2 \cdot s^{-1}$, which showed reductions of 84.7% and 72.2%, respectively, compared to neat PP. Additionally, high FPI and low FGI values further confirmed the improved fire safety. These enhancements are primarily attributed to aluminum ions promoting stronger interactions among acid, gas, and carbon sources in the IFR system, resulting in more compact and protective char layers. Beyond flame retardancy, this study also aimed to introduce thermal conductivity to the PP matrix without compromising fire safety. To this end, three thermal conductive fillers, including alumina, boron nitride, and multi-walled carbon nanotubes, were evaluated. Among them, Al_2O_3 was selected for further investigation due to its superior synergy with Al-IFR in maintaining flame retardancy. With appropriate loading, Al_2O_3 not only enhanced thermal conductivity but also reinforced flame retardancy and smoke suppression. Specifically, the LOI of 1Al_2O_3/20Al-IFR/PP increased to 33.8%, while the PHRR of 1Al_2O_3/20Al-IFR/PP and 5Al_2O_3/20Al-IFR/PP dropped to 90 and 135 $kW \cdot m^{-2}$, representing reductions of 93.8% and 90.8%, respectively, relative to neat PP. In terms of thermal conductivity, the 5Al_2O_3/20Al-IFR/PP composite achieved a thermal diffusivity of 2.07×10^{-7} $m^2 \cdot s^{-1}$ and a thermal conductivity of 0.414 $W \cdot m^{-1} \cdot K^{-1}$- enhancements of 27.0% and 48.9%, respectively, compared to unmodified PP. Importantly, mechanical testing confirmed that the Al-IFR/Al_2O_3-modified PP composites retained excellent toughness, particularly in elongation at break, even at a total additive content of 25 wt.%. In conclusion, this study demonstrates a viable strategy for simultaneously achieving flame retardancy, thermal conductivity, and smoke suppression in PP composites. The introduction of the Al-PAP macromolecule was key to unlocking these multifunctional properties, providing a promising path for the development of advanced flame-retardant polymeric materials suitable for practical applications.

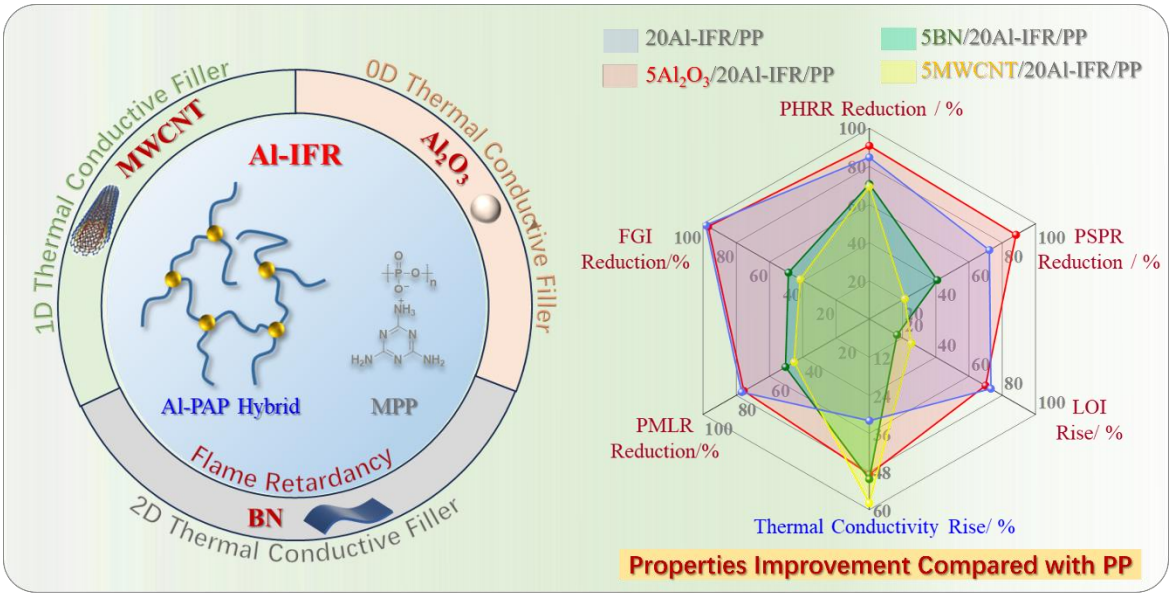

Fig. 5.22 The graphical summary of this chapter.

CHAPTER 6

Conclusion and Future Work

6.1 Conclusions

In this dissertation, a series of novel intumescent flame retardant systems were developed and systematically investigated to enhance the flame retardancy, mechanical performance, and multifunctional properties of polypropylene composites. The research focused on the rational design of macromolecular charring agents and their synergistic interactions with phosphorus-based acid and gas sources, aiming to overcome the limitations of traditional flame retardants and enable high-performance, application-ready PP materials.

(1) First, a class of N/Si-based charring macromolecules (MNSi-n) was synthesized by incorporating aggregation-controlled piperazine/phenyl-silicon structures into MCA frameworks. The resulting (MNSi-n/APP)/PP composites exhibited substantially enhanced flame retardancy, as evidenced by higher LOI, GWFI, GWIT, and UL-94 V-0 ratings, along with significantly reduced PHRR and THR. These enhancements were attributed to the synergistic charring behavior facilitated by the highly aggregated NSi-n cores, which promoted the formation of compact, silicon- and phosphorus-rich char layers. The results demonstrated that tailored molecular aggregation in the flame retardant design plays a pivotal role in improving condensed-phase protection and fire safety in PP systems.

(2) Building on this, covalently bonded copolymers (PNSi-co-MP) were developed to address the dispersion and compatibility challenges of physically mixed IFR systems. Compared to their physically blended counterparts, PNSi-co-MP/PP composites exhibited superior mechanical performance, including increased elongation at break and impact strength, owing to improved interfacial interactions and thermal softening behavior during melt blending. Moreover, these copolymers also outperformed physical blends in flame retardancy, achieving higher LOI, GWFI, and FRI values. The results underscore the importance of molecular-level integration of flame-retardant components to achieve both structural reinforcement and rapid, synergistic charring during combustion.

(3) Finally, a hybrid charring macromolecule (Al-PAP) was synthesized through coordination between aluminum and phosphate species, resulting in an Al-IFR system with excellent flame-retardant efficacy at low loading levels. The Al-IFR/PP composites achieved high LOI values and significant reductions in PHRR and PSPR, highlighting the role of aluminum ions in strengthening char formation and gas-phase inhibition. Furthermore, the

incorporation of alumina (Al_2O_3) as a thermally conductive filler enabled simultaneous improvements in thermal conductivity, flame retardancy, and smoke suppression without compromising mechanical integrity. These multifunctional composites present a practical solution for advanced applications where both fire safety and thermal management are critical.

In summary, this dissertation establishes a comprehensive framework for the molecular and functional design of intumescent flame retardant systems in polypropylene. Significant progress has been made in the development of high-efficiency, cost-effective, and application-oriented flame-retardant polypropylene composites by employing macromolecular-level structural innovations, including controlled aggregation, covalent copolymerization, and metal coordination.

6.2 Future work

This dissertation presents a systematic study on the construction of high-efficiency intumescent flame-retardant polypropylene composites, achieving a series of innovative and practically valuable results. However, to further advance this field, several important research directions merit continued exploration:

(1) Design and development of bio-based molecules and green intumescent flame-retardant systems with high charring efficiency

The current research has demonstrated the significant role of specific organosilicon and metal phosphate structures in enhancing the flame-retardant performance and char-forming ability of polypropylene. Future efforts can focus on identifying and utilizing novel structures derived from bio-based resources, such as phytic acid, tannic acid, lignin, chitosan, and cellulose derivatives. By introducing functional groups such as phosphorus-nitrogen moieties or siloxane segments through chemical modification, these bio-based structures can be transformed into effective flame-retardant macromolecules.

(2) Development of multifunctional flame-retardant polypropylene materials

In addition to achieving flame retardancy, the integration of multifunctional characteristics into polypropylene materials represents an important future direction. Potential functionalities include antistatic behavior, ultraviolet resistance, thermal conductivity, and electromagnetic shielding. The realization of these properties requires not only the co-design of functional additives but also a comprehensive optimization of compatibility, processability, and mechanical performance to ensure balanced and reliable material behavior.

(3) Design and optimization of fiber-reinforced flame-retardant polypropylene composites

With growing industrial demand, fiber-reinforced polypropylene composites are widely applied in sectors such as automotive, electronics, and home appliances. Future research should explore the use of reinforcement phases such as glass fibers, basalt fibers, and carbon fibers to develop materials with both high mechanical strength and flame retardancy. It is important to note that fiber additives may interfere with the formation of the protective char layer in intumescent systems, which introduces new challenges for the development of efficient charring strategies compatible with fiber reinforcement.

(4) Application of flame-retardant polypropylene composites in emerging industries

The flame-retardant systems developed in this study show promising application potential in a range of emerging industries. These include the use of polypropylene composites in electric vehicle battery housings and trays, interior components for rail transportation, electronic device enclosures, and structural elements of 5G communication equipment. These applications demand materials with excellent flame retardancy and thermal stability. Future research should therefore include performance evaluations under practical service conditions, such as resistance to aging, thermal cycling stability, and electrical insulation reliability, to support the transition from laboratory research to real-world applications.

In conclusion, future research should emphasize systematic innovation spanning from molecular design to material integration, with the aim of achieving environmentally friendly, high-performance, multifunctional, and industrially viable flame-retardant polypropylene composites.

CHAPTER 7

List of Publications

[1] **Wei Tang,** Lijun Qian*, Silvia González Prolongo, Yong Qiu, De-Yi Wang*. Macromolecular piperazine/aluminum phosphate hybrid and its efficient intumescent flame retardant/thermal conductive polypropylene. Chemical Engineering Journal, 2024, 495: 153162.

[2] **Wei Tang,** Lijun Qian*, Silvia González Prolongo, De-Yi Wang*. Dendritic copolymers from P-, N-and Si-based monomer and melamine phosphate generate thermal deformation toughening and a rapid charring flame retardant effect in polypropylene. Chemical Engineering Journal, 2023, 471: 144716.

[3] **Wei Tang,** Lijun Qian*, Silvia González Prolongo, De-Yi Wang*. Small core of piperazine/silane aggregation initiate efficient charring flame retardant effect in polypropylene composites. Polymer Degradation and Stability, 2023, 208: 110265.

Reference

[1]. Natta, G., Pino, P., Corradini, P., Danusso, F., Mantica, E., Mazzanti, G., & Moraglio, G. (1955). Crystalline high polymers of α-olefins. Journal of the American Chemical Society, 77(6), 1708-1710.

[2]. Ziegler, K., Holzkamp, E., Breil, H., & Martin, H. (1955). Das mülheimer normaldruck-polyäthylen-verfahren. Angewandte Chemie, 67(19-20), 541-547.

[3]. Pino, P. and Mülhaupt, R. (1980), Stereospecific Polymerization of Propylene: An Outlook 25 Years after Its Discovery. Angew. Chem. Int. Ed. Engl., 19: 857-875.

[4]. Brintzinger, H.H., Fischer, D., Mülhaupt, R., Rieger, B. and Waymouth, R.M. (1995), Stereospecific olefin polymerization with chiral metallocene catalysts. Angew. Chem. Int. Ed. Engl., 34: 1143-1170.

[5]. Hagihara, H., Tsuchihara, K., Takeuchi, K., Murata, M., Ozaki, H. and Shiono, T. (2004), Copolymerization of ethylene or propylene with α-olefins containing hydroxyl groups with zirconocene/methylaluminoxane catalyst. J. Polym. Sci. A Polym. Chem., 42: 52-58.

[6]. Van Der Ven, S. (2012). Polypropylene and other polyolefins: polymerization and characterization. Elsevier.

[7]. Matyjaszewski, K., & Davis, T. P. (2002). Handbook of radical polymerization (Vol. 922). New York: Wiley-Interscience.

[8]. Maddah, H. A. (2016). Polypropylene as a promising plastic: A review. Am. J. Polym. Sci, 6(1), 1-11.

[9]. Karger-Kocsis, J., & Bárány, T. (2019). Polypropylene handbook. Switzerland: Springer Nature.

[10]. Hossain, M. T., Shahid, M. A., Mahmud, N., Habib, A., Rana, M. M., Khan, S. A., & Hossain, M. D. (2024). Research and application of polypropylene: a review. Discover Nano, 19(1), 2.

[11]. Seidi, F., Movahedifar, E., Naderi, G., Akbari, V., Ducos, F., Shamsi, R., Vahabi, H., & Saeb, M. R. (2020). Flame retardant polypropylenes: A review. Polymers, 12(8), 1701.

[12]. Xu, Z. Z., Huang, J. Q., Chen, M. J., Tan, Y., & Wang, Y. Z. (2013). Flame retardant mechanism of an efficient flame-retardant polymeric synergist with ammonium polyphosphate for polypropylene. Polymer Degradation and Stability, 98(10), 2011-2020.

[13]. Kruse, T. M., Wong, H. W., & Broadbelt, L. J. (2003). Mechanistic modeling of polymer pyrolysis: polypropylene. Macromolecules, 36(25), 9594-9607.

[14]. Hayashi, J. I., Nakahara, T., Kusakabe, K., & Morooka, S. (1998). Pyrolysis of polypropylene in the presence of oxygen. Fuel Processing Technology, 55(3), 265-275.

[15]. Sojak, L., Kubinec, R., Jurdakova, H., Hájeková, E., & Bajus, M. (2006). GC-MS of polyethylene and polypropylene thermal cracking products. Petroleum & Coal, 48(1), 1-14.

[16]. Purohit, V., & Orzel, R. A. (1988). Polypropylene: A literature review of the thermal decomposition products and toxicity. Journal of the American College of Toxicology, 7(2), 221-242.

[17]. Matzen, M., Kandola, B., Huth, C., & Schartel, B. (2015). Influence of flame retardants on the melt dripping behaviour of thermoplastic polymers. Materials, 8(9), 5621-5646.

[18]. Gairola, S., Sinha, S., & Singh, I. (2025). Improvement of flame retardancy and anti-dripping properties of polypropylene composites via ecofriendly borax cross-linked lignocellulosic fiber. Composite Structures, 354, 118822.

[19]. Sharkey, M., Harrad, S., Abdallah, M. A. E., Drage, D. S., & Berresheim, H. (2020). Phasing-out of legacy brominated flame retardants: The UNEP Stockholm Convention and other legislative action worldwide. Environment International, 144, 106041.

[20]. van der Schyff, V., Kalina, J., Abballe, A., Iamiceli, A. L., Govarts, E., & Melymuk, L. (2023). Has regulatory action reduced human exposure to flame retardants?. Environmental Science & Technology, 57(48), 19106-19124.

[21]. de Boer, J., Harrad, S., & Sharkey, M. (2024). The European Regulatory Strategy for flame retardants-The right direction but still a risk of getting lost. Chemosphere, 347, 140638.

[22]. Enescu, D., Frache, A., Lavaselli, M., Monticelli, O., & Marino, F. (2013). Novel phosphorous-nitrogen intumescent flame retardant system. Its effects on flame retardancy and thermal properties of polypropylene. Polymer Degradation and Stability, 98(1), 297-305.

[23]. Song, P. A., Xu, L., Guo, Z., Zhang, Y., & Fang, Z. (2008). Flame-retardant-wrapped carbon nanotubes for simultaneously improving the flame retardancy and mechanical properties of polypropylene. Journal of Materials Chemistry, 18(42), 5083-5091.

[24]. Sang, B., Li, Z. W., Li, X. H., Yu, L. G., & Zhang, Z. J. (2016). Graphene-based flame retardants: a review. Journal of Materials Science, 51, 8271-8295.

[25]. Evans, A., Morris, L. J., Turner, Z. R., & O'Hare, D. (2025). Phosphonate-functionalized polypropylenes: single-component flame retardants. ACS Applied Polymer Materials, 7(4), 2508-2516.

[26]. Zhang, X., Shao, Z., Wei, T., Hou, X., Liu, X., Du, J., & Deng, H. (2025). Alkali-Induced transformation of salt lake magnesium slag into novel magnesium hydroxide-coated aluminum hypophosphite nanomaterials and their synergistic flame retardant effects. Surfaces and Interfaces, 56, 105745.

[27]. Qian, Y., Wei, P., Jiang, P., Zhao, X., & Yu, H. (2011). Synthesis of a novel hybrid synergistic flame retardant and its application in PP/IFR. Polymer Degradation and Stability, 96(6), 1134-1140.

[28]. Mai Nguyen Tran, T., MN, P., Lee, D. W., & Song, J. I. (2024). Effect of hybrid eco-friendly reinforcement and their size on mechanical and flame retardant properties of polypropylene composites for technical applications. Polymer Composites, 45(3), 2427-2443.

[29]. Wang, M., Yin, G. Z., Yang, Y., Fu, W., Palencia, J. L. D., Zhao, J., Wang, N., Jiang, Y., & Wang, D. Y. (2023). Bio-based flame retardants to polymers: A review. Advanced Industrial and Engineering Polymer Research, 6(2), 132-155.

[30]. Xu, Y. J., Zhang, K. T., Wang, J. R., & Wang, Y. Z. (2025). Biopolymer-based flame retardants and flame‐retardant materials. Advanced Materials, 37(22), 2414880.

[31]. Hörold, S. (2014). Phosphorus-based and intumescent flame retardants. In Polymer Green Flame Retardants (pp. 221-254). Elsevier.

[32]. Ho, Q. B., & Kontopoulou, M. (2021). Compatibilized polypropylene nanocomposites containing expanded graphite and graphene nanoplatelets. Polymer Engineering & Science, 61(4), 1116-1128.

[33]. Chung, D. D. L. (1987). Exfoliation of graphite. Journal of materials science, 22, 4190-4198.

[34]. Cheng, Z., Liao, D., Hu, X., Li, W., Xie, C., Zhang, H., & Yang, W. (2020). Synergistic fire retardant effect between expandable graphite and ferrocene-based non-phosphorus polymer on polypropylene. Polymer Degradation and Stability, 178, 109201.

[35]. Li, J., Wang, S., Zhang, G., Li, H., Sun, J., Gu, X., & Zhang, S. (2022). Burning behavior analysis of polypropylene composite containing poly-siloxane encapsulated expandable graphite. Polymer Degradation and Stability, 202, 110006.

[36]. Zheng, Z., Liu, Y., Zhang, L., & Wang, H. (2016). Synergistic effect of expandable graphite and intumescent flame retardants on the flame retardancy and thermal stability of polypropylene. Journal of Materials Science, 51, 5857-5871.

[37]. Bai, G., Guo, C., & Li, L. (2014). Synergistic effect of intumescent flame retardant and expandable graphite on mechanical and flame-retardant properties of wood flour-polypropylene composites. Construction and Building Materials, 50, 148-153.

[38]. Shi, Z., Yu, R., Lou, S., Li, N., Liu, J., Xing, H., Ma, L., Li, L., & Tang, T. (2022). A new strategy for constructing polypropylene composite foams with excellent ablation resistance and flame retardancy. Polymer, 251, 124940.

[39]. Guo, C., Zhou, L., & Lv, J. (2013). Effects of expandable graphite and modified ammonium polyphosphate on the flame-retardant and mechanical properties of wood flour-polypropylene composites. Polymers and Polymer Composites, 21(7), 449-456.

[40]. Bourbigot, S., Sarazin, J., Bensabath, T., Samyn, F., & Jimenez, M. (2019). Intumescent polypropylene: Reaction to fire and mechanistic aspects. Fire Safety Journal, 105, 261-269.

[41]. Chen, X., Wu, H., Luo, Z., Yang, B., Guo, S., & Yu, J. (2007). Synergistic effects of expandable graphite with magnesium hydroxide on the flame retardancy and thermal properties of polypropylene. Polymer Engineering & Science, 47(11), 1756-1760.

[42]. Liang, S., Liu, J., Guo, Y., Luo, J., Liu, H., & Peng, S. (2022). Role of expandable graphite on flame retardancy, smoke suppression, and acid resistance of polypropylene/magnesium hydroxide composites. Polymer Engineering & Science, 62(10), 3168-3179.

[43]. Dong, X., Yang, X., Liang, S., Li, J., Wang, K., Liu, J., & Chang, H. (2024). Flame retardancy of polypropylene filled with expandable graphite and magnesium hydroxide: The impact of particle size of expandable graphite and its mechanism. Journal of Vinyl and Additive Technology, 30(1), 142-155.

[44]. Qi, F., Tang, M., Wang, N., Liu, N., Chen, X., Zhang, Z., Zhang, K., & Lu, X. (2017). Efficient organic–inorganic intumescent interfacial flame retardants to prepare flame retarded polypropylene with excellent performance. RSC Advances, 7(50), 31696-31706.

[45]. Wang, N., Chen, S., Li, L., Bai, Z., Guo, J., Qin, J., Zhang, K., & Wu, H. (2021). An environmentally friendly nanohybrid flame retardant with outstanding flame-retardant efficiency for polypropylene. The Journal of Physical Chemistry C, 125(9), 5185-5196.

[46]. Yang, Z., Xi, W., Qian, L., Qiu, Y., Wang, J., Chen, Y., & Tang, W. (2023). Adsorption charring flame retardant effect of phosphaphenanthrene derivate intercalated micro-expanded graphite composite system in rigid polyurethane foams. Polymer Degradation and Stability, 216, 110493.

[47]. Tan, W., Tian, Y., Zuo, C., Zhang, Y., Liu, X., Ye, Z., Bai, L., Ren, Y., & Liu, X. (2025). Curcumin derivative intercalated expandable graphite: Imparting flame retardancy, anti-

dripping and smoke suppression for polylactic acid composites. Industrial Crops and Products, 224, 120305.

[48]. Malkappa, K., Prasad, C., Kang, C. S., Jeong, S. G., Sangaraju, S., Shin, E. J., & Choi, H. Y. (2025). Recent developments of phosphorous–nitrogen-based effective intumescent flame-retardant for polymers and textiles. Polymer Bulletin, 1-61.

[49]. Lim, K. S., Bee, S. T., Sin, L. T., Tee, T. T., Ratnam, C. T., Hui, D., & Rahmat, A. R. (2016). A review of application of ammonium polyphosphate as intumescent flame retardant in thermoplastic composites. Composites Part B: Engineering, 84, 155-174.

[50]. Liu, B. W., Zhao, H. B., & Wang, Y. Z. (2022). Advanced flame-retardant methods for polymeric materials. Advanced Materials, 34(46), 2107905.

[51]. Bourbigot, S. (2021). Intumescence-based flame retardant. Non-Halogenated Flame Retardant Handbook, 169-238.

[52]. Bellayer, S., Dilger, M., Duquesne, S., & Jimenez, M. (2024). Flame-retardants for polypropylene: A review. Polymer Degradation and Stability, 230, 111008.

[53]. Zhao, W., Kundu, C. K., Li, Z., Li, X., & Zhang, Z. (2021). Flame retardant treatments for polypropylene: Strategies and recent advances. Composites Part A: Applied Science and Manufacturing, 145, 106382.

[54]. Camino, G., & Costa, L. (1986). Mechanism of intumescence in fire retardant polymers. Reviews in inorganic chemistry, 8(1-2), 69-100.

[55]. Camino G, Costa L, Trossarelli L. Study of the mechanism of intumescence in fire retardant polymers: Part I – Thermal degradation of ammonium polyphosphate-pentaerythritol mixtures. Polymer Degradation and Stability, 1984, 6(4), 243-252.

[56]. Camino G, Costa L, Trossarelli L. Study of the mechanism of intumescence in fire retardant polymers: Part II – Mechanism of action in polypropylene-ammonium polyphosphate- pentaerythritol mixtures. Polymer Degradation and Stability, 1984, 7(1): 25-31.

[57]. Camino G, Costa L, Trossarelli L. Study of the mechanism of intumescence in fire retardant polymers: Part III – Effect of urea on the ammonium polyphosphate-pentaerythritol system. Polymer Degradation and Stability, 1984, 7(4): 221-229.

[58]. Camino G, Costa L, Trossarelli L. Study of the mechanism of intumescence in fire retardant polymers: Part IV – Evidence of ester formation in ammonium polyphosphate-pentaerythritol mixture. Polymer Degradation and Stability, 1984, 8(1): 13-22.

[59]. Zheng, A., Xia, Y., Li, N., Mao, Z., & Guan, Y. (2013). Synergistic effects of tetrabutyl titanate on intumescent flame-retarded polypropylene. Journal of Applied Polymer Science, 130(6), 4255-4263.

[60]. Gao, Q., Zhao, H., Zhou, X. L., Liu, F. Y., Jiao, Y. H., Xie, J. X., Qu, H. Q., Xu, J. Z., & Ma, H. Y. (2022). Flame retardant, combustion and thermal degradation properties of polypropylene composites treated with the mixture of pentaerythritol, nickel hydroxystannate and expandable graphite. Polymer Degradation and Stability, 203, 110084.

[61]. Bourbigot, S., Le Bras, M., & Delobel, R. (1995). Fire degradation of an intumescent flame retardant polypropylene using the cone calorimeter. Journal of fire sciences, 13(1), 3-22.

[62]. Zhou, S., Song, L., Wang, Z., Hu, Y., & Xing, W. (2008). Flame retardation and char formation mechanism of intumescent flame retarded polypropylene composites containing melamine phosphate and pentaerythritol phosphate. Polymer Degradation and Stability, 93(10), 1799-1806.

[63]. Xia, Y., Jin, F., Mao, Z., Guan, Y., & Zheng, A. (2014). Effects of ammonium polyphosphate to pentaerythritol ratio on composition and properties of carbonaceous foam deriving from intumescent flame-retardant polypropylene. Polymer Degradation and Stability, 107, 64-73.

[64]. Lai, X., Qiu, J., Li, H., Zeng, X., Tang, S., Chen, Y., & Chen, Z. (2015). Flame-retardant and thermal degradation mechanism of caged phosphate charring agent with melamine pyrophosphate for polypropylene. International Journal of Polymer Science, 2015(1), 360274.

[65]. Peng, H. Q., Zhou, Q., Wang, D. Y., Chen, L., & Wang, Y. Z. (2008). A novel charring agent containing caged bicyclic phosphate and its application in intumescent flame retardant polypropylene systems. Journal of Industrial and Engineering Chemistry, 14(5), 589-595.

[66]. Jiang, W., Hao, J., & Han, Z. (2012). Study on the thermal degradation of mixtures of ammonium polyphosphate and a novel caged bicyclic phosphate and their flame retardant effect in polypropylene. Polymer Degradation and Stability, 97(4), 632-637.

[67]. Li, X., Ou, Y. X., Zhang, Y. H., & Lian, D. J. (2000). Synthesis and structure of a novel caged bicyclic phosphate flame retardant. Chinese Chemical Letters, 11(10), 887-890.

[68]. He, Q., Lu, H., Song, L., Hu, Y., & Chen, L. (2009). Flammability and thermal properties of a novel intumescent flame retardant polypropylene. Journal of fire sciences, 27(4), 303-321.

[69]. Tian, N., Wen, X., Jiang, Z., Gong, J., Wang, Y., Xue, J., & Tang, T. (2013). Synergistic effect between a novel char forming agent and ammonium polyphosphate on flame retardancy and thermal properties of polypropylene. Industrial & Engineering Chemistry Research, 52(32), 10905-10915.

[70]. Huang, J., Zhang, Y., Yang, Q., Liao, X., & Li, G. (2012). Synthesis and characterization of a novel charring agent and its application in intumescent flame retardant polypropylene system. Journal of applied polymer science, 123(3), 1636-1644.

[71]. Zhang, S., Li, B., Lin, M., Li, Q., Gao, S., & Yi, W. (2011). Effect of a novel phosphorus-containing compound on the flame retardancy and thermal degradation of intumescent flame retardant polypropylene. Journal of Applied Polymer Science, 122(5), 3430-3439.

[72]. Xiao, D., Li, Z., De Juan, S., Gohs, U., Wagenknecht, U., Voit, B., & Wang, D. Y. (2016). Preparation, fire behavior and thermal stability of a novel flame retardant polypropylene system. Journal of Thermal Analysis and Calorimetry, 125, 321-329.

[73]. Chen, W., Yuan, S., Sheng, Y., & Liu, G. (2015). Effect of charring agent THEIC on flame retardant properties of polypropylene. Journal of Applied Polymer Science, 132(1), 41214.

[74]. Gao, S., Zhao, X., & Liu, G. (2017). Synthesis of tris (2-hydroxyethyl) isocyanurate homopolymer and its application in intumescent flame retarded polypropylene. Journal of Applied Polymer Science, 134(13), 44663.

[75]. Duan, L., Yang, H., Song, L., Hou, Y., Wang, W., Gui, Z., & Hu, Y. (2016). Hyperbranched phosphorus/nitrogen-containing polymer in combination with ammonium polyphosphate as a novel flame retardant system for polypropylene. Polymer Degradation and Stability, 134, 179-185.

[76]. Ding, S., Liu, P., Zhang, S., Gao, C., Wang, F., Ding, Y., & Yang, M. (2020). Crosslinking of β-cyclodextrin and combining with ammonium polyphosphate for flame-retardant polypropylene. Journal of Applied Polymer Science, 137(4), 48320.

[77]. Horacek, H., & Grabner, R. (1996). Advantages of flame retardants based on nitrogen compounds. Polymer Degradation and Stability, 54(2-3), 205-215.

[78]. Hu, X. P., Li, Y. L., & Wang, Y. Z. (2004). Synergistic effect of the charring agent on the thermal and flame retardant properties of polyethylene. Macromolecular Materials and Engineering, 289(2), 208-212.

[79]. Lai, X., Zeng, X., Li, H., Liao, F., Yin, C., & Zhang, H. (2012). Synergistic effect between a triazine-based macromolecule and melamine pyrophosphate in flame retardant polypropylene. Polymer composites, 33(1), 35-43.

[80]. Li, B., & Xu, M. (2006). Effect of a novel charring-foaming agent on flame retardancy and thermal degradation of intumescent flame retardant polypropylene. Polymer Degradation and Stability, 91(6), 1380-1386.

[81]. Chen, H., Wang, J., Ni, A., Ding, A., Han, X., & Sun, Z. (2018). The effects of a macromolecular charring agent with gas phase and condense phase synergistic flame retardant capability on the properties of PP/IFR composites. Materials, 11(1), 111.

[82]. Wang, Y., Xu, M. J., & Li, B. (2016). Synthesis of N-methyl triazine-ethylenediamine copolymer charring foaming agent and its enhancement on flame retardancy and water resistance for polypropylene composites. Polymer Degradation and Stability, 131, 20-29.

[83]. Feng, C., Liang, M., Jiang, J., Huang, J., & Liu, H. (2016). Synergistic effect of a novel triazine charring agent and ammonium polyphosphate on the flame retardant properties of halogen-free flame retardant polypropylene composites. Thermochimica Acta, 627, 83-90.

[84]. Feng, C., Li, Z., Liang, M., Huang, J., & Liu, H. (2015). Preparation and characterization of a novel oligomeric charring agent and its application in halogen-free flame retardant polypropylene. Journal of Analytical and Applied Pyrolysis, 111, 238-246.

[85]. Feng, C., Zhang, Y., Liu, S., Chi, Z., & Xu, J. (2012). Synthesis of novel triazine charring agent and its effect in intumescent flame-retardant polypropylene. Journal of applied polymer science, 123(6), 3208-3216.

[86]. Su, X., Yi, Y., Tao, J., Qi, H., & Li, D. (2014). Synergistic effect between a novel triazine charring agent and ammonium polyphosphate on flame retardancy and thermal behavior of polypropylene. Polymer degradation and stability, 105, 12-20.

[87]. Lai, X., Yin, C., Li, H., & Zeng, X. (2015). Synergistic effect between silicone-containing macromolecular charring agent and ammonium polyphosphate in flame retardant polypropylene. Journal of Applied Polymer Science, 132(10), 41580.

[88]. Chen, L., Yuan, Y., Wang, B., Liu, N., Xing, Y., & Li, Y. (2017). Synthesis and application of novel triazine-based charring-foaming agents in intumescent flame retardant polypropylene. Transactions of Tianjin University, 23, 221-229.

[89]. Yang, R., Ma, B., Zhao, H., & Li, J. (2016). Preparation, thermal degradation, and fire behaviors of intumescent flame retardant polypropylene with a charring agent containing

pentaerythritol and triazine. Industrial & Engineering Chemistry Research, 55(18), 5298-5305.

[90]. Wang, W., Wen, P., Zhan, J., Hong, N., Cai, W., Gui, Z., & Hu, Y. (2017). Synthesis of a novel charring agent containing pentaerythritol and triazine structure and its intumescent flame retardant performance for polypropylene. Polymer Degradation and Stability, 144, 454-463.

[91]. Yang, K., Xu, M. J., & Li, B. (2013). Synthesis of N-ethyl triazine–piperazine copolymer and flame retardancy and water resistance of intumescent flame retardant polypropylene. Polymer degradation and stability, 98(7), 1397-1406.

[92]. Wu, Q., Guo, J., Fei, B., Li, X., Sun, J., Gu, X., Li, H., & Zhang, S. (2020). Synthesis of a novel polyhydroxy triazine-based charring agent and its effects on improving the flame retardancy of polypropylene with ammonium polyphosphate and zinc borate. Polymer Degradation and Stability, 175, 109123.

[93]. Dai, J., & Li, B. (2010). Synthesis, thermal degradation, and flame retardance of novel triazine ring-containing macromolecules for intumescent flame retardant polypropylene. Journal of Applied Polymer Science, 116(4), 2157-2165.

[94]. Yang, T., Wu, Y., Cheng, Y., Huang, T., Yu, B., Zhu, M., & Yu, H. (2022). Synthesis of a charring agent containing triazine and benzene groups and its intumescent flame retardant performance for polypropylene. Polymer Degradation and Stability, 204, 110107.

[95]. Liu, S., Qiu, Y., Wang, T., Li, D., Qian, L., Xi, W., Wang, J., Qu, L., & Tang, W. (2025). Intumescent flame retardant behavior of aryl Schiff base triazine piperazine char-forming agent with heat-induced cyclization self-crosslinking trait in polypropylene. Chemical Engineering Journal, 508, 160959.

[96]. Xie, H., Lai, X., Li, H., & Zeng, X. (2016). Synthesis of a novel macromolecular charring agent with free-radical quenching capability and its synergism in flame retardant polypropylene. Polymer Degradation and Stability, 130, 68-77.

[97]. Peck, D. S. (1986, April). Comprehensive model for humidity testing correlation. In 24th International Reliability Physics Symposium (pp. 44-50). IEEE.

[98]. Tang, W., Qian, L., Chen, Y., Qiu, Y., & Xu, B. (2019). Intumescent flame retardant behavior of charring agents with different aggregation of piperazine/triazine groups in polypropylene. Polymer Degradation and Stability, 169, 108982.

[99]. Wang, J., Li, J., Meng, X., Gao, X., & Yan, H. (2022). Synthesis of a novel DOPO-substituted charring agent containing triazine for reducing the fire hazard of polypropylene. Journal of Polymer Research, 29(9), 380.

[100]. Liu, S., Tan, Y. L., Shao, S. C., Hui, Y. Y., & Peng, Z. H. (2013). Synthesis and characterization of a novel polyhydroxy triazine charring agent and properties of its flame retarded polyproylene. Advanced Materials Research, 746, 23-27.

[101]. Xu, M., Chen, Y., Qian, L., Wang, J., & Tang, S. (2014). Component ratio effects of hyperbranched triazine compound and ammonium polyphosphate in flame-retardant polypropylene composites. Journal of Applied Polymer Science, 131, 41006.

[102]. Qin, Y., Li, M., Huang, T., Shen, C., & Gao, S. (2022). A study on the modification of polypropylene by a star-shaped intumescent flame retardant containing phosphorus and nitrogen. Polymer Degradation and Stability, 195, 109801.

[103]. Zhu, C., He, M., Cui, J., Tai, Q., Song, L., & Hu, Y. (2018). Synthesis of a novel hyperbranched and phosphorus-containing charring-foaming agent and its application in polypropylene. Polymers for Advanced Technologies, 29(9), 2449-2456.

[104]. Wang, Y., Gao, S., Yin, N., Chen, Y., Shen, C., & Yu, Y. (2024). Synthesis of a charring-foaming agent containing triazine and triazole groups and its flame retardancy in PP. Polymer Bulletin, 81(14), 13183-13206.

[105]. Wen, P., Wang, X., Xing, W., Feng, X., Yu, B., Shi, Y., Tang, G., Hu, Y., Song, L., & Yuen, R. K. (2013). Synthesis of a novel triazine-based hyperbranched char foaming agent and the study of its enhancement on flame retardancy and thermal stability of polypropylene. Industrial & Engineering Chemistry Research, 52(48), 17015-17022.

[106]. Ye, X., Wang, Y., Zhao, Z., & Yan, H. (2017). A novel hyperbranched poly (phosphorodiamidate) with high expansion degree and carbonization efficiency used for improving flame retardancy of APP/PP composites. Polymer Degradation and Stability, 142, 29-41.

[107]. Yan, H., Zhao, Z., Ge, W., Zhang, N., & Jin, Q. (2017). Hyperbranched polyurea as charring agent for simultaneously improving flame retardancy and mechanical properties of ammonium polyphosphate/polypropylene composites. Industrial & Engineering Chemistry Research, 56(30), 8408-8415.

[108]. Meng, Z., Liu, Y., Wang, S., Zhang, A., & Li, S. (2023). Application of the PAPP/MCA/APP intumescent flame retardant system in polypropylene. Fire and Materials, 47(8), 1064-1073.

[109]. Tang, W., Zhu, H., Xi, W., Qiu, Y., & Qian, L. (2023). Cage-shaped octaphenyl silsesquioxane with micro-nano dispersibility for strengthening intumescent flame

retardancy in polypropylene composites. Journal of Applied Polymer Science, 140(22), e53907.

[110]. Pan, Y., Luo, Z., & Wang, B. (2021). Synergistic flame retardant effect of piperazine salt and ammonium polyphosphate as intumescent flame retardant system for polypropylene. Journal of Applied Polymer Science, 138(6), 49813.

[111]. Dong, F., Luo, Z., & Wang, B. (2021). Preparation of Mn^{2+} doped piperazine phosphate as a char-forming agent for improving the fire safety of polypropylene/ammonium polyphosphate composites. Materials, 14(24), 7589.

[112]. Wen, P., Tai, Q., Hu, Y., & Yuen, R. K. (2016). Cyclotriphosphazene-based intumescent flame retardant against the combustible polypropylene. Industrial & Engineering Chemistry Research, 55(29), 8018-8024.

[113]. Yuan, J., Wang, H., Wang, Y., Ma, Y., Zhu, Z., & Lin, X. (2022). A novel highly efficient intumescent flame-retardant polypropylene: Thermal degradation, flame retardance and mechanism. Journal of Polymer Research, 29(5), 205.

[114]. Bras, M. L., Bugajny, M., Lefebvre, J. M., & Bourbigot, S. (2000). Use of polyurethanes as char‐forming agents in polypropylene intumescent formulations. Polymer International, 49(10), 1115-1124.

[115]. Liu, M., Liu, Y., & Wang, Q. (2007). Flame‐retarded poly (propylene) with melamine phosphate and pentaerythritol/polyurethane composite charring agent. Macromolecular Materials and Engineering, 292(2), 206-213.

[116]. Zhang, T., Tao, Y., Zhou, F., Sheng, H., Qiu, S., Ma, C., & Hu, Y. (2019). Synthesis of a hyperbranched phosphorus-containing polyurethane as char forming agent combined with ammonium polyphosphate for reducing fire hazard of polypropylene. Polymer Degradation and Stability, 165, 207-219.

[117]. Almeras, X., Dabrowski, F., Le Bras, M., Poutch, F., Bourbigot, S., Marosi, G., & Anna, P. (2002). Using polyamide-6 as charring agent in intumescent polypropylene formulationsI. Effect of the compatibilising agent on the fire retardancy performance. Polymer degradation and stability, 77(2), 305-313.

[118]. Liu, Y., Feng, Z., & Wang, Q. (2009). The investigation of intumescent flame‐retardant polypropylene using a new macromolecular charring agent polyamide 11. Polymer Composites, 30(2), 221-225.

[119]. Chen, M., Tang, M., Ma, Y., Chen, X., Qin, J., He, W., & Zhang, Z. (2015). Influence of polyamide 6 as a charring agent on the flame retardancy, thermal, and mechanical

properties of polypropylene composites. Polymer Engineering & Science, 55(6), 1355-1360.

[120]. Tang, Y., Hu, Y., Xiao, J., Wang, J., Song, L., & Fan, W. (2005). PA-6 and EVA alloy/clay nanocomposites as char forming agents in poly (propylene) intumescent formulations. Polymers for advanced technologies, 16(4), 338-343.

[121]. Ma, Z. L., Zhang, W. Y., & Liu, X. Y. (2006). Using PA6 as a charring agent in intumescent polypropylene formulations based on carboxylated polypropylene compatibilizer and nano-montmorillonite synergistic agent. Journal of applied polymer science, 101(1), 739-746.

[122]. Yang, B., Liu, H., He, B., Leng, J., & Chen, X. (2013). Effect of novel copolyamide charring agents on flame-retarded polypropylene. Polymer composites, 34(5), 634-640.

[123]. Yi, J., Liu, Y., Pan, D., & Cai, X. (2013). Synthesis, thermal degradation, and flame retardancy of a novel charring agent aliphatic - aromatic polyamide for intumescent flame retardant polypropylene. Journal of applied polymer science, 127(2), 1061-1068.

[124]. Liu, J., Xu, J., Li, K., & Chen, Y. (2013). Synthesis and application of a novel polyamide charring agent for halogen-free flame retardant polypropylene. International Journal of Polymer Science, 2013(1), 616859.

[125]. Yi, J., Yin, H., & Cai, X. (2013). Effects of common synergistic agents on intumescent flame retardant polypropylene with a novel charring agent. Journal of Thermal Analysis and Calorimetry, 111(1), 725-734.

[126]. Zhang, Y., Qian, L., Wang, J., Qiu, Y., & Xi, W. (2024). A zinc-embedded multicomponent copolymer customized for polypropylene and its synergistic flame-retardant effect and outstanding mechanical properties. Polymer Degradation and Stability, 224, 110762.

[127]. Tao, M., Qian, L., Wang, J., Zhu, H., Tang, W., Chen, Y., Xi, W., & Qiu, Y. (2023). From physical mixtures to block copolymer: Impose outstandingly toughening and flame retardant effect to polypropylene. Composites Part B: Engineering, 253, 110538.

[128]. Tao, M., Tang, W., Qian, L., Wang, J., Xi, W., Xu, B., & Qiu, Y. (2023). Toughening behavior and synergistic flame retardant effect of a ternary block copolymer with amorphous morphology and thermal softening property in polypropylene. Chemical Engineering Journal, 461, 141963.

[129]. Zhu, C., He, M., Liu, Y., Cui, J., Tai, Q., Song, L., & Hu, Y. (2018). Synthesis and application of a mono-component intumescent flame retardant for polypropylene. Polymer Degradation and Stability, 151, 144-151.

[130]. Gao, S., Zhao, X., & Liu, G. (2017). Synthesis of an integrated intumescent flame retardant and its flame retardancy properties for polypropylene. Polymer Degradation and Stability, 138, 106-114.

[131]. Makhlouf, G., Abdelkhalik, A., & Hassan, M. A. (2020). Combustion toxicity of polypropylene containing melamine salt of pentaerythritol phosphate with high efficiency and stable flame retardancy performance. Process Safety and Environmental Protection, 138, 300-311.

[132]. Liu, H., Li, S., Zhang, Z., Li, B., & Xu, M. (2019). An efficient and convenient strategy toward fire safety and water resistance of polypropylene composites through design and synthesis of a novel mono-component intumescent flame retardant. Polymers for Advanced Technologies, 30(7), 1543-1554.

[133]. Li, G., Wang, W., Cao, S., Cao, Y., & Wang, J. (2014). Reactive, intumescent, halogen-free flame retardant for polypropylene. Journal of Applied Polymer Science, 131, 40054.

[134]. Li, H., Liu, J., Zhao, W., Wang, X., & Wang, D. (2016). Synthesis of a novel self-intumescent flame retardant with spiro and triazine structure and its performance for polypropylene. Journal of Fire Sciences, 34(2), 104-119.

[135]. Lai, X., Tang, S., Li, H., & Zeng, X. (2015). Flame-retardant mechanism of a novel polymeric intumescent flame retardant containing caged bicyclic phosphate for polypropylene. Polymer Degradation and Stability, 113, 22-31.

[136]. Qi, H., Liu, S., Chen, X., Shen, C., & Gao, S. (2020). The flame retardant and thermal performances of polypropylene with a novel intumescent flame retardant. Journal of Applied Polymer Science, 137(36), 49047.

[137]. Yang, R., Ma, B., Zhang, X., & Li, J. (2019). Fire retardance and smoke suppression of polypropylene with a macromolecular intumescent flame retardant containing caged bicyclic phosphate and piperazine. Journal of Applied Polymer Science, 136(25), 47593.

[138]. Zhang, C., Guo, X., Ma, S., Zheng, Y., Xu, J., & Ma, H. (2019). Synthesis of a novel branched cyclophosphazene-PEPA flame retardant and its application on polypropylene. Journal of thermal analysis and calorimetry, 137(1), 33-42.

[139]. Li, S., Qian, L., Tang, W., Qiu, Y., Wang, J., Xi, W., Chen, Y., & Wu, X. (2024). Microparticle-aggregation effect of intumescent flame retardants on flame retardancy and toughening property of polypropylene. Polymer Degradation and Stability, 222, 110705.

[140]. Li, S., Tang, W., Qian, L., Li, J., Qu, L., Wang, J., Xi, W., & Qiu, Y. (2025). Micron-level aggregate initiated ultra hydrophobicity with enhanced intumescent flame retardancy, smoke suppression, and toughness simultaneously in polypropylene. Chemical Engineering Journal, 504, 159040.

[141]. Li, S., Tang, W., Qian, L., Wang, J., Wu, X., Qiu, Y., & Xi, W. (2024). In-suit cemented strategy enables intumescent flame retardant transition from hyper-hydrophilic to hydrophobic and aggregation flame retardant effect simultaneously in polypropylene. Composites Part B: Engineering, 287, 111874.

[142]. Deng, C. L., Du, S. L., Zhao, J., Shen, Z. Q., Deng, C., & Wang, Y. Z. (2014). An intumescent flame retardant polypropylene system with simultaneously improved flame retardancy and water resistance. Polymer degradation and stability, 108, 97-107.

[143]. Huang, Z., Ruan, B., Wu, J., Ma, N., Jiang, T., & Tsai, F. C. (2021). High-efficiency ammonium polyphosphate intumescent encapsulated polypropylene flame retardant. Journal of Applied Polymer Science, 138(20), 50413.

[144]. Zhang, N., Zhang, J., Yan, H., Guo, X., Sun, Q., & Guo, R. (2019). A novel organic-inorganic hybrid K-HBPE@APP performing excellent flame retardancy and smoke suppression for polypropylene. Journal of Hazardous Materials, 373, 856-865.

[145]. Yu, S., Xiao, S., Zhao, Z., Huo, X., & Wei, J. (2019). Microencapsulated ammonium polyphosphate by polyurethane with segment of dipentaerythritol and its application in flame retardant polypropylene. Chinese Journal of Chemical Engineering, 27(7), 1735-1743.

[146]. Ding, S., Liu, P., Zhang, S., Ding, Y., Wang, F., Gao, C., & Yang, M. (2020). Preparation and characterization of cyclodextrin microencapsulated ammonium polyphosphate and its application in flame retardant polypropylene. Journal of Applied Polymer Science, 137(34), 49001.

[147]. Shao, Z. B., Deng, C., Tan, Y., Chen, M. J., Chen, L., & Wang, Y. Z. (2014). An efficient mono-component polymeric intumescent flame retardant for polypropylene: preparation and application. ACS applied materials & interfaces, 6(10), 7363-7370.

[148]. Zheng, Z., Liu, Y., Zhang, L., Dai, B., Yang, X., & Wang, H. (2017). Fabrication of halogen-free ammonium phosphate with two components via a simple method and its flame

retardancy in polypropylene composites. Journal of Thermal Analysis and Calorimetry, 127(3), 2013-2023.

[149]. Shao, Z. B., Deng, C., Tan, Y., Chen, M. J., Chen, L., & Wang, Y. Z. (2014). Flame retardation of polypropylene via a novel intumescent flame retardant: Ethylenediamine-modified ammonium polyphosphate. Polymer degradation and stability, 106, 88-96.

[150]. Xiao, D., Gohs, U., Wagenknecht, U., Voit, B., & Wang, D. Y. (2022). Thermal stability and pyrolysis behavior of an efficient fire-retarded polypropylene containing allylamine polyphosphate and pentaerythritol. Thermochimica Acta, 708, 179083.

[151]. Xiao, D., Li, Z., Gohs, U., Wagenknecht, U., Voit, B., & Wang, D. Y. (2017). Functionalized allylamine polyphosphate as a novel multifunctional highly efficient fire retardant for polypropylene. Polymer Chemistry, 8(40), 6309-6318.

[152]. Liu, Z., Xing, S., Li, Y., Sun, J., Li, H., Gu, X., & Zhang, S. (2024). Surface modification of zinc oxide and its application in polypropylene with excellent fire performance and ultra-violet resistance. Journal of Colloid and Interface Science, 661, 307-316.

[153]. Cheng, C., Shuqian, S., Mingmei, S., Zhengwen, W., Xingrong, Z., & Linsheng, T. (2023). Synergistic flame retardancy of ZnO with piperazine pyrophosphate/melamine polyphosphate in PP. Polymer Testing, 117, 107878.

[154]. Ma, Z. L., Fan, C. R., Lu, G. Y., Liu, X. Y., & Zhang, H. (2012). Synergy of magnesium and calcium oxides in intumescent flame-retarded polypropylene. Journal of applied polymer science, 125(5), 3567-3574.

[155]. Feng, C., Zhang, Y., Liu, S., Chi, Z., & Xu, J. (2012). Synergistic effect of La_2O_3 on the flame retardant properties and the degradation mechanism of a novel PP/IFR system. Polymer Degradation and Stability, 97(5), 707-714.

[156]. Wang, Y. L., Tang, X. P., & Tang, X. D. (2014). Study of Synergistic Effects of Cerium Oxide on Intumescent Flame Retardant Polypropylene System. Advanced Materials Research, 887, 90-93.

[157]. Feng, C., Liang, M., Jiang, J., Huang, J., & Liu, H. (2016). Synergism effect of CeO_2 on the flame retardant performance of intumescent flame retardant polypropylene composites and its mechanism. Journal of Analytical and Applied Pyrolysis, 122, 405-414.

[158]. Qin, Z., Li, D., Li, Q., & Yang, R. (2016). Effect of nano-aluminum hydroxide on mechanical properties, flame retardancy and combustion behavior of intumescent flame retarded polypropylene. Materials & Design, 89, 988-995.

[159]. Xu, M. J., Wang, J., Ding, Y. H., & Li, B. (2015). Synergistic effects of aluminum hypophosphite on intumescent flame retardant polypropylene system. Chinese Journal of Polymer Science, 33(2), 318-328.

[160]. Xu, B., Shao, L., Wang, J., Liu, Y., & Qian, L. (2020). Enhancement of the intumescent flame retardant efficiency in polypropylene by synergistic charring effect of a hypophosphite/cyclotetrasiloxane bi-group compound. Polymer Degradation and Stability, 181, 109281.

[161]. Qin, Z., Yang, R., Zhang, W., Li, D., & Jiao, Q. (2019). Synergistic barrier effect of aluminum phosphate on flame retardant polypropylene based on ammonium polyphosphate/dipentaerythritol system. Materials & Design, 181, 107913.

[162]. Zhao, W., Cheng, Y., Li, Z., Li, X., & Zhang, Z. (2021). Improvement in fire-retardant properties of polypropylene filled with intumescent flame retardants, using flower-like nickel cobaltate as synergist. Journal of Materials Science, 56(3), 2702-2716.

[163]. Dong, X., Nie, S., Liu, Z., & Wang, D. Y. (2016). Study of the synergistic effect of nickel phosphate nanotubes (NiPO-NT) on intumescent flame retardant polypropylene composites. Journal of Thermal Analysis and Calorimetry, 126(3), 1323-1330.

[164]. Chen, K., Cheng, J., Wu, B., Liu, C., & Guo, J. (2021). Synergistic effects of strontium carbonate on a novel intumescent flame-retardant polypropylene system. Polymers for Advanced Technologies, 32(8), 3018-3027.

[165]. Xu, J., Deng, H., & Luo, M. (2021). Preparation of MWCNTs@ SiO2 hybrids and its flame retardant synergistic effects with hyperbranched triazine-based flame retardant on polypropylene. SPE Polymers, 2(4), 276-287.

[166]. Liu, Q., Chu, J., Xie, Y., Li, Z., Wu, F., Feng, D., Meng, Y., Mei, Y., & Xie, D. (2025). Novel Si-MXene/PAPP hybrid system for high-performance flame-retardant polypropylene composites. Polymer Degradation and Stability, 239, 111376.

[167]. Jiang, S., Liu, L., Yang, X., Li, B., & Xu, M. (2023). Nickel-Aluminum Hydrotalcite for Improving Flame Retardancy and Smoke Suppression of Intumescent Flame Retardant Polypropylene: Preparation, Synergy, and Mechanism Study. Macromolecular Materials and Engineering, 308(4), 2200533.

[168]. Wang, X., Spörer, Y., Leuteritz, A., Kuehnert, I., Wagenknecht, U., Heinrich, G., & Wang, D. Y. (2015). Comparative study of the synergistic effect of binary and ternary LDH with intumescent flame retardant on the properties of polypropylene composites. RSC Advances, 5(96), 78979-78985.

[169]. Turgut, G., Dogan, M., Tayfun, U., & Ozkoc, G. (2018). The effects of POSS particles on the flame retardancy of intumescent polypropylene composites and the structure-property relationship. Polymer Degradation and Stability, 149, 96-111.

[170]. Pappalardo, S., Russo, P., Acierno, D., Rabe, S., & Schartel, B. (2016). The synergistic effect of organically modified sepiolite in intumescent flame retardant polypropylene. European polymer journal, 76, 196-207.

[171]. Ren, Q., Zhang, Y., Li, J., & Li, J. C. (2011). Synergistic effect of vermiculite on the intumescent flame retardance of polypropylene. Journal of Applied Polymer Science, 120(2), 1225-1233.

[172]. Feng, C., Zhang, Y., Liu, S., Chi, Z., & Xu, J. (2013). Synergistic effects of 4A zeolite on the flame retardant properties and thermal stability of a novel halogen-free PP/IFR composite. Polymers for advanced technologies, 24(5), 478-486.

[173]. Yuan, Y., Yu, B., & Wang, W. (2022). The influence of poorly-/well-dispersed organo-montmorillonite on interfacial compatibility, fire retardancy and smoke suppression of polypropylene/intumescent flame retardant composite system. Journal of Colloid and Interface Science, 622, 367-377.

[174]. Wang, S., Li, J., Wang, W., Wang, X., Li, H., Sun, J., Fei, B., Gu, X., & Zhang, S. (2021). Silicone filled halloysite nanotubes for polypropylene composites: Flame retardancy, smoke suppression and mechanical property. Composites Part A: Applied Science and Manufacturing, 140, 106170.

[175]. Feng, C., Zhang, Y., Liang, D., Liu, S., Chi, Z., & Xu, J. (2015). Influence of zinc borate on the flame retardancy and thermal stability of intumescent flame retardant polypropylene composites. Journal of Analytical and Applied Pyrolysis, 115, 224-232.

[176]. Yang, H., Guan, Y., Ye, L., Wang, S., Li, S., Wen, X., Chen, X., Mijowska, E., & Tang, T. (2019). Synergistic effect of nanoscale carbon black and ammonium polyphosphate on improving thermal stability and flame retardancy of polypropylene: A reactive network for strengthening carbon layer. Composites Part B: Engineering, 174, 107038.

[177]. Xie, J., Shi, X., Zhang, M., Dai, X., & Wang, X. (2019). Improving the flame retardancy of polypropylene by nano metal–organic frameworks and bioethanol coproduct. Fire and Materials, 43(4), 373-380.

[178]. Shen, R., Quan, Y., Zhang, Z., Ma, R., & Wang, Q. (2022). Metal–Organic Framework as an Efficient Synergist for Intumescent Flame Retardants against Highly Flammable Polypropylene. Industrial & Engineering Chemistry Research, 61(21), 7292-7302.

[179]. Duquesne, S., Samyn, F., Bourbigot, S., Amigouet, P., Jouffret, F., & Shen, K. (2008). Influence of talc on the fire retardant properties of highly filled intumescent polypropylene composites. Polymers for Advanced Technologies, 19(6), 620-627.

[180]. Liu, Y., Zhang, A., Cheng, Y., Li, M., Cui, Y., & Li, Z. (2023). Recent advances in biomass phytic acid flame retardants. Polymer Testing, 124, 108100.

[181]. Gao, Y. Y., Deng, C., Du, Y. Y., Huang, S. C., & Wang, Y. Z. (2019). A novel bio-based flame retardant for polypropylene from phytic acid. Polymer Degradation and Stability, 161, 298-308.

[182]. Li, W. X., Zhang, H. J., Hu, X. P., Yang, W. X., Cheng, Z., & Xie, C. Q. (2020). Highly efficient replacement of traditional intumescent flame retardants in polypropylene by manganese ions doped melamine phytate nanosheets. Journal of Hazardous Materials, 398, 123001.

[183]. Yan, W. J., Xu, S., Ding, C. J., Liu, Z. H., Hu, Y., Fan, Q. X., Li, J. S., Tian, X. Y., & Zeng, H. Y. (2022). Novel bio-derived phytic acid and melamine interlayered/surface dual modified layered double hydroxide by one-pot method and its highly efficient flame retardant performance for polypropylene. Applied Clay Science, 228, 106620.

[184]. He, S., Gao, Y. Y., Zhao, Z. Y., Huang, S. C., Chen, Z. X., Deng, C., & Wang, Y. Z. (2021). Fully bio-based phytic acid-basic amino acid salt for flame-retardant polypropylene. ACS Applied Polymer Materials, 3(3), 1488-1498.

[185]. He, S., Deng, C., Zhao, Z. Y., Chen, Z. X., & Wang, Y. Z. (2023). Hyperbranched polyamide-amine based phosphorous-containing flame retardant for simultaneous flame retardancy and high performance of polypropylene. Composites Part B: Engineering, 250, 110431.

[186]. Wang, X., Wang, Z., & Li, J. (2019). Effects of a semi-bio-based triazine derivative on intumescent flame-retardant polypropylene. Polymers for Advanced Technologies, 30(5), 1259-1268.

[187]. Ma, D., & Li, J. (2020). Synthesis of a bio-based triazine derivative and its effects on flame retardancy of polypropylene composites. Journal of Applied Polymer Science, 137(1), 47367.

[188]. Yu, G., Ma, C., & Li, J. (2020). Flame retardant effect of cytosine pyrophosphate and pentaerythritol on polypropylene. Composites Part B: Engineering, 180, 107520.

[189]. Xu, Y., Hu, H., Tao, B., Yin, R., Liu, L., & Li, B. (2025). Safe and economical preparation of amino acid-derived bio-based triazine char-forming agent for efficient

intumescent flame retardant polypropylene. Construction and Building Materials, 484, 141876.

[190]. Jung, D., & Bhattacharyya, D. (2018). Keratinous fiber based intumescent flame retardant with controllable functional compound loading. ACS Sustainable Chemistry & Engineering, 6(10), 13177-13184.

[191]. Wang, Z., Liu, Y., & Li, J. (2017). Regulating effects of nitrogenous bases on the char structure and flame retardancy of polypropylene/intumescent flame retardant composites. ACS Sustainable Chemistry & Engineering, 5(3), 2375-2383.

[192]. Huang, Z., Li, S., Tsai, L. C., Jiang, T., Ma, N., & Tsai, F. C. (2022). Flame retardant polypropylene with a single molecule intumescent flame retardant based on chitosan. Materials Today Communications, 33, 104689.

[193]. Wang, K., Wang, Q., Wang, L., Chen, D., Ma, Y., & Yang, W. (2024). Sustainable furfuryl alcohol-based flame retardants with regular spherical morphology: Endow polypropylene with excellent flame retardancy, smoke suppression, and mechanical properties. Chemical Engineering Journal, 496, 153848.

[194]. Zheng, Z., Liu, Y., Dai, B., Meng, C., & Guo, Z. (2019). Fabrication of cellulose-based halogen-free flame retardant and its synergistic effect with expandable graphite in polypropylene. Carbohydrate polymers, 213, 257-265.

[195]. Xia, Y., Chai, W., Liu, Y., Su, X., Liao, C., Gao, M., Li, Y., & Zheng, Z. (2022). Facile fabrication of starch-based, synergistic intumescent and halogen-free flame retardant strategy with expandable graphite in enhancing the fire safety of polypropylene. Industrial Crops and Products, 184, 115002.

[196]. Xu, S., Li, S. Y., Zhang, M., Zeng, H. Y., Wu, K., Tian, X. Y., Chen, C. R. & Pan, Y. (2020). Fabrication of green alginate-based and layered double hydroxides flame retardant for enhancing the fire retardancy properties of polypropylene. Carbohydrate Polymers, 234, 115891.

[197]. Yan, W. J., Ding, C. J., Min, J. J., Liu, S. C., Jian, J., Hu, J., & Xu, S. (2023). Fabrication of green and scalable N/P/S/Mn containing biobased layered double hydroxide as a novel flame retardant and efficient char forming agent for polypropylene. ACS Sustainable Chemistry & Engineering, 11(13), 5216-5228.

[198]. Wang, L., Wu, K., Ding, C. J., Min, J. J., Chen, H. P., Liu, Z. H., Xi, D. N., Zeng, H. Y., Jian, J., & Xu, S. (2023). Novel hierarchical carbon microspheres @ layered double hydroxides @ copper lignosulfonate architecture for polypropylene with enhanced flame

retardant and mechanical performances. International Journal of Biological Macromolecules, 235, 123726.

[199]. Wu, K., Xu, S., Tian, X. Y., Zeng, H. Y., Hu, J., Guo, Y. H., & Jian, J. (2021). Renewable lignin-based surfactant modified layered double hydroxide and its application in polypropylene as flame retardant and smoke suppression. International Journal of Biological Macromolecules, 178, 580-590.

[200]. Wang, Z., Liu, Y., & Li, J. (2016). Preparation of nucleotide-based microsphere and its application in intumescent flame retardant polypropylene. Journal of Analytical and Applied Pyrolysis, 121, 394-402.

[201]. Liang, J. Z., Zhu, B., Pan, M. S., & Feng, J. Q. (2019). Melt shear flow behavior of flame-retardant polypropylene composites filled with microencapsulated red phosphorus. Journal of Thermoplastic Composite Materials, 32(10), 1361-1377.

[202]. Wang, N., Li, L., Xu, Y., Zhang, K., Chen, X., & Wu, H. (2020). Synergistic effects of red phosphorus masterbatch with expandable graphite on the flammability and thermal stability of polypropylene/thermoplastic polyurethane blends. Polymers and Polymer Composites, 28(3), 209-219.

[203]. Chen, X., Yu, J., Qin, J., Luo, Z., Hu, S., & He, M. (2011). Combustion behaviour and synergistic effect of zinc borate and microencapsulated red phosphorus with magnesium hydroxide in flame-retarded polypropylene composites. Polymers and Polymer Composites, 19(6), 491-496.

[204]. Liang, J. Z., Feng, J. Q., Tsui, C. P., Tang, C. Y., Liu, D. F., Zhang, S. D., & Huang, W. F. (2015). Mechanical properties and flame-retardant of PP/MRP/Mg (OH) 2/Al (OH) 3 composites. Composites Part B: Engineering, 71, 74-81.

[205]. Pham, L. H., Nguyen, H. D., Kim, J., & Hoang, D. (2019). Thermal properties and fire retardancy of polypropylene/wood flour composites containing eco-friendly flame retardants. Fibers and Polymers, 20(11), 2383-2389.

[206]. Evans, A., Morris, L. J., Turner, Z. R., & O'Hare, D. (2025). Phosphonate-functionalized polypropylenes: single-component flame retardants. ACS Applied Polymer Materials, 7(4), 2508-2516.

[207]. Zhang, Z., Han, Z., Pan, Y. T., Li, D., Wang, D. Y., & Yang, R. (2020). Dry synthesis of mesoporous nanosheet assembly constructed by cyclomatrix polyphosphazene frameworks and its application in flame retardant polypropylene. Chemical Engineering Journal, 395, 125076.

[208]. Ai, L., Liu, J., Chen, S., Xu, Z., & Liu, P. (2022). Synthesis of melamine phenyl hypophosphite and its synergistic flame retardance with SiO_2 on polypropylene. Journal of Thermal Analysis and Calorimetry, 147(11), 6207-6217.

[209]. Nazir, R., Gooneie, A., Lehner, S., Jovic, M., Rupper, P., Ott, N., Hufenus, R., & Gaan, S. (2021). Alkyl sulfone bridged phosphorus flame-retardants for polypropylene. Materials & Design, 200, 109459.

[210]. Sain, M., Park, S. H., Suhara, F., & Law, S. (2004). Flame retardant and mechanical properties of natural fibre–PP composites containing magnesium hydroxide. Polymer degradation and stability, 83(2), 363-367.

[211]. Hong, C. H., Lee, Y. B., Bae, J. W., Jho, J. Y., Uk Nam, B., Chang, D. H., Yoon, S. H., & Lee, K. J. (2005). Tensile properties and stress whitening of polypropylene/polyolefin elastomer/magnesium hydroxide flame retardant composites for cable insulating application. Journal of Applied Polymer Science, 97(6), 2311-2318.

[212]. Yang, J., Zhang, J., & Tang, L. (2013). Flame Retardant Synergism of Bentonite and Magnesium Hydroxide in Polypropylene. Asian Journal of Chemistry, 25(11), 6121-6124.

[213]. Wang, W., Peng, Y., Zammarano, M., Zhang, W., & Li, J. (2017). Effect of ammonium polyphosphate to aluminum hydroxide mass ratio on the properties of wood-flour/polypropylene composites. Polymers, 9(11), 615.

[214]. Liang, J. Z., Chen, Y., & Jiang, X. H. (2012). Flame-Retardant Properties of PP/Al (OH) 3/Mg (OH) 2/POE/ZB Nanocomposites. Polymer-Plastics Technology and Engineering, 51(5), 439-445.

[215]. Xu, S., Li, S. Y., Zhang, M., Zeng, H. Y., Du, J. Z., & Chen, C. R. (2018). Effect of $P_3O_{10}^{5-}$ intercalated hydrotalcite on the flame retardant properties and the degradation mechanism of a novel polypropylene/hydrotalcite system. Applied Clay Science, 163, 196-203.

[216]. Hajibeygi, M., Mousavi, M., Shabanian, M., Habibnejad, N., & Vahabi, H. (2021). Design and preparation of new polypropylene/magnesium oxide micro particles composites reinforced with hydroxyapatite nanoparticles: A study of thermal stability, flame retardancy and mechanical properties. Materials Chemistry and Physics, 258, 123917.

[217]. Sheng, Y., Li, P., & Chen, Y. (2014). The synergistic effect of transition metal nitrate in polypropylene/magnesium hydroxide flame retarded composite. Advances in Polymer Technology, 33(S1), 2144701-2144708.

[218]. Shen, H., & Liu, Y. (2018). One-step synthesis of hydrophobic magnesium hydroxide nanoparticles and their application in flame-retardant polypropylene composites. Chinese Journal of Chemical Engineering, 26(10), 2199-2205.

[219]. Chen, X., Yu, J., Guo, S., Lu, S., Luo, Z., & He, M. (2009). Surface modification of magnesium hydroxide and its application in flame retardant polypropylene composites. Journal of Materials Science, 44(5), 1324-1332.

[220]. Chen, D., Zheng, Q., Liu, F., Xu, L., Xu, K., & Chen, M. (2009). Effects of magnesium hydroxide containing copper compound on the properties of polypropylene composites. Polymer-Plastics Technology and Engineering, 48(4), 432-439.

[221]. Battaglia, G., Domina, M. A., Lo Brutto, R., Lopez Rodriguez, J., Fernandez de Labastida, M., Cortina, J. L., Pettignano, A., Cipollina, A., Tamburini, A., & Micale, G. (2022). Evaluation of the purity of magnesium hydroxide recovered from saltwork bitterns. Water, 15(1), 29.

[222]. Tian, X. S., Zhang, Y. F., Li, Y., & Zhong, J. R. (2022). Effect of char-forming agents rich in tertiary carbon on flame retardant properties of polypropylene. Journal of Thermal Analysis and Calorimetry, 147(19), 10391-10401.

[223]. Wang, C., Wei, P., Qian, Y., & Liu, J. (2011) The synthesis of a novel flame retardant and its synergistic efficiency in polypropylene/ammonium polyphosphate system. Polymers for Advanced Technology, 22(7), 1108-1114.

[224]. Huang, Y. W., Song, M. L., Ma, J. J., Lu, Z. Y., Yang, J. X., & Cao, K. (2013). Synthesis of a phosphorus/silicon hybrid and its synergistic effect with melamine polyphosphates on flame retardant polypropylene system. Journal of applied polymer science, 129(1), 316-323.

[225]. Qian, Y., Wei, P., Jiang, P., Hao, J., & Du, J. (2013). Preparation of hybrid phosphamide containing polysilsesquioxane and its effect on flame retardancy and mechanical properties of polypropylene composites. Composites Part B: Engineering, 45(1), 1541-1547.

[226]. Yuan, G., Yang, B., Chen, Y., & Jia, Y. (2019). Synthesis of a novel multi-structure synergistic POSS-GO-DOPO ternary graft flame retardant and its application in polypropylene. Composites Part A: Applied Science and Manufacturing, 117, 345-356.

[227]. Qiu, Y., Qian, L., Chen, Y., & Hao, J. (2019). Improving the fracture toughness and flame retardant properties of epoxy thermosets by phosphaphenanthrene/siloxane cluster-like molecules with multiple reactive groups. Composites Part B: Engineering, 178, 107481.

[228]. Qiu, Y., Qian, L., Feng, H., Jin, S., & Hao, J. (2018). Toughening effect and flame-retardant behaviors of phosphaphenanthrene/phenylsiloxane bigroup macromolecules in epoxy thermoset. Macromolecules, 51(23), 9992-10002.

[229]. Cai, B., Qian, L., Qiu, Y., Wang, J., Xi, W., Chen, Y., & Tang, W. (2022). Group aggregation effect of polyphenolic phosphaphenanthrene macromolecule on enhancing fire safety and toughness of epoxy thermoset. Polymer Degradation and Stability, 205, 110154.

[230]. Nie, S., Hu, Y., Song, L., He, Q., Yang, D., & Chen, H. (2008). Synergistic effect between a char forming agent (CFA) and microencapsulated ammonium polyphosphate on the thermal and flame retardant properties of polypropylene. Polymers for Advanced Technologies, 19(8), 1077-1083.

[231]. Zhang, Feng, Jun Zhang, and Daoxing Sun. "Study on thermal decomposition of intumescent fire-retardant polypropylene by TG/Fourier transform infrared." Journal of Thermoplastic Composite Materials 22.6 (2009): 681-701.

[232]. Li, N., Xia, Y., Mao, Z., Wang, L., Guan, Y., & Zheng, A. (2012). Influence of antimony oxide on flammability of polypropylene/intumescent flame retardant system. Polymer Degradation and Stability, 97(9), 1737-1744.

[233]. Wang, B., Wang, X., Tang, G., Shi, Y., Hu, W., Lu, H., Song, L., & Hu, Y. (2012). Preparation of silane precursor microencapsulated intumescent flame retardant and its enhancement on the properties of ethylene–vinyl acetate copolymer cable. Composites Science and Technology, 72(9), 1042-1048.

[234]. Xia, S., Zhang, Z., Leng, Y., Li, B., & Xu, M. (2018). Synthesis of a novel mono-component intumescent flame retardant and its high efficiency for flame retardant polyethylene. Journal of Analytical and Applied Pyrolysis, 134, 632-640.

[235]. Vahabi, H., Kandola, B. K., & Saeb, M. R. (2019). Flame retardancy index for thermoplastic composites. Polymers, 11(3), 407.

[236]. Zheng, Z., Xia, Y., Liao, C., Liu, Y., Dai, B., Guo, Z., & Chai, W. (2021). Facile fabrication of cyclodextrin-based and integrated flame retardant in intumescent flame-retarding polypropylene. Journal of Thermal Analysis and Calorimetry, 146(6), 2375-2386.

[237]. Wang, Z., Qiu, Y., Liu, A., Tang, W., Xi, W., Wang, J., Gao, L. B., & Qian, L. (2023). Micro-crosslinking of phosphaphenanthrene/siloxane molecule initiate aggregation flame retardant and toughening enhancement effects on its polycarbonate composite. Chemical Engineering Journal, 466, 143169.

[238]. Tsai, K. C., Kuan, C. F., Chen, C. H., Kuan, H. C., Hsu, S. W., Lee, F. M., & Chiang, C. L. (2013). Study on thermal degradation and flame retardant property of halogen-free polypropylene composites using XPS and cone calorimeter. Journal of applied polymer science, 127(2), 1084-1091.

[239]. Wang, Z. H., Liu, B. W., Zeng, F. R., Lin, X. C., Zhang, J. Y., Wang, X. L., Wang, Y. Z. & Zhao, H. B. (2022). Fully recyclable multifunctional adhesive with high durability, transparency, flame retardancy, and harsh-environment resistance. Science Advances, 8(50), eadd8527.

[240]. Yue, X., Li, C., Ni, Y., Xu, Y., & Wang, J. (2019). Flame retardant nanocomposites based on 2D layered nanomaterials: a review. Journal of Materials Science, 54(20), 13070-13105.

[241]. Lin, X. C., Li, S. L., Li, W. X., Wang, Z. H., Zhang, J. Y., Liu, B. W., Zhao, H. B. & Wang, Y. Z. (2023). Thermo-responsive self-ceramifiable robust aerogel with exceptional strengthening and thermal insulating performance at ultrahigh temperatures. Advanced Functional Materials, 33(27), 2214913.

[242]. Zeng, F., He, L., Ma, J., Fang, D., Zeng, Z., Bai, T., Ding, R., Liu, B., Zhao, H., & Wang, Y. (2024). Microcage flame retardants with complete recyclability and durability via reversible interfacial locking engineering. Materials Horizons, 11(8), 1867-1876.

[243]. Guo, Y., Ruan, K., Shi, X., Yang, X., & Gu, J. (2020). Factors affecting thermal conductivities of the polymers and polymer composites: A review. Composites Science and Technology, 193, 108134.

[244]. Huang, C., Qian, X., & Yang, R. (2018). Thermal conductivity of polymers and polymer nanocomposites. Materials Science and Engineering: R: Reports, 132, 1-22.

[245]. Xu, X., Chen, J., Zhou, J., & Li, B. (2018). Thermal conductivity of polymers and their nanocomposites. Advanced Materials, 30(17), 1705544.

[246]. Tang, W., Song, L., Liu, F., Dessie, W., Qin, Z., Zhang, S., & Gu, X. (2022). Improving the flame retardancy and thermal stability of polypropylene composites via introducing glycine intercalated kaolinite compounds. Applied Clay Science, 217, 106411.

[247]. Yuan, B., Fan, A., Yang, M., Chen, X., Hu, Y., Bao, C., Jiang, S., Niu, Y., Zhang, Y., & Dai, H. (2017). The effects of graphene on the flammability and fire behavior of intumescent flame retardant polypropylene composites at different flame scenarios. Polymer Degradation and Stability, 143, 42-56.

[248]. Yang, B., Chen, Y., Zhang, M., & Yuan, G. (2019). Synergistic and compatibilizing effect of octavinyl polyhedral oligomeric silsesquioxane nanoparticles in polypropylene/intumescent flame retardant composite system. Composites Part A: Applied Science and Manufacturing, 123, 46-58.

[249]. Zhang, J., Fang, Y., Zhang, A., Yu, Y., Liu, L., Huo, S., Zeng, X., Peng, H., & Song, P. (2023). A Schiff base-coated ammonia polyphosphate for improving thermal and fire-retardant properties of unsaturated polyester. Progress in Organic Coatings, 185, 107910.

[250]. Yu, L., Yang, G., Wang, X., & Fang, J. (2023). Flame retardancy and degradation process of precipitation construction of double-shell flame-retardant microcapsules. Industrial Crops and Products, 205, 117551.

[251]. Sun, Y., Yuan, B., Shang, S., Zhang, H., Shi, Y., Yu, B., Qi, C., Dong, H., Chen, X., & Yang, X. (2020). Surface modification of ammonium polyphosphate by supramolecular assembly for enhancing fire safety properties of polypropylene. Composites Part B: Engineering, 181, 107588.

[252]. Tang, W., Qian, L., Chen, Y., Qiu, Y., Xu, B., & Li, J. (2020). Joint-aggregation intumescent flame‐retardant effect of ammonium polyphosphate and charring agent in polypropylene. Polymers for Advanced Technologies, 31(8), 1699-1708.

List of Figures

List of Tables